UNIVERSITY OF SOUTHAMPTON

FACULTY OF NATURAL AND ENVIRONMENTAL SCIENCES

School of Chemistry

THE DEVELOPMENT OF NANO-SIZED SILICAS AS ANALYTICAL TOOLS

By

Mohammed Mobarak Algaradah

Thesis for the degree of Doctor of Philosophy

November 2010

UNIVERSITY OF SOUTHAMPTON

ABSTRACT

FACULTY OF NATURAL AND ENVIRONMENTAL SCIENCES

SCHOOL OF CHEMISTRY

Doctor of Philosophy

THE DEVELOPMENT OF NANO-SIZED SILICAS AS ANALYTICAL TOOLS

by Mohammed Algaradah

Even at low concentrations the presence of toxic materials, such as metals or organic pesticides, in water can be harmful to humans. Extraction and preconcentration of these materials is an important part of many analytical procedures. In this work functionalised solid phase extractants, 250 nm in size (nanoscavenger), have been used to collect and concentrate metals and organic species from water using a nanoscavenger dispersion extraction (NSDE) approach.

Stöber-type silica with a mean diameter of ca. 250 nm and a surface area of ca. 20 m^2 g^{-1} has been synthesized by hydrolysis and condensation of tetraethoxysilane in a methanol and ammonium hydroxide medium. Increasing the surface area to increase the loading of functional groups on the surface was achieved by adopting mesoporous silica as the nanoscavenger core. This was successfully synthesized from tetramethoxysilane in the presence of a dodecyltrimethylammonium bromide template: 250 nm particles prepared in this manner had a surface area of ca. 1325 m^2 g^{-1}. The properties of synthesized sub-micron silicas have been investigated using various techniques.

One of the main aims of this work was to use the nanoscavengers for the analytical recovery of trace analytes from water. Nanoscavengers were prepared by chemically modifying mesoporous silicas with groups such as mono- and diamines, dithiocarbamates, hydroxyquinoline, mercaptobenzamide and, for organic extractions, a mixed functionality diol and C_{18} modification. The nanoscavengers were characterized by Fourier transform infrared spectroscopy, scanning electron microscope, transmission electron microscope and thermogravimetric analysis. Copper capacity measurements for complexant nanoscavengers ranged between 0.1 and 2 mmol g^{-1} depending on the type of silica and the loading group.

The nanoscavengers were evaluated for the preconcentration of trace analytes from water. The dithiocarbamate, hydroxyquinoline and mercaptobenzamide nano-scavengers were used to preconcentrate eight metal ions (Cu^{2+}, Cd^{2+}, Ni^{2+}, Pb^{2+}, Co^{2+}, Cr^{3+}, Mn^{2+} and Zn^{2+}) from water. A dual functionality diol/C_{18}-nanoscavenger was used to collect four estrogenic compounds, polynuclear aromatic hydrocarbons and tributyltin from water. The recovery of extracted analytes by nanoscavengers exhibited good results.

Table of contents

DECLARATION OF AUTHORSHIP

I, Mohammed M. Algaradah declare that the thesis entitled: The Development of Sub-Micron Sized Silicas as Analytical Tools and the work presented in the thesis are both my own, and have been generated by me as the result of my own original research. I confirm that:

- this work was done wholly or mainly while in candidature for a research degree at this University;
- the study of the applications of the HOC_{18}-nanoscavenger in the extraction of TBT from water was carried out jointly with Awad Alrashdy (PhD student and member of Alan Howard group)
- where I have quoted from the work of others, the source is always given. With the exception of such quotations, this thesis is entirely my own work;
- I have acknowledged all main sources of help;
- where the thesis is based on work done by myself jointly with others, I have made clear exactly what was done by others and what I have contributed myself;
- none of this work has been published before submission.

Signed: ……..

Date: ……

Acknowledgements

I would like to thank several people for supporting me in the last five years to the end of my PhD project. First, I extend great thanks to my supervisor Dr. Alan Howard who has spent an enormous amount of time on the project. During the time that I spent in his group, he gave me an intensive supervision, considerable time to discuss the results and valuable suggestions. At the end of my PhD period I feel that I have adopted several skills from him, especially the ability to solve problems. I am very fortunate to have had the opportunity to work with him.

Next, I would like to thank Dr. Andrew Hector for advising in the pursuit my PhD. His feedback in the quarterly reports and in the transfer report were helpful for planning further work.

Some of the instruments were not available in our groups and therefore several instruments have been used outside in other laboratories. I would like to thank all of those who gave me full access to their laboratory, especially Professor George Attard and Professor Richard Brown, for allowing me to use their instruments. Many thanks to all members of the School of Chemistry who trained me to use the instruments, especially Dr Mamdoh Abdalsalam. Many thanks to Dr Saad Alghamidi who has carried out the statistic analysis of some of the data.

I also take this opportunity to gratefully thank His Royal Highness Prince Motab bin Abdullah bin Abdulaziz, the head of the National Guard and all members of king Khalid military academy for supporting me to obtain the scholarship and for their efforts in extending this until I finished my study.

Many thanks to all my brothers, sisters and friends for their encouragement and support. Thanks also go to those people who contributed directly to my thesis project: Awad Alrashdy, who carried out some of the application of the HOC_{18}-nanoscavenger in the extraction of TBT from water.

With the oversight of my main supervisor, editorial advice has been sought. No changes of intellectual content were made as a result of this advice. Many thanks go to Dr. Sherif B. Abdel Ghani, Dr Nadeem Shike and Jill Doubleday for their proofreading and comments on my thesis.

Finally, I wish to express my deepest appreciation to my parents, Mobarak and Salma for their continuing help and support and for their patience in being away from me for more than six years despite their need for me, especially after they lost my older brother. My special thanks also to my wife Haia for taking care of our children Salma, Mobarak and Raid during my study commitment.

ABBREVIATIONS

AMP	4-Amino-2-mercaptopyrimidine
ANOVA	Analysis of variance
BET	Multipoint Brunauer, Emmett and Teller method
BJH	Barrett, Joyner and Halenda method
$BNCS_2@SiO_2$	Bis-dithiocarbamate-nanoscavenger
BTEE	1,2-Bis(triethoxysilyl)ethane
C_8	Octyl
C_{18}	Octadecyl
CS_2	Carbon disulfide
$C_{18}SiCl_3$	Octadecyltrichlorosilane or trichloro(octadecyl)silane
$C_{18}Si(OMe)_3$	Octadecyltrimethoxysilane or trimethoxy(octadecyl)silane
CTMABr	Cetyltrimethylammonium bromide
C_{10}TMABr	Decyltrimethylammonium bromide
C_{12}TMABr	Dodecyltrimethylammonium bromide
C_{16}TMABr	Hexadecyltrimethylammonium bromide
C_{16}TMACl	Hexadecyltrimethylammonium chloride
CPTMOS	Chloropropyltrimethoxysilane
$DiNH_2@SiO_2$	Diamino-nanoscavenger
DL	Detection limit
DLVO	Derjaguin-Landau-Verwey-Overbeek
$DMC_{18}ClSi$	Dimethyloctadecylchlorosilane
DRIFT	Diffuse reflectance infrared Fourier transform
DSPE	Dispersive solid phase extraction
EPA	Environmental Protection Agency
EtOH	Ethanol
EU	European Union
FAAS	Flame atomic adsorption spectrometry
FHQ	5-Formyl-8-hydroxyquinoline
FID	Flame Ionization Detector
FSM	Folded sheet material

FT-IR	Fourier transform infrared
g	Earth gravitational acceleration
GC	Gas chromatography
GC/MS	Gas chromatography/Mass spectrometry
$GSi(OMe)_3$	3-Glycidoxypropyltrimethoxysilane
$HOC_{18}@SiO_2$	Dual functionality nanoscavenger
HPLC	High performance liquid chromatography
HQ	8-Hydroxyquinoline
$HQ@SiO_2$	Hydroxyquinoline-nanoscavenger
ICP-AES	Inductively coupled plasma atomic emission spectrometry
IR	Infrared
IUPAC	International Union of Pure and Applied Chemistry
LC	Liquid chromatography
LCT	Liquid crystal templating
LSPSA	Laser scattering particle size analysis
MCM-41	Mobil composition of matter No. 41
MDL	Method detection limit
MeOH	Methanol
MIP	Molecularly imprinted polymer
$MNCS_2@SiO_2$	Mono-dithiocarbamate-nanoscavenger
MPMP	2-[(2-Mercaptophyenylimino)methyl]phenol
MWCNTs	Multi-walled carbon nanotubes
$NCS_2@SiO_2$	Dithiocarbamate-nanoscavenger
$NH_2@SiO_2$	Aminopropyl-nanoscavenger
$NH_2Si(OEt)_3$	3-Aminopropyltriethoxysilane
$NH_2Si(OMe)_3$	3-Aminopropyltrimethoxysilane
NMR	Nuclear magnetic resonance
NSDE	Nanoscavenger dispersion extraction
PAHs	Polynuclear aromatic hydrocarbons
PAN	1-(2-Pyridylazo)-2-naphtol
PDMS	Polydimethylsiloxane
PF	Preconcentration factor
PFPD	Pulsed flame photometric detector

PTFE	Polytetrafluoroethylene
PUHs	Phenylurea herbicides
PVDF	Polyvinylidene fluoride
Ref	Reference
RSD	Relative standard deviation
SD	Standard deviation
SE	Solvent extraction
SEM	Scanning electron microscope
SH@SiO_2	Mercaptobenzamide-nanoscavenger
SLC	Silicatropic liquid crystal
S_N2	Nucleophilic substitution
SPDE	Solid phase dispersion extraction
SPE	Solid phase extraction
SPME	Solid phase microextraction
SWCNTs	Single-walled carbon nanotubes
TBT	Tributyltin
TBTCl	Tributyltin chloride
TEOS	Tetraethoxysilane
TGA	Thermogravimetric analysis
THF	Tetrahydrofuran
TMB	1,3,5-Trimethylbenzene
TMOS	Tetramethoxysilane
WHO	World Health Organization
XRD	X-ray diffraction
Z-6094	N-[3-(trimethoxysilyl)propyl]ethylenediamine

Chapter 1

The measurement of contaminants in water

The presence of inorganic and organic contaminants in water even at low concentration levels is a problem of widespread concern. Regulations are in place in most countries which specify permitted levels of concentration in water. Compliance with their regulations must be monitored through the application of suitable analytical techniques. When concentrations are too low for direct measurement or measurements are impeded by the presence of interfering species, preconcentration is often employed.

1.1 The nature of the problem

Water is vital for the existence of all life forms. For humans, it is used for drinking, agriculture, cooking, washing, transport and almost all sorts of industries. A wide variety of materials have been identified as contaminants in natural water. These include inorganic materials, organic chemicals, radionuclides and pathogens. Some of these materials naturally exist in water while others can come from industrial sources. Whilst at low levels of concentration the vast majority of the toxic contaminants of water are colourless, tasteless and odourless, they nevertheless render it unsuitable for human use. Specific analytical techniques must therefore be employed to detect the presence of each[1].

The difficulty is that on some occasions these materials contaminate the water at concentrations so low that they can not be directly detected by commonly available analytical techniques. The word "trace" applies to this kind of contamination and the term "trace analysis" is widely used to describe the application of analytical chemistry to measure a very small quantity or concentration of analyte[2]. Some analysts, however, prefer to define the term more specifically as applying to analyses where the concentration of the analyte is at such a low level that it causes a problem for those attempting to obtain accurate results[3]. Thus the term trace analysis is, in this case, applied to the measurement of analytes which have a concentration equal to or

less than 1 µg g^{-1} or 1 µg mL^{-1} for liquids. Chemist's definitions of the term continuously change as sample preparation and analytical techniques improve, meaning that what is considered today to be trace analysis, may become easier to determine in the near future with the development of new analytical instruments.

The following two sections provide a more detailed discussion of inorganic and organic contaminants present in water.

1.1.1 Inorganic contaminants

This section explains the nature and sources of inorganic contaminants, as well as the problems they cause. It will be restricted to metal contaminants in water since these are the focus of this study.

Metals such as arsenic, mercury and copper have been introduced to the environment as a result of natural processes, industrialisation and other human activities. During the processing of products containing metals, loss of the metal results in the contamination of air, water and soils. The metals then directly contaminate human drinking water or contaminate food in an indirect manner, as is seen in the first case below.

Mercury is probably the metal contaminant with the worst reputation. In a small village on Minamata Bay in Japan, at least 3000 people suffered from birth defects and nervous system damage after inadvertently eating mercury-tainted shellfish and fish. This occurred because a fertiliser and petrochemical company released around 27 tons of mercury compounds into Minamata Bay during the period between 1932 and 1968, resulting in the shellfish and fish absorbing the methyl mercury that accumulated in the water[4]. Cadmium also poisoned Japanese farmers between 1940 and 1960, after their rice crop was irrigated by the contaminated water. Thousands of men and women in contaminated regions suffered from kidney failure and severe osteoporosis as a result of eating the contaminated rice. Cadmium remains a major source of rice contamination in Asia[5].

A recent example of metal contaminated water occurred in Bangladesh. The concentration of arsenic in drinking water is currently up to 1000 μg L^{-1}, considerably higher than the limit recommended for drinking water by the World Health Organization (WHO) (10 μg L^{-1}) or that set by the Bangladesh authorities (50 μg L^{-1}). Many people were killed as a consequence of consumption of this water[6-8]. Berg *et al.*[9], investigating arsenic in drinking water from Hanoi, Vietnam and surrounding areas, found that the average concentration in ground water used directly as drinking water was 436 μg L^{-1}. They pointed out that such high levels of arsenic can lead to many deaths and diseases.

In addition to affecting humans, metal pollutants can also affect plants and animals. For example, in the 1850s, arsenic caused the death of deer in Germany[10], and thousands of cattle, deer and horses were killed when copper smelting first began in 1900, in the USA[11]. It was reported that metals such as copper, silver and zinc affects phytoplankton in lakes in Canada and marine waters in the USA[12, 13]. Measurement of metal concentration in water, especially when they are under the detection limit of the available instruments, is therefore important.

Preconcentration of metal is widely applied to the metal ions prior to their measurements using any analytical technique. The preconcentration process can be defined as increasing the analytes concentration by transferring them from large volume of solution to small one. This process may also lead to removal of the interfering materials from the matrix[14]. The challenge for analytical chemists is to improve preconcentration techniques to achieve lower detection limits, so that it may become possible to determine metals at very low concentrations. This aspect is highlighted in Section 1.3.

1.1.2 Organic contaminants

Organic materials contaminate drinking water supplies sourced from surface and ground waters. Contamination of surface water can lead to contaminate ground water as it is the main source of ground water recharge. When organic contaminants are introduced to the ground water through the recharge process, they will either

move with the water to reach the aquifer or be adsorbed by the solid surfaces such as soil. Whenever such retained contaminates do not decompose, they will accumulate in the aquifer. This accumulation may have a long term impact, as shown by one study which concluded that more than fifty volatile organic compounds lasted more than 50 years[15].

Agriculture is the main source of contamination of water by organic materials. It is very difficult to prevent, since herbicides, pesticides and fertilizers are used extensively in the field. Animal farms are another source of water contamination, as pharmaceuticals (antibiotics and hormones) are frequently used to prevent and treat microbial infection and as growth promoters. Following medication, the animals excrete between 40 and 90 % of the dosage. This bioactive residue then contaminates water, in some cases with contaminants that are even more harmful than the original compound[16].

Chromatography provides a unique tool to determine complex matrices of water samples which typically contain different types of organic compounds. The low concentrations, complexities and varieties of organic pollutants in water make their recovery and identification challenging. Since ordinary analytical techniques are usually inapplicable due to lacking the required sensitivity to detect extremely low concentration, new specific methods are necessary to detect these substances. Preconcentration of the materials is therefore required. Many analytical methods can be applied to isolate and preconcentrate organic materials which will be discussed in Section 1.3.

1.2 Regulations for permitted levels

International legislation has been required to ensure that water is clean enough for human consumption. Water quality criteria, standards or guidelines have been established above which metals and organic compounds are considered to be hazardous for human health. Drinking water quality guidelines focus on permissible values of [17]:

- Micro-organisms, e.g pathogenic bacteria, viruses, toxic algae.

- Inorganic chemicals, e.g nitrate, heavy metals.
- Organic chemicals, e.g toxic organic compounds, pesticides, disinfection by-products.
- Radioactive materials.

International organizations which produce regular reports specifying permissible levels of contaminants in water, include the WHO[18,19] and the US Environmental Protection Agency (EPA). In addition, most countries publish their own guidelines. Many organizations have set guidelines for organic compounds. For example WHO set a guideline value for atrazine as an organic compound up to 2 μg L^{-1}. This can be determined by GC/MS which has a detection limit of 0.01 μg L^{-1} [20-22].

Rules have been set for the metals based on their level of human toxicity. Table 1.1 shows some guidelines, instrumental detection limits and health risks of some metals which may contaminate aquatic environments.

Table 1.1 Risk-based drinking water criteria recommended by WHO[18, 23] (2004)

Metal	Drinking water criteria (μg L^{-1})	The detection limit	Health risk
As	10	0.1 μg L^{-1} by ICP/MS, 2 μg L^{-1} by hydride generation AAS or FAAS	Skin damage or problems with circulatory system, and may increase risk of getting cancer
Mn	400	0.01 μg L^{-1} by AAS, 0.05 μg L^{-1} by ICP/MS, 0.5 μg L^{-1} by ICP/optical emission spectroscopy, 1 μg L^{-1} by EAAS, 10 μg L^{-1} by FAAS	Particularly harmful for newborns and children
Cd	3	0.01 μg L^{-1} by ICP/MS, 2 μg L^{-1} by FAAS	Damaged kidney, liver, bone and blood
Co	50	7 μg L^{-1} by FAAS	-
Cr	50	0.05-0.2 μg L^{-1} by AAS	Damage to liver, kidney circulatory and nerve tissues; dermatitis
Cu	2000	0.02-0.01 μg L^{-1} by ICP/MS, 0.5 μg L^{-1} by FAAS	Cause stomach and intestinal distress, liver and kidney damage, and anaemia.
Ni	20	0.1 μg L^{-1} by ICP/optical emission spectroscopy, 15 μg L^{-1} by ICP, 20 μg L^{-1} by FAAS	Decreased body weight, heart and liver damage and dermatitis
Pb	10	1 μg L^{-1} by FAAS	Cause cancer, cereb-rovascular and kidney disease in humans.

Maximum permissible concentrations have changed over time as the recognition of the risk posed by the material increased. For example, in 1958 the WHO International Standards for drinking water recommended a maximum concentration of 0.1 mg L^{-1} for lead, and this value was lowered to 0.05 mg L^{-1} in 1963. However, it was raised to 0.1 mg L^{-1} again in 1971 as no evidence of health problems had been observed. In 1984, the acceptable level was reduced to 0.05 mg L^{-1}, when lead was found to be an accumulative poison in children. The guidelines issued in 1993 recommended 0.01 mg L^{-1} as a maximum of concentration of lead in water[18].

It is well documented that in some places metal and organic contamination levels in the environment has declined in recent decades, due to strict regulations. However, the level of contaminants in water must still be monitored frequently to ensure that the water is safe, and the example of lead above illustrates the need to develop new techniques to detect lower and lower concentrations.

Instrumental techniques are required to measure the concentrations of contaminants in water. But sometimes the analytes are present in the water below the detection limit of the instrument. In addition, in some cases the water sample is very complex, containing other components that interfere with the direct measurement by the instrument; even if the analyte concentration is above the detection limit. Preconcentration/extraction techniques can bring the concentration of the analytes to the instrumental detection limit and can isolate the analyte from interfering species.

1.3 Preconcentration approaches

Analytical instruments with sufficient sensitivity and selectivity are not always available to directly determine analytes in water, therefore preconcentration of the water samples prior to the analysis then becomes essential. In some cases preconcentration is also used to eliminate substances that may be present in water sample which can interfere with the determination of the analytes of interest or render them difficult to measure. Many analytical techniques have been developed to preconcentrate and extract the analyte to a level high enough for detection and some examples will be discussed in the following section.

1.3.1 Conventional preconcentration techniques

There are many classical techniques that have been applied to preconcentrate the analytes from aqueous samples which include evaporation, solvent extraction, ion exchange, co-precipitation, precipitation and electrochemical deposition. Solvent extraction and co-precipitation have both been widely applied to preconcentrate the analytes from water. While the former can be used to extract either organic or inorganic material, co-precipitation is generally applied to preconcentrate metal ions.

1.3.1.1 Solvent extraction

Solvent extraction, also known as liquid-liquid extraction, can be used to extract both inorganic and organic contaminants. When two immiscible phases are shaken together, solutes partition between the two phases, the polar solutes prefer to dissolve in more polar solvents, while less polar solutes prefer to partition into less polar solvents.

The key factor affecting the efficiency of this method is to be the choice of solvent. It is crucial that the solute does not react with the solvent as it may lead to the formation of a new species. Furthermore, the solute should be easily recoverable from the solvent

Chloroform, dichloromethane and hexane are the most popular solvents used to extract trace analytes[24]. Sometimes, it is possible to improve the efficiency of solvent extraction by adopting a mixed solvent system. For example, a mixture of ether and alcohol is commonly used in the thiocyanate extraction of some metals. Similarly thorium was extracted from a nitrate solution using a mixture of dibutoxytetraethylene glycol and ether[24].

Jain *et al.*[25] reported the extraction of thorium (IV) from an ethyl acetate solution using octa-functionalized calyx[4]resorcinarene hydroxide acid. A 133-fold preconcentration factor was obtained with this approach. A complete recovery of thorium was obtained when ethyl acetate was used as a solvent but the recovery

dropped to 11, 36 and 85 % when benzene, toluene and chloroform respectively were used instead of the ethyl acetate.

Cadmium has been extracted from river water by solvent extraction (chloroform) of its dithizone complex. A 50-fold preconcentration factor was achieved with this method[26]. Copper, iron (III) and nickel have been extracted from HNO_3 leachate from waste printed circuit board by extracting into a solution of LK-C2 (one of the hydroxyl oxime extractants) in kerosene. The separation and recovery of copper, iron and nickel was based on the pH dependence of their extraction behaviour. The copper was extracted at pH 2.6 with 100 % recovery; the iron and nickel were extracted at pH 3 and 10 with recoveries of 96 and 99 %, respectively[27]. Makrlik *et al.*[28] recently extracted microamounts of strontium and barium into nitrobenzene using hydrogen dicarbollycobaltate in the presence of dicyclohexano-24-crown-8. They found that the stability complex between barium and ligand to be higher than that of the strontium complex.

Solvent extraction has been successfully applied to extract a wide range of organic materials from water. For example, dichloromethane was used to enrich trace amounts of herbicides from water collected from the Elorn River [29]. LC-MS confirmed the presence of triazines such as atrazine, simazine, metolachlor, isoproturon and diuron in the sample[30]. Chou and co-workers developed a dispersive liquid-liquid microextraction technique to selectively preconcentrate phenylurea herbicides (PUHs) from the aqueous samples. Tetrahydrofuran (THF) was used as dispersive while dichloromethane as an extraction solvent. The technique yielded a high preconcentration factor (68-126), good recovery results (91-104 %), short extraction time and low cost when compared to solid phase extraction techniques used to preconcentrate PUH compounds[31].

Recently, conventional solvent extraction has been developed to overcome some of its disadvantages such techniques include liquid-phase microextraction and microfluidic chip based microextraction. Early studies (1996) in this field demonstrated the efficiency of systems based on microextraction with 1.3 µL and 8 µL single droplets of organic solvent[32, 33]. Chen *et al.*[34] developed a microfluidic sub-nanoliter liquid-liquid extraction in which the organic solvent (1-hexane) droplet was

trapped in the channel wall of a microfabricated glass chip. The analytes in aqueous solution passed through the channel and were enriched within organic droplets. A 100 % preconcentration factor was achieved in a 12.5 minute period. Aluminium (III) was extracted using improved microfluidic liquid-liquid extraction system with chemiluminescence detection. A 12 minute period was required to do one analysis and an enrichment factor of 85 was obtained in the extraction, consuming just 1.8 µL of sample[35]. The advantages of these kinds of technique are low consumption of sample and extractant (in the nL-µLs ranges) and high extraction efficiency due to the microscale effect in microchannels. In addition, they provide a short analysis time and occupy only small space. However, the negative aspects are that they are generally expensive, and their design and operation are complicated[36].

To sum up, solvent extraction is simple and convenient, but has many drawbacks that limit its use as a preconcentration technique. These drawbacks include the high cost of some organic solvents, the difficulty of disposing of organic solvents, and the fact that the technique is both labour-intensive and time consuming.

1.3.1.2 Co-precipitation

Co-precipitation is the simultaneous precipitation of a normally soluble component with a macro-component from the same solution by the formation of mixed crystals, by absorption, occlusion or mechanical processes. This method is mainly used to preconcentrate trace elements from matrices that adversely influence atomic absorption spectrometric detection. One of the main requirements for this technique to be effective is that the collector should easily separate from the matrix solution; this can be achieved by filtration or centrifugation and then washing the precipitate with a suitable solvent. Furthermore, the collector should be pure[37]. The main advantages of this technique are that it is a simple, fast approach and several analyte ions can be simultaneously preconcentrated[38].

The collectors most widely used to preconcentrate trace metal ions from different matrices are metal hydroxides such as iron (III), indium, gallium, cerium (IV), lanthanum, and aluminium. For instance, Kagaya *et al.*[39] successfully used yttrium

phosphate to quantitatively coprecipitate lead, iron (III), chromium (III), manganese (II), cobalt, nickel, copper and zinc.

A number of studies have recently reported the use of co-precipitation to preconcentrate trace analytes. For example, dysprosium hydroxide was applied as a co-precipitant to enrich Cr (III) and Cr (VI) from tap water. The recoveries of the chromium species were affected by the pH. The Cr (III) was quantitatively recovered over the pH range 9-12, but the recovery of Cr (VI) was 10 % lower over the pH range 11- 12. The method detection limits were 0.65 µg L^{-1} for Cr (III) and 0.78 µg L^{-1} for Cr (VI)[40]. Co, Pb, Cu, Fe and Zn were preconcentrated using a Ni^{2+}/2-nitroso-1-naphthol-4-sulfonic acid precipitate prior to their determination using FAAS. Nitric acid was used to dissolve the precipitate and the recovery results for the metal ions were above 95 %. Table 1.2 summarizes some of the different materials used as precipitants in co-precipitation techniques as reported in the literature[41]. The pH needs to be adjusted depending on the type of precipitant if good recovery results are to be achieved (Table 1.2).

In conclusion, co-precipitation is a convenient technique for the preconcentration of metal ions from water. However, the many stages employed in the process may cause the loss of analytes and may result in interferences which can occur as a result of the high concentration of contaminating material present in the precipitant. Reagent purity is critical to avoid obtaining high blank values[42].

Table 1.2 Comparison of some trace metal extractions using different batches of coprecipitant (reproduced from reference[41] with permission from the publisher)

Metal ions	Precipitant	Carrier element	pH	PF	DL ($\mu g\ L^{-1}$)	Ref
Pb, Cd, Cr, Ni, Mn	Dibenzyldithio-carbamate	Cu	9	50	0.34-0.87	43
Pb, Fe	Violuric acid	Cu	7	50-100	0.16-0.18	44
Fe, Pb, Co, Cr, Mn, Ni, Cd, Au, Bi, U,	9-Phenyl-3-fluorone	Cu	7	30	6.1	45
Cu, Fe, Pb, Mn, Zn ,Cd, Ni, Bi, Cr	Diethyldithio-carbamate	Co	6	225	4-64	46
Cr	8-Quinolinol /tannic acid	Pb	5	-	0.02	47
Pb, Cr	5-Chloro-2-hydroxyaniline	Cu	8	50	1.2	48
Au, Pd, Pb	5-Methyl-4-(2-thiazolylazo) resorcinol	Ni	4	25	1.5-2.6	49
Cd, Pb, Ni	Diethyldithio-carbamate	Cu	9	22-45	0.23-3.2	50
Co, Pb, Cu Fe, Zn	2-Nitroso-1-naphthol-4-sulfonic acid	Ni	8	25	0.5-2.67	41
Mn (II), Mn (VII)	Zirconium (IV) hydroxide	-	8	50	0.75	51

(PF: preconcentration factor, DL: detection limit, Ref: references)

1.3.2 Solid phase extraction

Solid phase extraction (SPE) is widely used for the isolation and concentration of analytes. The principle of SPE is similar to that of solvent extraction, involving partitioning between two phases, whereas in solvent extraction the partitioning occurs between two immiscible liquids, in SPE it takes place between a liquid (sample matrix) and a solid phase (sorbent). The analytes must have a greater affinity for the solid phase than for the sample matrix. The collected analytes are eluted from the sorbent using either an organic or an inorganic eluent[52] that causes the extracted materials to release from the solid phase. Many different sorbents, for instance poly(styrene divinylbenzene), Schiff bases functionalized Amberlite XAD4[53, 54] ,C_{18}-silica and activated carbon, have been used in solid phase extraction.

SPE can be applied in several different ways. The sorbents can be dispersed in the sample matrix and shaken for a period of time. Later on, it is separated from the bulk matrix by filtration or centrifugation[55, 56]. Alternatively, most commonly in modern SPE, the sorbent is packed into a polyethylene cartridge as a small column or incorporated into a membrane disk.

As with any technique, SPE has advantages and disadvantages. The benefits are that it is fast because the sample can be quickly passed through the SPE column or cartridge under gentle pressure or suction; it requires only a small quantity of organic solvent; and it provides high concentration factors[57]. However, overloading the sorbent, blocking of the pores and the pressure or sucking required can be disadvantages of SPE.

The choice of adsorbent is critical, as this controls selectivity, capacity and affinity for the analytes. Solid phase extractants are frequently classified as polar, nonpolar or ion exchangers, based on chemical characters of the functional groups bonded to the support phases (Table 1.3). These functional groups can be physically loaded or chemically bonded to a solid phase support, the most common of which is silica gel. Silica does not swell or strain in solvent, and it demonstrates good mechanical and thermal stability[58], high capacity and it is easily modified due to the presence of reactive hydroxyl groups.

Table 1.3 Nonpolar, polar and ion exchange phases commonly used in SPE (reproduced from reference[59] with permission from the publisher)

Type of reagent	Name	Structure
Nonpolar	Octadecylsilane	-Si-$(CH_2)_{17}$-CH_3
	Octylsilane	-Si-$(CH_2)_7$-CH_3
	Ethylsilane	-Si-CH_2-CH_3
	Phenylsilane	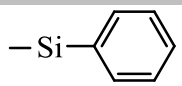
	Cyclohexylsilane	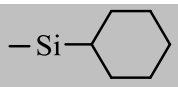
Polar	Silica	-Si-OH
	Cyanopropylsilane	-Si-$CH_2CH_2CH_2CN$
	Diolsilane	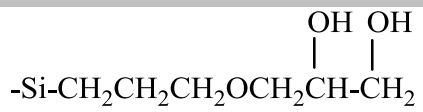
	Aminopropylsilane	-Si-$CH_2CH_2CH_2NH_2$
Ion exchange	Benzenesulfonylpropylsilane	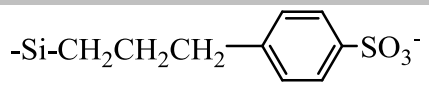
	Sulfonylpropylsilane	-Si-$CH_2CH_2CH_2$-SO^-_3
	Carboxymethylsilane	-Si-CH_2COO^-
	Diethylaminopropylsilane	-Si-$CH_2CH_2CH_2{}^+NH(CH_2CH_3)_2$
	Trimethylaminopropylsilane	-Si-$CH_2CH_2CH_2{}^+N(CH_3)_3$

In recent years, a considerable number of publications have reported the use of modified silica in solid phase techniques. He *et al.*[60] immobilized *p*-toluene-sulfonylamide on a silica surface for use in the extraction of metal ions from water. Trace amounts of Cr (III), Cu (II), Pb (II) and Zn (II) were taken onto the *p*-toluene-sulfonylamide-silica at pH 4 but recoveries were lower below this pH. The preconcentration factor was in the range of 125 to 250 and the detection limit was

between 0.19 and 1.59 ng mL^{-1}, depending on the type of metal ion. A new solid phase extractant was prepared by loading 2,6-pyridine dicarboxylic acid on the surface of nano-sized silica[61], and this was applied to selectively preconcentrate Hg (II) from water using a batch equilibration approach prior to its determination by inductively coupled plasma atomic emission spectrometry (ICP-AES). The pH affected the efficiency of Hg (II) extraction in the presence of other metals. It was found that the maximum uptake capacity of the 2,6-pyridine dicarboxylic acid-silica for Hg (II) was 92 mg g^{-1} at pH 3. 4-Amino-2-mercaptopyrimidine (AMP) chelate was attached onto the surface of silica gel through an organosilane reaction. This sorbent showed a high affinity for the Cu (II) present in fresh water samples but the recovery was affected by some interferences by other ions that were present in the samples[62].

In order to improve the handling of solid phase extraction materials, they have been developed into a number of alternative physical forms such as cartridges; disk and solid phase microextraction.

1.3.2.1 Cartridge formats

A SPE cartridge is generally a commercially produced small column made of polypropylene or polyethylene and packed with 100 mg to 1 g of a functional sorbent. During the process of extraction, the sample passes through the sorbent and the extracted analytes are then eluted using a suitable solvent. The sample flow rate usually is slow and the presence of small particles in the sample can block the channels between the particles, reducing the flow rate and capacity of the cartridge to retain the analytes. This is considered one of the main disadvantages of this technique[63].

Cartridges can be used to extract organic and inorganic contaminants from water samples. For example, Cd (II) was enriched from water samples using cartridge containing 2-(2-quinolinylazo)-4-methyl-1,3-dihydroxydibenzene loaded on a graphitized carbon black sorbent. A preconcentration factor of 500 was obtained and a detection limit was reached of 0.05 µg L^{-1} [64]. In another study, Bahramifar and Yamini applied a cartridge filled with octadecyl-silica loaded with 1-(2-pyridylazo)

2-naphtol (PAN) to preconcentrate some rare earth elements and uranium. A low detection limit up to 11 ng L^{-1}, an enhancement preconcentration factor (382) and high recoveries (between 95 and 106 %) demonstrated the main advantages of this type of extraction technique[65]. In a further experiment, carbon nanotubes were packed into cartridge and applied to extract three herbicide compounds (nicosulfuron, thifensulfuron and metsulfuron-methyl). The extracted compounds were eluted from the sorbent using acetonitrile containing 1 % acetic acid to achieve recovery results in the range of 87 to 111 %. The detection limits for nicosulfuron, thifensulfuron and metsulfuron-methyl were 6.8, 11.2 and 5.9 ng L^{-1}, respectively[66].

1.3.2.2 Disk

In the solid phase extraction disk, sorbent particles (8-12 µm diameters) are immobilised in a web of polytetrafluoroethylene (PTFE) microfibrils, with typical composition of 90 % w/w adsorbent and 10 % PTFE fibers[67, 68]. Such disks are usually employed for large volume, low concentration samples which are difficult to extract using the cartridge technique. Since the disk has a large surface area with a thinner sorbent bed, the sample flow rate is higher than in the cartridge and blockages are minimized. This method has been further developed by incorporating the disks into multiwall extraction plates to extract small volume samples, particularly those of biological origin[69].

As with SPE cartridges, the disks can be used together with metal chelators to extract contaminants metal ions. A number of studies have produced good results using this technique. For example, octadecyl bonded silica disks impregnated with bis(2,2,4-trimethylpentyl)monophosphinic acid (Cyanex 302) could be applied to preconcentrate cobalt (II) from urine samples prior to its determination by FAAS. The Co (II) was absorbed on the disk at pH 6 and eluted using hydrochloric acid (0.003 M). The recovery of Co (II) was 99 % with the Cyanex 302 but only 9.7 % without the complexant. This experiment demonstrated positive features such as good reusability (>35 cycles) and a high preconcentration factor (133)[70]. Similarly, mercury (II) and methyl mercury have been extracted from water samples using octadecyl-silica membrane disks modified with 2-[(2-mercaptophyenylimino)-methyl]phenol (MPMP). The MPMP chelate was capable of separating mercury ions

from solution by complex formation, whereas the unmodified disk did not show any tendency to retain mercury ions. The recovery of mercury was affected by the amount of MPMP loaded to the disk; recovery of only 80 % was obtained when 5 mg of MPMP was loaded, but 7 mg or more was found to achieve approximately 100 % recovery. A preconcentration factor of 500 was achieved with low concentrations of mercury (3.8 ng L^{-1})[71]. This octadecyl-silica disk, modified by MPMP, was also used to preconcentrate silver[72].

C_{18}-silica disks were originally developed for the collection of organic materials from water. Just one of the many direct applications of such disks was their application in the determination of approximately 100 pesticides in drinking water. Following GC-MS analysis of water extractant, at around 0.1 µg L^{-1}, the recoveries ranged from 72-120 %[73]. Recently, Niu *et al.*[74] reported a new kind of solid phase extraction disk based on a sheet of single-walled carbon nanotubes (SWCNTs). These disks permitted fast sample flow rates to be used; with one litre of water sample being passed through the disk within 10-100 minutes with reasonable recoveries. The performance of the SWCNT-disks in the extraction of some organic compounds (phthalate esters) from water samples was compared with commercial C_{18}-disks. The SWCNT-disks have showed extraction ability for all the studied analytes, even though the SWNT-disks contained only 60 mg of adsorbent whilst there was 500 mg of adsorbent packed into the commercial C_{18}-disk. The SWCNTs-disk showed some attractive features such as strong extraction ability of compounds with different polarities and that a large volume of sample could be extracted at a high flow rate. However, the main disadvantage is that the preparation of the sorbent is currently expensive.

1.3.2.3 Solid phase micro-extraction

Solid phase micro-extraction (SPME) employs a fibre coated with an extraction phase such as poly(dimethylsiloxane)/divinylbenzene and Carbowax/divinyl-benzene. For protection, the fibre can be retracted inside the needle of a syringe. Analytes are usually adsorbed onto the fibre by placing it in an agitated sample for between 2 to 15 minutes. The analytes are desorbed from the fibre by introducing the needle into the heated injector of a gas chromatograph[59]. Invented by Pawliszyn

and co-workers[75] in 1989 the technique incorporates sampling, extraction, concentration and sample introduction into a single solvent-free step. It has been successfully applied to extract a wide variety of analytes (volatile or non-volatile) from environmental, food, clinical and pharmaceutical samples. It has been directly coupled to HPLC and HPLC/MS[76].

In order to improve the ability of SPME to extract/preconcentrate a wider range of compounds, alternative approaches have been developed for the production of SPME fibres[29, 77-83]. SPME fibres coated with multi-walled carbon nanotubes (MWCNTs) have, for example, been applied to the preconcentration of polar aromatic compounds from water. The average thickness of MWCNTs/Nafion was found to be 12.5 μm according to scanning electron microscope (SEM) (Figure 1.1). The MWCNT coated Nafion fibre showed a high ability to extract polar compounds in low concentration (0.03-0.57 ng mL^{-1}) compared to commercial fibre[84].

Bagheri *et al.*[85] synthesized a sol-gel based amino functionalized fibre to be used for the SPME of organophosphorus pesticides in water. Chemical bonding of the coating to the surface of the silica led to chemical and thermal stability of the fibre coating. It was found that the fibre could be used more than 120 times for extractions with 250 ºC desorption, without any significant change in its stability. A novel SPME fibre based on a molecularly imprinted polymer (MIP) template with 17 β-estradiol was reported by Hu *et al.*[86]. This MIP-coated fibre was developed for the extraction of estrogenic compounds and give recoveries between 80 and 83 %. The attraction of SPME is that it is a simple, low cost, rapid, complete desorption of analytes and solventless extraction approach that is convenient to use. However, its main disadvantage is the limited number of commercially available stationary phases for extracting different types of analytes.

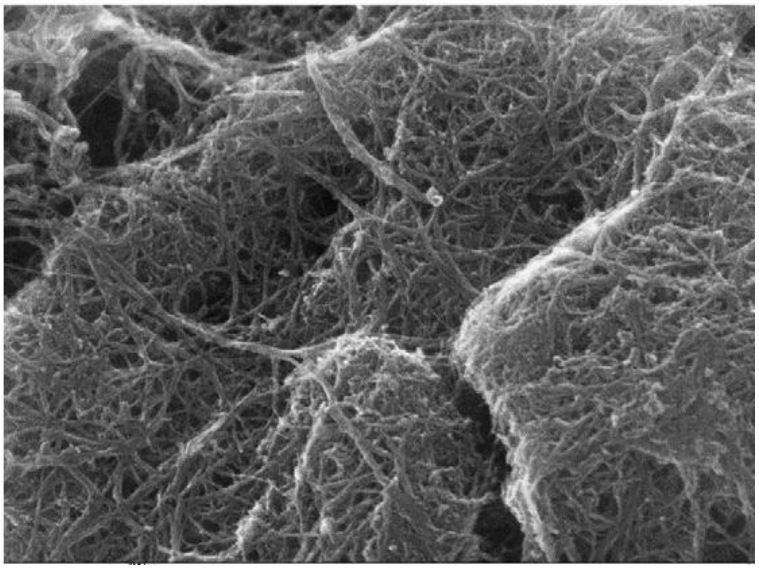

Figure 1.1 SEM image (50,000X) of MWCNT coated Nafion fibre surface (taken from reference[84] with permission from the publisher)

1.3.3 The nanoscavenger dispersion extraction

Solid phase dispersion extraction (SPDE), or dispersive solid phase extraction (DSPE) as it is called in some literatures, was originally introduced by Anastassiades *et al*.[87] as a clean up step. A small amount of solid phase extraction sorbent is initially dispersed into the crude extract to remove co-extracted materials. The clean up process can be easily carried out by shaking and the sorbent can then be removed by centrifugation. Silicas functionalized with primary, secondary amines or C_{18} (octadecyl), graphitized carbon black and carbon nanotubes have been used as sorbents in SPDE[87-90]. Since its original introduction, there have been many reports of SPDE being used in the analysis of samples. Phthalates have been extracted from fruit jellies[91] and soil[92], estrogens from aquatic animals[93], sulfonylurea herbicides from soil[94], pesticides from honey and wine[95]. The technique can however be lengthy, it requires the use of organic solvent and can after only be used to achieve a clean up of the sample extract.

In 2005, a novel SPDE technique was developed by Howard and Khdary[96] that employed carefully size-selected modified Stöber-type silica particles modified with

an extracting agent. Many contaminants, both organic and inorganic, could be directly preconcentrated from an aqueous samples using these designed particles.

In this study functionalized spherical mesoporous silica particles have been developed to preconcentrate metal ions and organic materials from water. Mesoporous silica has been chosen as the core support because it is relatively cheap, stable material with a large surface area that does not significantly swell or shrink in different solvent. Spherical mesoporous silica particles of 250 nm were synthesized and modified for use as analytical tools. These modified mesoporous silica particles are called nanoscavengers. Their size is critical. It falls within the colloidal range and the particles can therefore be dispersed easily in aqueous solution where they move naturally without external agitation. They sediment very slowly and therefore remain dispersed in the sample for sufficiently long for them to achieve complete analyte extraction. They can however be easily recovered by centrifugation or filtration (Figure 1.2). Modified silica particles will be employed to extract analytes from water using a technique will be called nanoscavenger dispersion extraction (NSDE).

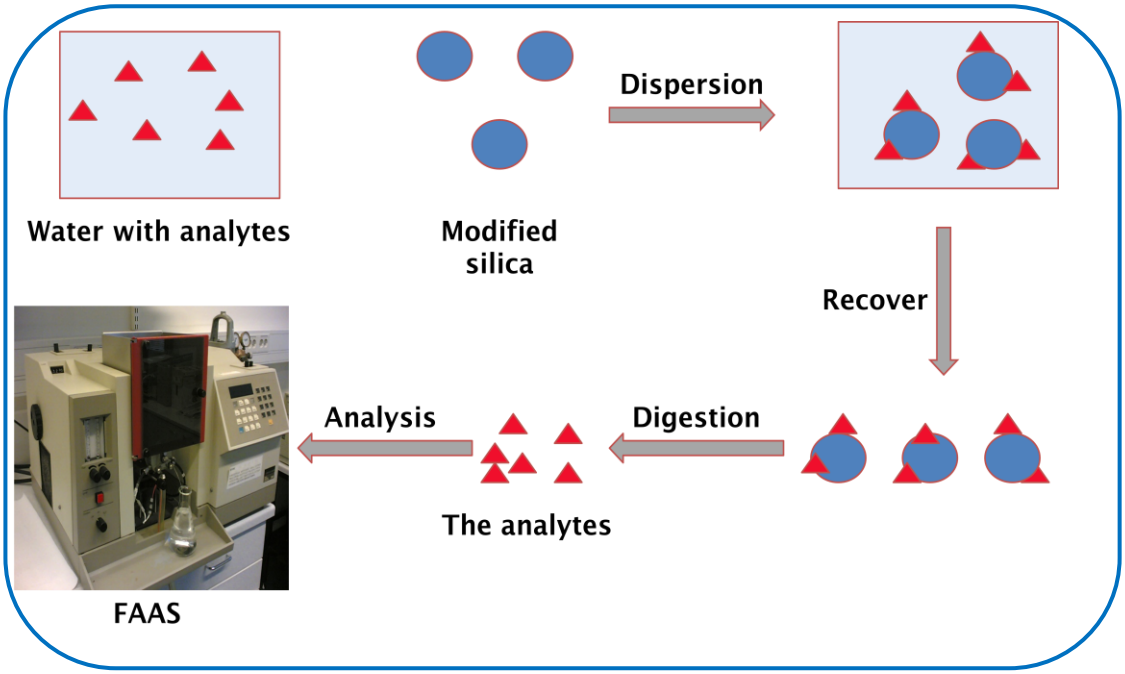

Figure 1.2 Diagram illustrating the process of preconcentrating metal analytes using nanoscavenger dispersion extraction

This method requires no mechanical agitation facilitating its use in the field. This results in the need to transport only small quantities of solid sample, as opposed to carrying litres of liquid. Furthermore, performing this process in the field limits sample contamination, oxidation and loss which might otherwise occur during transportation.

1.4 Conclusion

In conclusion, water contamination is a worldwide problem that becomes more difficult to assess when the contaminants are at levels below the detection limit of available analytical instruments. Even with major technological developments in analytical instruments, contaminants at low concentration level can still not be detected satisfactorily without a preconcentration step. In addition to raising the concentration of the analytes, preconcentration can also overcome interferences between the target analytes and other materials in the sample matrix. Various methods have been used to enrich the analytes to detectable level of concentration, including solvent extraction, co-precipitation and various solid phase extractions. However, some of these techniques have drawbacks such as the use of harmful solvents, the difficulty of dealing with large quantities of sample, slow processes and high cost. Hence, it has been necessary to further develop techniques that give high recovery of the analytes whilst is not damaging to the environment.

Among the numerous preconcentration techniques that are available, a novel nanoscavenger dispersion extraction technique is clearly one of the simplest and most effective procedures. The procedure can be designed to be highly analyte selective, fast and can be carried out in the field, with no mechanical or manual shaking required. In addition only small amounts of organic solvent are used to elute organic analytes and no organic solvent are normally required to elute metal ions from a nanoscavenger.

For these reasons, the nanoscavenger dispersion extraction technique has been selected for further development as a main preconcentrating/extracting of a number of metal ions and organic compounds from water.

1.5 References

(1) Wilson, A. L. *The Chemical Analysis of Water*, 1st ed.; The Society for Analytical Chemistry: London, **1974**.

(2) Tianbin, W.; Yangchuan, K. *Eur. Polym. J.* **2006**, *42*, 274-285.

(3) Prichard, E.; Mackay, G. M.; Points, J. *Trace analysis: a structured approach to obtaining reliable results*, 1st ed.; The Royal Society of Chemistry: Cambridge, **1996**.

(4) Harada, M. *Crit. Rev. Toxicol.* **1995**, *25*, 1-24.

(5) Arao, T.; Kawasaki, A.; Baba, K.; Mori, S.; Matsumoto, S. *Environ. Sci. Technol.* **2009**, *43*, 9361-9367.

(6) Nickson, R.; McArthur, J.; Burgess, W.; Ahmed, K. M.; Ravenscroft, P.; Rahman, M. *Nature* **1998**, *395*, 338-338.

(7) Mukherjee, A. B.; Bhattacharya, P. *Environ. Revs.* **2001**, *9*, 189-220.

(8) Anawar, H. M.; Akai, J.; Mostofa, K. M. G.; Safiullah, S.; Tareq, S. M. *Environ. Int.* **2002**, *27*, 597-604.

(9) Berg, M.; Tran, H. C.; Nguyen, T. C.; Pham, H. V.; Schertenleib, R.; Giger, W. *Environ. Sci. Technol.* **2001**, *35*, 2621-2626.

(10) Newman, J. R.; Schreiber, R. K. *Environ. Toxicol. Chem.* **1988**, *7*, 381-390.

(11) Harkins, W. D.; Swain, R. E. *J. Am. Chem. Soc.* **1908**, *30*, 928-946.

(12) Sunda, W. G.; Tester, P. A.; Huntsman, S. A. *Estuar. Coast. Shelf Sci.* **1990**, *30*, 207-221.

(13) Moffett, J. W.; Brand, L. E.; Croot, P. L.; Barbeau, K. A. *Limnol. Oceanogr.* **1997**, *42*, 789-799.

(14) Mizuike, A. *Fresen. Z. Anal. Chem.* **1986**, *324*, 672-677.

(15) Barber, L. B.; Thurman, E. M.; Schroeder, M. P.; Leblanc, D. R. *Environ. Sci. Technol.* **1988**, *22*, 205-211.

(16) Silvia Diaz-Cruz, M.; Barcelo, D. *Chemosphere* **2008**, *72*, 333-342.

(17) Burden, F. R.; McKelvie, I.; Forstner, U.; Guenther, A. *Environmental Monitoring Handbook*; McGraw Hill: New York, **2001**.

(18) WHO *Guidelines for Drinking Water Quality*, 3rd ed.; WHO, Geneva, **2004**.

(19) Al-Khashman, O. A.; Abu-Hamatteh, Z. S. H.; Eyad, S.; Abbassi, B.; Al-Whoosh, K. S. *Water Int.* **2010**, *35*, 78-93.

(20) Achilli, G.; Cellerino, G. P.; Deril, G. M.; Bird, S. *J. Chromatogr. A* **1995**, *697*, 357-362.

(21) Gawdzik, J.; Gawdzik, B.; Czerwinskabil, U. *Chromatographia* **1988**, *25*, 504-506.

(22) Chriswell, C. D.; Chang, R. C.; Fritz, J. S. *Anal. Chem.* **1975**, *47*, 1325-1329.

(23) Buschmann, J.; Berg, M.; Stengel, C.; Winkel, L.; Sampson, M. L.; Trang, P. T. K.; Viet, P. H. *Environ. Int.* **2008**, *34*, 756-764.

(24) Morrison, G. H.; Freiser, H. *Solvent Extraction in Analytical Chemistry*, 1st ed.; Wiley: New York, **1957**.

(25) Jain, V. K.; Pillai, S. G.; Pandya, R. A.; Agrawal, Y. K.; Shrivastav, P. S. *Anal. Sci.* **2005**, *21*, 129-135.

(26) Shimizu, T.; Hiraoka, Y.; Kikuchi, M.; Uehara, N. *Anal. Sci.* **2005**, *21*, 1-2.

(27) Zhang, X. J.; Li, X. G.; Cao, H. B.; Zhang, Y. *Sep. Purif. Technol.* **2010**, *70*, 306-313.

(28) Makrlik, E.; Vanura, P.; Selucky, P. *J. Radioanal. Nucl. Chem.* **2010**, *283*, 615-619.

(29) Llop, A.; Pocurull, E.; Borrull, F. *J. Chromatogr. A* **2010**, *1217*, 575-581.

(30) Molina, C.; Durand, G.; Barcelo, D. *J. Chromatogr. A* **1995**, *712*, 113-122.

(31) Chou, T. Y.; Lin, S. L.; Fuh, M. R. *Talanta* **2009**, *80*, 493-498.

(32) Liu, H. H.; Dasgupta, P. K. *Anal. Chem.* **1996**, *68*, 1817-1821.

(33) Jeannot, M. A.; Cantwell, F. F. *Anal. Chem.* **1996**, *68*, 2236-2240.

(34) Chen, H.; Fang, Q.; Yin, X. F.; Fang, Z. L. *Lab Chip* **2005**, *5*, 719-725.

(35) Shen, H.; Fang, Q. *Talanta* **2008**, *77*, 269-272.

(36) Sun, M.; Du, W. B.; Fang, Q. *Talanta* **2006**, *70*, 392-396.

(37) Doner, G.; Ege, A. *Anal. Chim. Acta* **2005**, *547*, 14-17.

(38) Soylak, M.; Saracoglu, S.; Divrikli, U.; Elci, L. *Talanta* **2005**, *66*, 1098-1102.

(39) Kagaya, S.; Araki, Y.; Hasegawa, K. *Chem. Lett.* **2000**, 208-209.

(40) Karatepe, A.; Korkmaz, E.; Soylak, M.; Elci, L. *J. Hazard. Mater.* **2010**, *173*, 433-437.

(41) Uluozlu, O. D.; Tuzen, M.; Mendil, D.; Soylak, M. *J. Hazard. Mater.* **2010**, *176*, 1032-1037.

(42) Hill, S. J.; Arowolo, T. A.; Butler, O. T.; Chenery, S. R. N.; Cook, J. M.; Cresser, M. S.; Miles, D. L. *J. Anal. At. Spectrom.* **2002**, *17*, 284-317.

(43) Tuzen, M.; Soylak, M. *J. Hazard. Mater.* **2009**, *162*, 724-729.

(44) Saracoglu, S.; Soylak, M.; Peker, D. S. K.; Elci, L.; Dos Santos, W. N. L.; Lemos, V. A.; Ferreira, S. L. C. *Anal. Chim. Acta* **2006**, *575*, 133-137.

(45) Aydin, F. A.; Soylak, M. *Talanta* **2007**, *73*, 134-141.

(46) Elci, L.; Sahin, U.; Oztas, S. *Talanta* **1997**, *44*, 1017-1023.

(47) Zhang, Q. B.; Minami, H.; Inoue, S.; Atsuya, I. *Anal. Chim. Acta* **1999**, *401*, 277-282.

(48) Tuzen, M.; Citak, D.; Soylak, M. *J. Hazard. Mater.* **2008**, *158*, 137-141.

(49) Soylak, M.; Tuzen, M. *J. Hazard. Mater.* **2008**, *152*, 656-661.

(50) Chen, H. W.; Jin, J. C.; Wang, Y. F. *Anal. Chim. Acta* **1997**, *353*, 181-188.

(51) Citak, D.; Tuzen, M.; Soylak, M. *J. Hazard. Mater.* **2010**, *173*, 773-777.

(52) Imamoglu, M.; Gunes, V. *Instrum. Sci. Technol.* **2008**, *36*, 105-116.

(53) Kara, D.; Fisher, A.; Hill, S. J. *Analyst* **2005**, *130*, 1518-1523.

(54) Kara, D.; Fisher, A.; Hill, S. J. *J. Hazard. Mater.* **2009**, *165*, 1165-1169.

(55) Scheepers, P. T. J.; Velders, D. D.; Straetemans, M. M. E.; Ouwerkerk, J. C.; Vanvliet, L. A.; Bos, R. P. *J. Chromatogr.-Biomed. Appl.* **1993**, *619*, 215-221.

(56) Rosenfeld, J. M.; Moharir, Y.; Hill, R. *Anal. Chem.* **1991**, *63*, 1536-1541.

(57) Fritz, J. S.; Macka, M. *J. Chromatogr. A* **2000**, *902*, 137-166.

(58) Tong, A.; Akama, Y.; Tanaka, S. *Analyst* **1990**, *115*, 947-949.

(59) Berrueta, L. A.; Gallo, B.; Vicente, F. *Chromatographia* **1995**, *40*, 474-483.

(60) He, Q.; Chang, X. J.; Huang, X. P.; Hu, Z. *Microchim. Acta* **2008**, *160*, 147-152.

(61) Zhang, L.; Chang, X. J.; Hu, Z.; Zhang, L. J.; Shi, J. P.; Gao, R. *Microchim. Acta* **2010**, *168*, 79-85.

(62) Pereira, A. S.; Ferreira, G.; Caetano, L.; Martines, M. A. U.; Padilha, P. M.; Santos, A.; Castro, G. R. *J. Hazard. Mater.* **2010**, *175*, 399-403.

(63) Camel, V. *Spectroc. Acta Pt. B-Atom. Spectr.* **2003**, *58*, 1177-1233.

(64) Li, Y. K.; Huang, Y.; Xu, Y. R.; Fan, P.; Hu, Q. F.; Yang, G. Y. *Asian J. Chem.* **2009**, *21*, 5319-5327.

(65) Bahramifar, N.; Yamini, Y. *Anal. Chim. Acta* **2005**, *540*, 325-332.

(66) Zhou, Q. X.; Wang, W. D.; Xiao, J. P. *Anal. Chim. Acta* **2006**, *559*, 200-206.

(67) Hagen, D. F.; Markell, C. G.; Schmitt, G. A.; Blevins, D. D. *Anal. Chim. Acta* **1990**, *236*, 157-164.

(68) Poole, C. F. *Trends. Anal. Chem.* **2003**, *22*, 362-373.

(69) Thurman, E. M.; Snavely, K. *Trac-Trends Anal. Chem.* **2000**, *19*, 18-26.

(70) Karve, M.; Rajgor, R. V. *Anal. Lett.* **2009**, *42*, 2520-2532.

(71) Ashkenani, H.; Dadfarnia, S.; Shabani, A. M. H.; Jaffari, A. A.; Behjat, A. *J. Hazard. Mater.* **2009**, *161*, 276-280.

(72) Shabani, A. M. H.; Dadfarnia, S.; Jafari, A. A.; Shahbasi, Z. *Can. J. Anal. Sci. Spectrosc.* **2006**, *51*, 194-199.

(73) Leandro, C. C.; Bishop, D. A.; Fussell, R. J.; Smith, F. D.; Keely, B. J. *J. Agric. Food Chem.* **2006**, *54*, 645-649.

(74) Niu, H. Y.; Cai, Y. Q.; Shi, Y. L.; Wei, F. S.; Liu, J. M.; Bin Jiang, G. *Anal. Bioanal. Chem.* **2008**, *392*, 927-935.

(75) Arthur, C. L.; Pawliszyn, J. *Anal. Chem.* **1990**, *62*, 2145-2148.

(76) Chong, S. L.; Wang, D. X.; Hayes, J. D.; Wilhite, B. W.; Malik, A. *Anal. Chem.* **1997**, *69*, 3889-3898.

(77) Chun, M. H.; Kim, E. K.; Lee, K. R.; Jung, J. H.; Hong, J. *Microchem. J.* **2010**, *95*, 25-31.

(78) Bahri, M.; Driss, M. R. *Desalination* **2010**, *250*, 414-417.

(79) Lopez-Darias, J.; Pino, V.; Anderson, J. L.; Graham, C. M.; Afonso, A. M. *J. Chromatogr. A* **2010**, *1217*, 1236-1243.

(80) Rastkari, N.; Ahmadkhaniha, R.; Samadi, N.; Shafiee, A.; Yunesian, M. *Anal. Chim. Acta* **2010**, *662*, 90-96.

(81) Qin, Z. P.; Bragg, L.; Ouyang, G. F.; Niri, V. H.; Pawliszyn, J. *J. Chromatogr. A* **2009**, *1216*, 6979-6985.

(82) Zeng, J. B.; Chen, J. M.; Song, X. H.; Wang, Y. R.; Ha, J.; Chen, X.; Wang, X. R. *J. Chromatogr. A* **2010**, *1217*, 1735-1741.

(83) Hii, T. M.; Basheer, C.; Lee, H. K. *J. Chromatogr. A* **2009**, *1216*, 7520-7526.

(84) Chen, W.; Zeng, J.; Chen, J.; Huang, X.; Jiang, Y.; Wang, Y.; Chen, X. *J. Chromatogr. A* **2009**, *1216*, 9143-9148.

(85) Bagheri, H.; Ayazi, Z.; Babanezhad, E. *Microchem. J.* **2010**, *94*, 1-6.

(86) Hu, Y. L.; Wang, Y. Y.; Chen, X. G.; Hu, Y. F.; Li, G. K. *Talanta* **2010**, *80*, 2099-2105.

(87) Anastassiades, M.; Lehotay, S. J.; Stajnbaher, D.; Schenck, F. J. *J. AOAC Int.* **2003**, *86*, 412-431.

(88) Diez, C.; Traag, W. A.; Zommer, P.; Marinero, P.; Atienza, J. *J. Chromatogr. A* **2006**, *1131*, 11-23.

(89) Walorczyk, S. *J. Chromatogr. A* **2008**, *1208*, 202-214.

(90) Valcarcel, M.; Cardenas, S.; Simonet, B. M.; Moliner-Martinez, Y.; Lucena, R. *Trac-Trends Anal. Chem.* **2008**, *27*, 34-43.

(91) Ma, Y. W.; Hashi, Y.; Ji, F.; Lin, J. M. *J. Sep. Sci.* **2010**, *33*, 251-257.

(92) Zhang, Y.; Zhang, X. S.; Yang, P.; Zhang, D. *Chin. J. Anal. Chem.* **2009**, *37*, 1535-1538.

(93) Dong, X. Z.; Zhao, L. X.; Guo, G. S.; Lin, J. M. *Anal. Lett.* **2009**, *42*, 29-44.

(94) Wu, Q. H.; Wang, C.; Liu, Z. M.; Wu, C. X.; Zeng, X.; Wen, J. L.; Wang, Z. *J. Chromatogr. A* **2009**, *1216*, 5504-5510.

(95) Zhang, K.; Wong, J. W.; Hayward, D. G.; Sheladia, P.; Krynitsky, A. J.; Schenck, F. J.; Webster, M. G.; Ammann, J. A.; Ebeler, S. E. *J. Agric. Food Chem.* **2009**, *57*, 4019-4029.

(96) Howard, A. G.; Khdary, N. H. *Analyst* **2005**, *130*, 1432-1438.

Chapter 2
Silica particles: types, characteristics and applications

This chapter reviews the process of preparation of silica materials and highlights some porous materials and their major applications. Particular attention has been paid to mesoporous silica, as it is the main material under development as a nanoscavenger. Its synthesis, control of its pore size and different formation mechanisms are discussed. In addition, different types of silica modification and the physical characteristics of the silica particles are discussed.

2.1 The historical development of silicas

2.1.1 Gel materials

A sol can be defined as a colloidal dispersion of particles in a liquid, and a gel is a substance that consists of a solid skeleton enclosing a continuous liquid phase. The presence of the liquid phase and solid phase together is necessary, as the liquid prevents the solid collapsing and the solid keeps the liquid from escaping. Therefore, the process of sol-gel formation is defined as a growth of colloidal particles, joining together to produce a gel[1]. The precursor of colloidal particles usually contains metal or metalloid elements surrounded by various reactive groups. The starting materials proceed to form colloidal particles (sol) in contact with water or diluted acid. Different types of material can then be produced[2].

2.1.1.1 Sol-gel processing

Sol-gel materials can be prepared using alcohol as a solvent with a suitable silica precursor. The most commonly used alkoxide resources in the sol-gel production of silicas are tetraethoxysilane (TEOS) and tetramethoxysilane (TMOS)[3]. The sol-gel process can be carried out in the following steps: hydrolysis and condensation, gelation and aging and drying, as described below.

I- Hydrolysis

The hydrolysis of a silica precursor (tetraalkoxysilane) takes place either with a base or in an acid-catalyzed process. The hydrolysis reaction mechanism in both cases follows nucleophilic substitution (S_N2), which involves a penta-coordinated intermediate (Figure 2.1)[4]. Catalysis using acid or base is essential, as the water has poor nucleophilic properties and the reaction is sterically hindered , which occurs as a result of forming a penta-coordinated transition state with a silica atom, which has a small size[5].

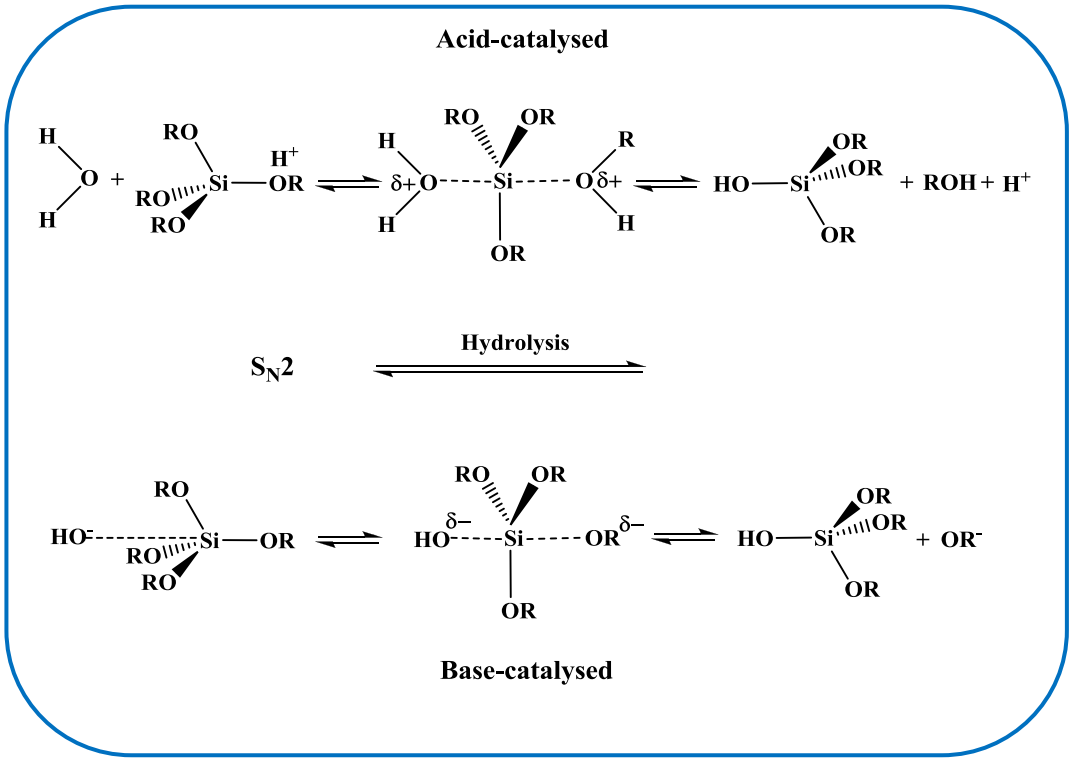

Figure 2.1 Mechanisms of hydrolysis of alkoxysilane

As a result of this process, the replacement of alkoxide groups with hydroxyl groups occurs, as seen in Figure (2.2).

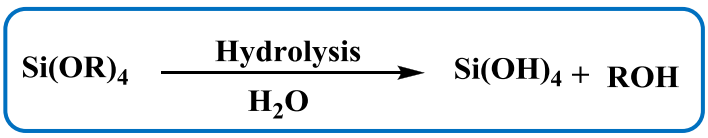

Figure 2.2 The hydrolysis of alkoxysilane

During the hydrolysis process under acid or base catalysis, nucleophilic attack by the oxygen of water on the alkoxide silicon atom leads to nucleophilic substitution by proton transfer and to the elimination of alcohol. In base catalysed hydrolysis a nucleophilic hydroxyl anion is formed, due to the dissociation of water. The hydroxyl anion attacks the silicon atom and replaces the alkoxide groups to form a penta-coordinated intermediate state. That process is followed by the removal of alkoxide. However, in the acid-catalyzed hydrolysis process, the alkoxide is protonated to form an alcohol. The electron density which is withdrawn from the silicon makes it more electrophilic and highly positioned to be attacked by the oxygen of water. A transition state forms as a result of attacking the silicon by water. The positive charge of the protonated alkoxide is then reduced, which makes alcohol a good leaving group. Removal of alcohol occurs by displacement of alkoxide in the tetrahedral transition state[2].

II- Condensation

Condensation occurs simultaneously with the hydrolysis, the reactions producing water or alcohol and involving the formation of siloxane bonds in both processes. Figure 2.3 shows the condensation mechanisms under acid and base catalysis[4]. In all cases, the rapid formation of a charged intermediate takes place from reaction with a proton or hydroxide ion. The process is followed by slow attack of another neutral silicon species on the intermediate.

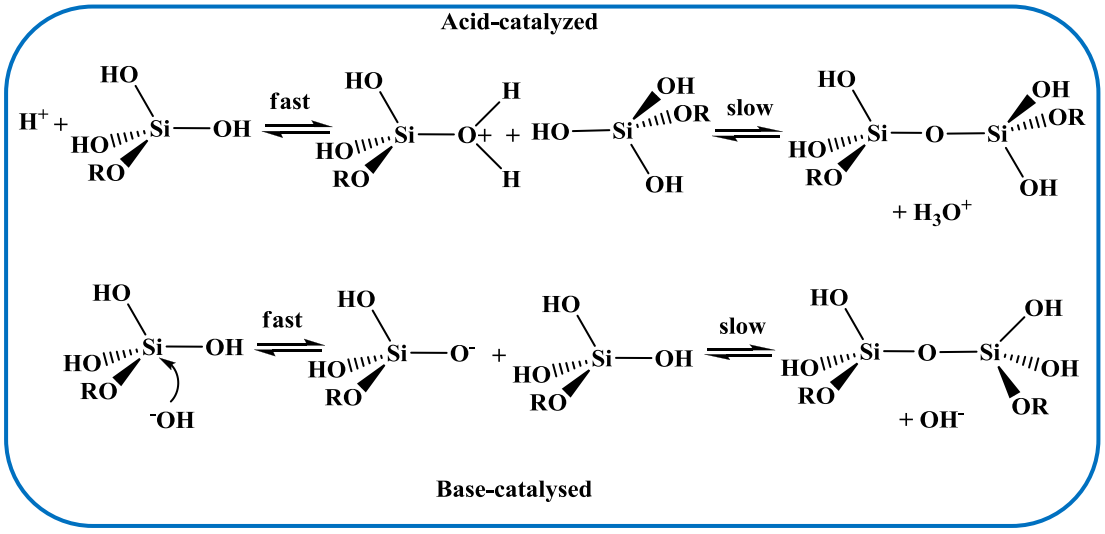

Figure 2.3 The mechanisms of condensation

The condensation process is pH-dependent, as the transition state is protonated under the acidic conditions and deprotonated under the base conditions. The effect of acid catalysis is to promote the growth of a polymeric chain to produce a highly cross-linked system and, under basic condition of catalysis, dense particles are produced. Therefore, the reaction conditions (acid or base) can be adjusted to control the properties of the produced materials (gel or sols)[5]. Iler[2] divided the condensation process into three approximate pH ranges: pH < 2, 2-7 and > 7. At pH less than 2, the hydrolysis reaction rate is fast and complete, without the formation of a gel. Highly cross-linked systems are produced as a result of particle aggregation at pH between 2 and 7. At pH value above 7, the solubility and dissolution rate reach their maximum, leading to particle growth without aggregation, and no gelation occurs at this pH range. Monomers, dimers, linear trimers, cyclic trimers, tetramers, and higher order rings are the products of the condensation process (Figure 2.4).

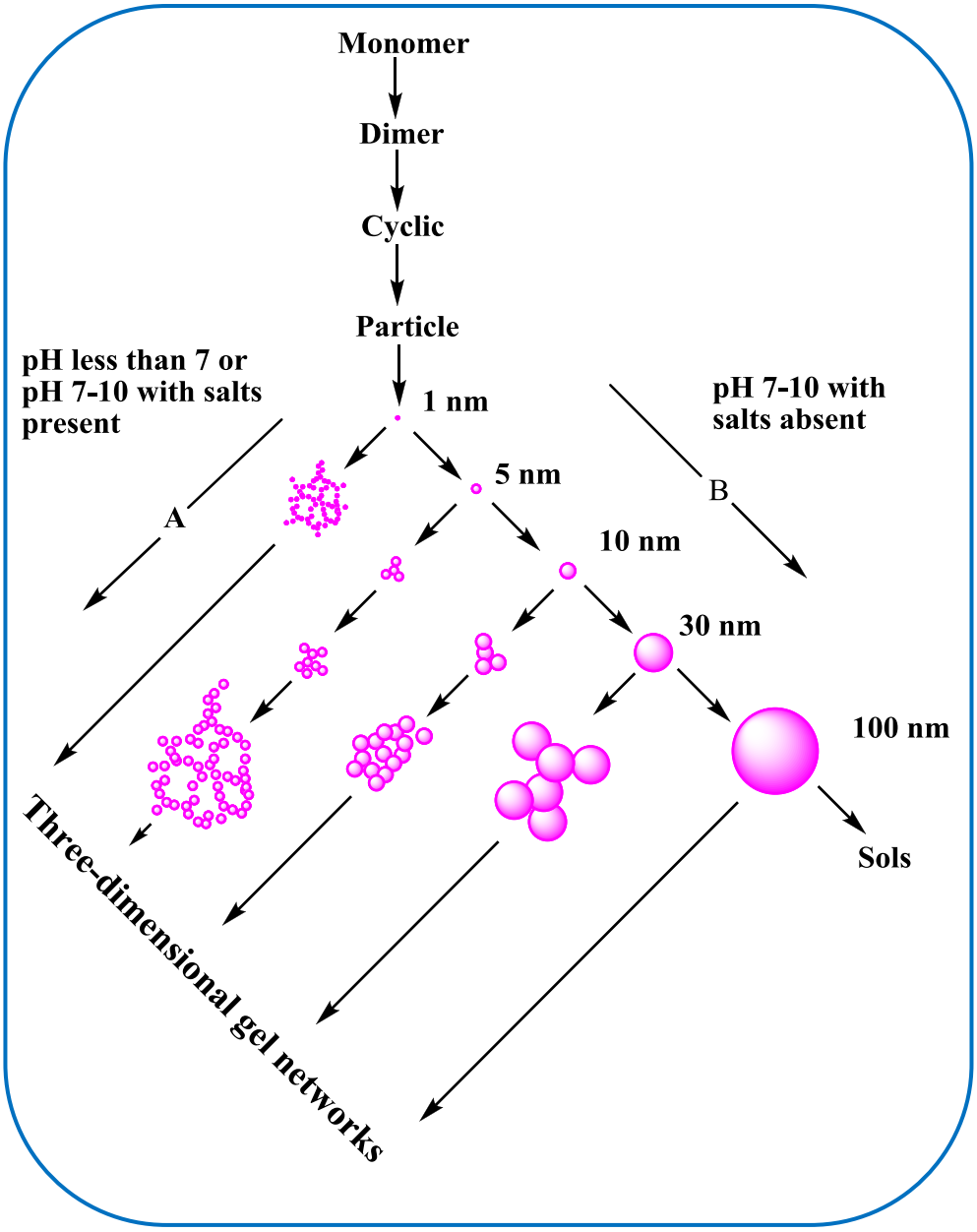

Figure 2.4 The polymerization pathway to form silica. Under acid conditions, the particles aggregate and link together into branched chains and networks of gels, under basic condition, particles grow without aggregation. (from reference[2])

III- Aging and drying

The hydrolysis and condensation steps lead to colloidal particles linked together to form a gel. After the gel network has formed an aging process take place. Shrinkage of the network occurs during aging and this can cause removal of liquid from the pores of the gel. In addition, continuing reactions increase the linkages of the network. The solid phase separating from the liquid is the final step in aging. The structure of the gel matrix becomes more of a solid network as the gel dries and shrinks. At a critical point, the gel structure becomes strong enough to resist shrinkage during liquid evaporation[4].

Different types of materials can be produced by varying the drying process. When the liquid is removed from the gel by evaporation at or near ambient pressure, xerogel is produced. In this case shrinkage leads to a decrease in the surface area. It was reported that the surface area of silica xerogel decreased from 330 m^2 g^{-1} to 63 m^2 g^{-1} when xerogel gel was heated at 250 ºC for 5 hours[6]. When the liquid in the gel is replaced by a gaseous phase an aerogel is produced. It was introduced by Kistler[7], who replaced most of the water with alcohol and then the alcohol was replaced by air. No shrinkage or cracking in the silica aerogel was observed.

2.1.1.2 Major applications of sol-gel materials

The sol-gel process is a useful approach for the preparation of materials with a variety of applications in many different fields. It plays an important role in the preparation of materials used in chemical sensing, catalysis and the extraction of analytes, as discussed below.

Sol-gel glasses are an amorphous form of silica which have been widely used as solid supports for immobilization of chemical and biochemical sensors and biosensors[8-10]. Various pH sensors have been developed using sol-gel technology as the preparation of thin film sensors can be carried out at low temperature. Jurmanovic *et al*.[11] prepared colorimetric pH indicators by immobilization of methyl red and bromocresol in organic-inorganic silica matrices, using a sol-gel method. The developed thin film has high porosity and good mechanical stability, which make

pH-based film sensors fast and sensitive to use in many applications, such as continuous pH monitoring in solutions and gases.

Many catalysis materials have been prepared by encapsulation of catalytic groups into sol-gel materials and immobilization of catalysts on the surface of sol-gel materials. For instance, two kinds of Co^{2+} Schiff base complexes were covalently bonded to a silica matrix using a sol-gel process. These two complexes showed good catalytic activity[12]. In addition, a Co/Fe catalyst was obtained using a sol-gel technique on a silica base support. Good catalytic performance was noted when it was applied as a catalyst for the conversion of trial organic compounds[13].

In the analytical field, sol-gel materials are widely used for the preparation of sorbents for separation and microextraction applications. For example, propylamine anchored silica was obtained by a sol-gel process using TMOS and 3-(diethoxymethylsilyl)propylamine[14]. Many researchers use similar propylamine silicas for further modification with more specific complexing groups. Amine silicas have been used to extract metal ions from water[15]. For example, an amino-silica[16] system was used as a solid phase extraction agent for the collection of copper (II) from water at pH 5.5. Malik and co-workers were the first to apply the sol-gel approach to the coating of SPME fibres. The outer surface of the fibre was coated with a bonded sol-gel layer of poly(dimethylsiloxane). These SPME fibres were used with GC for the preconcentration and determination of organic compounds such as polynuclear aromatic hydrocarbons in the aquatic environment[17]. Vinyl crown ether SPME fibres were also synthesized using sol-gel process. The new SPME fibres showed higher extraction efficiencies for some pesticide compounds than other fibres[18]. The recoveries of pesticides spiked in food samples were determined to be more than 55 %, with a detection limit in the range of 0.003-0.09 ng g^{-1}.

There are some drawbacks to sol-gel materials, such as their physical stability and mechanical strength which may limit their use in some applications.

2.1.2 Porous materials

Porous materials are widely used as adsorbents, as ion exchange media, in separation and as catalysts or catalytic supports, because of their high surface area. The porous structures come from the aggregation or intergrowth of small grains into solid particles, resulting in pores between these grains. In addition, using templating materials during the growth of the particles leads to the generation of pores after the template is removed. Thus, different materials with a variety of pore sizes can be obtained, depending on the method of preparation. According to their average pore size distribution, IUPAC classified them into three different materials[19]:

- Microporous materials which have a pore size not exceeding 2 nm in diameter
- Mesoporous materials with medium size pores around 2-50 nm.
- Macroporous materials having large pores; more than 50 nm.

The determination of the type of material based on its porosity is important from the point of view of the quantity and type of material that can be loaded on their surface.

The standard technique for the measurement of porosity is to use a gas adsorption isotherm, using either nitrogen or argon as the gas adsorbate. The BET method[20] is used to calculate the surface area and pore size distribution. The gas adsorption isotherms have different shapes according to the porosity of the sample (porous or non porous), its pore size and shape. There are six major types of gas adsorption isotherms as classified by the IUPAC (Figure 2.5).

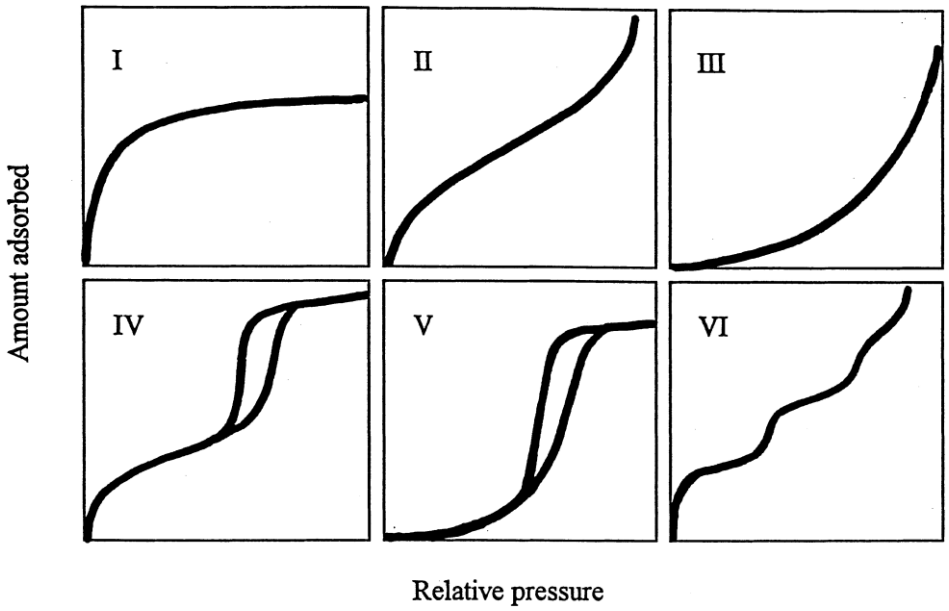

Figure 2.5 Types of adsorption isotherms (taken from reference[19] with permission from the publisher)

The Type I isotherm is concave and represents microporous materials with low external surface area. Examples of adsorbents of Type I are activated carbon and zeolite. Types II and III isotherms derive from non-porous or macroporous adsorbents. The Type III isotherm is convex and not common, only appearing in nitrogen adsorption isotherms of some systems, such as polyethylene. The Type IV isotherm derives from mesoporous adsorbents and is associated with capillary condensation inside mesopores. In its initial part it follows the Type II isotherm path. The Type V isotherm is related to Type III, but the pores are in the *meso* range and it is uncommon. Type VI has more than one step as a result of multilayer adsorption on a uniform non-porous surface. An example of this type is the isotherm obtained from the adsorption of argon or krypton on the surface of graphitised carbon blacks[19, 21]. It is noticeable that Type I, II and III isotherms are reversible systems, as the amounts of adsorbed and desorbed gas are equal. Microporous materials of Type I isotherm can exhibit hysteresis. Types IV and V isotherms, which are related to mesoporous systems, usually show hysteresis between adsorption and desorption. Although the IUPAC isotherm classifications cover a wide range of adsorption systems, there are

still some materials whose adsorption isotherm does not fit in any IUPAC classification.

2.1.2.1 Microporous materials

Microporous materials have an average pore diameter less than 2 nm. They can be divided into microporous (1-2 nm) and submicroporous (pores less than 1 nm). There are many types of silica which have microporous structures; these include fumed silica and Stöber-type silicas.

2.1.2.1a Fumed silica

Fumed silica (pyrogenic silica) is a fine white amorphous powder prepared in a high-temperature vapour process. The source of silica is silicon tetrachloride ($SiCl_4$) which is hydrolyzed in a hydrogen/oxygen flame, as shown in Figure 2.6. The combustion process leads to the production of silicon dioxide molecules which condense to form particles. The prepared silica has a large surface area[22]; the primary particles are non-porous and a microporous structure forms as a result of the linking of primary particles.

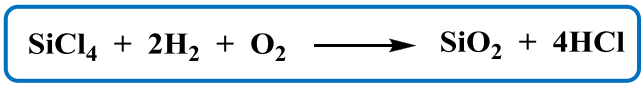

Figure 2.6 The formation of fumed silica

The most important applications of fumed silicas are as thickening agents in ink for printers and paint, thermal insulators and reinforced filler in rubbers[23]. Aerosil, arc and plasma silicas are three different classes of pyrogenic silicas.

I- Aerosil silicas

In 1942 Kloepfiner discovered a method to produce aerosil by flame hydrolysis, which involves burning $SiCl_4$ vapour with oxygen and hydrogen[24]. Particles with a unimodal size distribution are obtained (with diameters of 10-20 nm) as a result of the homogenous formation conditions[25]. Particles of aerosil are coagulated outside

the combustion area to form particles of 1-2 µm diameters. The surface area can be adjusted over the range 50-400 m^2 g^{-1} by manipulating the reaction conditions, such as the concentration of $SiCl_4$, the flame temperature and the residence time of the materials in the flame. The individual primary spheres of aerosil are not porous[26], the pores are generated between the arranged small aerosil particles. The diameter of the pores varies between 0.34 to 0.9 nm, based on a close-packing arrangement[24].

II- Arc silicas

Arc silicas are prepared commercially by reduction of high purity sand (quartz) to silicon monoxide at high temperature. The silicon monoxide is then oxidized to silicon dioxide in an air atmosphere[23]. The size of the particles varies and the surface area is around 170 m^2 g^{-1}.

III- Plasma silicas

Ultra-fine silica particles can be prepared by conversion of quartz to a plasma state at high temperature in an inert gas or nitrogen. It involves transferring an arc consisting of decomposed quartz ($SiO_{(g)} + O_2$), followed by an oxidizing quench back to SiO_2. No by-product like HCl is obtained if silica is produced by plasma technology. This is because cheap and easily available material (quartz) is used instead of $SiCl_4$. Pristavita *et al.*[23] studied the surface area of different batches of plasma silica. The measured surface areas ranged from 105 to 263 m^2 g^{-1}. They found that the specific surface area increased as a result of the formation of smaller particles at a higher quenching rate[23].

2.1.2.1b Stöber-type silica

Stöber *et al.*[27] synthesized spherical silica particles by hydrolysis of TEOS in a medium containing alcohol and ammonia. This type of silica is non-porous. However, micropores can be obtained by combustion of the silica or by using a template. Several attempts have been made to obtain spherical silica particles of different porosities. Most of these efforts were based on modifications of the Stöber method, by adding templating materials such as an alkylamine. The pore diameter of

the particles can be controlled by varying the length of the alkyl-chain of the surfactant. The shorter the alkyl-chain, the smaller the pore diameters. Two examples of attempts to prepare microporous spherical silica using modified Stöber methods are discussed below.

Yano and Fukushima synthesized spherical silica particles using TMOS with a decyltrimethylammonium bromide (C_{10}TMABr) template in a mixture of methanol and water. The particle diameters changed with varying the synthesis temperature, water: methanol ratio and silica precursor. However, the particle sizes remained unchanged when C_{10}TMABr and TMOS concentrations were varied. The surface area was between 700-1000 m^2 g^{-1}, with an average pore diameter in the microporous range (1.7-2 nm)[28].

Spherical microporous silica powders were synthesized using a TEOS silica precursor in a medium containing ethanol and ammonia. Microporosity in these particles was obtained by introducing either glycerol or 3-aminopropyl-triethoxysilane ($NH_2Si(OEt)_3$) during the formation of the particles. The micropores can be then generated by calcination of the organic materials. The surface area of the particles was 36.5 m^2 g^{-1}, with no organic materials added and the surface area increased with increasing the amount of added materials. The surface area reached 86 m^2 g^{-1} with 50/50 % $NH_2Si(OEt)_3$/TEOS. Increasing the added material to TEOS led to an increase in particle size and particles of irregular shape were obtained when the amount of added materials was more than 50 %[29].

2.1.3 Mesoporous silica

The mesoporous silicas have an average pore diameter of between 2-50 nm and usually show the Type IV adsorption isotherm of the IUPAC classification. Ordered mesoporous silicas were first discovered by Kresge and co-workers at the Mobil Oil Corporation in 1992[30]. The general procedure that the Mobil group applied was to produce mesoporous silica using surfactant supramolecular assemblies as a template. Silicas with a mesoporous structure were obtained after the template had been removed. The pore diameters fall in the range between 2 and 10 nm, with hexagonal

and cubic arrays. Since this breakthrough, a lot of research has been carried out to obtain mesoporous silicas of different pore sizes, by manipulating factors such as silica precursor, type of template and reaction solvents. So far, the Kresge *et al.* article has been cited over 8277 times in 18 years.

2.1.3.1 Method of preparations

The preparations of mesoporous silica involve three general steps: synthesis, drying and template removal. Synthesis of silica is the most important step among the three, as the silica characteristics are based on it. Thus, choosing the type of reagent and the reaction conditions is crucial to control the size and pore diameters of the particles. Once the materials are formed, they are isolated and rinsed with water to remove the residue of reagents and solvents. A drying process then takes place at temperatures between 25 and 45 ºC, which has little effect on porosity. The final step to obtain the mesoporous silica is the removal of the template. The method and conditions to remove the template affect the pore size and surface area of the silica[31].

2.1.3.1a Synthesis of mesoporous silica

Five reagents are normally required to synthesize mesoporous silica: a silica precursor, a surfactant, water, alcohol and a catalyst. All the materials except the silica precursor are mixed together to form micelles. To the micellar solution, a silica precursor which is usually TMOS or TEOS is added to form the phase. Three types of pure silica mesophase structure can be formed: hexagonal which is a 1-d system of hexagonally arrayed cylindrical pores (2.7a), cubic which consists of a bicontinuous system of pores (2.7b), and lamellar (2.7c), which is a 2-d system of metal oxide sheets interleaved by surfactant bilayers [31, 32] (Figure 2.7). When the template is removed, the structure will collapse to generate pores.

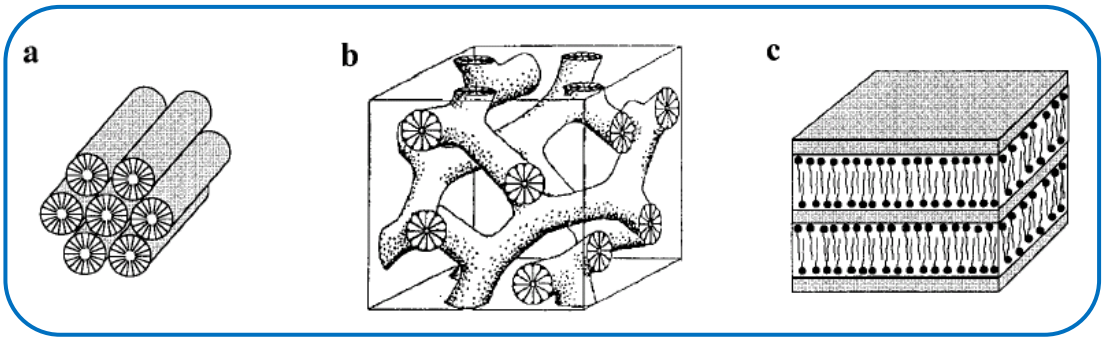

Figure 2.7 The silica-surfactant mesophase structures: a) hexagonal, b) cubic bicontinuous, c) lamellar (taken from reference[31] with permission from the publisher)

2.1.3.1a1 Control of pore diameter

The mesoporous silica materials exhibit specific surface areas varying from 400 m^2 g^{-1} to greater than 1000 m^2 g^{-1} with pore volumes of more than 0.5 cm^3 g^{-1}. The pore diameters can vary from 2 to 50 nm, depending mostly on the surfactant templates used. Surfactants are defined as bifunctional molecules that contain two ends, a head group, which is solvent-loving (lyophilic) and a tail which is solvent-hating (lyophobic). They are considered as amphiphiles[33]. There are three types of surfactants: charged, neutral and non-ionic surfactants. The charged surfactant can be either cationic or anionic, depending on the type of charge on the hydrophilic group. Examples of cationic surfactants include alkylammonium salts such as hexadecyl-trimethylammonium bromide (C_{16}TMABr). Alkylcarboxylic acids such as $C_{17}H_{35}COOH$ are examples of anionic surfactants[34]. In neutral surfactants such as primary amines[35] the hydrophilic group is not charged. The non-ionic surfactants, such as polyethylene oxide[36], are normally polymers. The type of surfactant affects the pore size. For example, a large pore size (> 20 nm) can be obtained using polymeric surfactants. Yu *et al.*[37] synthesized mesoporous silica with an average pore diameter of 23 nm and a surface area of 610 m^2 g^{-1}, using polymer as a surfactant. A pore size of less than 20 nm can be obtained using ionic and neutral surfactants. For example, silica particles of mesoporous type with particle diameters of 300-500 nm and pore sizes of 3 and 12 nm were synthesized using the ionic surfactant *N*-lauroylsarcosine sodium[38]. The surface area of the particles was 536 m^2 g^{-1} and the

pore volume was 0.83 cm^3 g^{-1}. The pore diameter can be manipulated by changing the length of the hydrophobic chain.

The simplest way to tune the pore size is by altering the surfactant tail length. Cationic surfactants, suitable for use as templates, are available with the general formula:

$C_nH_{2n+1}(CH_3)_3NX$ where n = 8, 10, 12, 14, 16, 18 and X= Br, Cl, OH

It has been found that the pore diameter of as-synthesized materials increases by about 2.25 Å with each carbon atom added to the hydrocarbon chain in the surfactant. The smallest pore size that can be obtained is around 15 Å, using the shortest surfactant chain with 8 carbon atoms. The maximum pore size can be achieved by using surfactants, with a hydrocarbon chain length of 18, is around 45 Å[31, 32, 39]. Increasing the number of carbons in the surfactant chain to more than 18 may cause problems such as low solubility and high melting point of the surfactants. These theoretical calculations of the pore diameter alter in practice as the surfactant's form changes according to the nature of the medium used, as discussed later.

There are many reports about controlling the pore size by adjusting the surfactant's tail length. Hamoudi *et al.*[40] synthesized mesoporous silica with pore diameters ranging from 2.9 to 4.4 nm using alkyltrimethylammonium chloride with different hydrocarbon chain lengths (n = 8, 12, 14, 16, 18). They found that the pore diameters of prepared mesoporous silicas increased in parallel with the surfactant carbon chain length. Alkylammonium surfactants of various alkyl chain lengths (n = 12, 14, 16, 18) were used by Xia and Mokaya to prepare mesoporous silicas with pore sizes tunable from 2.3 to 4.1 nm. It was found that variations in surfactant chain lengths not only changed the pore size but also changed the morphology of the particles. Irregular particles were formed when the surfactant's chain length had more than 12 carbon atoms[41].

The pore size of mesoporous silicas can depend not only on the type and surfactant alkyl chain length; there are many minor factors that affect the pore diameters. These factors include the concentration of the silica precursor, addition of a swelling agent

and a condensation catalyst (NaF) and the reaction temperature. Generally, increasing or adding these factor increase the pore diameter[42, 43]. Boissiere *et al*.[44] studied the influence of the factors on the pore size of mesoporous silica. They found that adding swelling agent such as 1,3,5-trimethyl benzene (TMB) led to an expansion of the pore diameter. The pore diameter increased by 1 nm when the reaction temperature was varied between 35 and 75 ºC, as well as when the NaF/Si molar ratio was changed from 1 to 6 %. A small increase was observed when changing the Si/surfactant ratio[44].

2.1.3.1a2 Formation mechanisms

Several models have been proposed to describe the formation of mesoporous materials. Understanding the synthesis procedure and interaction of the materials during the reaction is important for designing the final product. Most proposed mechanisms consider the template molecules to play key roles in controlling mesostructure formation[45]. Some other factors can be considered such as condensation degree and the structure of the silica precursor. Although these mechanisms offer some explanations of the manner of formation of mesostructures, the templating mechanism is still not completely understood. The mesostructure formation reaction involves numerous and complex species and equilibria, diffusion, nucleation, and a growth process which is affected by concentration, pH, temperature and reaction time. Some of the proposed mechanisms in the literature will be discussed in the following sections.

I. Liquid Crystal Templating (LCT) mechanism

The LCT mechanism was proposed when Mobil scientists noted that the resulting silica/surfactant mesophases strongly resembled the mesophases seen in simple surfactant-water systems[30, 32]. Two pathways were suggested (Figure 2.8).

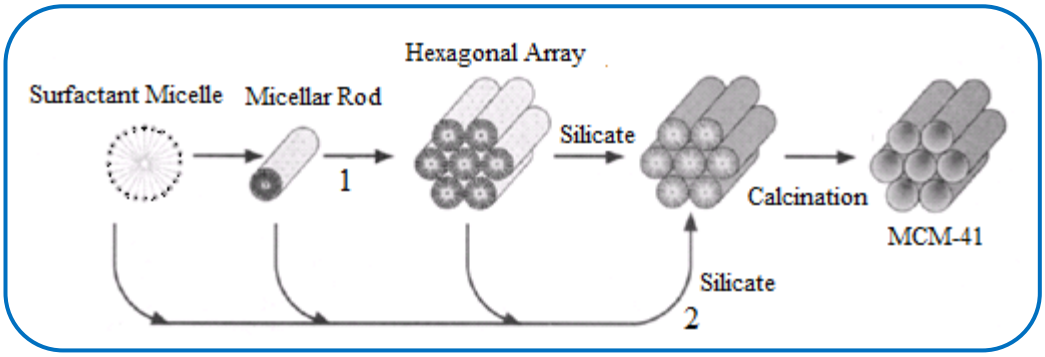

Figure 2.8 The liquid-crystal templating mechanisms scheme. Path 1 is liquid initiated and path 2 is silica anion initiated (taken from reference[31] with permission from the publisher)

In the first path, the surfactant liquid crystal is already present in the solution prior to the addition of the silica precursor and it acts as a template. The inorganic (silicate) species are located at the external surface of micelles and then condense to form the inorganic network. The second pathway postulates that interactions between the silicate species and the surfactant influences the ordering of surfactant micelles to the desired liquid crystal phase. In both pathways, there is a strong electrostatic interaction between the surfactant and the silica species, and through the condensation of silica species around the surfactant arrays, an ordered inorganic structure is ultimately produced.

II. The cooperative Self-Assembly pathway

Monnier *et al.*[46] postulated this mechanism based on their observation of the formation of a lamellar phase prior to the hexagonal MCM-41(Mobil Composition of Matter No. 41) phase. Three processes in the formation of mesostructures have been suggested. In the first step, the oligomeric silicate polyanions act as multidentate ligands for the cationic head groups of the surfactant. This leads to a strong interaction at the surfactant-silicate interface with a lamellar phase. Secondly, as the negative charge of the silica species is balanced by the surfactant, there is a possibility that the silicate concentration is high at the surfactant-silicate interface; therefore polymerization of the silicate species is preferred. Once the condensation of silica starts, the negative charge density is reduced. This new situation leads to a

charge rearrangement that induces the phase transition from lamellar to hexagonal (Figure 2.9)[45, 46].

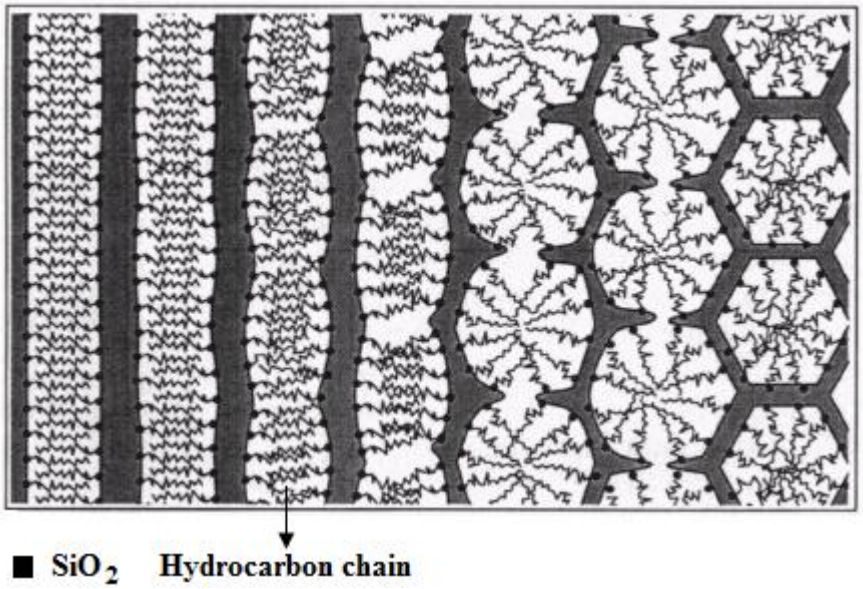

Figure 2.9 The transformation mechanism of a surfactant-silicate system from a lamellar (left side) to a hexagonal (right side) mesophase (taken from reference[46] with permission from the publisher)

An experimental observation supported this lamellar to hexagonal transition, in which kanemite, a single layered hydrated sodium silicate is used as the inorganic source for the preparation of a mesostructured phase[47, 48]. This phenomenon was also observed in materials called folded sheet materials (FSM), which were prepared by intercalation of an alkyltrimethylammonium surfactant into kanemite. After ionic exchange of sodium for alkyltrimethylammonium ions, the surfactant was folded by silica layers, leading to a hexagonal structure. However, the postulated synthesis mechanism is still debated, for instance by Linden *et al.*[49]. They used in-situ X-ray diffraction (XRD) to study the formation of MCM-41 in a tubular reactor. It was found that the hexagonal silica-surfactant mesostructure was directly formed by precipitation in alkaline media.

Firouzi *et al.*[50] revealed the formation mechanism for MCM-41. The formation of silicate-surfactant mesophases was investigated at high pH and low temperature; thus the silica condensation was hindered, in order to separate the effects of self-assembly

from the kinetics of silica polymerization. It was demonstrated that in a micellar solution of C_{16}TMABr the counterions were ion exchanged for silicate oligomers, forming aggregations of inorganic-organic silica whose structure can be different from that of micelles (Figure 2.10). The multidentate interaction of the silicate oligomers with surfactant prevents the electrostatic repulsion between the head groups of the surfactant. This process induces self-assembly of the silicatropic liquid crystal (SLC). This behaviour is analogous to the effect of electrolytes on micellar systems. Heating of the synthesis mixture results in condensation, leading to MCM-41[45, 50].

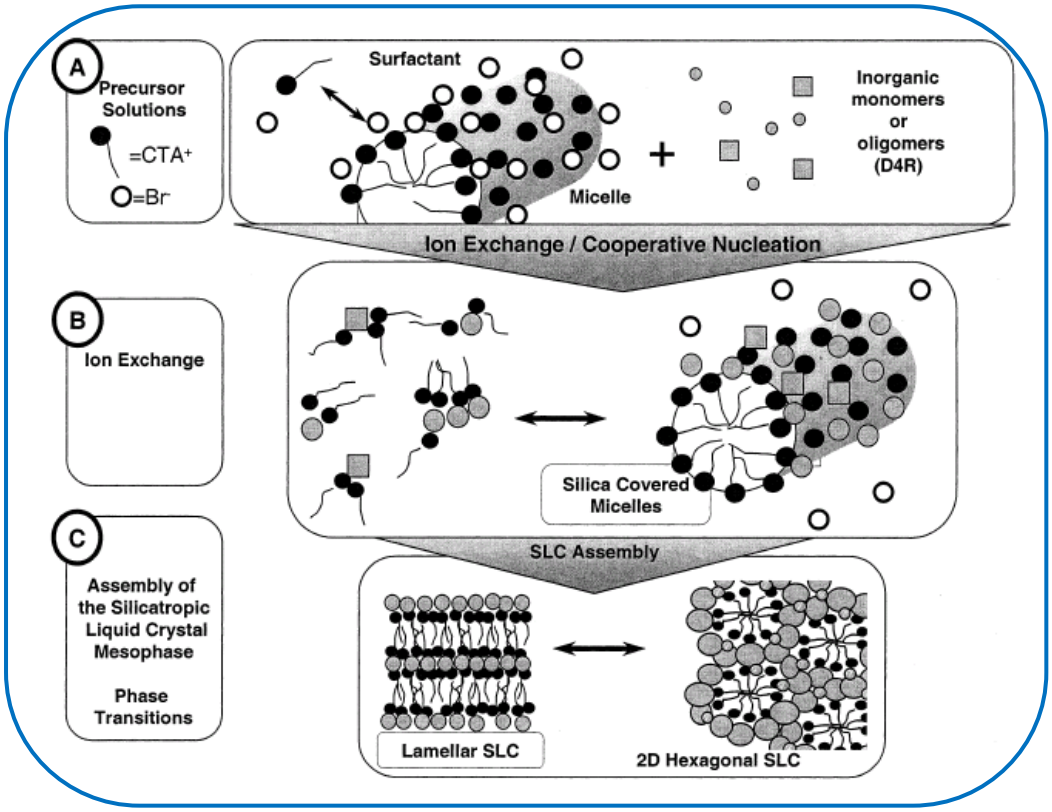

Figure 2.10 Schematic pathways for the cooperative organization of silicate-surfactant mesophases (taken from reference[45] with permission from the publisher)

2.1.3.2 Template removal

There are generally two methods for removal of the template: solvent extraction and calcination[51, 52]. In solvent template extraction, acidic ethanol is widely used. Hue *et al.*[53] used solvent extraction to remove the template from the silica structure and by Fourier transform infrared (FT-IR) spectroscopy confirmed a complete extraction

into ethanol/HCl solution. Weak bonding between the template ions and the inorganic species is believed to help achieving a complete extraction of the template. The average pore diameter of the mesoporous silica was 2.4 nm, (from the N_2 adsorption isotherm). Solvent extraction with ethanolic HCl has also been used to remove the template from MCM-48 mesoporous silica. Around 90 % of the template was removed at room temperature over 24 hours. XRD study of the prepared materials revealed that the extraction process did not destroy the mesostructure of the MCM-48 material[54].

The advantage of removal of the surfactant using solvent extraction is that the mesophase structure does not shrink. Therefore the pore size does not change, and the mesostructure could be easily maintained after extraction. In addition, it is possible to recycle the template, and the concentration of silanol groups on the pore walls and on the surface does not change. However, incomplete removal of surfactant and time consumption are the main disadvantages of solvent extraction.

Calcination is the most common method used to remove templates from mesostructured silicas. The calcination process is normally carried out by heating as-synthesized materials to a high temperature in oxygen, nitrogen or air, to burn off the organic materials from the structure. Removal of the template by calcination can lead to a decrease in pore size and surface area, and could lead to the collapse of the mesoporous channel[55, 56]. MCM-41 samples were originally calcinated at 540 ºC in N_2 for one hour and then in O_2 for six hours by Mobil scientists[32]. Chen *et al.*[57] investigated the effect of calcination on the mesostructure of MCM-41 samples under heating to 540 ºC over a period of 10 hours. They observed variation of up to 25 % of pore sizes according to synthetic conditions. Heating the mesoporous silicas (MCM-41) at more than 900 ºC caused collapse of the framework of the silicas, as observed by Chen *et al.*[57]. Therefore, it is advisable when removing the surfactant by thermal treatment to keep the calcination temperature lower than 650 ºC, to avoid the collapse of the mesostructure of the materials and condensation of the silanol groups.

2.1.3.3 Surface functionality of mesoporous silicas

Many silica properties are based on the chemistry and geometry of their surfaces, and these properties determine the practical applications of silicas. Therefore, the chemistry of the silica surface is an interesting field of study. The surface of silica was studied using transmission infrared spectroscopy by Hair[58]. In addition, continuous studies were carried out in the field, using different techniques and methods, such as diffuse reflectance infrared Fourier transform (DRIFT) spectroscopy, ^{29}Si nuclear magnetic resonance (NMR)[59] and BET method[20], to identify the functional groups on the surface.

Many groups have been identified on the surface of silicas. These groups involve Si-O bonds either as silanols or siloxanes. The silanol groups are formed on the silica surface during the process of the condensation of $Si(OH)_4$ to synthesize silica, and they can also be obtained by aqueous treatment of thermally dehydroxylated silicas. The silanol groups can be classified according to their nature and type of association to the following types[60]:

a) An isolated group, also known as a single or free silanol, consists of a hydroxyl group placed at a sufficient distance from a neighboring hydroxyl group to prevent hydrogen bonding (Figure 2.11). In the IR spectrum, the isolated silanol group shows a sharp band at around 3750 cm^{-1}.

b) Geminal (silanediol) groups have two hydroxyl groups on the same silicon atom. Hensley postulated the existence of this group and they were experimentally confirmed by ^{29}Si NMR spectroscopy[61].

c) Silanetriol groups consist of three hydroxyl groups bonded to one silicon atom. The existence of these groups on the surface of silica was proven by solid-state NMR[62, 63].

d) Vicinal or hydrogen-bonded silanol groups are hydroxyl groups located on silicon atoms and close enough to make hydrogen bonding (Figure 2.11).

The silanol groups are not only present on the surface of silica but also inside the pores and within the structure.

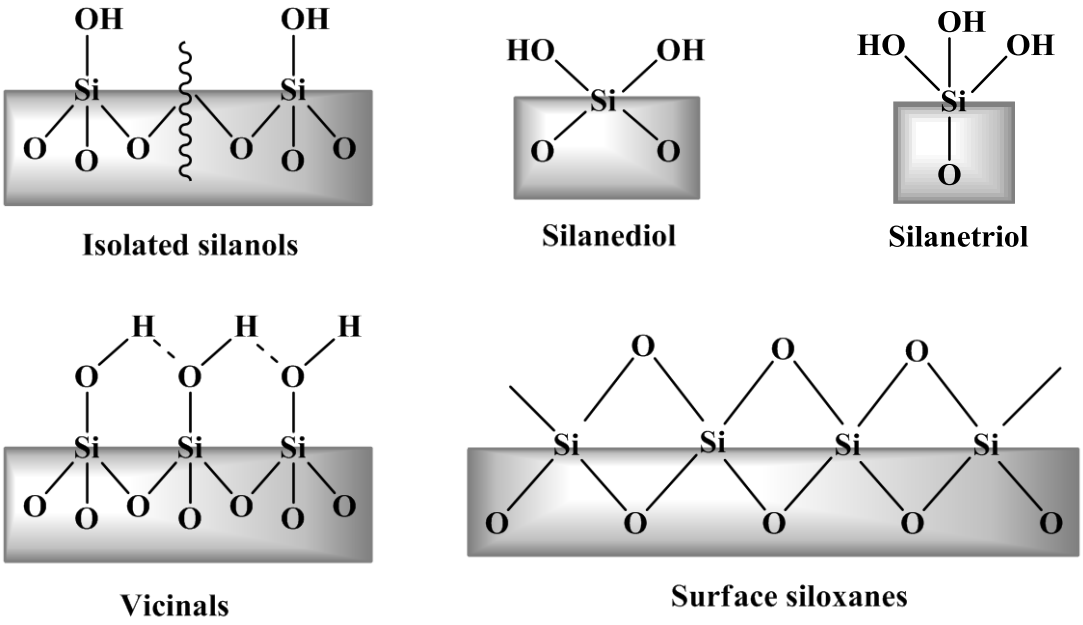

Figure 2.11 Different types of silanol groups and siloxane bridges on the surface of silica

The external and internal silanol groups of silica may thermally dehydroxylate to form strained siloxane bridges (Figure 2.11). At high temperature (> 500 ºC), the strained siloxane groups are converted to form stable siloxane groups. The type of silanol affects the process of dehydroxylation to produce siloxane. It was found that vicinal silanol groups are easy to dehydroxylate because of the existence of neighboring silanol groups. These vicinal silanol groups can be condensed at temperatures between 150-600 ºC. However, the isolated silanol may be thermally removed in the range of temperature between 600-900 ºC[64]. The stable siloxane bridge can be rehydroxylated, but at a slow rate. For example, silica with a surface area of 340 m^2 g^{-1} was completely dehydroxylated at 900 ºC. It has been found that this dehydroxylated silica needed five years of contact with water at room temperature to be rehydroxylated completely[65]. The rate of dehydroxylation of the silica surface can be encouraged by catalyzing the aqueous solution with acid or base.

2.1.3.4 Major applications of mesoporous silicas

The unique properties of mesoporous silicas make them attractive materials to use in the areas of separation, catalysis, nanotechnology etc. The applications of mesoporous silicas in the fields of catalysis and environment remediation will be discussed in the following sections as they may be considered to be the most important applications of mesoporous silicas reported in the literature.

2.1.3.4a Catalysis

Mesoporous silicas have been functionalized as catalysts for oxidation and as acid and base catalysts. Titanium dioxide has been immobilized into mesoporous silicas for use as an oxidation catalyst for organic materials in the presence of H_2O_2. It has been found that the activity of the Ti is affected by the nature of the silica matrix. A possible explanation is that it is related to the hydrophobicity of the surface of the silica. The more hydrophobic the surface, the higher the reaction rate, as the concentration of organic materials increases at the hydrophobic surface, which contains a Ti active site. Many researchers have enhanced Ti-mesoporous silicas, making the surface more hydrophobic by post synthesis silylation by alkylsilane[66] or chloroalkylsilane[67]. The enhanced Ti-mesoporous silica was used as catalyst for oxidation of several substrates, such as alkenes[68], ketones[69], aromatic or aliphatic hydrocarbons and fatty esters[70], in the presence of H_2O_2 or *tert*-butyl hydroperoxide. Various organometallic complexes have also been grafted on aminopropyl-mesoporous silica and applied as oxidation catalysts[71, 72].

Mesoporous silicas have been used as solid supports to prepare both acid and base catalysts. For example, sulfonic acid was immobilized onto MCM-41 mesoporous silica and applied as an acid catalyst for glycerol esterification by lauric acid[73]. The sulfonic acid could be loaded onto the silica by coating or silylation. On the other hand, a base catalyst can be prepared by post synthesis modification of mesoporous silicas. These modifications may be accomplished either by direct reaction of mesoporous silicas with trialkoxysilanes containing amine functional groups or *via* a two step synthesis. The two step synthesis consists of reaction between mesoporous silicas and chloroalkoxysilane, followed by reaction with a free secondary amine,

such as piperidine[74, 75]. In both preparations of basic catalysts, the residual hydroxyl groups were removed by reaction with hexamethyldisilazane. The catalytic activity of base catalyst-mesoporous silicas was investigated with various esterification and condensation reactions. For example, Cauvel and co-workers[76] found that when mesoporous silica modified with piperidines was used to catalyze the esterification of glycidol, the best yield was 90 %. This yield was high compared to those obtained using unmodified materials and aminopropyl-mesoporous silicas. The high surface area of the mesoporous silica made it a good host material for immobilizing catalysts.

2.1.3.4b Environmental applications

Mesoporous silicas have been extensively used in environmental applications. The surface of mesoporous silica can be easily modified to act as extraction agents and the materials can be used for many kinds of environmental applications. They can either be used for removal or the extraction/preconcentration of pollutants.

I. Removal applications

The removal of heavy metals from wastewater can be achieved using modified mesoporous silicas. For instance, mesoporous silica modified with 3-mercaptopropyltrialkoxysilane has been applied to the removal of Hg^{2+}, Cu^{2+}, Zn^{2+}, Cr^{2+} and Ni^{2+} from wastewaters. It was found that the adsorption capacity for the metals was not only proportional to the concentration of the thiol groups on the surface but was also strongly depended on pore size[77, 78]. In more recent work, amine functionalized hexagonal and cubic silicas (type MCM-41 and MCM-48) were applied to remove Cd^{2+}, Co^{2+}, $Cu^{2+}$and Pb^{2+} from water. The affinity of metal ions for the amino-mesoporous silicas depended on the metal[79]. The adsorption capacity order was $Cu^{2+} > Pb^{2+} > Cd^{2+} > Co^{2+}$.

Modified mesoporous silicas can also be applied for the remediation of water contaminated by organic materials. Sawicki and Mercier[80] prepared cyclodextrin-mesoporous silica as an organic adsorbent. These materials were shown to be promising agents for the removal of low concentrations of pesticides from water.

Recently, various types of mesoporous silicas (MCM-41, MCM-48, SBA-15) were directly used (without modification) to remove large-molecule pesticides such as 1,1,1-trichloro-2,2`-bis(*p*-chlorophenyl)ethane (DDT) from water. All materials exhibited high efficiency for DDT removal and adsorption was rapid. The efficiency of DDT removal was affected by pore volume, pore diameter, pore connectivity and hydroxyl groups on the surface. SBA-15 has the highest adsorption efficiency (around 95 %) among all the mesoporous silicas, as a result of its large pore diameter and volume. After removal of DDT, the silicas were thermally treated and almost 100 % of the DDT was decomposed. The materials could be reused several times to remove organic materials[81].

II. Preconcentration applications

Since the discovery of mesoporous silicas, significant effort has been devoted to synthesize mesoporous silicas of high surface areas, defined sizes and pore diameters for extraction/preconcentration purposes. The mesoporous silica is used as a supporting phase to immobilize the extraction agent. The selectivity of the sorbent relies strongly on the affinity of the surface-coated functional ligand for specific pollutants. The modification of mesoporous silica with 2-mercaptopyridine, for example, has been carried out in two steps. The 2-mercaptopyridine was first reacted with 3-chloropropyltriethoxysilane and the product was used to functionalize the silica surface. Using a batch technique, the mercapto-mesoporous silica showed a high affinity for extracting Cr^{6+} from aqueous solution, with a maximum adsorption value of 0.35 mmol g^{-1} [82]. Noble metal ions such as Pt^{2+} and Pd^{2+} have been selectively extracted from water using an imidazole-functionalized mesoporous silica adsorbent. This adsorbent was prepared by grafting *N*-(3-triethoxysilylpropyl)-4,5-dihydroimidazole onto the surface of the mesoporous silica. It showed a high selectivity for extraction of Pt^{2+} and Pd^{2+} in the presence of other competing metal ions[83].

Enhancing the method of immobilization of the extraction agent can lead to improvements in the extraction ability of modified mesoporous silica. Dai *et al.*[84] developed a novel synthesis of selective functionalized mesoporous sorbents, based on imprint coating. In this method the functional groups were introduced onto the

surface of the mesoporous silica. The key enhancement in this work was that the surface was modified not just with the ligand, but also with the target metal. After removal of the metal ions, ligand imprints of the template metal ions are created on the mesoporous surface. The selectivity of the new sorbent was investigated using an aqueous solution of Zn^{2+} and Cu^{2+}. They found that the new sorbent materials exhibited higher binding selectivity towards the target metal ions than sorbents prepared by the conventional coating method. This comes as a result of the memory of the size and stereochemical signature of the template ion.

The large surface area of mesoporous silicas allows them to be loaded with more than one functional group for metal ions uptake, as described by Olkhovyk and Jaroniec[85]. They functionalized periodic mesoporous silicas with two functional groups, and the product was used as an adsorbent for heavy metal ions, such as mercury. In the synthesis of the bi-functional adsorbent, heterocyclic isocyanurate rings were incorporated into the structure during the formation of the particles. A second functional (thioether bridging) group was then introduced to the surface after the particles had formed. They noted no change in pore size and structure when the first groups were incorporated into the framework. On the other hand, after introduction of the thiol functionality along with isocyanurate moieties, the structure changed. Incorporation of the functional groups during the formation of the particles causes them to be distributed within the structure and inside the pore, and this will not hinder further modification of the surface. The method of modification can lead to enhanced metal adsorption[85].

Mesoporous silicas are widely used as a supporting phase to immobilise extraction agents, such as C_{18}, for the extraction and separation of organic compounds[86, 87]. Ma *et al*.[88] synthesized large pore mesoporous silica and the surface was functionalized by dimethyloctadecylchlorosilane ($DMC_{18}ClSi$). The C_{18}-silica was packed into an HPLC column for separation of small aromatic molecules, and large molecules, such as proteins.

To sum up, the mesoporous silicas are not normally effective in environemental applications without prior modification of their surface to give the silica with functionality suited to the particular application.

2.2 Modification of silica

Solid phase extraction of analytes from water involves transferring them from a water medium to the adsorbent matrix. The adsorbent usually consists of a solid support, linked chemically to a hydrocarbon chain, terminating in functional groups that work as the main extraction agent (Figure 2.12). The hydrocarbon chain used to carry the extraction groups is often a propyl chain as this keeps the extraction groups away from the surface of the solid and reduces a steric hindrance effects at the silanol site, allowing more extraction groups to react with analytes[89].

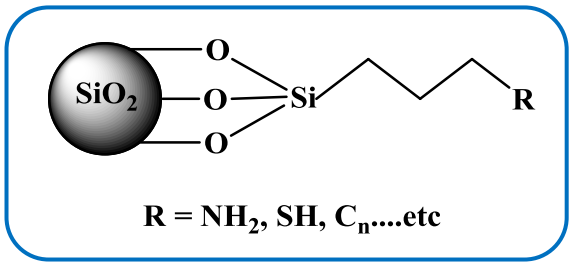

Figure 2.12 Silica surface functionalization

Silica is one of the most popular substrates for carrying functional groups. It has many advantages over other substrates, such as thermal and mechanical stability, no swelling and great resistance to organic solvents. In addition to the ease of linkage of the functional groups to the silica surface, which is covered by different types of active silanol groups, as discussed earlier.

The surface of silica can be modified either by physical adsorbing or chemically grafting the functional groups to the surface. The chemical bonding of the functional groups to the surface is preferable, as the grafted groups have a strong covalent bonded with the surface, which prevents leaching of the groups during the sample preparation. Modification of silica using a silane agent and organically modified silicates (ormosils) are widely used to functionalize the surface of silicas and prepared modified silicas. These methods will be discussed in the following sections.

2.2.1 Modification of silica by silane agents

Modification of the silica surface using organosilane agents is extensively practised by many researchers. The organosilanes of type RSiX, where R is the functional group and X is the reactive group, such as halogen, ethoxy and methoxy, firstly hydrolyse and react with the hydroxyl groups to covalently link the extraction groups to the surface of the silica[90].

Among the functional groups of interest for loading onto the surface of the silica are amine derivatives, which can be used for metal ions and DNA extraction. The 3-(2-aminoethylamino)propyl group was grafted to the surface of the silica and applied to preconcentrate Au, Pd and Cu prior to their determination by FAAS. The recovery results were more than 90 % for all metal ions. In addition, amino-silica was also functionalized to the surface of silica using $NH_2Si(OMe)_3$. The prepared amino-silica was packed in a column and applied to extract and purify DNA. The 50 mM of DNA was dissolved in tris(hydroxylmethyl)aminomethane-EDTA buffer at pH 7 and eluted using 300 mM of potassium phosphate solution at pH 10. No organic solvent was used for elution or washing the column[91].

Grafting the organic groups for extraction of metal ions can be done *via* the reaction between the silanol on the silica surface and alkoxysilane. Hernàndez and Rodríguez[92] modified the silica surface with mercaptopropyltrimethoxysilane. They found that the adsorption properties of silica particles were improved after the attachment of thiol groups to the surface. This increase in the adsorption of metal ions is due to the strong affinity of thiol groups to various metal ions, such as Hg, Pb and Cu. Moreover, mercapto groups were grafted to silica gel and applied by Howard and co-workers[93] to selectively preconcentrate arsenite from a water sample using column and batch techniques. The recovery results were in the range between 94-96 %. The good selectivity of mercapto-silica gel towards arsenite over other arsenic speciation allowed it to be used as storage stabilizer of arsenic prior to analysis.

The surface of silica can be reacted with alkyltrichlorosilanes to immobilize the hydrocarbon groups, such as octyl (C_8) and octadecyl (C_{18}), for extraction of organic materials. Yoo *et al.*[94] inserted C_{18} onto the surface of silica *via* a reaction with octadecyltrichlorosilane ($C_{18}SiCl_3$). Silicas modified with C_{18} groups are commonly used as solid stationary phase in the chromatography column and as sorbents in solid phase extraction for extraction/preconcentration of organic compounds. The key attraction mechanism between organic analytes and alkyl groups is based on hydrophobic forces. The length of alkyl groups could affect the extraction ability. Therefore, C_{18}-silica is more commonly used for extracting organic compounds than C_8-silica[95].

2.2.2 Organically modified silicates (ormosils)

Organically modified silicates (ormosils) are composites containing organic /inorganic hybrid materials. These materials have the potential to provide unique combination properties, such as no crack coating and bulk monoliths, which cannot be achieved with other materials[96]. Ormosil materials can be produced by using various organotrialkoxysilane agents. For example, when a tetraalkoxysilane is combined with different types of trialkoxysilane, it results in the formation of ormosils as described below.

The polydimethylsiloxane (PDMS) oligomer was added to TEOS as a modifier to produce silica xerogels and give toughness and flexibility to the product. The final structure of this type of hybrid material can be governed by many factors, such as catalysis type, the amount and molecular weight of added organic material, solvent and water quantities, temperature and reaction time[97]. In similar research, it has been found that using basic catalysis enhances co-condensation between PDMS and TEOS. However, an acidic catalysis has more influence on the hydrolysis reaction and a large amount of free organic species was found when acid was used as the catalyst. Moreover, the prepared silica xerogel was affected by water and the pH of the reaction solution. The hydrolysis rate of the sol was increased by increasing the water quantity[98].

Organo modified alkoxysilane can be used directly to prepare ormosil materials. For example, surface modified ormosil nanoparticles were prepared by hydrolysis and a polycondensation reaction of vinyl triethoxysilane. The vinyl groups were produced out from the surface of the particles. The prepared particles were spherical, with an average size of 87 nm[99]. In addition, Das *et al*.[100] prepared organic/silica hybrid spherical nanoparticles (100 nm) using octyltrimethoxysilane. Organic modified silica nanoparticles with high surface hydrophobicity due to octyl groups were obtained.

2.3 The physical characteristics of silica particles

2.3.1 Brownian motion

This phenomenon was firstly observed in 1827 by Robert Brown when he studied the movement of pollen grains and other small particles in water. In 1888, the French scientist Lèon Gouy investigated this motion and revealed that it was more active in low viscosity liquid. He believed that the random motion was generated by thermal molecular collisions. After a few years, Jean Perrin won the Nobel Prize for proving the reality of atoms. He studied the motion of colloidal particles in water and studied the isolated particles under a microscope[101, 102].

The theoretical analysis of Brownian motion can be explained using Einstein's equation.

The mean displacement due to Brownian motion (υ) is shown in Equation 2.1

$$\upsilon = \sqrt{2Dt} \qquad (2.1)$$

Where D is the diffusion coefficient and t is the time required for a particle to move a distance from its original position[103].

Spherical sub-micron sized silica particles follow Brownian motion when suspended in water. The motion of each particle leads to movement through the liquid, and collision between particles and liquid molecules causes a change in direction of the particles.

2.3.2 Stability of colloidal silica

Colloidal silica is an expression referring to the dispersion of silica particles with diameters of 5 to 1500 nm in a liquid. In an aqueous solution, silica particles with sizes in the range of 5 to 100 nm may remain for a long time without settling or loss of stability. The stability of a silica sol means that the particles do not aggregate at a significant rate to cause settlement of the particles. There are two forces present between colloidal particles according to Derjaguin-Landau-Verwey-Overbeek (DLVO)[104]. These are London-van der Waals and electrostatic forces, which generate as a result of particle electrostatic forces. The repulsive force between particles of same charge prevents aggregation. On the other hand, an interaction force between colloidal particles through London-van der Waals forces encourages aggregation between the particles[1, 103, 104].

The DLVO theory postulated that when two particles become close to each other, the repulsive forces prevent them from approaching and adhering together. An energy barrier is created as a result of this process. An aggregation and adhering can take place when colloidal particles have sufficient energy to overcome the energy barrier otherwise they will remain stable (Figure 2.13).

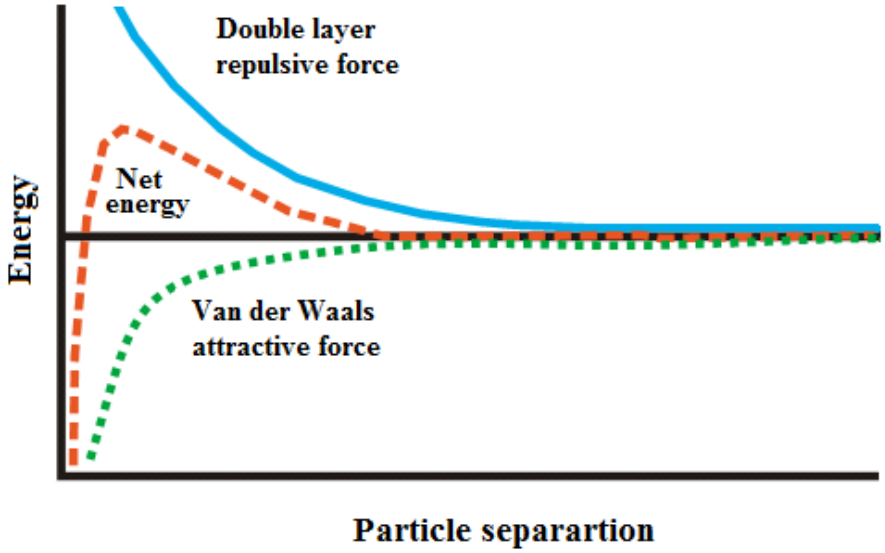

Figure 2.13 DVLO interaction potential against particles distance (taken from reference[105] with permission from the publisher)

Hamaker calculated the interaction energy[106] between spherical particles as seen in Equation 2.2[107].

$$V_{att} = \frac{-Aa}{12H} \qquad (2.2)$$

Where *A* is the Hamaker constant which depends strongly on the nature of the particles and the medium and *a* is the spherical particle radius. The minimum distance between the particle surfaces was expressed by *H* and can be calculated from Equation 2.3.

$$H = R\text{-}2a \qquad (2.3)$$

Where *R* is the distance between particle centres.

When the dispersion medium used is liquid instead of a vacuum or the air, the attraction energy is lower and the Hamaker constant can be calculated from Equation 2.4.

$$A = \left(\sqrt{A2} - \sqrt{A1}\right)^2 \quad (2.4)$$

Where *A1* is the Hamaker constant of liquid-liquid interaction and *A2* for particle-particle interaction. The interparticle attraction will be the lost state, when the chemistry of particles and the dispersion medium are similar[108].

There are generally two types of repulsion forces: steric and electrostatic, which lead to stabilization of the particles (Figure 2.14). Steric repulsion can be generated as a result of coating the surface of the particles by long chain molecules. In this case some of these molecules are insoluble in the medium; they repel each other leading to repulsion between the particles.

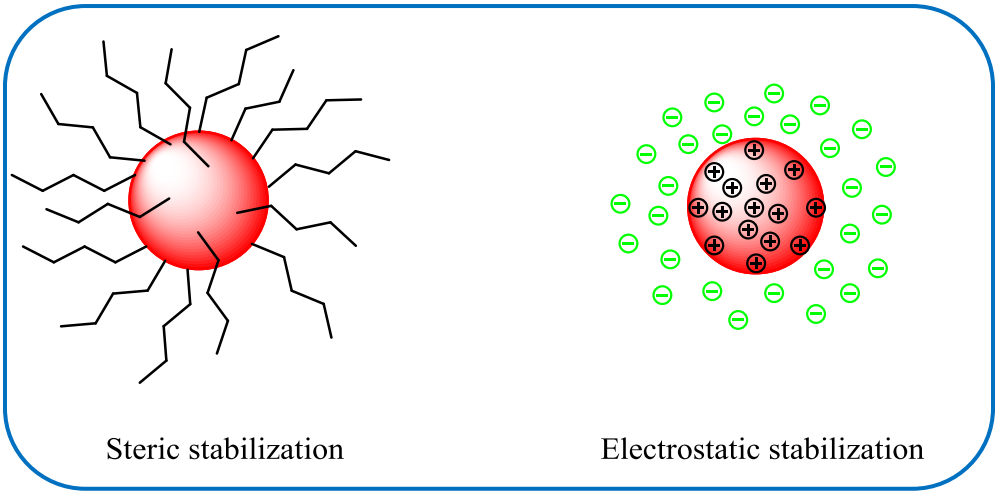

Figure 2.14 The two types of colloidal stabilization as a result of repulsion forces

Steric repulsion occurs because of the two effects, osmotic and volume restriction. The osmotic effect take places as a result of high concentration of chain molecules in the overlap area (Figure 2.15a). The volume restriction effect is obtained from possible loss of chain conformation in the narrow space between the two surfaces (Figure 2.15b). Steric repulsion is highly affected by the length and nature of the modified groups, the adsorption energy and by changing the solvent properties[109].

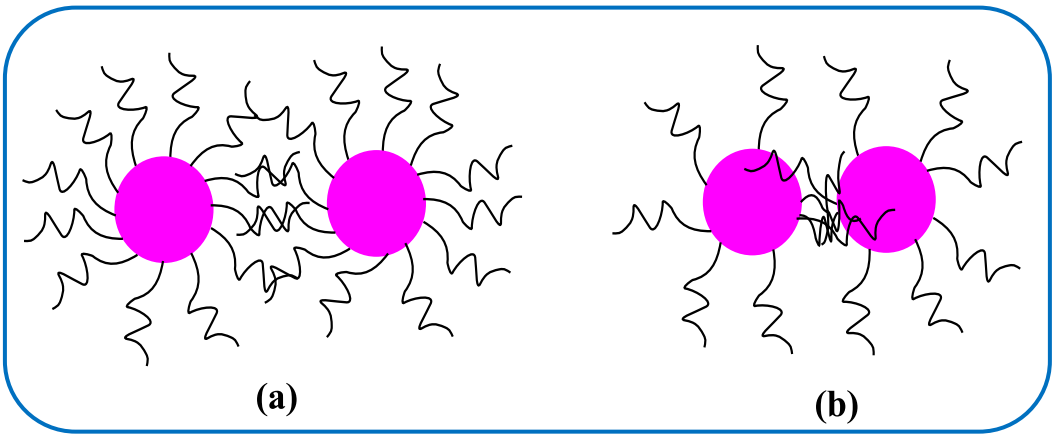

Figure 2.15 The two types of steric repulsion: (a) osmotic effect and (b) volume restriction effect

On the other hand, the electrostatic repulsion is based on the charge of the particles, either positive or negative, and similar charged particles repelling each other. It is not, however, as simple as normal repulsion, since the charged particles surrounded by the opposite charge ions create an electric double layer (Figure 2.16). The difference between the charge of this transferable layer and that of the suspended liquid is called zeta potential. The electric double layer is affected by addition of electrolyte. Adding electrolyte to stable colloidal particles leads to a decreasing the zeta potential, which causes aggregation of the particles and loss of stability[109].

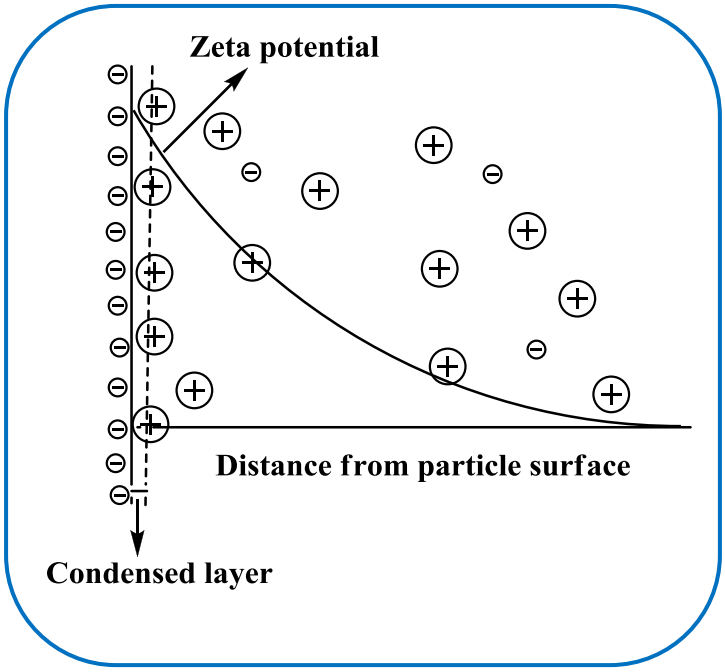

Figure 2.16 Double layer formation (taken from reference[110] with permission from the publisher)

2.4 Conclusion

A number of different types of silica have been reviewed in this chapter, ranging from silica gel monoliths to porous materials. TMOS and TEOS are the most popular precursors for the preparation of controlled particle size silica, as they are cheap and commercially available. The synthesis of silica occurs in two major steps, hydrolysis and condensation. These two steps can be catalysed by addition of acid or base, the choice of which can control the properties of the final product. Acidic catalysis

promotes the growth of polymeric chains to yield a network system of silica. However, dense particles with spherical morphology are produced by base catalysis.

Porous materials can be divided according to the pore size into microporous (< 2 nm), mesoporous (2-50 nm) and macroporous materials (>50 nm). Many factors may control the pore size of silica particles, such as type of silica precursor, concentration of water and solvent and types of template. The pore size of the particles is influenced by high temperature and the porous structure of silicas may collapse by heating the silica particles over 900 ºC. In addition, high temperature leads to condensation of the silanols on the silica surface that are very important for further modification of the silica.

Modification of the silica surface is essential to give it the unique properties for specific applications in catalysis, drug delivery or extracting materials. Organotrialkoxysilanes are widely used to link chosen functional groups to the surface of silica through hydrolysis of the alkoxy moiety and condensation with silanol groups on the silica. The nature of the functionalized groups on the surface of silica affects the stability of silica particles in water.

2.5 Overall objectives

This project develops the use of sub-micron sized silica particles in the extraction of analytes from aqueous solution. There are three basic research aims:

I) The synthesis and characterization of sub-micron sized silica particles, having high surface areas resulting from mesoporosity or disruption of structural regularity. The research will focus on a particle size of around 250 nm, as such particles will disperse as a colloidal sol under the right conditions and will sediment very slowly. The extraction of samples does not require external agitation, because the particles move naturally throughout the sample by Brownian motion, convection and sedimentation. Finally, it is easy to recover the particles by filtration.

II) Chemical modification of the silica surface with amino, dithiocarbamate, hydroxyquinoline, mercaptobenzamide and with dual functionality (octadecyl and diol groups).

III) The use of the modified silica particles in analytical applications such as the analytical preconcentration of metal ions (copper, nickel, cobalt, chromium, cadmium, lead, manganese and zinc) and organic compounds (estrogenic compounds, polynuclear aromatic hydrocarbons and tributyltin).

2.6 References

(1) Bergna, H. E.; Roberts, W. O. *Colloidal Silica: Fundamentals and Applications*; Taylor and Francis Group: New York, **2006**.

(2) Iler, R. K. *The chemistry of silica : solubility, polymerization, colloid and surface properties, and biochemistry*; Wiley: New York, **1979**.

(3) Winter, R.; Chan, J. B.; Frattini, R.; Jonas, J. *J. Non-Cryst. Solids* **1988**, *105*, 214-222.

(4) Kijak, A. M. Ph.D. Thesis, Miami University, Ohio, USA, **2003**.

(5) Hector, A. L. *Chem. Soc. Rev.* **2007**, *36*, 1745-1753.

(6) Kiselev, A.; Nikitin, S.; Oganesyan, B. *Colloid J.* **1969**, *31*, 525-531.

(7) Kistler, S. *J. Phys. Chem.* **1932**, *36*, 52-64.

(8) Jeronimo, P. C. A.; Araujo, A. N.; Montenegro, M. *Talanta* **2007**, *72*, 13-27.

(9) Wolfbels, O. S. *Anal. Chem.* **2008**, *80*, 4269-4283.

(10) Zusman, R.; Rottman, C.; Ottolenghi, M.; Avnir, D. *J. Non-Cryst. Solids* **1990**, *122*, 107-109.

(11) Jurmanovic, S.; Kordic, S.; Steinberg, M. D.; Steinberg, I. M. *Thin Solid Films* **2010**, *518*, 2234-2240.

(12) Chen, L. J.; Mei, F. M.; Li, G. X. *Catal. Commun.* **2009**, *10*, 981-985.

(13) Mirzaei, A. A.; Babaei, A. B.; Galavy, M.; Youssefi, A. *Fuel Process. Technol.* **2010**, *91*, 335-347.

(14) Sarussi, L.; Blum, J.; Avnir, D. *J. Sol-Gel Sci. Technol.* **2000**, *19*, 17-22.

(15) El-Ashgar, N. M.; El-Nahhal, I. M.; Chehimi, M. M.; Babonneau, F.; Livage, J. *Int. J. Environ. Anal. Chem.* **2009**, *89*, 1057-1069.

(16) El-Ashgar, N.; El-Nahhal, I. *J. Sol-Gel Sci. Technol.* **2005**, *34*, 165-172.

(17) Chong, S. L.; Wang, D. X.; Hayes, J. D.; Wilhite, B. W.; Malik, A. *Anal. Chem.* **1997**, *69*, 3889-3898.

(18) Cai, L. S.; Gong, S. L.; Chen, M.; Wu, C. Y. *Anal. Chim. Acta* **2006**, *559*, 89-96.

(19) Sing, K. S. W.; Everett, D. H.; Haul, R. A. W.; Moscou, L.; Pierotti, R. A.; Rouquerol, J.; Siemieniewska, T. *Pure Appl. Chem.* **1985**, *57*, 603-619.

(20) Brunauer, S.; Emmett, H.; Teller, E. *J. Am. Chem. Soc.* **1938**, *60*, 309-319.

(21) Donohue, M. D.; Aranovich, G. L. *Adv. Colloid Interface Sci.* **1998**, *77*, 137-152.

(22) Zou, H.; Wu, S. S.; Shen, J. *Chem. Rev.* **2008**, *108*, 3893-3957.

(23) Pristavita, R.; Munz, R. J.; Addona, T. *Ind. Eng. Chem. Res.* **2008**, *47*, 6790-6795.

(24) Parfitt, G. D.; Sing, K. S. W. *Characterization of Powder Surfaces*; Academic Press: London, **1976**.

(25) Bode, R.; Feach, H.; Fartzscher, H. *J. Paint Oil Colour Chem. Associ.* **1968**, *2*, 415-422.

(26) Broekhoff, J. C. P.; Linsen, B. G. *Physical and Chemical Aspects of Adsorbents and Catalysis*; Academic Press: London and New York, **1970**.

(27) Stöber, W.; Fink, A.; Bohn, E. *J. Colloid Interface Sci.* **1968**, *26*, 62-69.

(28) Yano, K.; Fukushima, Y. *J. Mater. Chem.* **2003**, *13*, 2577-2581.

(29) Vacassy, R.; Flatt, R. J.; Hofmann, H.; Choi, K. S.; Singh, R. K. *J. Colloid Interface Sci.* **2000**, *227*, 302-315.

(30) Kresge, C. T.; Leonowicz, M. E.; Roth, W. J.; Vartuli, J. C.; Beck, J. S. *Nature* **1992**, *359*, 710-712.

(31) Raman, N. K.; Anderson, M. T.; Brinker, C. J. *Chem. Mat.* **1996**, *8*, 1682-1701.

(32) Beck, J. S.; Vartuli, J. C.; Roth, W. J.; Leonowicz, M. E.; Kresge, C. T.; Schmitt, K. D.; Chu, C. T. W.; Olson, D. H.; Sheppard, E. W.; McCullen, S. B.; Higgins, J. B.; Schlenker, J. L. *J. Am. Chem. Soc.* **1992**, *114*, 10834-10843.

(33) Rosen, M. J. *Surfactants and Interfacial Phenomena*; Wiley: New York, **1989**.

(34) Huo, Q. S.; Margolese, D. I.; Ciesla, U.; Feng, P. Y.; Gier, T. E.; Sieger, P.; Leon, R.; Petroff, P. M.; Schuth, F.; Stucky, G. D. *Nature* **1994**, *368*, 317-321.

(35) Tanev, P. T.; Pinnavaia, T. J. *Science* **1995**, *267*, 865-867.

(36) Bagshaw, S. A.; Prouzet, E.; Pinnavaia, T. J. *Science* **1995**, *269*, 1242-1244.

(37) Yu, T.; Zhang, H.; Yan, X. W.; Chen, Z. X.; Zou, X. D.; Oleynikov, P.; Zhao, D. Y. *J. Phys. Chem. B* **2006**, *110*, 21467-21472.

(38) He, W. C.; Wang, J. G.; Chen, T. H. *Sci. China Ser. B-Chem.* **2009**, *52*, 1423-1426.

(39) Luca, V.; MacLachlan, D. J.; Hook, J. M.; Withers, R. *Chem. Mater.* **1995**, *7*, 2220-2223.

(40) Hamoudi, S.; Yang, Y.; Moudrakovski, I. L.; Lang, S.; Sayari, A. *J. Phys. Chem. B* **2001**, *105*, 9118-9123.

(41) Xia, Y. D.; Mokaya, R. *J. Phys. Chem. B* **2006**, *110*, 3889-3894.

(42) Boissiere, C.; van der Lee, A.; El Mansouri, A.; Larbot, A.; Prouzet, E. *Chem. Commun.* **1999**, 2047-2048.

(43) Prouzet, E.; Pinnavaia, T. J. *Angew. Chem.-Int. Edit.* **1997**, *36*, 516-518.

(44) Boissiere, C.; Martines, M. A. U.; Tokumoto, M.; Larbot, A.; Prouzet, E. *Chem. Mater.* **2003**, *15*, 509-515.

(45) Soler-Illia, G. J. D.; Sanchez, C.; Lebeau, B.; Patarin, J. *Chem. Rev.* **2002**, *102*, 4093-4138.

(46) Monnier, A.; Schuth, F.; Huo, Q.; Kumar, D.; Margolese, D.; Maxwell, R. S.; Stucky, G. D.; Krishnamurty, M.; Petroff, P.; Firouzi, A.; Janicke, M.; Chmelka, B. F. *Science* **1993**, *261*, 1299-1303.

(47) Yanagisawa, T.; Shimizu, T.; Kuroda, K.; Kato, C. *Bull. Chem. Soc. Jpn.* **1990**, *63*, 988-992.

(48) Inagaki, S.; Fukushima, Y.; Kuroda, K. *J. Chem. Soc.-Chem. Commun.* **1993**, 680-682.

(49) Linden, M.; Schunk, S. A.; Schuth, F. *Angew. Chem.-Int. Edit.* **1998**, *37*, 821-823.

(50) Firouzi, A.; Kumar, D.; Bull, L. M.; Besier, T.; Sieger, P.; Huo, Q.; Walker, S. A.; Zasadzinski, J. A.; Glinka, C.; Nicol, J.; Margolese, D.; Stucky, G. D.; Chmelka, B. F. *Science* **1995**, *267*, 1138-1143.

(51) Schuth, F. *Ber. Bunsen-Ges. Phys. Chem. Chem. Phys.* **1995**, *99*, 1306-1315.

(52) Dattelbaum, A. M.; Amweg, M. L.; Ruiz, J. D.; Ecke, L. E.; Shreve, A. P.; Parikh, A. N. *Mechanism of surfactant removal from ordered nanocomposite silica thin films by deep-UV light exposure*; Materials Research Society: Warrendale, **2004**.

(53) Hua, Z. L.; Shi, J. L.; Wang, L.; Zhang, W. H. *J. Non-Cryst. Solids* **2001**, *292*, 177-183.

(54) Ji, H.; Fan, Y. Q.; Jin, W. Q.; Chen, C. L.; Xu, N. P. *J. Non-Cryst. Solids* **2008**, *354*, 2010-2016.

(55) Hozumi, A.; Yokogawa, Y.; Kameyama, T.; Hiraku, K.; Sugimura, H.; Takai, O.; Okido, M. *Adv. Mater.* **2000**, *12*, 985-987.

(56) Kundu, D.; Zhou, H. S.; Honma, I. *J. Mater. Sci. Lett.* **1998**, *17*, 2089-2092.

(57) Chen, C. Y.; Li, H. X.; Davis, M. E. *Micropor. Mater.* **1993**, *2*, 17-26.

(58) Hair, M. L. *J. Non-Cryst. Solids* **1975**, *19*, 299-309.

(59) Maciel, G. E.; Sindorf, D. W. *J. Am. Chem. Soc.* **1980**, *102*, 7606-7607.

(60) Legrand, A. P.; Hommel, H.; Tuel, A.; Vidal, A.; Balard, H.; Papirer, E.; Levitz, P.; Czernichowski, M.; Erre, R.; Vandamme, H.; Gallas, J. P.; Hemidy, J. F.; Lavalley, J. C.; Barres, O.; Burneau, A.; Grillet, Y. *Adv. Colloid Interface Sci.* **1990**, *33*, 91-330.

(61) Fyfe, C. A.; Gobbi, G. C.; Kennedy, G. J. *J. Phys. Chem.* **1985**, *89*, 277-281.

(62) Severin, J. W.; Vankan, J. M. J. *Philips J. Res.* **1990**, *45*, 35-39.

(63) Takei, T.; Kato, K.; Meguro, A.; Chikazawa, M. *Colloid Surf. A-Physicochem. Eng. Asp.* **1999**, *150*, 77-84.

(64) Sneh, O.; George, S. M. *J. Phys. Chem.* **1995**, *99*, 4639-4647.

(65) Zhuravlev, L. T. *Colloid Surf. A-Physicochem. Eng. Asp.* **1993**, *74*, 71-90.

(66) Tatsumi, T.; Koyano, K. A.; Igarashi, N. *Chem. Commun.* **1998**, 325-326.

(67) Krijnen, S.; Abbenhuis, H. C. L.; Hanssen, R.; Van Hooff, J. H. C.; Van Santen, R. A. *Angew. Chem.-Int. Edit.* **1998**, *37*, 356-358.

(68) Corma, A.; Jorda, J. L.; Navarro, M. T.; Rey, F. *Chem. Commun.* **1998**, 1899-1900.

(69) Rao, Y. V. S.; De Vos, D. E.; Jacobs, P. A. *Angew. Chem.-Int. Edit.* **1997**, *36*, 2661-2663.

(70) Diaz, I.; Marquez-Alvarez, C.; Mohino, F.; Perez-Pariente, J.; Sastre, E. *J. Catal.* **2000**, *193*, 295-302.

(71) Sayari, A.; Hamoudi, S. *Chem. Mater.* **2001**, *13*, 3151-3168.

(72) Zhou, X. G.; Yu, X. Q.; Huang, J. S.; Li, S. G.; Li, L. S.; Che, C. M. *Chem. Commun.* **1999**, 1789-1790.

(73) Bossaert, W. D.; De Vos, D. E.; Van Rhijn, W. M.; Bullen, J.; Grobet, P. J.; Jacobs, P. A. *J. Catal.* **1999**, *182*, 156-164.

(74) Jaenicke, S.; Chuah, G. K.; Lin, X. H.; Hu, X. C. *Micropor. Mesopor. Mater.* **2000**, *35-6*, 143-153.

(75) Lin, X. H.; Chuah, G. K.; Jaenicke, S. *J. Mol. Catal. A-Chem.* **1999**, *150*, 287-294.

(76) Cauvel, A.; Renard, G.; Brunel, D. *J. Org. Chem.* **1997**, *62*, 749-751.

(77) Liu, J.; Feng, X. D.; Fryxell, G. E.; Wang, L. Q.; Kim, A. Y.; Gong, M. *Chem. Eng. Technol.* **1998**, *21*, 97-100.

(78) Perez-Quintanilla, D.; Del Hierro, I.; Fajardo, M.; Sierra, I. *J. Hazard. Mater.* **2006**, *134*, 245-256.

(79) Benhamou, A.; Baudu, M.; Derriche, Z.; Basly, J. P. *J. Hazard. Mater.* **2009**, *171*, 1001-1008.

(80) Sawicki, R.; Mercier, L. *Environ. Sci. Technol.* **2006**, *40*, 1978-1983.

(81) Tian, H.; Li, J. J.; Zou, L. D.; Mua, Z.; Hao, Z. P. *J. Chem. Technol. Biotechnol.* **2009**, *84*, 490-496.

(82) Perez-Quintanilla, D.; Del Hierro, I.; Fajardo, M.; Sierra, I. *Mater. Res. Bull.* **2007**, *42*, 1518-1530.

(83) Kang, T.; Park, Y.; Choi, K.; Lee, J. S.; Yi, J. *J. Mater. Chem.* **2004**, *14*, 1043-1049.

(84) Dai, S.; Burleigh, M. C.; Shin, Y.; Morrow, C. C.; Barnes, C. E.; Xue, Z. L. *Angew. Chem.-Int. Edit.* **1999**, *38*, 1235-1239.

(85) Olkhovyk, O.; Jaroniec, M. *Ind. Eng. Chem. Res.* **2007**, *46*, 1745-1751.

(86) Li, Y. Y.; Cheng, S. Y.; Dai, P. C.; Liang, X. M.; Ke, Y. X. *Chem. Commun.* **2009**, 1085-1087.

(87) Zhao, J. W.; Gao, F.; Fu, Y. L.; Jin, W.; Yang, P. Y.; Zhao, D. Y. *Chem. Commun.* **2002**, 752-753.

(88) Ma, Y. R.; Qi, L. M.; Ma, J. M.; Wu, Y. Q.; Liu, O.; Cheng, H. M. *Colloid Surf. A-Physicochem. Eng. Asp.* **2003**, *229*, 1-8.

(89) Jal, P. K.; Patel, S.; Mishra, B. *Talanta* **2004**, *62*, 1005-1028.

(90) Unger, K. K. *Porous silica: its properties and use as support in column liquid chromatography*; Elsevier: Amsterdam, **1979**.

(91) Liu, L. J.; Yu, S. B.; Yang, S. X.; Zhou, P.; Hu, J. M.; Zhang, Y. B. *J. Sep. Sci.* **2009**, *32*, 2752-2758.

(92) Hernandez, G.; Rodriguez, R. *J. Non-Cryst. Solids* **1999**, *246*, 209-215.

(93) Howard, A. G.; Volkan, M.; Ataman, O. Y. *Analyst* **1987**, *112*, 159-162.

(94) Yoo, H. J.; Kim, S. K.; Kim, J. H.; Kang, H. J. *Polym.-Korea* **2003**, *27*, 555-561.

(95) Pocurull, E.; Sanchez, G.; Borrull, F.; Marce, R. M. *J. Chromatogr. A* **1995**, *696*, 31-39.

(96) Schmidt, H. *J. Non-Cryst. Solids* **1985**, *73*, 681-691.

(97) Guo, L.; Hyeon, L. J.; Beaucage, G. *J. Non-Cryst. Solids* **1999**, *243*, 61-69.

(98) Chakrabarti, K.; Kim, S. M.; Oh, E. O.; Whang, C. M. *Mater. Lett.* **2002**, *57*, 192-197.

(99) Sharma, R. K.; Das, S.; Maitra, A. *J. Colloid Interface Sci.* **2004**, *277*, 342-346.

(100) Das, S.; Jain, T. K.; Maitra, A. *J. Colloid Interface Sci.* **2002**, *252*, 82-88.

(101) Frey, E.; Kroy, K. *Ann. Phys.-Berlin* **2005**, *14*, 20-50.

(102) Abe, S.; Thurner, S. *Phys. A* **2005**, *356*, 403-407.

(103) Khdary, N. H. Ph.D. Thesis, Southampton University, Southampton, UK, **2006**.

(104) Verwey, E. J. W.; Overbeek, J. T. G. *Theory of the Stability of Lyophobic Colloids*; Elsevier: New York, **1948**.

(105) Nel, A. E.; Madler, L.; Velegol, D.; Xia, T.; Hoek, E. M. V.; Somasundaran, P.; Klaessig, F.; Castranova, V.; Thompson, M. *Nat. Mater.* **2009**, *8*, 543-557.

(106) Chiarle, S.; Ratto, M.; Rovatti, M. *Water Res.* **2000**, *34*, 2971-2978.

(107) Vera, P.; Gallardo, V.; Salcedo, J.; Delgado, A. V. *J. Colloid Interface Sci.* **1996**, *177*, 553-560.

(108) Shaw, D. J. *Introduction to colloid and surface chemistry* ; Butterworths: London, **1970**.

(109) Goodwin, J. W. *Colloidal dispersions : the papers given at a Review Symposium on Colloid Science, University of Bristol, 8-10th September 1981*; Royal Society of Chemistry: London, **1982**.

(110) Gouy, G. *J. Phys.* **1910**, *9*, 457-468.

Chapter 3

Synthesis of nano-sized silica particles

The development of synthetic methods for the production of nano-sized spherical silica particles is reported in this chapter. There were two main targets to achieve. The first was to synthesize monodisperse spherical silica particles with a mean diameter of around 250 nm. This size of the particles was selected according to several criteria. Their size had to fall within the colloidal range, so that they remain suspended in aqueous samples and they must be easy to recover. The second aim was to increase the surface area of the silica particles so that the loading of the functional groups on the surface could be enhanced.

The Stöber method of preparing spherical silica particles was the starting point. Spherical silica particles of ca. 250 nm diameter were synthesised from TEOS. A number of approaches were evaluated to increase the surface area of the particles. In one such method 1,2-bis(triethoxysilyl)ethane (BTEE) [1] was added to the reaction mixture during the formation of the particles to disrupt the growth of the particles and increase the surface area. This method was not however successful.

Mesoporous silica particles were found to have the required high surface area. These were prepared from TMOS using a dodecyltrimethylammonium bromide (C_{12}TMABr) template.

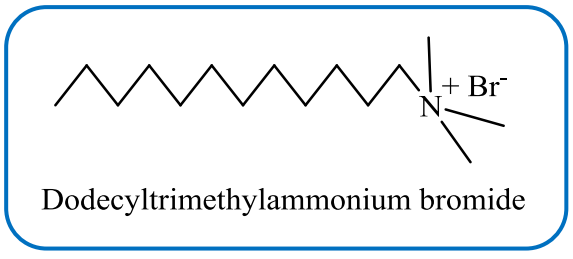

Dodecyltrimethylammonium bromide

3.1 Preparation of Stöber-type silica

The synthesis of spherical silica particles is commonly carried out using methods derived from that which was originally reported by Stöber *et al.*[2]. In their syntheses a tetraalkoxysilane is used as a silica precursor, with polymerization catalyzed by ammonia. Tetraethoxysilane and tetramethoxysilane are the most common tetraalkoxysilanes used to produce silica particles, as many other alkoxysilanes are immiscible with water. Under neutral conditions the rate of hydrolysis of the tetraalkoxysilane in water and alcohol is slow but the rate can be enhanced by adding acid or base to initiate the hydrolysis and condensation of the reaction intermediates. Using tetraalkoxysilane based systems spherical silica particles, can be then synthesized with controlled morphology and properties. Silica particles are produced through the hydrolysis of the alkoxysilane to give silanols, which then condense to give Si-O-Si linkages, which ultimately lead to solid silica. The condensation process can occur either *via* alcohol or water producing mechanisms[3] (Figure 3.1).

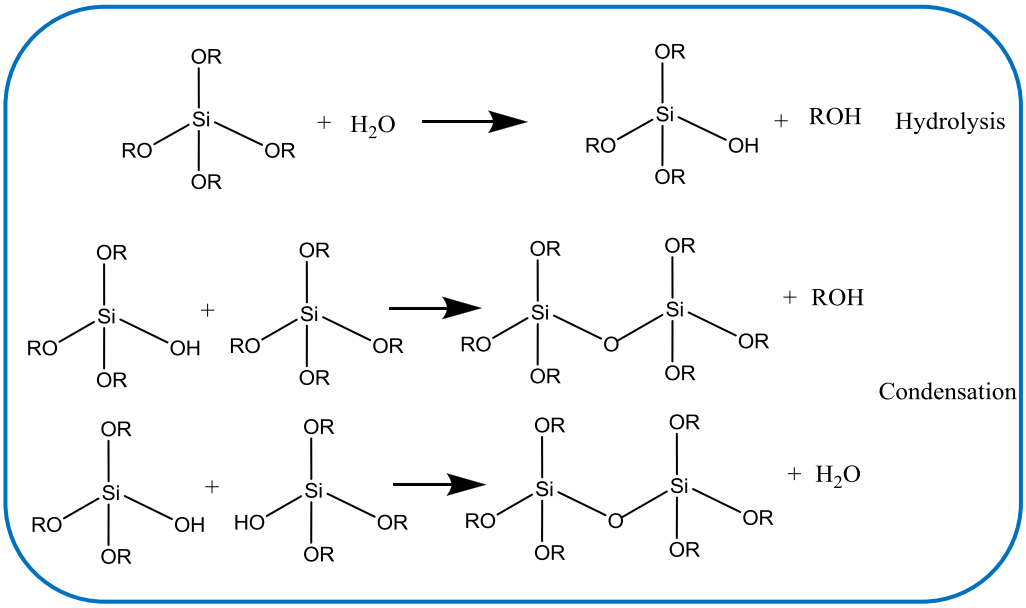

Figure 3.1 The hydrolysis and condensation mechanisms to form silica particles

The formation of the silica particles from primary particles can be carried out by two possible mechanisms, monomer addition[4, 5] and controlled aggregation[6-8]. These models divide the formation of silica into two events: nucleation and growth, and use different approaches to describe particle growth. The monomer addition model suggests that the growth of the particles occurs through the addition of hydrolyzed monomers to the particle surface. The second model, controlled aggregation, claims that growth occurs continuously throughout the reaction as small particles aggregate to form bigger particles.

Jafarzadeh *et al.*[9] supposed that the concentrations of tetraalkoxysilane, ammonia, water, as well as the types of co-solvent (alcohol) and reaction temperature were the main parameters governing the particle size and distribution. By controlling these parameters, Park *et al.*[10] prepared silica particles within the range of 13.7 ± 4.0 nm. Rahman *et al.*[11] reported that monodispersed silica, with an average size of 20.5 ± 3.5 nm, can be synthesized in the presence of a small quantity of NH_4Br. Normally nanospherical silica particles are synthesized using ethanol as a solvent but Venkatathri[12] was also able to prepare a monodisperse nanosilica using acetone, isopropanol and n-octanol solvents. *Razo et al.*[13] controlled the particle diameter over a wide range by varying only the amount of the alkoxide, whilst keeping the concentration of all the other parameters fixed. Most recently, Rahman *et al.*[14] reported that the synthesis of silica nanoparticles depends on the optimization of parameters such as the concentration of reactants, ammonia and temperature under ultrasonic mixing.

The specific surface area ($m^2\ g^{-1}$), specific pore volume, the distribution of pore size or pore area and particle size are fundamental parameters which physically characterize the surface area. Knowledge of the specific surface area is critical as a measure of the concentration of surface functional groups that can be modified. Pore size distribution provides deeper information about silanol group availability. Specific surface area can be estimated from a nitrogen adsorption isotherm. The specific areas of Stöber-type silicas fall in the range of 18 to 24 $m^2\ g^{-1}$. Poor surface area is one of the main disadvantages of Stöber-type silicas.

3.1.1 Materials

Octadecyltrimethoxysilane ($C_{18}Si(OMe)_3$) (90 %), tetraethoxysilane (TEOS) (98 %), tetramethoxysilane (TMOS), 1,2-bis(triethoxysilyl)ethane (BTEE) (96%) **,** and sodium fluoride were purchased from Aldrich (Poole, UK). Methanol and ethanol (laboratory grade), ammonium hydroxide (SG = 0.88, 35 % (w/v)), hydrochloric acid (36 % (w/v)), ethylene glycol and sodium hydroxide were bought from Fisher Scientific (Loughborough, UK). Hexadecyltrimethylammonium chloride (C_{16}TMACl) (98 %) was obtained from Fluka (Gillingham, UK). Dodecyltrimethylammonium bromide (C_{12}TMABr) was supplied by Alfa Aesar, (Heysham, UK). Sucrose ($C_{12}H_{22}O_{11}$, analytical grade) was purchased from BDH chemicals Ltd (Poole, UK). Water was purified by deionisation using an Elga Option 4 system.

3.1.2 Characterization of the particles

The prepared silica particles in the Thesis were characterized using a wide variety of techniques and devices:

- A laser scattering particle size analyzer (COULTER N4 Plus) equipped with size distribution processor (SDP) and multi-angles options was used to measure the particle size and assess the size distribution. When suspended particles are irradiated with a laser beam, light is scattered by particles over a wide angle range. The particle size distribution can be obtained through the analysis of scattered light. The silica particles (10 mg) were prepared for the measurement by dispersion in deionised water (10 mL) and sonication for an hour. The suspension was transferred to a quartz cuvette and the measurement was carried out using the following conditions:
Angle selected: 90°, equilibrium time: 1 minute, run times: 5 minutes, refractive index: 1.333 and temperature: 20 °C,

- The surface area and pore size distribution was measured using a Micromeritics Gemini 2375 and Quantachrome NovaWin apparatus. The silica

sample was dried overnight at 150 ºC and kept in evacuated desiccator before measurement and the run was carried out under the following conditions:
Evacuation time: 5 minutes, evacuation rate: 300.0 mmHg min^{-1}, equilibration time: 5 seconds, saturation pressure: 760.00 mmHg.

- SEM was utilized to measure the particle size and to evaluate the morphology of the particles. Silica particles (10 mg) were dispersed in deionised water (10 mL) using ultrasonicator and the sample was then prepared by dispensing drops of pre-dispersed silica onto a glass plate. The water was allowed to evaporate at room temperature and the glass surface was then coated with a thin gold film. SEM measurement was carried out using a Philips XL-30 ESEM instrument under these conditions:
Mode: high vacuum, detector: Secondary Electron (SE).

- The structure of mesoporous silica was evaluated using a Jeol JEM-3010 transmission electron microscope (TEM). Mesoporous silica particles (1 mg) were dispersed in methanol (10 mL) for an hour using ultrasonicator. A small drop of the suspended particles was placed on a copper grid with holey carbon film and then kept in a desiccator for commencing measurement.

- The settling time of a colloidal suspension of the nanoscavenger was measured using a Perkin Elmer Lambda 3 spectrophotometer. The silica suspension was prepared by dispersing of silica particles (10 mg) in deionised water (10 mL), held in a 1 cm pathlength quartz cuvette and the light transmission at 600 nm was measured over time.

- The thermal analysis of the particles was carried out using thermogravimetric analysis (TGA), type Perkin-Elmer TGS-2 instrument attached to a Perkin-Elmer Datastation-3700 and a System 4 thermal analysis microprocessor. An accurate weight of sample (7-10 mg) was analyzed using temperature program that run from 25 to 800 ºC at temperature rate of 2 ºC min^{-1}, under air.
- Fourier transform Infrared spectroscopy was carried out using a Perkin-Elmer 1600 series instrument. The silica samples were directly measured as solid materials.

3.1.3 Experiments

3.1.3.1 Syntheses of silica particles with undiluted tetraethoxysilane

In this experiment, undiluted TEOS was added to the ammonium hydroxide solution directly according to the method described by Howard and Khdary[15]. Methanol (250 mL) and ammonium hydroxide (250 mL) were transferred to a conical flask (1000 mL) and mixed for 5 minutes using a magnetic stirrer. TEOS (5 mL) was then slowly added. The reaction was left to proceed at 20 ºC for one hour. The product was then centrifuged for 30 minutes at 8400 *g* and the supernatant was isolated and discarded. The silica was then rinsed with methanol six times and the product was dried under continuous vacuum for an hour giving a white solid (1.46 g).

3.1.3.2 Pre-diluted tetraethoxysilane

In this method the TEOS was pre-diluted with methanol to improve its dispersion in the hydrolysis medium.
Methanol (250 mL) and TEOS (5 mL) were transferred to a conical flask (1000 mL) and mixed for 2 minutes using a magnetic stirrer. Ammonium hydroxide (250 mL) was then added. The reaction was left to proceed at 20 ºC for one hour. The solid product was then isolated by centrifugation for 30 minutes at 8400 *g*. The silica was then rinsed with methanol six times and the product was dried under continuous vacuum for an hour giving a white powder (1.12 g).

3.1.4 Results and discussion

For preparation of Stöber-type silicas, two approaches have been applied: un-diluted and pre-diluted approach. Three main criteria have been considered for the production the silica particles: particle size, particle size distribution and wettability of the particles. 250 nm sized spherical particles were synthesized by adding neat TEOS to a mixture of methanol and ammonium hydroxide. The laser scattering particle size analysis (LSPSA) of silica from the un-diluted approach showed a broad

particle size distribution compared to narrow size distribution obtained from the pre-diluted approach (Table 3.1).

Table 3.1 Particle size analysis of the prepared silica particles

Main approach	Method	Mean diameter
Pure alkoxysilane synthesis	Un-diluted	272 ± 62 nm
	Pre-diluted	244 ± 15 nm

The two approaches produced monodispersed silica particles (Figure 3.2 and 3.3) of similar size although the diameter of silica particles decreased slightly using the pre-diluted method. The pre-diluted method produced silica particles with a more uniform size distribution than the un-diluted method. The pre-dilution of the TEOS helps to disperse the silica precursor prior the addition of the catalyst (NH_4OH). The hydrolysis, condensation and growth of the particles therefore takes place more uniformly to generate similarly sized particles. Poor dispersion of TEOS in the reaction mixture leads to the production of silica with wide standard deviation.

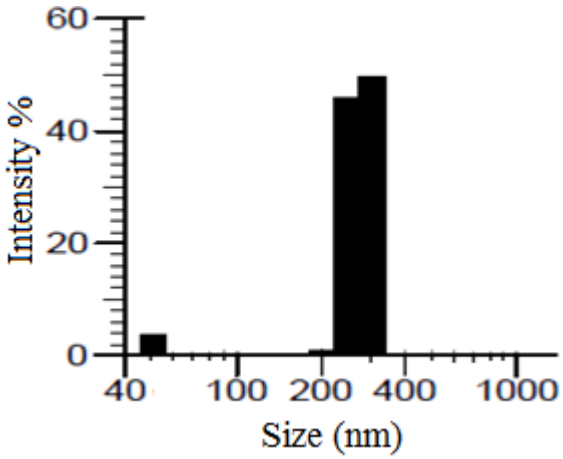

Figure 3.2 LSPSA of silica particles prepared using undiluted alkoxide

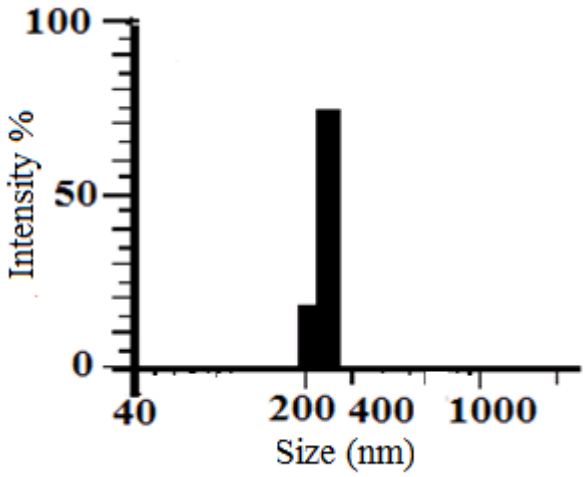

Figure 3.3 LSPSA of silica prepared by adding NH_4OH to pre-diluted TEOS and methanol

Scanning electron microscope was carried out to confirm the morphology of the prepared silica particles. Figures 3.4 and 3.5 show that the silica particles are spherical with highly by uniform sizes.

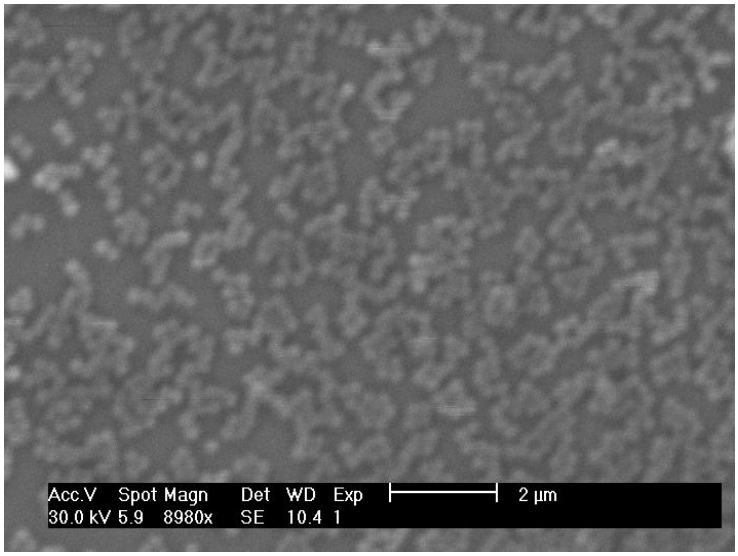

Figure 3.4 SEM image (8980X magnification) of the silica particles prepared using undiluted alkoxide

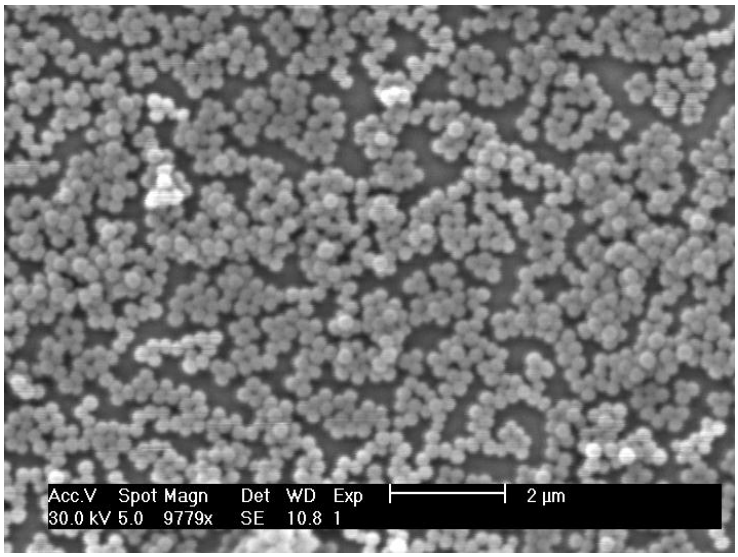

Figure 3.5 SEM image (9779X magnification) of silica particles prepared by adding NH_4OH to pre-diluted TEOS and methanol

3.2 Efforts to increase the silica surface area

The surface of Stöber-type silica particles is highly dense and the specific surface area is therefore too low to permit a high loading of analytically useful functional groups to be grafted on the surface of Stöber-type silica[16]. Many researchers have tried to manipulate the chemical parameters to increase the surface area of the particles. Hai *et al.*[17] managed to increase the surface area of Stöber-type silica to 200 m^2 g^{-1} by reducing the silica using magnesium under pressure and at 750 ºC for 5 hours. A high surface area was formed after removing the MgO. Sodium chloride (NaCl) has also been employed as a templating medium during the synthesis of silica particles. Spherical nanosized mesoporous silica particles were attained after removing NaCl from the silica by washing. After removing the salt from silica structure, surface areas from 17 to 700 m^2 g^{-1} were obtained that varied with the hydrolysis time (from 1 to 50 hours). Salt templating offers the advantages of being inexpensive and easy to remove by aqueous rinsing[18]. Recently silica particles with high surface area have been synthesized using low cost sodium silicate as a silica precursor[19]. A cetyltrimethylammonium bromide (CTMABr) was used as an additive to control the particle shape and produce a large surface area. The particle size and

specific surface area were controlled by manipulating the molar ratios of a silica precursor, CTMABr, ethyl acetate and deionised water.

3.2.1 Pilot study of silica preparations

3.2.1.1 Preparation of nano-sized silica particles using BTEE and TEOS

In this method, BTEE was added during the formation of the silica particles to disrupt the growth of the particles. The BTEE has two silane moieties linked by ethylene bridge. The surface area increases eventually after the organic materials had been removed.

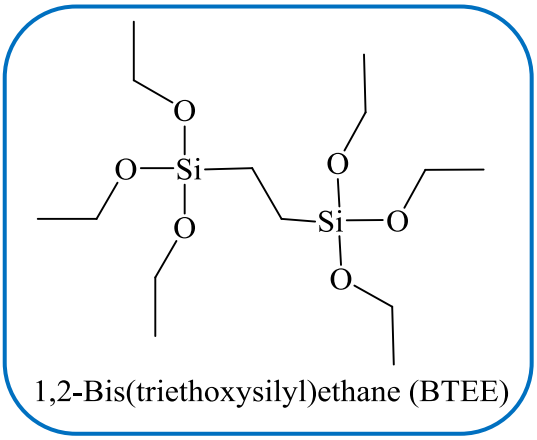

1,2-Bis(triethoxysilyl)ethane (BTEE)

Two approaches were used. In the first, TEOS was added to prehydrolyzed BTEE. In another approach, BTEE and TEOS were dissolved in methanol before the addition of ammonium hydroxide. Introducing the BTEE into the silica structure may generate pores after combustion of BTEE and increase the surface area.

3.2.1.1a The pre-hydrolysed BTEE method

In this experiment BTEE was added to a mixture of methanol and ammonium hydroxide solution to prehydrolyze the BTEE before adding TEOS. Methanol (250 mL) and ammonium hydroxide (250 mL) were transferred to a conical flask (1000 mL) and mixed for 5 minutes using a magnetic stirrer. BTEE (0.1 mL) was added. After 3 minutes, TEOS (4.9 mL) was slowly added. The reaction was left to proceed at 20 ºC for an hour. The solid product was isolated by centrifugation for 30 minutes

at 8400 *g*. The silica was then rinsed with methanol six times and the product was dried under vacuum for one hour. Combustion in air at 500 ºC for 6 hours gave a white powder (1.15 g).

3.2.1.1b The premixed BTEE and TEOS method

In this experiment BTEE and TEOS were dissolved in methanol before ammonium hydroxide solution was added. The concentrations of BTEE and TEOS were varied and the total added volume of silica precursor was 5 mL.
Methanol (250 mL), BTEE (0.1, 0.25 and 0.5 mL) and TEOS (4.9, 4.75 and 4.5 mL) were transferred to a conical flask (1000 mL) and mixed for 1 minute using a magnetic stirrer. Ammonium hydroxide (250 mL) was then added. The reaction was left to proceed with stirring at 20 ºC for two hours. The product was then isolated by centrifugation for 30 minutes at 8400 *g*. The silica was then rinsed with methanol six times and the product was dried under continuous vacuum for one hour. Combustion in air at 500 ºC for 6 hours produced a white powder (1.12 g).

3.2.1.2 Silica synthesized using NaF

Several researchers[20-22] have implied NaF during the preparation of mesoporous silicas to improve the hydrothermal stability of these materials as the fluorinated silica surface is much more hydrophobic and more resistant against water molecules attack than a silanol silica surface[22, 23]. In addition, several studies have reported the etching of silica by HF[24]. In this experiment NaF was added during the formation of the silica. After the addition of NaF some HF (weak acid) will be formed which attacks the surface of the silica with an anticipated increase in surface area.

Methanol (125 mL), TEOS (2.5 mL) and ammonium hydroxide (125 mL) were transferred to a conical flask (500 mL), and the mixture was agitated using a magnetic stirrer for 15 minutes at room temperature. NaF (50 mL of 1 mol L^{-1}) was added. The flask was left for 48 hours at 20 ºC with a magnetic stirring. The silica was isolated by centrifugation and rinsed with water 10 times. The silica was left in air to dry, giving a white powder (0.74 g).

3.2.1.3 Silica preparation using sucrose as a template

In this experiment, sucrose was used as a template and TEOS as the silica precursor[25]. The organic template will be trapped inside the structure during the silica formation. The removal of the template was easily carried out by rinsing with water. Methanol (125 mL) and ammonium hydroxide (125 mL) were transferred to a conical flask (500 mL) and mixed for 5 minutes using a magnetic stirrer. Sucrose (25 mL, 1M) and TEOS (2.5 mL) were then added. The reaction was left to proceed at 20 ºC for 8.5 hours. The product was then centrifuged for 15 minutes at 8400 *g* and the supernatant was isolated and discarded. The silica was rinsed with water five times and three additional times with methanol. The product was dried under continuous vacuum for 3 hours.

3.2.2 Results and discussion

3.2.2.1 Synthesis of nano-sized sized silicas using TEOS and BTEE

In this approach, BTEE was introduced to the reaction mixture anticipating that this would disturb the growth of the silicas particles, leading to enhancement in the surface area after burning off the organic species. The pre-hydrolysed BTEE method afforded particles that were 375.4 ± 98.2 nm before combustion and 257.3 ± 25 .3 nm after combustion (Table 3.2). With premixed BTEE and TEOS, the particles shrank from 240.5 ± 20.3 nm to 229.1 ± 29 nm on combustion (Table 3.2).

Table 3.2 Particle size analyses of silica particles prepared using BTEE and TEOS

Main approach	Method	Mean diameter	
		Not combusted	Combusted at 500 °C
Preparation using BTEE and TEOS	Pre-hydrolysed BTEE	375.1 ± 98.2 nm	257.3 ± 25 .3 nm
	Pre-mixed BTEE and TEOS	240.5 ± 20.3 nm	229.1 ± 29 nm

Thermogravimetric analyses carried out from 25 to 800 ºC showed four regions of weight loss. The first change occurred between 37 and 160 ºC, a weight loss thought

to be that of water adsorbed on the silica surface and residual solvent[26]. There was then a large weight loss from 160 to 450 ºC, followed by another between 450 and 500 ºC. Most of the weight was lost between 160 to 450 ºC (Figure 3.6). No significant change was observed between 500 to 800 ºC. There was a sharp weight loss between 450 and 470 ºC for material prepared from BTEE and TEOS.

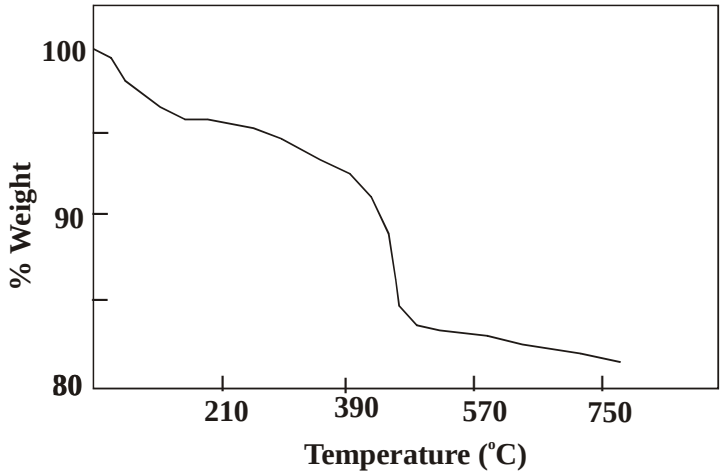

Figure 3.6 Thermal analysis of silica produced by the premixed BTEE-TEOS method

Surface areas of the two silicas were 18 m^2 g^{-1}. BET isotherm is of Type II according to IUPAC classification[27], characteristic of non porous materials (Figure 3.7). This means that the BTEE did not break up the structure of the silica as expected. The BTEE might possibly hydrolyse and polymerize to produce its own particles, but be fragmented by combustion of the organic bridge within the particles.

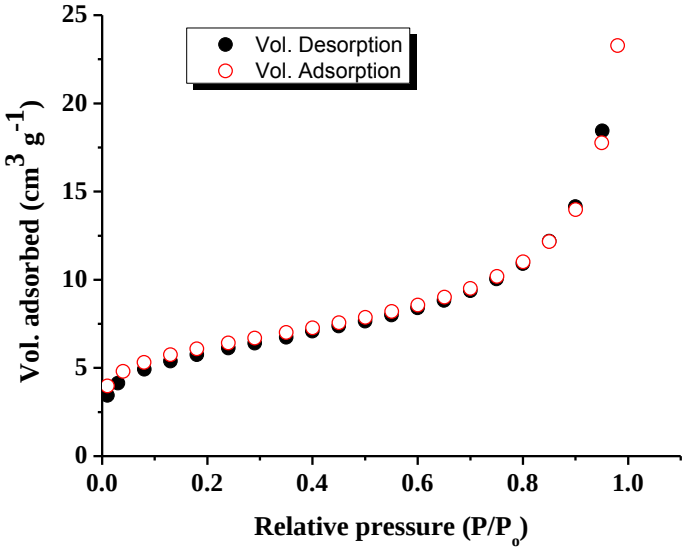

Figure 3.7 N_2 adsorption isotherm of nano-sized sized silica prepared by the premixed TEOS- BTEE method

3.2.2.2 NaF as an additive during the silica formation

In this method, NaF was added to the reaction mixture during the formation of the silica to attack the surface of the silica to make it rough and increase the surface area. The LSPSA illustrates a bimodal distribution of silica particles (Figure 3.8). The existence of small particles may be due to the effect of the electrolyte. It has been reported that addition of NaF to the reaction mixture leads to an increase in the population of the silica seed particles and decreases the size of the particles[20]. Growth of the particles is achieved *via* aggregation of primary particles and the presence of electrolyte in the reaction medium inhibits the growth of the particles and produces smaller size particles. This is due to the electrolyte enhancing the electric charge on the particle surface[28]. The average size of the particles (main population) was found to be 324 nm with 100 nm standard deviation.

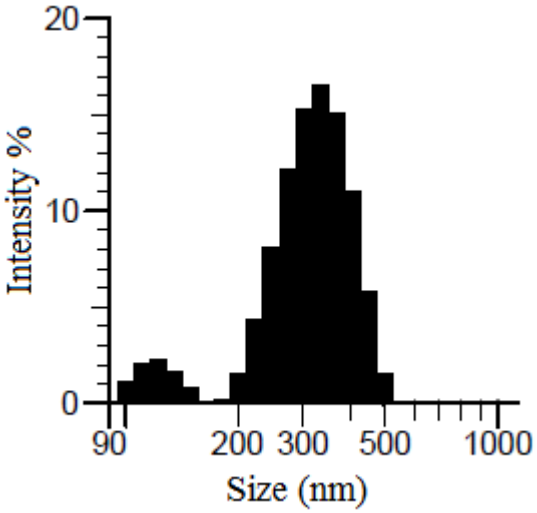

Figure 3.8 LSPSA of silica particles prepared by addition of NaF during silica formation

Scanning electron microscopy showed spherical particles with a mean diameter of around 259 ± 47 nm. Figure 3.9a shows a chunk of aggregated particles. This may occur whilst evaporating the water during the preparation of the sample for SEM or the sonication process was not enough to disaggregate these particles.

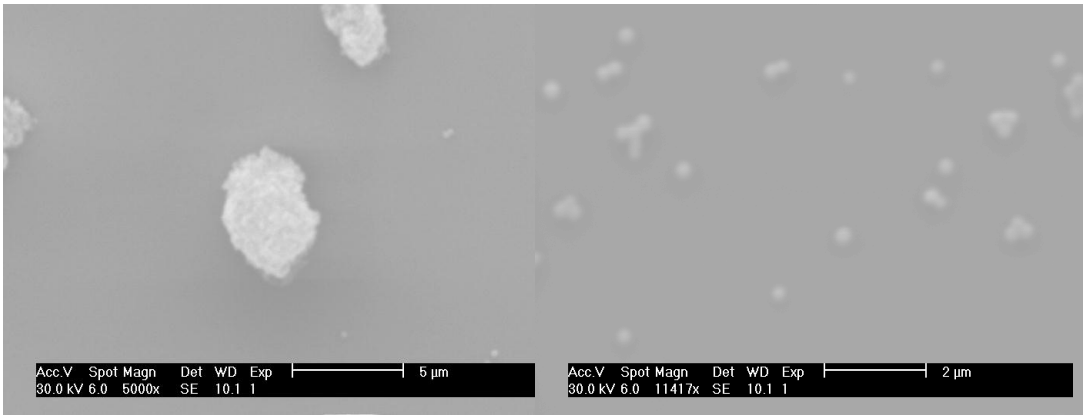

Figure 3.9 SEM images of silica particles prepared by addition of NaF to silica reaction mixture

The surface area (BET) was around 20 m^2 g^{-1} indicating that the surface area was not improved by the addition of NaF during the formation of the particles. NaF did not give the hoped for results.

3.2.2.3 Silica preparation using sucrose as a template

In the previous methods spherical silica particles were synthesized but an improvement in the surface area remained a challenge. Therefore sucrose was tested as a template to create pores with the template being removed by washing with deionised water. Sugar was used by Sang *et al.*[29] as template to prepare zeolite materials. The templating is reported to take place on glucose and fructose generated by the hydrolysis of sucrose. It was reported that glucose increased the surface area whilst the fructose was responsible for the formation of a large pore size[25]. The templating mechanism may take place by condensation of hydroxyl groups of sucrose isomers and silica precursor.

Figure 3.10 shows monodispersed silica particles prepared using sucrose as a template. The average particle size was of 412 nm with a standard deviation of 24 nm. The expected average particle diameter is around 250 nm as obtained in the same condition without using sucrose.

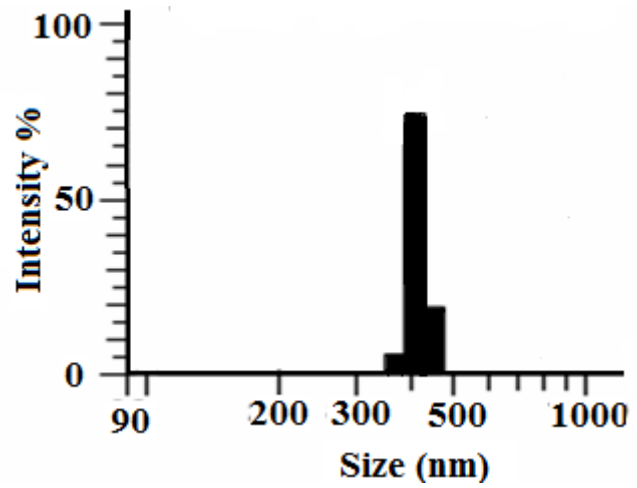

Figure 3.10 LSPSA of silica prepared using sucrose as a template

The N_2 adsorption isotherm was Type I according to the IUPAC classification[27] (microporous) (Figure 3.11) and the BET surface area was 109 m^2 g^{-1}

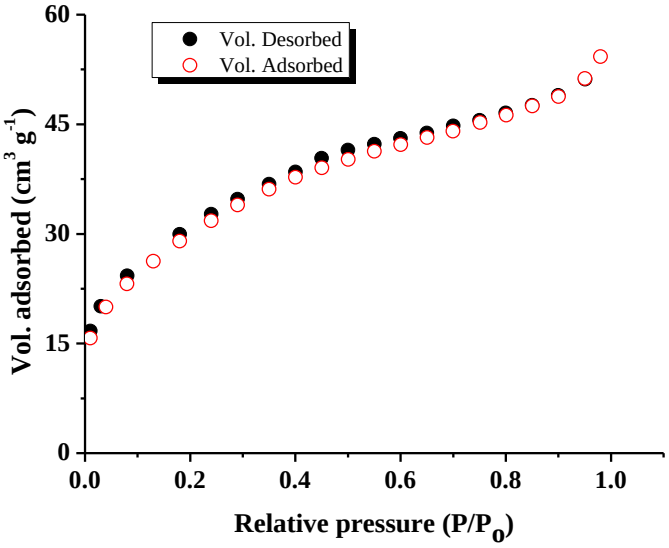

Figure 3.11 N_2 adsorption isotherm of nano-sized sized silica prepared using a sucrose template

Templating the Stöber-type silica using sugar increased the surface area from 20 m^2 g^{-1} to 109 m^2 g^{-1}. The increase in the surface area may be attributed to the generation of pores inside the structure of silica. It was reported that silica gel surface area was increased by more than two folds up to 750 m^2 g^{-1} using a sucrose template. It was found that the surface area increased with increasing the sugar ratio in the reaction[25]. However, the size of the prepared silica particles (412 nm) is not suitable to use as a substrate materials for the preparation of nanoscavenger as their large size results in particle sedimentation (by observation).

3.3 Synthesis of controlled size mesoporous silica particles

The formation of mesoporous silica involves the templating of silicate materials between ordered surfactant micelles. Controlling the size of the particles is the most challenging part in the preparation of mesoporous silica, as increasing the pore size of the particles may lead to an increase in the size of the particles. A few reports in the literature have reported the production of mesoporous silicas with average sizes

of less than 500 nm. There are a number of factors that can be taken to control particle size, including changing the length of the alkyl chain of the surfactant , changing the reaction temperature[30], using a double surfactant system, selecting the appropriate type of solvent, quenching the formation of the silica after a short period of time by the addition of water[31], controlling the stirring speed and etc. Some of the most important factors will be discussed below.

Long chain alkyltrimethylammonium halides are known to template mesoporous silica; the pore size of which can be controlled by adjusting the alkyl chain length from C_{12} to C_{18}. Yano and Fukushima[32] synthesized mesoporous silicas using TMOS as a silica precursor and alkyltrimethylammonium chlorides of different alkyl lengths (C_{14}, C_{16} and C_{18}) as templates in a mixture of methanol, water and NaOH. The specific surface areas of the prepared silicas were in the range 1150-1200 $m^2\ g^{-1}$, with pore volumes in the range 0.60-0.81 $cm^3\ g^{-1}$. They found that the average particle size increased from 490 nm to 1002 nm when the alkyl-chain length of the surfactant was increased[32].

The reaction temperature also affects the particle size when the length of the alkyl-chain of the surfactant is C_{12} or fewer. Since a decrease in temperature results in larger particles, it was supposed that an increase would lead to increased nucleation and thus generate small particles[33]. However, no size change was observed with mesoporous silica when the reaction temperature was varied between 10-50 ºC, when C_{16}TMACl was used as a surfactant[32]. Mesoporous silica with an average particle size of 110 nm was obtained when the temperature of the reaction of TEOS, C_{12}TMABr, water, ethanol and NH_4OH was increased from 25 to 40 ºC. The surface area of the prepared silica was 910 $m^2\ g^{-1}$ with an average pore diameter of 2.5 nm[34].

Mesoporous silica particles with an average particle size of 50 nm were obtained using a double surfactant system according to work carried out by Suzuki *et al.*[35]. They used two types of surfactant, a cationic surfactant (CTMACl) and a non-ionic surfactant triblock copolymer (Pluronic F127, $EO_{106}PO_{60}EO_{106}$). Large size particles (100-200 nm) were obtained when silica was templated only with CTMACl. However, the size of the particles dropped to 50 nm with addition of Pluronic F127. It was assumed that the triblock copolymer surfactant hindered the growth of the

mesostructured CTMA-silica composites. The existence of the Pluronic F127 micelles stabilizes the mesostructure by covering nanoparticles and leading to the generation of small particles. However, the drawback of this approach is that the particles have an irregular morphology and a wide pore diameter[35].

A simple method for producing small particles is to use a highly diluted aqueous solution of surfactant-silica. A dilute solution of CTMABr and sodium silicate was used to synthesise particles with an average size between 30-100 nm. It was found that the size decreased as the pH value decreased: the former was reduced to 30 nm when the latter was lowered to 5.5. This is because the pH value turned the strong electrostatic interaction between the surfactant and silicate into a weak hydrogen bonding leading to a wormhole-like mesostructure. However, the reduction of the pH value may produce particles with irregular sizes[36].

Finally, the type of solvent affects the particle dimensions. Methanol and ethanol are the most commonly used solvents in the preparation of mesoporous silica, and it has been reported that a low concentration of methanol[37] and ethanol[38] led to smaller particles. Significant work carried out by Japanese researchers[39] involved the synthesis of mesoporous silica spheres of different particle diameters (100-400 nm) using TMOS and C_{12}TMABr as a template, and using ethylene glycol as a co-solvent instead of methanol or ethanol. It was postulated that increasing the reaction solution viscosity caused a higher generation of primary particles, resulting in the eventual production of smaller particles. Moreover, this research demonstrated that particles became larger as the concentration of ethylene glycol in the reaction mixture increased[39]. This clearly shows that a decrease in the concentration of solvent produces reduced particle size.

To sum up, it is clear that changing the alkyl chain length of the surfactant and the reaction composition are the most powerful factors available to control the particle size.

3.3.1 Experiments

In previous work, nano-sized silica with a mean particle size of ca. 250 nm was successfully prepared, but the surface area was found to be low (~ 20 m^2 g^{-1}). New approaches have therefore been taken to synthesise nano-sized silicas using surfactant templates to create pores in the silica structure and hence increase the available surface area. Four different methods have been applied in order to obtain spherical silica particles of 250 nm diameter and possessing high surface area.

3.3.1.1 Syntheses of mesoporous silicas using BTEE as a silica precursor and a C_{16}TMACl template (Method a)

In these approaches, hexadecyltrimethylammonium chloride was used to template silica formation from BTEE and hence produce a mesoporous product. Five variations of the method were carried out in attempts to change the size of the particles. These experiments involved changing the amount of ammonia, deionised water and the amount and type of alcohol.

General method

In a conical flask (50 mL), C_{16}TMACl (0.38 g) was dissolved in a mixture of deionised water, ethanol or methanol, and ammonia solution and stirred at room temperature. After 15 minutes, BTEE (0.4 mL) was then added. A white precipitate appeared. The mixture was stirred for two more hours. The product was then isolated by centrifugation for 30 minutes at 3000 *g*, rinsed with deionised water four times and one additional time with methanol. The product was left to dry in air overnight. Removal of the surfactant was carried out by Soxhlet extraction with a mixture of ethanol (200 mL) and concentrated HCl (6 mL) for 24 hours. The product was then dried under vacuum for an hour. Table 3.3 shows the materials and quantities used in the different experiments.

Table 3.3 The materials and quantities of mesoporous silicas synthesized using BTEE as a silica precursor and using a C_{16}TMACl template

Experiment	Materials and quantities			
	EtOH (mL)	MeOH (mL)	NH_4OH (mL)	H_2O (mL)
1a	5	-------	5	8
2a	-------	12	1	12
3a	6	-------	1	6
4a	-------	10	1	10
5a	15	-------	1	15

3.3.1.2 Mesoporous silica prepared using TEOS and C_{16}TMACl (Method b)

In a conical flask, C_{16}TMACl (0.38 g) was dissolved in a mixture of deionised water, methanol or ethanol and ammonium hydroxide solution (conc.) and stirred at room temperature. After 15 minutes, TEOS (0.4 mL) was added and a white solid formed. The mixture was stirred for two more hours and then filtered. The solid was rinsed with deionised water (four times) and then once with methanol. The product was left to dry in air overnight. Removal of the surfactant was carried out by burning the silica in a furnace for 12 hours at 550 ºC; this final temperature being reached at a heating rate of 5 ºC / min. Table 3.4 shows the materials and quantities used in the different experiments which have been carried out.

Table 3.4 The materials and quantities of mesoporous silicas prepared using TEOS and C_{16}TMACl

Experiment	Materials and quantities			
	EtOH (mL)	MeOH (mL)	NH_4OH (mL)	H_2O (mL)
1b	-------	6	1	6
2b	-------	10	1	10
3b	10	-------	1	10
4b	25	-------	1	25

3.3.1.3 Mesoporous silica prepared using TEOS and ethylene glycol (Method c)

In these experiments, C_{16}TMACl or C_{12}TMABr was used as a template and TEOS as a silica precursor. Ethylene glycol was used instead of methanol or ethanol.

General method

In a conical flask (250 mL), a suitable amount of C_{16}TMACl or C_{12}TMABr was dissolved in a mixture of deionised water, ethylene glycol and ammonium hydroxide (conc.) or sodium hydroxide (1M) under stirring at room temperature. After 15 minutes, TEOS (0.45 mL) was added. The reaction mixture was left to proceed at 20 ºC for a period of time (2 – 24 hours). The product was isolated by centrifugation and the white solid was rinsed with water 5 times and left to dry. The removal of surfactant was carried out by combustion of the silica at 550 ºC, rating at 5 ºC / min in air. Table 3.5 shows the materials and quantities used in the different experiments that were carried out.

Table 3.5 The materials and quantities used to prepare mesoporous silica

Experiment	Materials and quantity					
	Ethylene glycol (mL)	H_2O (mL)	NH_4OH (mL)	NaOH (mL)	$C_{16}TMACl$ (g)	$C_{12}TMABr$ (g)
1c	10	10	1	-------	0.42	----------
2c	40	60	1	-------	0.42	----------
3c	22.5	75	1	-------	0.42	---------
4c	27	30	---------	1	---------	0.42
5c	20	73	---------	1	--------	0.42

3.3.1.4 Synthesis of a large batch of mesoporous silica using TMOS (Method d)

In this approach, $C_{12}TMABr$ was used as a template, TMOS as a silica precursor, ethylene glycol as a co-solvent and NaOH as a base[39].

Ethylene glycol (90 mL), deionised water (310 mL), NaOH (3 mL, 1M) and $C_{12}TMABr$ (1.68 g) were transferred into a conical flask (1000 mL). The mixture was stirred for 15 minutes at 20 ºC. TMOS (1.8 mL) was then slowly added and the reaction was allowed to proceed for 8 hours under stirring. The mixture was then aged overnight. The white solid was isolated by centrifugation for an hour at 8300 *g*, rinsed with water five times, and then dried at 45 ºC for three days. The white powder was calcinated to remove the surfactant at 550 ºC for 12 hours after taken to that temperature at 1 ºC / min. The experiment was repeated five times and the combined products were gently ground and mixed together

3.3.2 Results and discussion

3.3.2.1 Controlling the size and surface area of the silica particles

One of the aims of this study was to synthesise spherical silica particles with an average diameter of 250 nm and possessing a high surface area. Mesoporous silica is

a material with a high surface area which allows control of the particle size. There are many factors that play important roles in determining the size and surface area of mesoporous silica. The factors investigated in this study were: silica precursor, alkyl chain length of the surfactant, solvent type and concentration and base type.

Four methods were applied in order to achieve the aim stated above. In all of these, the silica precursors were BTEE, TEOS or TMOS.

3.3.2.1a Syntheses of mesoporous silicas using BTEE and C_{16}TMACl (Method a)

In this approach mesoporous silica particles were synthesized using BTEE as the silica precursor, and templated by C_{16}TMACl. Experiments were carried out in which the solvent type and base concentration were changed to achieve particle size and surface area characteristics suitable for the work.

Figure 3.12 shows the SEM image and LSPSA of mesoporous silica prepared using approach 1a. The SEM images showed aggregated particles, these results support the result obtained by the LSPSA in which the average particle diameter was 2400 nm (Figure 3.12). The solvent was changed from ethanol to methanol in Experiment 2a. The particle diameter might be expected to decrease with the decreasing the molecular weight of the solvent[2]. The LSPSA of the batch showed a bimodal distribution of silica particles (Figure 3.13) with 90 % of the particles were larger than 5000 nm. The main reason for these results was aggregation of the particles and the existence of some amorphous particles as shown in the SEM image (Figure 3.13). Sometimes the aggregation of particles occurs due to weak static attraction between the particles that can be overcome by sonication of the particles in a suitable solvent. With these samples, despite sonication prior to the particle sizing, aggregation of nano-sized particles remained, a feature that can occur when the particles are chemically linked.

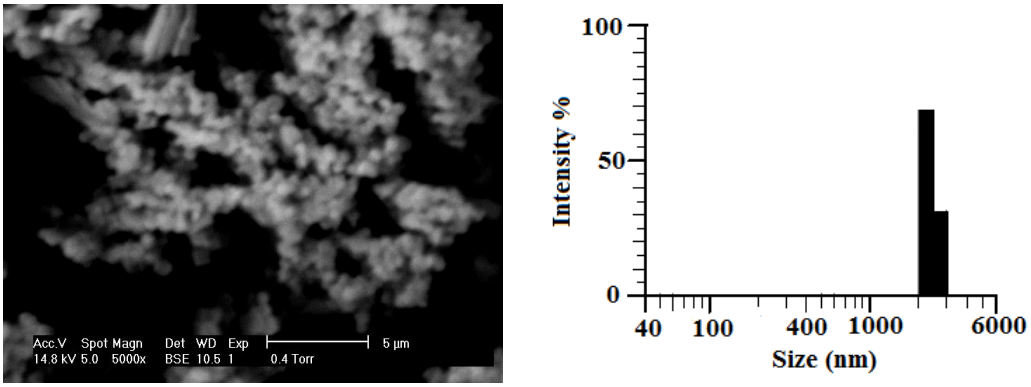

Figure 3.12 SEM image and LSPSA of mesoporous silica prepared using [BTEE (0.4 mL), C_{16}TMACl (0.38 g), EtOH (5 mL), NH_4OH (5 mL) and H_2O (8 mL) (Experiment 1a)]

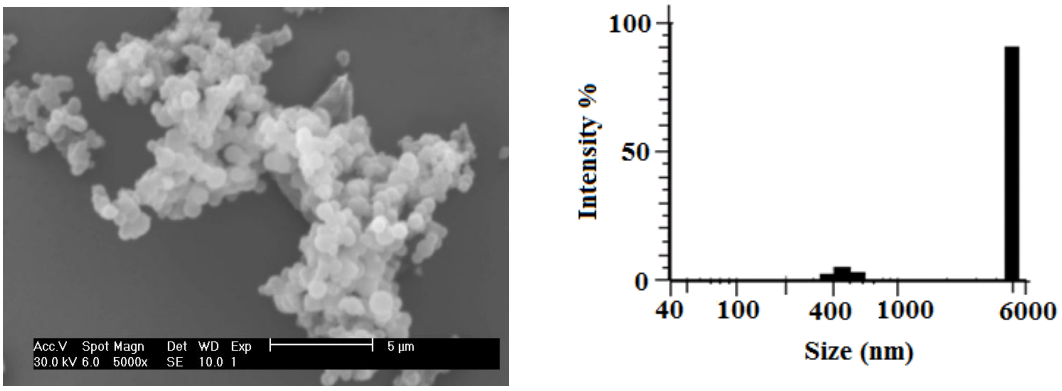

Figure 3.13 SEM image and LSPSA of mesoporous silica prepared using [BTEE (0.4 mL), C_{16}TMACl (0.38 g), MeOH (12 mL), NH_4OH (1 mL) and H_2O (12 mL) (Experiment 2a)]

Further experiments (3a and 4a) were carried out by varying the amount and type of alcohol. Scanning electron micrographs of the resulting particles (Figure 3.14)

showed them to be spherical with an average diameter between 450 and 700 nm. In addition, some of the particles were amorphous. Despite the alteration of the type of alcohol, ammonia and water concentrations resulting in some improvement in dispersity, no significant change was observed in particle size. In Figure 3.14, the silica particles appear as a lump of aggregated particles. The solid silica particles can usually be dispersed in water using an ultrasonicator bath within 1 to 3 hours but these particles could not be disaggregated (Figure 3.14), even over a period of 10 hours.

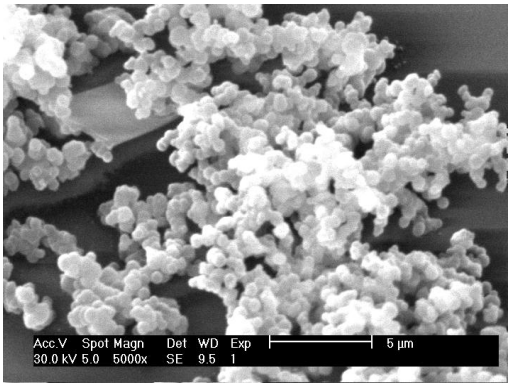

SEM image of mesoporous silica prepared using ethanol [BTEE (0.4 mL), C_{16}TMACl (0.38 g), NH_4OH (1 mL) and H_2O (6 mL) (Experiment 3a)]

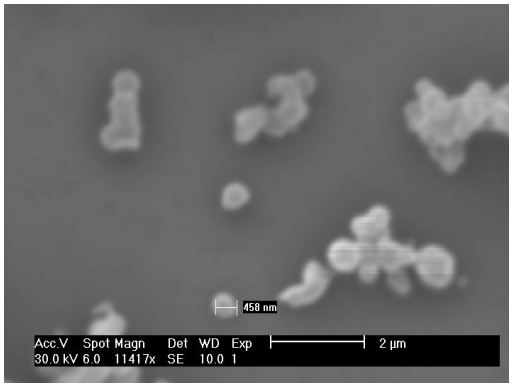

SEM image of mesoporous silica prepared using methanol [BTEE (0.4 mL), C_{16}TMACl (0.38 g), NH_4OH (1 mL) and H_2O (10 mL) (Experiment 4a)]

Figure 3.14 SEM images of different batches of mesoporous silica prepared using (Method a)

Experiment (5a) was carried out by increasing the proportion of ethanol in the reaction but still the dispersion of the obtained silica in water was very poor. No SEM and further characterization of this batch was carried out as it sedimented rapidly making it unsuitable for the job. The ethylene bridge of the silica precursor could hinder the growth of the particles, possibly accounting for the poor spherical

shape of the particles and some apparently amorphous materials. Bridging between particles may account for the tendency for these particles to irreversibly aggregate.

3.3.2.1b Mesoporous silica prepared from TEOS with a C_{16}TMACl template (Method b)

In these experiments BTEE was replaced by TEOS, which does not have a bridge and ethanol and methanol quantities were varied in an attempt to obtain the desired particle diameter. In Experiment 1b methanol was used as a solvent. An SEM image of the product showed aggregated particles with an average diameter of 337 ± 68 nm (Figure 3.15). The aggregation was reflected in the LSPSA particle size (main population) of 1551 ± 553 nm (Figure 3.15). The proportion of methanol used in the synthesis was then increased (Experiment 2b) in an attempt to reduce the size of the particles and improve the dispersity. SEM images of these silicas showed the particles to be spherical with an average diameter of 323 ± 71 nm. Pre-assessment of the particles show rapid sedimentation.

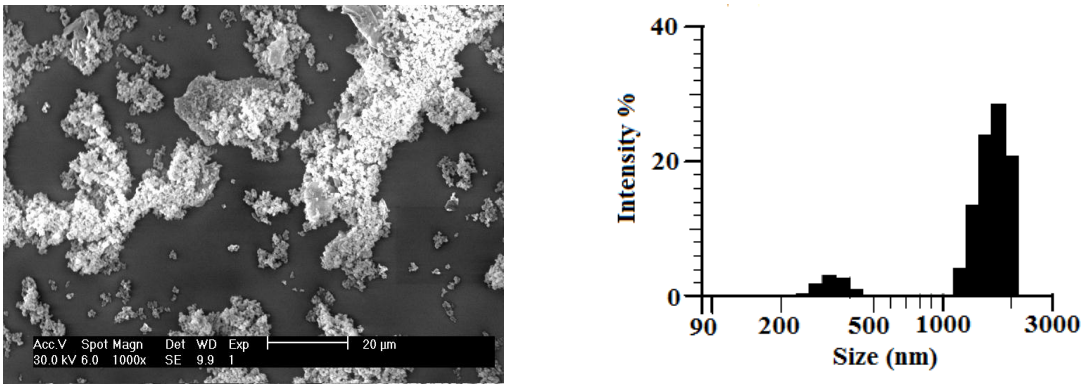

Figure 3.15 SEM image and LSPSA of mesoporous silica prepared using TEOS (0.4 mL), C_{16}TMACl (0.38 g), MeOH (6 mL), NH_4OH (1 mL) and H_2O (6 mL) (Experiment 1b)

Further experiments were carried out using different concentrations of ethanol instead of methanol (Experiment 3b and 4b). Pre-assessment of the production by dispersion in water showed poor dispersion and rapid settlement due to large or aggregated particles as shown in SEM images (Figure 3.16). These particles were

not therefore suitable for use as substrates to prepare nanoscavengers. Generally the particles prepared using this method were smaller than those prepared from BTEE, but they are still bigger than desired.

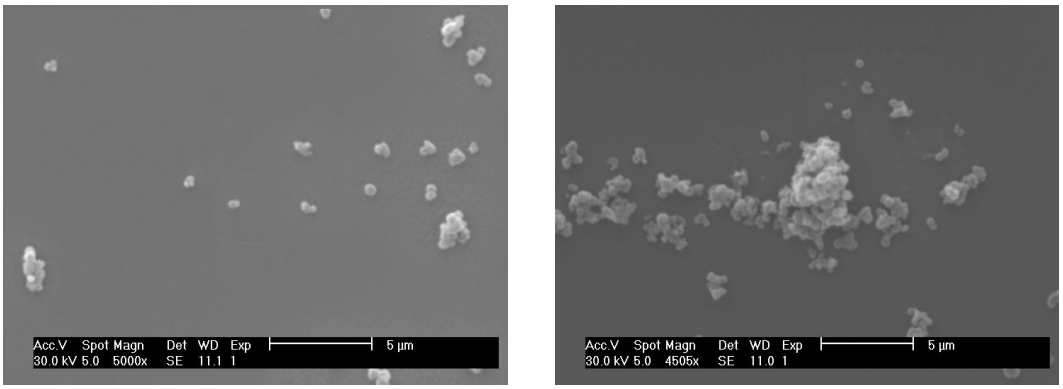

Figure 3.16 SEM image of mesoporous silica prepared using TEOS (0.4 mL), C_{16}TMACl (0.38 g), EtOH (10 mL), NH_4OH (1 mL) and H_2O (10 mL) (Experiment 3b)

3.3.2.1c Mesoporous silica prepared using TEOS and ethylene glycol (Method c)

In these experiments ethylene glycol replaced ethanol or methanol, to increase the viscosity of the reaction solution. This was predicted to lead to the generation of larger numbers of primary particles and hence particles of smaller particle size[39]. The silica precursor was TEOS. A surfactant of shorter chain length (C_{12}TMABr) was adopted as it was expected to reduce the size of the particles[32]. Method c was catalysed by NH_4OH or NaOH, bigger particles being anticipated when the NH_4OH was used. Using NH_4OH as a catalyst is reported to produce long silicate rod-like micelles leading to big particles. Whilst NaOH gives short silicate rod-like micelles leading to small particles[40].

SEM images of silica particles prepared in Experiment 1c (Figure 3.17) show spherical particles and the average particles diameter (SEM) is 288 ± 60 nm. The average particle diameter seemed to have decreased using ethylene glycol. However, the dispersion of the particles in water was still poor, as shown in the LSPSA (Figure 3.17). The average size of the particles according to LSPSA was 2077 ± 1742 nm,

the result being attributable to the aggregation of the particles. The concentration of ethylene glycol were decreased (Experiment 2c and 3c) in order to reduce the size of the particles[39]. Pre-assessment of the particles obtained showed rapid sedimentation of the particles.

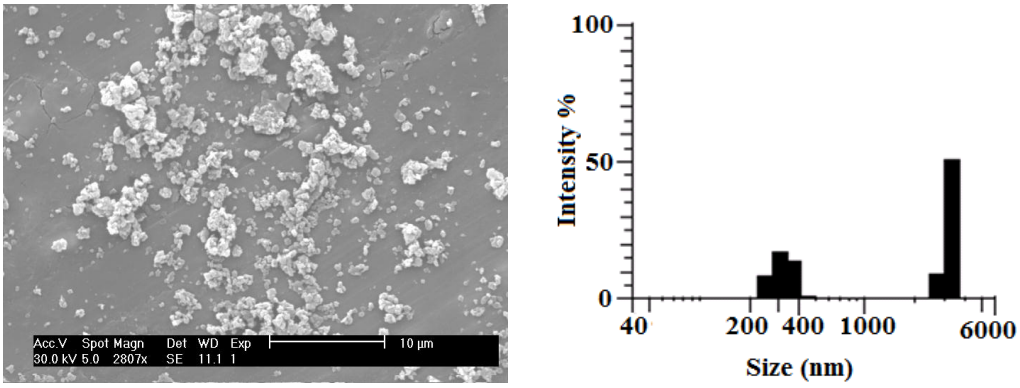

Figure 3.17 SEM image and LSPSA of silica prepared using TEOS (0.45 mL), C_{16}TMACl (0.42 g), ethylene glycol (10 mL), NH_4OH (1 mL) and H_2O (10 mL) (Experiment 1c)

The surfactant and base types were changed in order to obtain spherical silica with an average diameter of 250 nm (Experiments 4c and 5c). Sodium hydroxide was used instead of the NH_4OH and C_{12}TMABr was used instead of the C_{16}TMACl. SEM images of silica prepared in Experiment 4c showed spherical silica with an average diameter 614 ± 274 nm (Figure 3.18). The size of the particles decreased with a decreasing amount of ethylene glycol (Experiment 5c) giving an average particle diameter (SEM) of 332 ± 71 nm (Figure 3.18). This supports the results obtained by Yamada and Yano[39] who found that the size of mesoporous silica particles increases with increasing the proportion of ethylene glycol. There are however some amorphous silica particles (Figure 3.18) that may come about from reducing the proportion of NaOH in the reaction mixture; the spherical morphology of the particles is reported to increase with increasing the proportion of the base[2]. To sum up, changing the amount of ethylene glycol, base and surfactant types was not successful in obtaining the required size of particles.

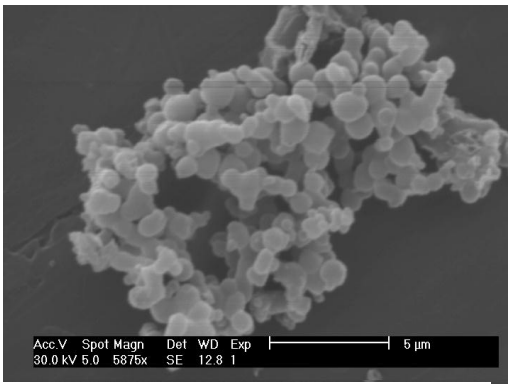

SEM image of mesoporous silica prepared using TEOS (0.45 mL), C_{12}TMABr (0.42 g), ethylene glycol (27 mL), NaOH (1 mL) and H_2O (30 mL) (Experiment 4c)

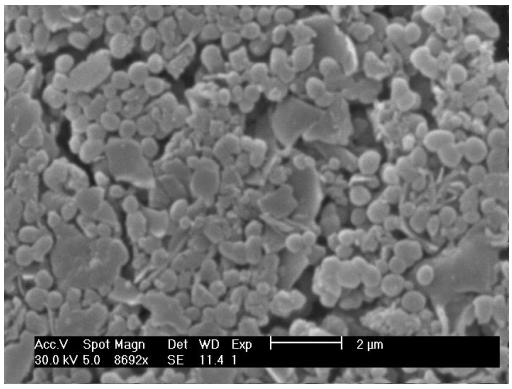

SEM image of mesoporous silica prepared using TEOS (0.45 mL), C_{12}TMABr (0.42 g), ethylene glycol (20 mL), NaOH (1 mL) and H_2O (73 mL) (Experiment 5c)

Figure 3.18 SEM images of different batches of mesoporous silica prepared using (Method c)

3.3.2.1d Mesoporous silica particles prepared using TMOS (Method d)

In this approach, mesoporous silica was successfully synthesized using TMOS as the silica precursor and a C_{12}TMABr template. TMOS hydrolyzes faster than TEOS due to the small leaving group on the TMOS. This phenomenon was noted in experiments as the reaction solution mixture changed from colourless to opalescent and then to a milky colour within one minute of adding TMOS to the solution mixture. This process takes place over 5 minutes in the case of TEOS. The rapid hydrolysis of TMOS can help to generate more (smaller) primary particles that grow to give the final product particles.

In order to increase the viscosity of the reaction mixture ethylene glycol was used instead of ethanol or methanol. The highly viscous solution mixture helps to generate more primary particles. These primary particles work as a seed for the formation of the final particles, and therefore the size of the final particle can be controlled by manipulating the concentration of the reaction mixture[39].

Scanning electron microscope imaging of the particles revealed them to be spherical, with a mean size of ca. 250 ± 35 nm (Figure 3.19), (the size of the particles was calculated by taking the size of 50 particles from the images). All the particles appeared spherical. The laser scattering particle size analyzer gave a mean diameter of 299 ± 52 nm (Figure 3.20), a little higher than the SEM results due to some aggregation of particles.

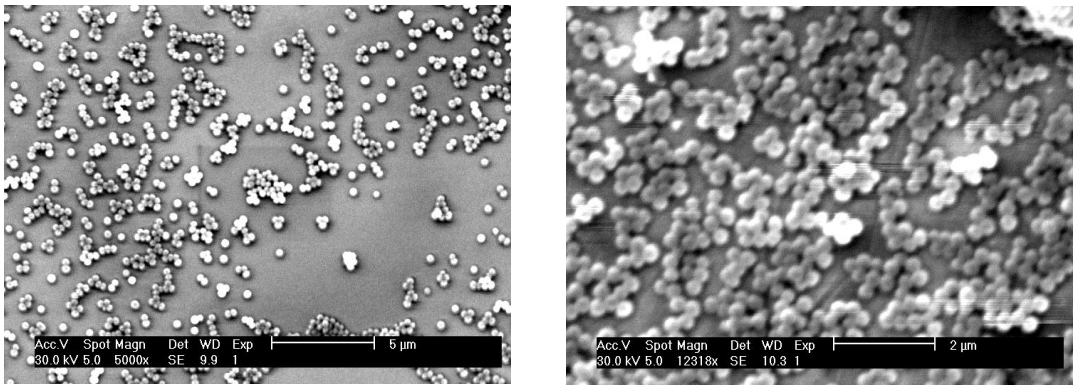

Figure 3.19 SEM images of silica particles prepared from TMOS using a C_{12}TMABr template in ethylene glycol as a solvent (Method d)

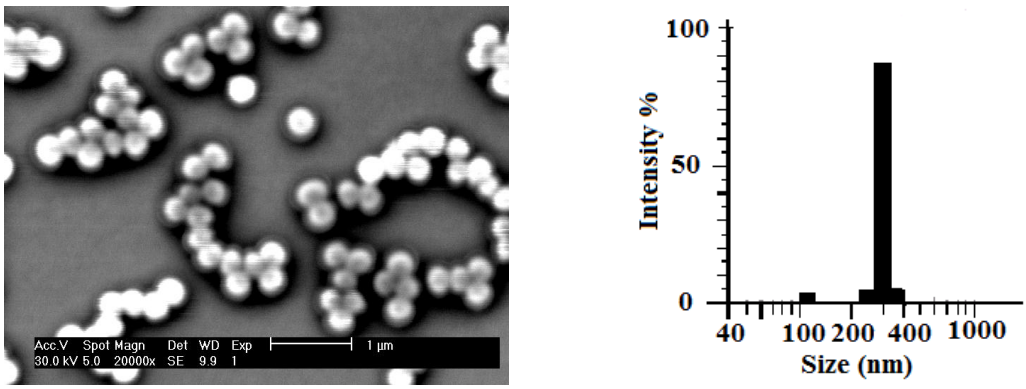

Figure 3.20 SEM and LSPSA of silica prepared using TMOS as silica precursor, a C_{12}TMABr template and ethylene glycol as a solvent (Method d)

The TEM images confirmed the spherical morphology of the silica (prepared in Method d) and the mesoporosity of the particles (Figure 3.21). The calculated pore diameter from the images was 2.88 ± 0.24 nm which indicate these materials classify

as mesoporous type materials. The obtained pore diameters coincide with the pore diameter calculated using the BJH method, as will discussed in Section 3.3.2.

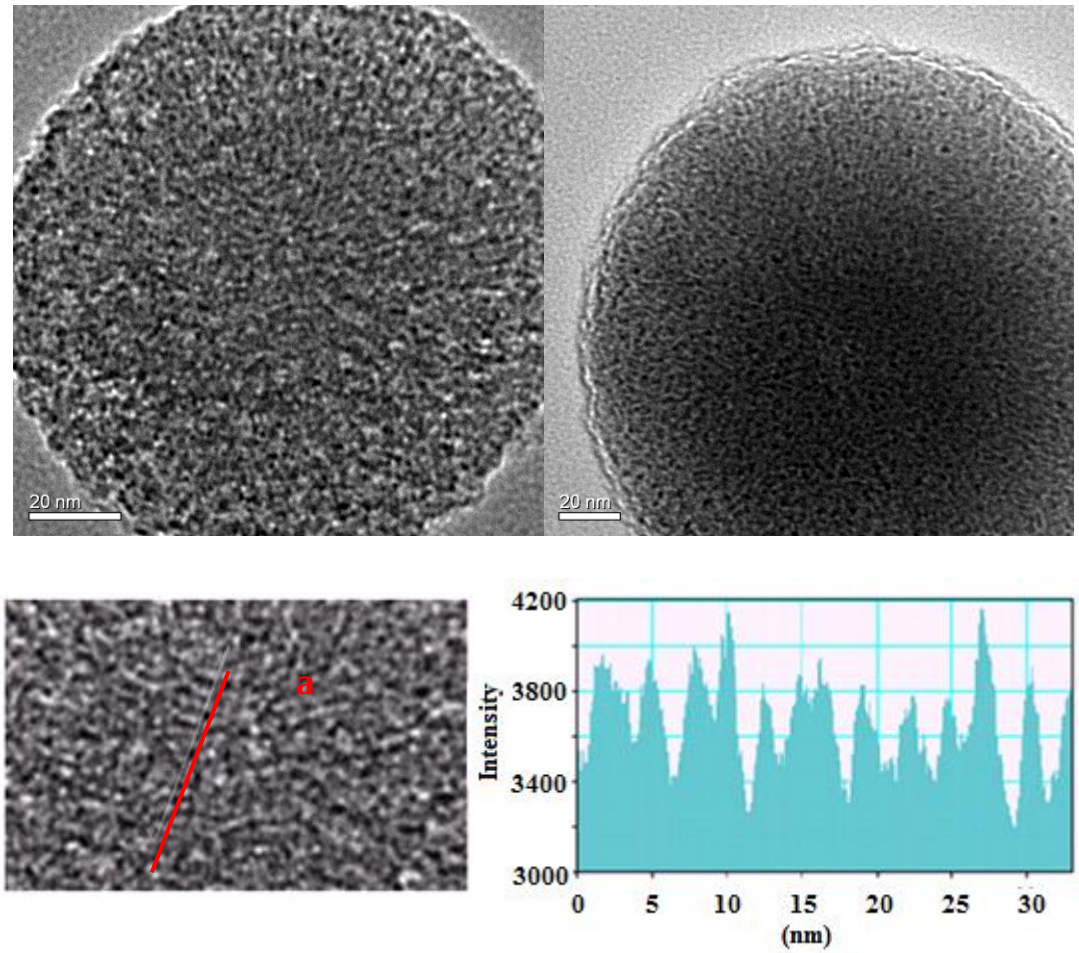

Figure 3.21 TEM images of mesoporous silica (prepared in method d) intensity through the line draw between point (a) and (b)

It has been noticed that some particles were linked together through a bridge of silica (Figure 3.22a). In this bridging area, the hexagonal array was more obvious than in the spherical particles (Figure 3.22b). This may be due to the fact that the formation of hexagonally arrayed cylindrical pores is easier in non-spherical surfaces.

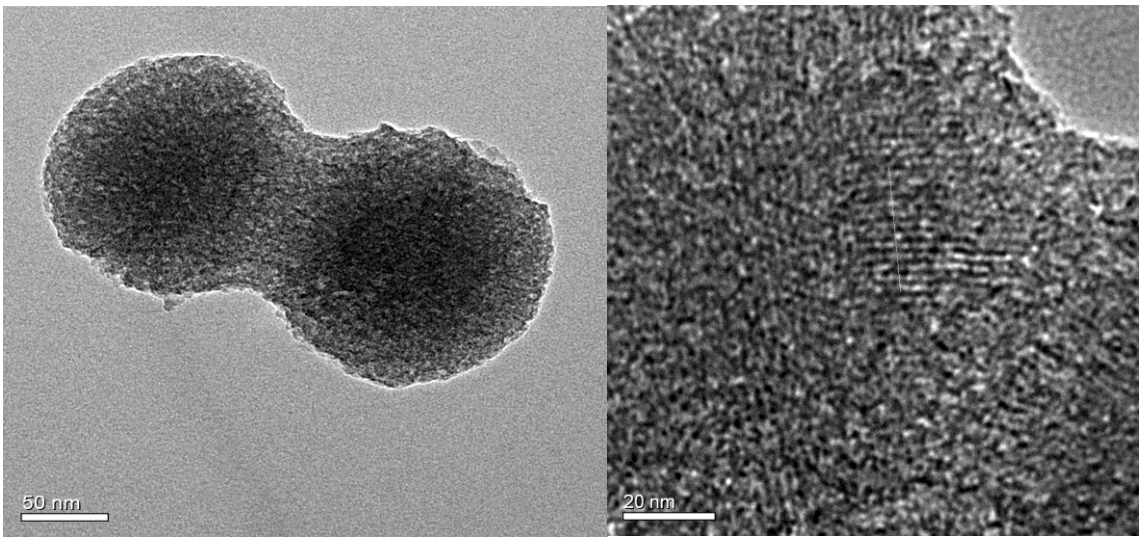

Figure 3.22 TEM images of : a) two particles joined together and b) the area between the particles

3.3.2.2 General comparison of the synthetic methods

Several factors influence the size of the particles such as choice of silica precursor, the length of alkyl chain in the surfactant, alcohol type and base choice. All of these factors were altered in an attempt to change the size of the particles. Table 3.6 summarizes the materials used in each method, together with some of characteristics of the particles produced by each approach.

The choice of silica precursor has a major impact on particle size. The largest particles were obtained when BTEE was used. This may be due to a physical enlargement due to the ethylene bridge in BTEE or its slow hydrolysis rate (no data available) (Method a). TEOS produced smaller particles but those with an average diameter of around 250 nm were easiest to prepare when TMOS was used as the silica precursor. The hydrolysis of TMOS is faster than that of TEOS due to the steric bulk of the EtO^- groups. The fast hydrolysis of TMOS is believed to lead to the rapid generation of small seed particles with limited precursor being available for subsequent particle growth.

Turning next to the solvent type, three were used: methanol, ethanol and ethylene glycol. It has been generally found that the particle size has increased as the proportion of this solvent increased[2, 37, 39, 41]. In order to reduce the size of the particles, the proportion of these solvents in the reaction mixture was therefore decreased. However, the reduction of the organic solvent in the reaction medium led to particles with a wide range of diameters. Thus, it is difficult to control the size whilst maintaining the monodispersity of the particles by changing the type and concentration of the solvent. One of the most effective ways to control the size was found to be using a solvent with a high viscosity such as ethylene glycol. This increases the viscosity of the reaction medium causing the production of a large number of primary particles and results in smaller product particles[39] (as seen in Method d).

Table 3.6 Some characteristics of mesoporous silicas prepared using four different methods

Method	Reaction contents	Particle size (nm)	Dispersion of the particles	Characteristics of the particles
a	BTEE, EtOH or MeOH, NH_4OH, H_2O, $C_{16}TMACl$	450-700	Poor dispersion, rapid sedimentation	Irregular spherical particles, some amorphous particles, aggregated particles
b	TEOS, EtOH or MeOH, NH_4OH, H_2O, $C_{16}TMACl$	300-400	Poor dispersion, rapid sedimentation	Aggregated particles, some amorphous particles
c	TEOS, ethylene glycol, NH_4OH or NaOH, H_2O, $C_{16}TMACl$ or $C_{12}TMABr$	250-400	Poor dispersion, rapid sedimentation	Aggregated particles, some amorphous particles
d	TMOS, ethylene glycol, NaOH, H_2O, $C_{12}TMABr$	299 ± 52	Good dispersion, particles last more than 5 hours without sedimentation	Spherical particles

3.3.2.3 Removal of the template from the structure

Removal of the surfactant from the silica structure was carried out using two approaches: solvent extraction and combustion in air. In Method a (BTEE precursor) solvent extraction was the only possible approach to remove the surfactant as removal of the template by burning would combust the ethylene bridge and lead to the collapse of the silica structure. A mixture of ethanol/hydrochloric acid solution was therefore used to remove the template from the silica structure. The weak electrostatic bond between inorganic materials and the cationic surfactant helps in getting good extraction of the template[42].

TGA of the sample before extraction showed four regions of weight loss (Figure 3.23). A 10 % weight loss appeared between 38 and 120 ºC which may be attributed

to the loss of adsorbed water and residual solvents. This is followed by a large weight loss (23 %) between 120 and 290 ºC due to burning of the surfactant. Ignition of organic materials continued between 290 and 310 ºC. The last area of weight loss for 310 to 775 ºC (9 %) may be assigned to the combustion of residual surfactant molecules or the BTEE ethyl bridge.

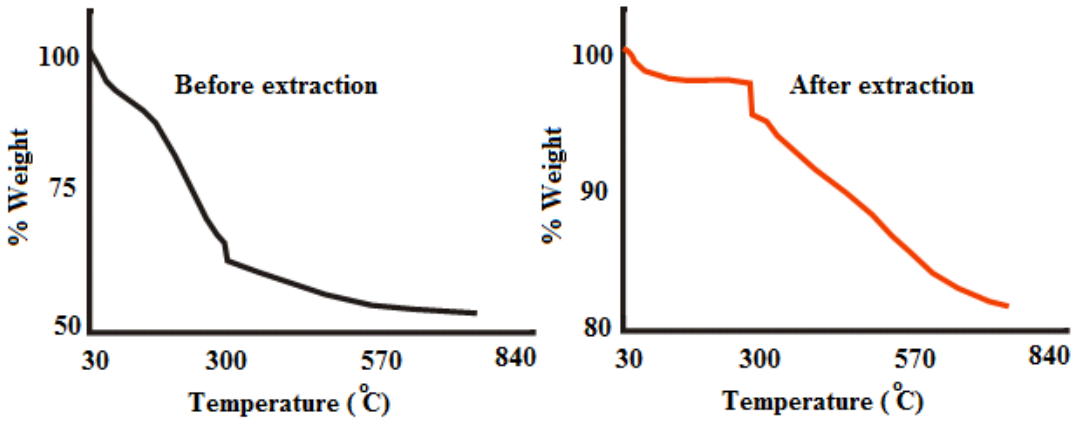

Figure 3.23 Thermogravimetric analysis of mesoporous silica prepared using (Method 1a) (BTEE (0.4 mL), C_{16}TMACl (0.38 mL), water (8 mL), NH_4OH (5 mL), ethanol (5 mL))

The TGA trace of the sample after extraction (Figure 3.23) illustrates three weight losses. The steep weight loss (2.23 %) between 271 and 290 ºC may be attributed to the combustion of residual surfactant from incomplete extraction of the template. A 13 % of weight loss between 290 and 778 ºC is due to the combustion of the ethylene bridge of the silica structure.

FT-IR spectra (Figure 3.24) of silica showed a significant reduction in organic content through a diminution of the CH bands (ca 2900 cm^{-1}) but complete removal of the template by solvent extraction could not be confirmed as, after extraction, the BTEE ethylene bridge should remain.

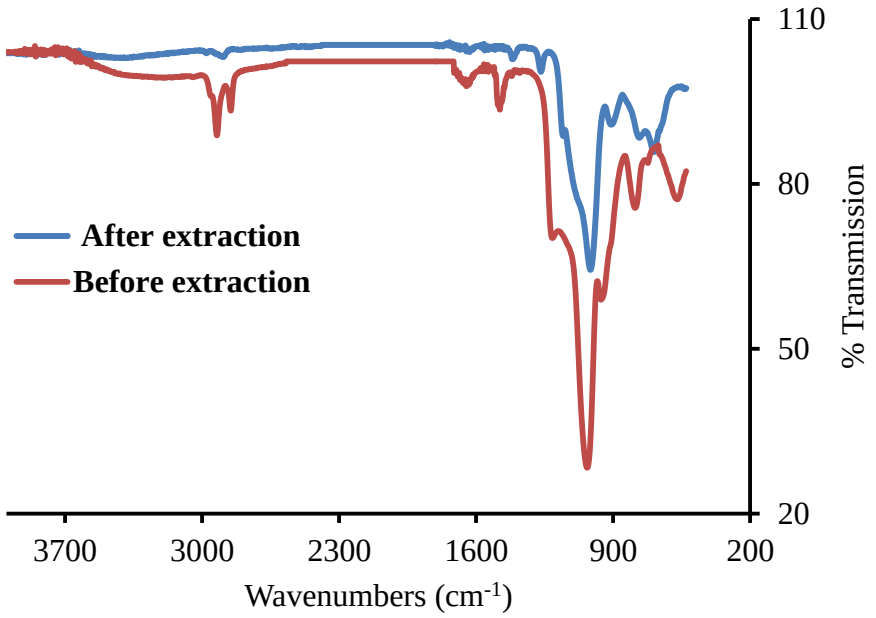

Figure 3.24 FT-IR spectroscopy of mesoporous silica prepared using (Method 1a) [BTEE (0.4 mL) as silica precursor, a C_{16}TMACl template and ethanol (5 mL) as a solvent], before and after solvent extraction of the surfactant

Removal of the template by solvent extraction has some drawbacks. These include solvent consumption; lengthy procedures and incomplete template removal. These drawbacks would limit its implementation unless it was the only option. Calcination was an easier and more efficient means of completely removing the surfactant. The calcination was carried out by burning the as-synthesized mesoporous silicas in air at around 550 ºC, raising the sample to this temperature at a low ramp rate. The removal of the surfactant was confirmed by thermogravimetric analyses in air. A 33.5 % weight loss between 154 ºC and 332 ºC weight loss disappeared from the TG trace after combustion of the silica approving complete removal of the surfactant (Figure 3.25).

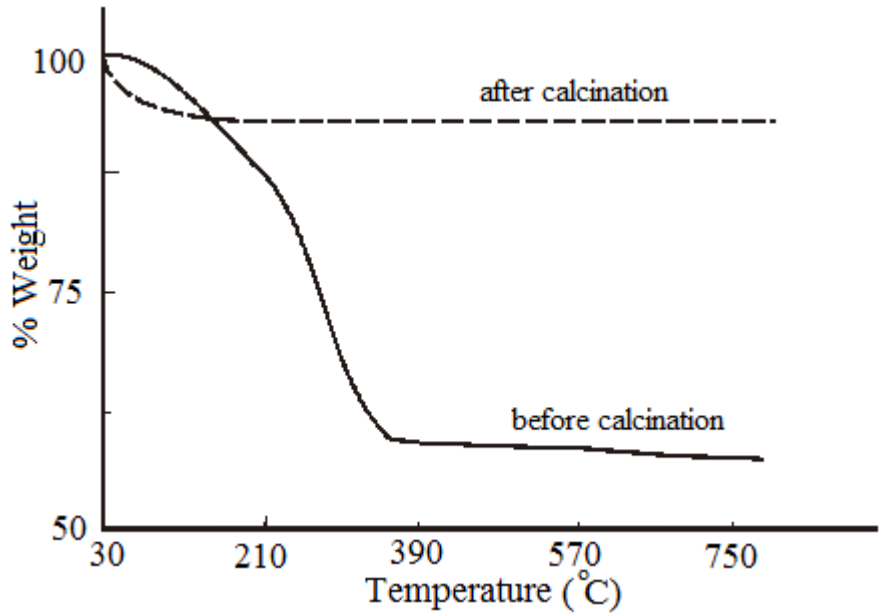

Figure 3.25 Thermal analysis of mesoporous silica (in air) prepared using (Method d) [TMOS as silica precursor, a C_{12}TMABr template and ethylene glycol as a solvent: before and after burning off the surfactant]

Additional confirmation of template removal was obtained by FT-IR spectroscopy. The CH_2 and CH_3 stretching peaks at 2942 and 2853 cm^{-1} were absent after burning off the organic materials (3.26). The siloxane (Si-O-Si) band appears as strong peak at 1059 cm^{-1}. The band appearing at 811 cm^{-1} belongs to Si-O.

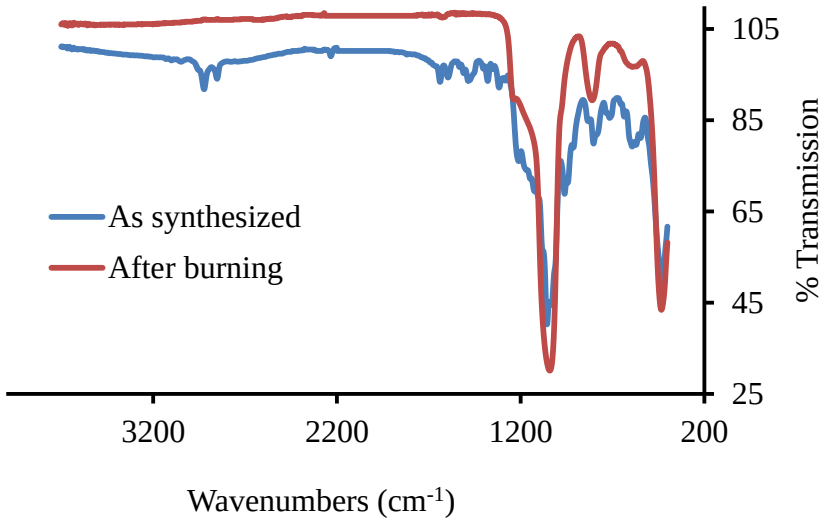

Figure 3.26 FT-IR spectroscopy of mesoporous silica prepared using (Method d) [TMOS as silica precursor, a C_{12}TMABr template and ethylene glycol as a solvent, as synthesized and after burning off the surfactant]

3.3.2.4 Surface area of prepared mesoporous silicas

The surface area of the mesoporous silica was determined using the Brunauer-Emmett-Teller (BET) method. Employing equation (3.1) to calculate the surface area.

$$\frac{1}{W\,[(P_o/P)-1]} = \frac{1}{Wm\,C} + \frac{C-1}{Wm\,C}\left(\frac{P}{P_o}\right) \qquad (3.1)$$

Where C is the BET constant, W is the weight of gas adsorbed at a relative pressure P/P_o and Wm is the weight of adsorbate constituting a monolayer of surface coverage[43]. The pore diameter was measured using Barret, Joyner and Halenda (BJH) method which is the most widely used method for calculations the pore size distribution of mesoporous materials[44].

Measurement of the mesoporous silica surface area, carried out using a N_2 adsorption isotherm, gave high surface areas for the mesoporous silicas (Table 3.7).

Table 3.7 Surface area and pore diameter of mesoporous silicas

Method	Reaction contents	Surface area (m^2 g^{-1})	Pore diameter (nm)
2a	BTEE, MeOH, NH_4OH, H_2O, $C_{16}TMACl$	1208	2.19
3b	TEOS, EtOH, NH_4OH, H_2O, $C_{16}TMACl$	1090	2
1c	TEOS, ethylene glycol, NH_4OH, H_2O, $C_{16}TMACl$	1205	2.18
d	TMOS, ethylene glycol, NaOH, H_2O, $C_{12}TMABr$	1325	2.96

Figure 3.27 to 3.29 show of N_2 adsorption isotherms of mesoporous silicas prepared using methods 2a, 3b and 1c respectively. The isotherms do not precisely belong to Type I or Type IV of the IUPAC isotherm classification [27, 41] but they do possess high surface areas and pores of mesopore dimension (Table 3.7). Despite using three different solvents (methanol, ethanol, ethylene glycol) in the preparations, the pore sizes and surface areas of the samples are quite similar.

The mesoporous silica prepared in Method d showed an isotherm clearly to belong to Type IV[27, 41] according to the IUPAC classification (Figure 3.30). Type IV curves occur when the material is mesoporous (pore widths between 2 and 50 nm)[27]. Similar adsorption isotherms have been reported by Yamada and Yano[39] for their synthesis of monodispersed mesoporous spherical particles using TMOS and $C_{12}TMABr$. The isotherm from the mesoporous silica can be divided to three divisions: the monolayer and multiple adsorption of N_2 on the wall of mesopores of silica, followed by capillary condensation of N_2 inside the mesopores and finally the saturation step[45]. The sudden N_2 uptake at P/Po = 0.96 is as a result of condensation of N_2 between particles[39] (Figure 3.30). The surface area of silica prepared in Method d (Table 3.7) is higher than that obtained in the previous three samples (2a, 3b and 1c). This may be due to a decrease in the size of the particles and enlargement of the pore diameter of the particles in Method d, allowing more N_2 to be adsorbed and leading to higher

surface area. In all figures the adsorption/desorption isotherm curves are reversible showing no hysteresis between the adsorption and desorption branches[46] and showing that the amount of adsorbed gas is almost equal to the amount of desorbed gas. This may due to symmetrical cylindrical pore structure.

The mesoporosities of all samples were confirmed by calculating the pore size distribution using the method proposed by Barrett, Joyner and Halenda (BJH) (Table 3.7). The BJH pore size is based on the Kelvin equation and is widely used for mesoporous materials[47]. This method calculates the pore diameters based on the desorption isotherm. The average pore diameters of mesoporous silicas of samples 2a, 3b and 1c are similar, which indicates little dependence on the type of solvent. A larger pore size was obtained using TMOS as the silica precursor, a C_{12}TMABr template and ethylene glycol solvent (Method d). The average pore diameter calculated based on the BJH method was 2.96 nm and it coincides with the pore diameter (2.88 nm) calculated from TEM images. These results confirm the mesoporosity of the prepared silicas.

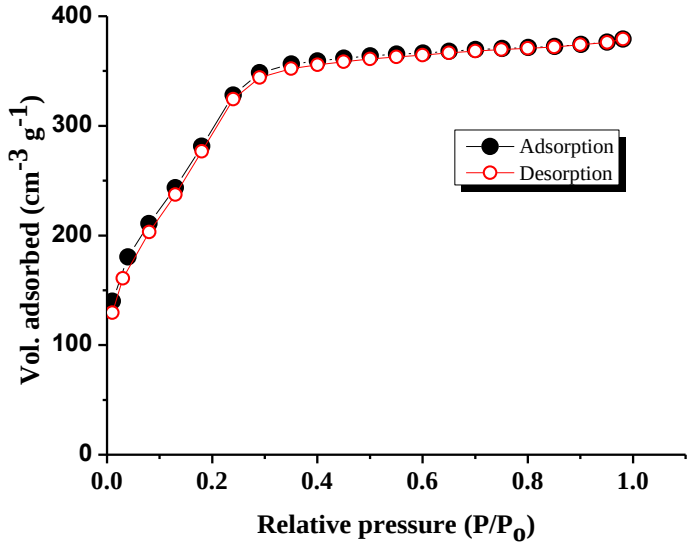

Figure 3.27 N_2 adsorption isotherm of mesoporous silica prepared using BTEE (0.4 mL), C_{16}TMACl (0.38 g), MeOH (12 mL), NH_4OH (1 mL) and H_2O (12 mL) (Experiment 2a)

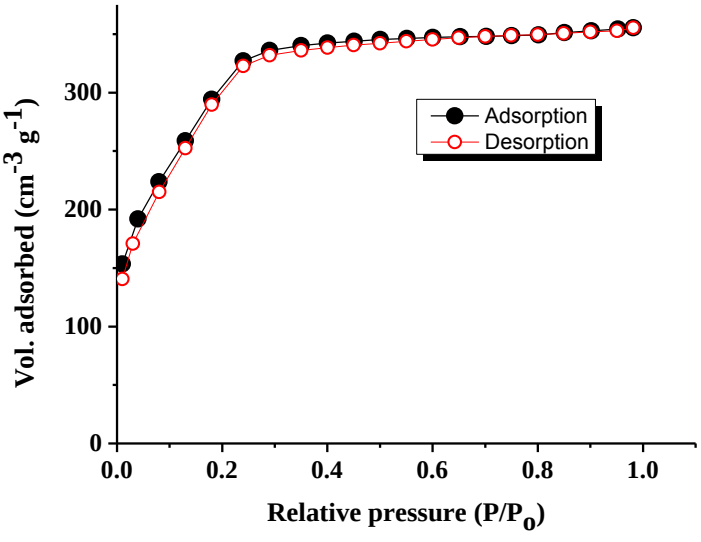

Figure 3.28 N_2 adsorption isotherm of mesoporous silica prepared using TEOS (0.4 mL), C_{16}TMACl (0.38 g), EtOH (10 mL), NH_4OH (1 mL) and H_2O (10 mL) (Experiment 3b)

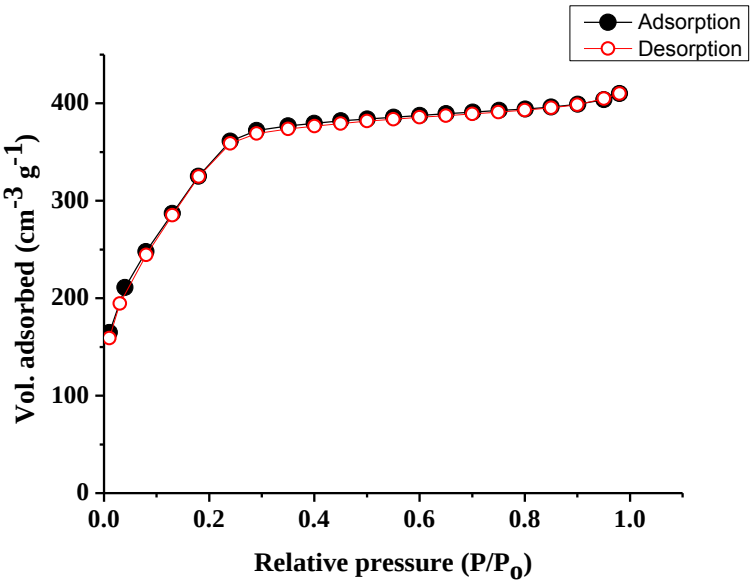

Figure 3.29 N_2 adsorption isotherm of mesoporous silica prepared using TEOS (0.45 mL), C_{16}TMACl (0.42 g), ethylene glycol (10 mL), NH_4OH (1 mL) and H_2O (10 mL) (Experiment 1c)

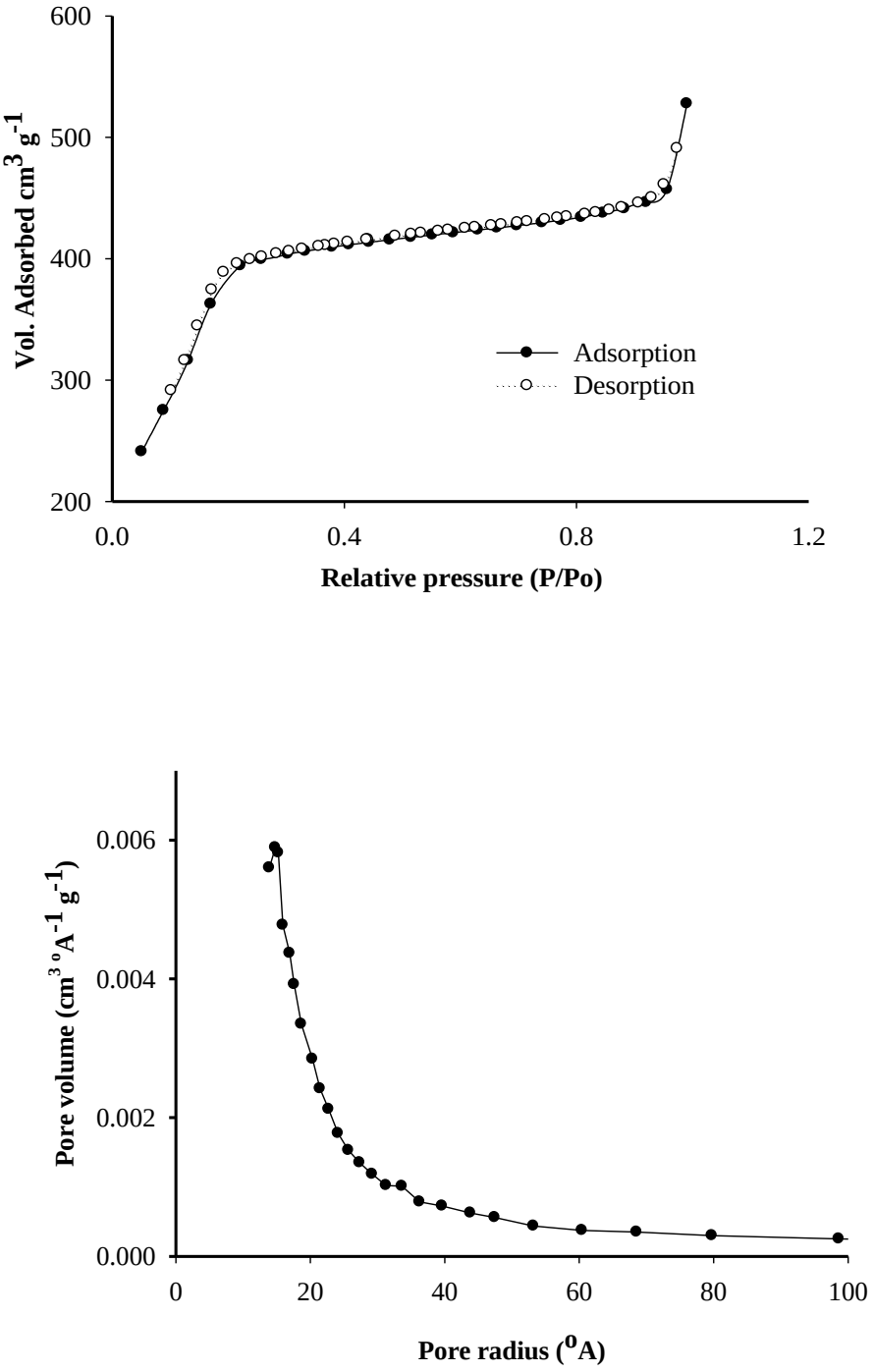

Figure 3.30 N_2 adsorption isotherm and pore size distribution (calculated from the desorption branch using the BJH method) of mesoporous silica prepared using TMOS as silica precursor, a C_{12}TMABr template and ethylene glycol as a solvent (Method d)

3.3.2.5 The settlement rate of mesoporous silica prepared using Method d

Mesoporous silica particles with a mean diameter of ca. 250 nm have been produced for use as a support solid for functionalization with specific active groups. The modified silica particles are then to be used in NSDE techniques. The concept of NSDE is to disperse the particles in water and to allow the particles to move naturally in the sample without external agitation. The particles should stay suspended in the sample long enough for the extraction process to be completed. The stability of the suspended particles in an aqueous solution was therefore examined. 10 mg of mesoporous silica was suspended in 10 mL of deionised water (pre-filtered using 0.1 μm cellulose nitrate membrane filter). 2 mL of the suspended particles were transferred to a 1cm pathlength quartz cuvette. The settling rate of the particles was assessed using a Perkin Elmer Lambda 3 spectrophotometer by monitoring light transmission over time. Figure 3.31 shows the light transmission remained essentially constant for more than 5 hours without obvious sedimentation. The result demonstrates the extremely low sedimentation rate of the particles.

The concentration of silica particles in the water sample influenced the stability of the particles. Increasing the concentration of the particles increased the probability of particle to particle interaction and interparticle collisions. This could cause aggregation of the particles and accelerate the sedimentation rate. The concentration of the silica particles in the deionised water was around 1 mg mL^{-1}. This concentration will be adequate for the nanoscavengers to preconcentrate the analytes from water and will be discussed later.

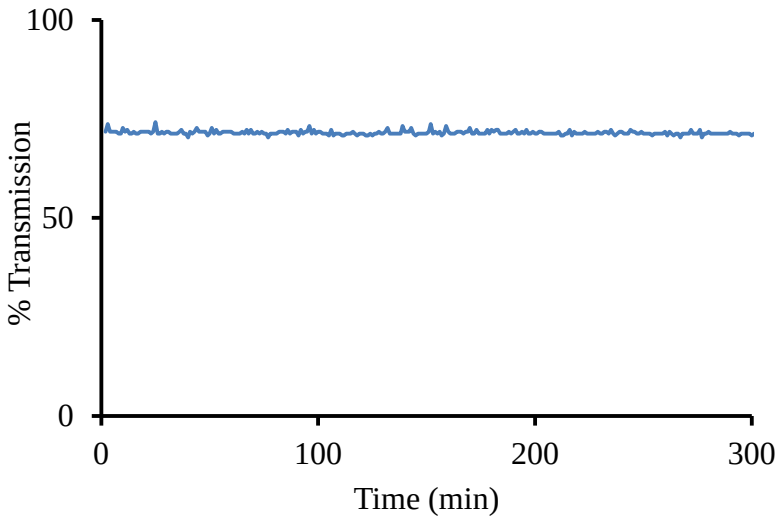

Figure 3.31 Settling of mesoporous silica prepared using TMOS as silica precursor, a C_{12}TMABr template and ethylene glycol as a solvent (Method d) from its suspension in water

3.4 Conclusion

Stöber-type silica particles of around 250 nm diameter were prepared from TEOS in a medium containing methanol and ammonium hydroxide (1:1). The reaction was carried out at room temperature for 2 hours. The particles presented good spherical morphology with monodisperse particle sizes but their surface area was very low according to their N_2 adsorption isotherm (~ 20 m^2 g^{-1}). The low surface area is not favourable to obtain high capacities of surface modification.

A number of attempts have been made to improve the surface area, such as adding BTEE to the reaction mixture during the synthesis of the Stöber-type silica to disrupt the growth of the silica particles. There was not however much change in the surface area after removing the organic materials from the silica particles. Moreover adding NaF during the formation of the Stöber-type silica particles did not improve the surface area. However, using sucrose as a template increased the surface area from

20 to 109 m^2 g^{-1}. The sizes of the particles were not however of the target size (250 nm).

The unique characterisation of mesoporous silica, such as its thermal stability, well-ordered pore size and high surface area makes it a good material for use as a supporting solid phase. Mesoporous silica particles were first synthesized using BTEE or TEOS as a silica precursor with different alkyl chain length of template. The surface areas attained were in the range 1000 to 1200 m^2 g^{-1}, and the size of the particles varied from 300 to 700 nm. The base, silica precursor and alcohol type and concentration were manipulated in an attempt to obtain the right particles size (250 nm). However, adjusting these factors was ineffective to obtain the target particle size (250 nm) with high surface area until TMOS was used as the silica precursor and ethylene glycol as a solvent. Ethylene glycol increased the viscosity of the reaction mixture and led to the generation of more primary particles and decreased the size of the final particles to 250-300 nm. N_2 adsorption isotherms of the mesoporous silica particles gave surface area of ca. 1325 m^2 g^{-1}. These mesoporous silica particles were deemed to possess suitable properties for their use as supporting solid phases, to be further modified to produce a variety of solid phase nanoscavenger extraction materials.

3.5 References

(1) Burleigh, M. C.; Markowitz, M. A.; Spector, M. S.; Gaber, B. P. *Langmuir* **2001**, *17*, 7923-7928.

(2) Stöber, W.; Fink, A.; Bohn, E. *J. Colloid Interface Sci.* **1968**, *26*, 62-69.

(3) Schubert, U.; Husing, N. *Synthesis of Inorganic Materials*; Wiley-VCH: Weinheim, **2005**.

(4) Matsoukas, T.; Gulari, E. *J. Colloid Interface Sci.* **1988**, *124*, 252-261.

(5) Matsoukas, T.; Gulari, E. *J. Colloid Interface Sci.* **1989**, *132*, 13-21.

(6) Bogush, G. H.; Zukoski, C. F. *J. Colloid Interface Sci.* **1991**, *142*, 19-34.

(7) Bogush, G. H.; Zukoski, I., C. F. *J. Colloid Interface Sci.* **1991**, *142*, 1-18.

(8) Green, D. L.; Lin, J. S.; Lam, Y. F.; Hu, M. Z. C.; Schaefer, D. W.; Harris, M. T. *J. Colloid Interface Sci.* **2003**, *266*, 346-358.

(9) Jafarzadeh, M.; Rahman, I. A.; Sipaut, C. S. *J. Sol-Gel Sci. Technol.* **2009**, *50*, 328-336.

(10) Park, S. K.; Do Kim, K.; Kim, H. T. *Colloid Surf. A-Physicochem. Eng. Asp.* **2002**, *197*, 7-17.

(11) Rahman, I. A.; Vejayakumaran, P.; Sipaut, C. S.; Ismail, J.; Abu Bakar, M.; Adnan, R.; Chee, C. K. *Ceram. Int.* **2006**, *32*, 691-699.

(12) Venkatathri, N. *J. Indian Chem. Soc.* **2008**, *85*, 1143-1145.

(13) Razo, D. A. S.; Pallavidino, L.; Garrone, E.; Geobaldo, F.; Descrovi, E.; Chiodoni, A.; Giorgis, F. *J. Nanopart. Res.* **2008**, *10*, 1225-1229.

(14) Rahman, I. A.; Vejayakumaran, P.; Sipaut, C. S.; Ismail, J.; Abu Bakar, M.; Adnan, R.; Chee, C. K. *Colloid Surf. A-Physicochem. Eng. Asp.* **2007**, *294*, 102-110.

(15) Howard, A. G.; Khdary, N. H. *Analyst* **2005**, *130*, 1432-1438.

(16) Etienne, M.; Sayen, S.; Lebeau, B.; Walcarius, A. *Nanopor. Mater. III* **2002**, *141*, 615-622.

(17) Hai, N. H.; Grigoriants, I.; Gedanken, A. *J. Phys. Chem. C* **2009**, *113*, 10521-10526.

(18) Kim, S. H.; Liu, B. Y. H.; Zachariah, M. R. *Langmuir* **2004**, *20*, 2523-2526.

(19) Ui, S. W.; Lim, S. J.; Lee, S. H.; Choi, S. C. *J. Ceram. Process. Res.* **2009**, *10*, 553-558.

(20) Prouzet, T.; Boissiere, C. *C. R. Chim.* **2005**, *8*, 579-596.

(21) Wang, L. Z.; Shao, Y. F.; Zhang, J. L.; Anpo, M. *Micropor. Mesopor. Mater.* **2007**, *100*, 241-249.

(22) Xia, Q. H.; Hidajat, K.; Kawi, S. *Chem. Lett.* **2001**, *7*, 654-655.

(23) Xia, Q. H.; Hidajat, K.; Kawi, S. *Mater. Lett.* **2000**, *42*, 102-107.

(24) Iler, R. K. *The chemistry of silica : solubility, polymerization, colloid and surface properties, and biochemistry*; Wiley: New York, **1979**.

(25) Da Costa, J. C. D.; Coombs, S.; Lim, J.; Lu, G. Q. *J. Sol-Gel Sci. Technol.* **2004**, *31*, 215-218.

(26) Chen, H.; Zhou, S. X.; Gu, G. X.; Wu, L. M. *J. Disper. Sci. Technol.* **2004**, *25*, 837-848.

(27) Balbuena, P. B.; Gubbins, K. E. *Langmuir* **1993**, *9*, 1801-1814.

(28) Kim, S. S.; Kim, H. S.; Kim, S. G.; Kim, W. S. *Ceram. Int.* **2004**, *30*, 171-175.

(29) Sang, H. J.; Jun, S.; Ryoo, R. *Micropor. Mesopor. Mater.* **2000**, *153*, 158-161.

(30) He, Q. J.; Cui, X. Z.; Cui, F. M.; Guo, L. M.; Shi, J. L. *Micropor. Mesopor. Mater.* **2009**, *117*, 609-616.

(31) Fowler, C. E.; Khushalani, D.; Lebeau, B.; Mann, S. *Adv. Mater.* **2001**, *13*, 649-652.

(32) Yano, K.; Fukushima, Y. *J. Mater. Chem.* **2004**, *14*, 1579-1584.

(33) Yano, K.; Suzuki, N.; Akimoto, Y.; Fukushima, Y. *Bull. Chem. Soc. Jpn.* **2002**, *75*, 1977-1982.

(34) Lin, Y. S.; Tsai, C. P.; Huang, H. Y.; Kuo, C. T.; Hung, Y.; Huang, D. M.; Chen, Y. C.; Mou, C. Y. *Chem. Mater.* **2005**, *17*, 4570-4573.

(35) Suzuki, K.; Ikari, K.; Imai, H. *J. Am. Chem. Soc.* **2004**, *126*, 462-463.

(36) Lin, H. P.; Tsai, C. P. *Chem. Lett.* **2003**, *32*, 1092-1093.

(37) Yano, K.; Fukushima, Y. *J. Mater. Chem.* **2003**, *13*, 2577-2581.

(38) Chen, Q. R.; Han, L.; Gao, C. B.; Che, S. N. *Micropor. Mesopor. Mater.* **2010**, *128*, 203-212.

(39) Yamada, Y.; Yano, K. *Micropor. Mesopor. Mater.* **2006**, *93*, 190-198.

(40) Cai, Q.; Luo, Z. S.; Pang, W. Q.; Fan, Y. W.; Chen, X. H.; Cui, F. Z. *Chem. Mater.* **2001**, *13*, 258-263.

(41) Rebbin, V.; Jakubowski, M.; Potz, S.; Froba, M. *Micropor. Mesopor. Mater.* **2004**, *72*, 99-104.

(42) Hua, Z. L.; Shi, J. L.; Wang, L.; Zhang, W. H. *J. Non-Cryst. Solids* **2001**, *292*, 177-183.

(43) Brunauer, S.; Emmett, H.; Teller, E. *J. Am. Chem. Soc.* **1938**, *60*, 309-319.

(44) Groen, J. C.; Peffer, L. A. A.; Perez-Ramirez, J. *Micropor. Mesopor. Mater.* **2003**, *60*, 1-17.

(45) Tai, X. M.; Wang, H. X.; Shi, X. Q. *Chin. Chem. Lett.* **2005**, *16*, 843-845.

(46) Zheng, S.; Gao, L.; Guo, J. K. *Mater. Chem. Phys.* **2001**, *71*, 174-178.

(47) Barrett, E. P.; Joyner, L. G.; Halenda, P. P. *J. Am. Chem. Soc.* **1951**, *73*, 373-380.

Chapter 4
Synthesis and characterization of amino-nano-scavengers

4.1 Introduction

Silica particles are just one of the many types of solid phase used in solid phase extraction. Their advantage over most other materials is that the surface of the silica can be readily modified with organic materials to optimize the selectivity of the particles. Covalent bonding of the organic modifier on the surface of silica generally results in a stable material which can be used over a relatively wide pH range.

Among the available organic modifiers which can be linked to silica are those containing amine groups. The amine groups can be grafted onto the silica either post synthesis of the silica particles or during particle formation. Functionalization during silica formation can be achieved by co-condensation of aminotrialkoxysilanes with TEOS or TMOS[1]. The post synthesis approach may be preferable as particle structure is stabilized before coverage of the surface and inside of the pores with the grafting agent. Incorporation of the amine groups during the process of forming the particles may also lead to the trapping of amine groups inside the structure of silica preventing the metal ions from reaching the ligand. Table 4.1 illustrates some of the differences between synthesis during formation of silica and post synthesis functionalization.

Table 4.1 Differences between the main two approaches to the synthesis of aminosilica

Characteristics	Incorporation of amine groups during silica formation	Post synthesis amination
Reaction step	One	Two
Amine position	Inside the structure and outer surface	Just on the surface and inside the pores.
Amine capacity	High	Low

A number of researchers have reported the immobilization of amino groups on the surface of silica[2, 3]. The amino-silicas can themselves be utilized as extractants, but they are also a useful base through which more specific functional groups can be linked to the silica. For example, amino-silica prepared by the post-synthesis approach was used to extract Pb^{2+} and Cu^{2+} from water[4]. The adsorption capacity was affected by the pH value. The best adsorption capacity achieved for Cu^{2+} was 0.57 mmol g^{-1} at pH 7.1 and 0.09 mmol g^{-1} for Pb^{2+} at pH 4.7. Amine-functionalized mesoporous silicas have also been prepared by post synthesis modification with N-N-dimethyldodecylamine and dodecylamine groups. The amino-silicas were capable of complexing Cd^{2+}, Co^{2+}, Cu^{2+} and Pb^{2+} from an aqueous solution[5].

Amine-functionalized silicas are not limited to metal extraction but can be employed to immobilize other materials. For example, functionalized spherical silica particles have been prepared by co-condensation of 3-aminopropyltrimethoxysilane ($NH_2Si(OMe)_3$) and TEOS. The aminopropyl-silica was applied to covalently link glucose oxide on the surface and the product exhibited high stability[6]. Amino-silica particles (25 nm) prepared by Kemin *et al.*[7] were used as carriers to deliver antisense oligonucleotides to treat cancer cells. Aminopropyl-silica was synthesized and used to immobilize o-hydroxybenzophenone onto the silica surface [8].

The quantity of amine groups that can be loaded onto a silica surface is governed by several factors, such as the types of silica used (porous or non-porous) and the method of preparation. It is clear that porous silicas can accept higher loads than non-porous silica materials because of their large surface areas. Typical synthetic approaches can immobilize between 1 and 1.5 mmol g^{-1} of amine groups. However, a special synthetic modification was developed using ethylenediamine to catalyze the reaction between 3-aminopropyldimethylethoxysilane and hydroxyl groups of silica surface that achieved more than 3 mmol g^{-1} of amine loading[9].

A further point to note is that with most commercially available amine modifiers the amino groups are linked to a propyl chain terminating in a silicon alkoxide. The reaction between silanol groups on the surface of the silica and the amino-silicon alkoxide molecules proceeds with the hydrolysis of the alkoxy groups (first step) followed by the covalent bonding of the hydroxysilane product (second step), resulting in the formation of an amino-silica[10, 11]. The silanization reaction can be carried out using unhydrated or hydrated (that is thermally untreated) silica. When the silanization is accomplished on silica under aqueous conditions or hydrated silica in toluene, the product illustrates a higher degree of polymerization on the silica surface as the water catalyzes the hydrolysis of alkoxysilane. The disadvantage of the wet method is that the amino-alkoxysilane can self polymerize outside the surface of the silica[12].

This chapter describes work carried out to synthesize and characterize amino-nanoscavengers, functionalized with a primary amine (Figure 4.1) and ethylenediamine (Figure 4.2). These amino-nanoscavengers are to be used as starting materials for the preparation of a range of new chelating nanoscavengers.

The amino-nanoscavengers were characterized using scanning electron microscopy, laser scattering particle size analysis; thermogravimetric analysis and Fourier transform infrared spectroscopy. Amino group loadings on the silica were assessed by measuring the copper capacity.

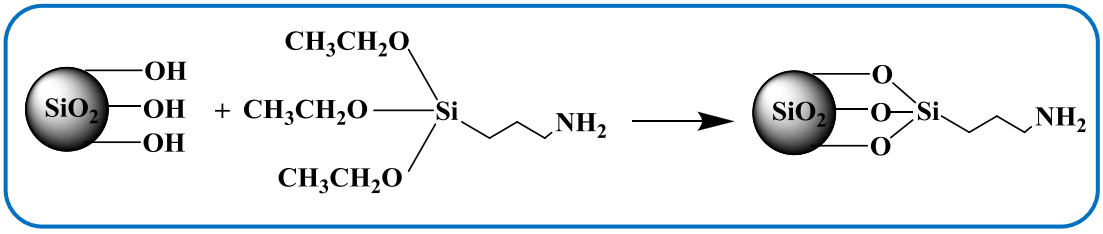

Figure 4.1 Modification of silica particles with 3-aminopropyltriethoxysilane ($NH_2Si(OEt)_3$)

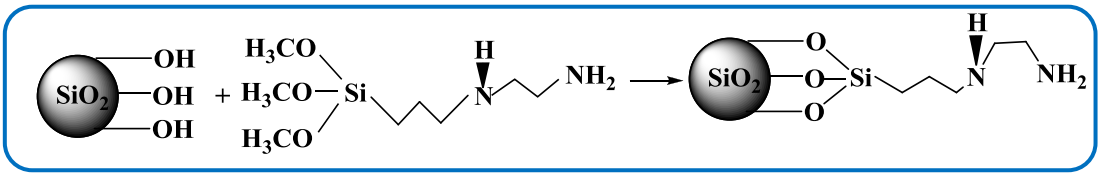

Figure 4.2 Modification of silica particles with [3-(2-aminoethyl)aminopropyl]-trimethoxysilane (Z-6094)

4.2 Experiments

4.2.1 Materials

TEOS (98 %) and $NH_2Si(OEt)_3$ (99 %) were obtained from Aldrich (Poole, UK). Z-6094 (96 %) and C_{12}TMABr were supplied by Alfa Aesar (Lancashire, UK). Ammonium hydroxide (SG = 0.88), methanol and ethanol were laboratory grade. Whatman cellulose nitrate membrane filters (47 mm diameter, pore size 0.2 µm) and toluene were supplied by Fisher Scientific (Loughborough, UK). The toluene was dried using Dean-Stark apparatus.

Acetate buffer was prepared by dissolving 3.402 g of sodium acetate trihydrate in 200 mL of 0.1 mol L^{-1} of acetic acid and the pH was adjusted to 5.7 using 0.5 M sodium hydroxide. The volume was then made up to 250 mL using deionised water. A standard copper solution containing 1000 µg mL^{-1} of Cu^{2+} was prepared by dissolving 0.393 g of copper (II) in 95 mL of deionised water and 5 mL of acetate

buffer. All apparatus was soaked in nitric acid (5 % v/v) and rinsed with deionised water before use.

4.2.2 Characterization of amine-nanoscavengers

Preparation of the samples for the instruments was carried out according to the methods described in Section 3.1.2.

4.2.3 Synthesis of diamino-nanoscavengers ($DiNH_2@SiO_2$)

4.2.3.1 Diamine modification of pre-formed Stöber-type silica

Dried toluene (80 mL) was transferred to a three necked round-bottomed flask (250 mL) fitted with a condenser and under a N_2 atmosphere. Nano-sized sized Stöber-type silica (1 g) with a BET surface area of ca. 20 m^2 g^{-1} (prepared as described in Section 3.1.3.2 and then dried in an oven at 120 ºC overnight) was dispersed in dried toluene. The mixture was stirred using a magnetic stirrer for 15 minutes and then heated at 95 ºC, whilst maintaining the stirring. Z-6094 (1 mL) was slowly added to the flask after the temperature had stabilized. After 8 hours, the reaction mixture was allowed to cool. The product was isolated by centrifugation, rinsed thoroughly with toluene five times and twice with methanol. The white solid was then dried for five hours under continuous vacuum.

4.2.3.2 Diamine modification of pre-formed mesoporous silica in dried toluene

This experiment was carried out according to the method described in Section 4.2.3.1, except that mesoporous silica (prepared as described in Section 3.3.1.4) was used instead of Stöber-type silica.

4.2.3.3 Diamine modification of pre-formed mesoporous silica in ethanol

Ethanol (30 mL) was transferred to a three necked round-bottomed flask (100 mL) fitted with a condenser. Mesoporous silica (0.07 g) (prepared as described in Section 3.3.1.4 and then dried overnight at 120 ºC in an oven) was dispersed in ethanol. The mixture was mixed using a magnetic stirrer for 15 minutes and then heated under N_2 to 80 ºC, whilst maintaining the stirring. 0.8 mL of Z-6094 was slowly added. After 8 hours, the reaction mixture was stirred overnight at room temperature. The white suspension was then centrifuged and the supernatant was removed. The product was rinsed with ethanol five times, and dried overnight under continuous vacuum.

4.2.4 Synthesis of aminopropyl-nanoscavengers ($NH_2@SiO_2$)

4.2.4.1 Grafting of the monoamine onto mesoporous silica in dry toluene

Mesoporous silica (4 g) (prepared as described in Section 3.3.1.4 and then dried overnight at 120 ºC) and dried toluene (200 mL) were transferred to a two necked round-bottomed flask (500 mL) fitted with a condenser. The mixture was sonicated for an hour and heated to 90 ºC under N_2 and stirring. Dried toluene (30 mL) and $NH_2Si(OEt)_3$ (4 mL) were transferred to the dropping funnel under N_2 and after mixing were added to the reaction flask slowly. The reaction was left to proceed at 90 ºC under N_2 and stirring for 8 hours. The mixture was left to cool for an hour. The solid product was isolated by centrifugation for 15 minutes at 8400 g, rinsed with dried toluene five times and three additional times with ethanol and dried under continuous vacuum.

4.2.4.2 Post-synthesis grafting of a monoamine onto mesoporous silica in ethanol

Mesoporous silica (0.1 g) (prepared as described in Section 3.3.1.4) and ethanol (20 mL) were transferred to a conical flask (50 mL). The mixture was sonicated for an

hour, $NH_2Si(OEt)_3$ (0.1 mL) was added and the reaction was left to proceed under stirring for 14 hours at 20 ºC. The white product was isolated by centrifugation for 5 minutes at 8500 g, and rinsed with ethanol five times, and then dried under continuous vacuum.

4.2.4.3 Grafting of a monoamine onto Stöber-type silica

This experiment was carried out according to the method described in Section 4.2.4.1, except that Stöber-type silica (prepared as described in Section 3.1.3.2) was used instead of the mesoporous silica.

4.2.4.4 Single pot synthesis of $NH_2@SiO_2$

C_{12}TMABr (1.68 g) was dissolved in a mixture containing ethylene glycol (90 mL), deionised water (310 mL) and NaOH (3 mL). The mixture was stirred for 15 minutes using a magnetic stirrer. TMOS (1.8 mL) and $NH_2Si(OEt)_3$ (1.8 mL) were mixed together and then added to the reaction mixture. The reaction was left to proceed at 20 ºC for three days. The white product was centrifuged, rinsed with water five times and left in a fume cupboard to dry. Removal of the surfactant was carried out by Soxhlet extraction using ethanol. The solvent was changed every 12 hours for 3 days. The product was dried under continuous vacuum.

4.2.5 Measurement of copper capacity

An accurate (10 mg) weight of modified nano-sized silica particles was placed in a polyethylene tube (10 mL). Buffered (pH 5.7) copper (II) solution (5 mL, 1000 µg mL^{-1}), was added to the tube. The mixture was shaken for 5 minutes, the tube was centrifuged and the supernatant discarded. The product was rinsed 5 times with deionised water. Hydrochloric acid (10 mL, 6 M) was added to the tube, the mixture was centrifuged and the acidic solution was then transferred to a volumetric flask (100 mL). A second aliquot of HCl (10 mL) was added to silica, and the resulting

acidic solution was added to the volumetric flask. The flask was made up to the mark and the copper content of the solution was measured by FAAS.

4.3 Results and discussion

Primary amine and ethylenediamine moieties were chemically immobilized on both Stöber-type silica and mesoporous silica. Two different synthetic approaches were evaluated. Post-synthesis grafting methods were based on the modification of pre-formed silica particles and a single pot synthesis, in which the amine precursor is added during the formation of the silica particles.

4.3.1 Diamino-nanoscavengers ($DiNH_2@SiO_2$)

The surface of silica particles were modified with diamino- groups using Z-6094. Post grafting synthesis was applied to immobilized diamino- groups on the silicas. Two solvent types were explored to maximize the loading groups on the silicas surface.

4.3.1.1 Morphology and size distribution of $DiNH_2@SiO_2$ particles

The particle sizes of the diaminosilicas were assessed using a laser scattering particle size analysis (LSPSA) (Table 4.2). It is clear from these measurements that the diamine silicas were significantly larger than the starting materials. This could be attributed to aggregation of the diaminosilica particles but no confirmatory SEM study was carried out for most of the diamine functionalized silicas as these batches exhibited low copper capacities as will be discussed in Section 4.3.1.5.

Whilst LSPSA of $DiNH_2@SiO_2$ (prepared using mesoporous silica in dried toluene), revealed particles with a mean diameter of 551 nm (standard deviation of 33 nm) (Figure 4.3). SEM (Figure 4.4) showed the particles to be spherical with a mean size of 249 ± 24 nm. This discrepancy in size results was believed to be due to aggregation of the particles in the sample suspension used for the LSPSA. The

morphology of the particles in this batch was spherical (Figure 4.4) indicating no apparent effect of the modification on the morphology.

Table 4.2 Average particle sizes of silicas and diaminosilicas

Batch	Solvent	LSPSA (nm) Size ± SD	SEM (nm) Size ± SD
Stöber-type silica	----	244 ± 15	----
$DiNH_2@SiO_2$ (I) (Stöber-type silica)	Toluene	350 ± 73	----
Mesoporous silica	----	299 ± 52	250 ± 35
$DiNH_2@SiO_2$ (II) (Mesoporous silica)	Toluene	551 ± 33	249 ± 24
$DiNH_2@SiO_2$ (III) (Mesoporous silica)	Ethanol	667 ± 120	----

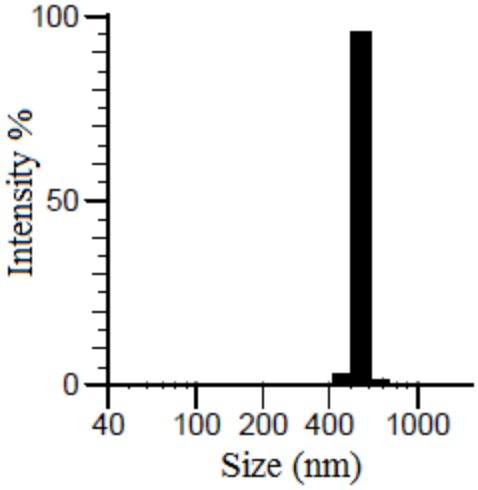

Figure 4.3 LSPSA of $DiNH_2@SiO_2$ (prepared using mesoporous silica in toluene)

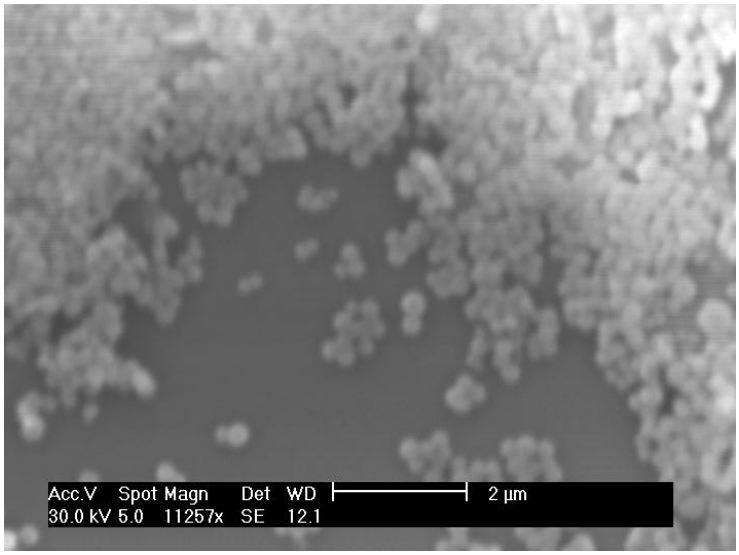

Figure 4.4 SEM image (11257X magnification) of $DiNH_2@SiO_2$ (II) (prepared using mesoporous silica in toluene)

4.3.1.2 Thermogravimetric analysis (TGA) study of $DiNH_2@SiO_2$

Thermogravimetric analysis was carried out to confirm the loading of diamino groups on the surface of the silica. The analysis was carried out between 25 and 800 ºC at a heating rate of 5 ºC / min in an air atmosphere. Figure 4.5 shows the thermogravimetric traces from different $DiNH_2@SiO_2$ syntheses. The TGA trace of $DiNH_2@SiO_2$ prepared using mesoporous silica in dried toluene shows 7 % weight loss (Figure 4.5c) between 27-126 ºC, attributed to residual solvent and adsorbed water. Around 13 % weight loss between 126 and 434 ºC, followed by 8 % weight loss, at a temperature range of 434-773 ºC due to oxidation of organic materials. On the other hand, 2 % and 12 % of the weight loss (Figure 4.5b) was observed between 126-254 ºC and 254-773 ºC, respectively, when ethanol was used as a solvent to immobilize diamino moiety on the surface of mesoporous silica. The modification carried out in dried toluene rather than ethanol, gave a higher diamine loading, as ethanol can hinder the hydrolysis process[12]. Modification of the Stöber-type silica shows just a 6 % weight loss between 126-773 ºC (Figure 4.5a) a low loading attributed to the low surface area of the silica. The highest loadings were found for mesoporous silica modified in toluene (Table 4.3).

Table 4.3 Total weight loss of different $DiNH_2@SiO_2$ batches according to TGA

Batch	Solvent	Total of weight loss (%) between 126 and 773 ºC
$DiNH_2@SiO_2$ (I) (Stöber-type silica)	Toluene	6
$DiNH_2@SiO_2$ (II) (Mesoporous silica)	Toluene	21
$DiNH_2@SiO_2$(III) (Mesoporous silica)	Ethanol	14

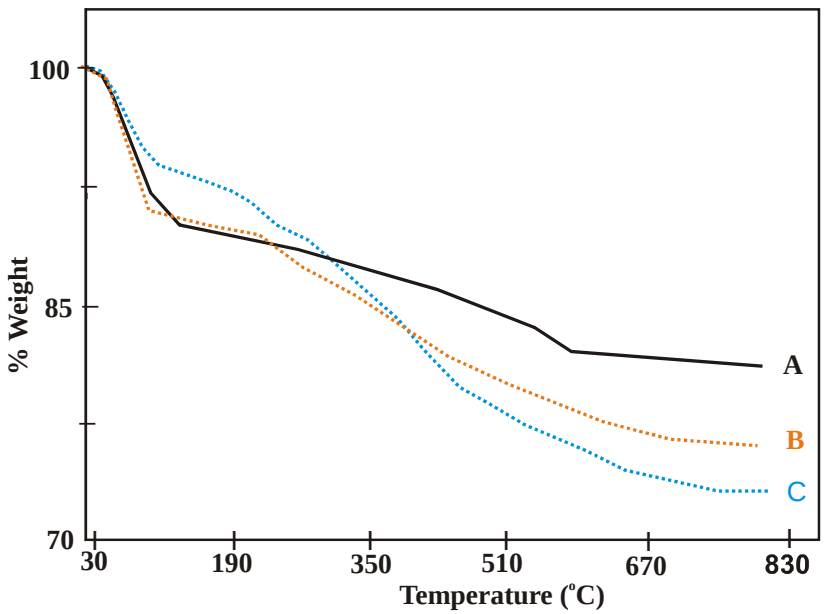

Figure 4.5 Thermogravimetric analyses of $DiNH_2@SiO_2$ prepared in A) dried toluene using Stöber-type silica B) ethanol using mesoporous silica C) dried toluene using mesoporous silica

4.3.1.3 Infrared spectroscopy of $DiNH_2@SiO_2$

$DiNH_2@SiO_2$ (II) (prepared using mesoporous silica in toluene) was selected for IR study. The FT-IR spectrum of $DiNH_2@SiO_2$ (II) between 4000 and 400 cm^{-1} (Figure 4.6) shows small bands at 2934 and 2884 cm^{-1} due to the CH_2 stretching vibration. The existence of CH_2 group bands on the spectrum can be a good indication of loading of the diamine reagent on the surface of the silica. On the other hand, no bands from the NH stretching vibration were distinguishable at around 3276 and 3295 cm^{-1} (as seen in the Z-6094 spectra) (Figure 4.6)[13].

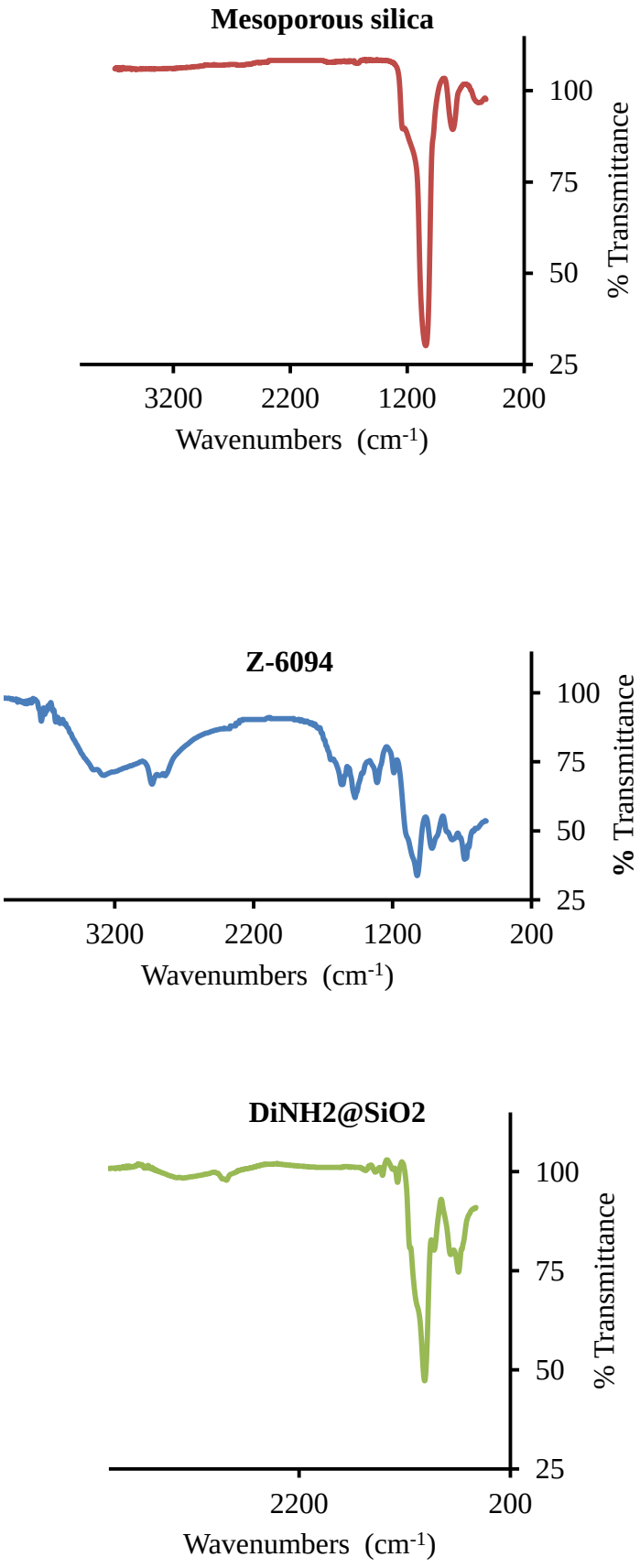

Figure 4.6 FT-IR spectra of mesoporous silica, Z-6094 and $DiNH_2@SiO_2$

4.3.1.4 Colour test of $DiNH_2@SiO_2$

The functionalization of the diamino moiety on the silica particles was assessed by a colour test in which 20 mg of $DiNH_2@SiO_2$ particles and 20 mg of unmodified SiO_2 were separately equilibrated with 5 mL of copper (II) solution (1000 µg Cu mL^{-1}). The colour of the $DiNH_2@SiO_2$ particles turned from white to blue but unmodified silica particles were unchanged. The colour change from white to blue is attributed to the diamine ligand chelating the Cu^{2+}.

4.3.1.5 Measurement of the copper capacity of $DiNH_2@SiO_2$

The number of diamine groups available on the silica was assessed by measurement of its copper capacity. The loading of diamine groups on the mesoporous silica is significantly higher than the loading on the Stöber-type silica, as a result of the high surface area of the mesoporous silica (Table 4.4). The copper capacity measurements of diamine-mesoporous silicas slightly decreased when the solvent was changed from toluene to ethanol.

Table 4.4 The copper capacities of different of $DiNH_2@SiO_2$ batches

Batch	Solvent	Copper capacity ± SD, mmol g^{-1}, (n = 3)
$DiNH_2@SiO_2$ (I) (Stöber-type silica)	Toluene	0.10 ± 0.01
$DiNH_2@SiO_2$ (II) (mesoporous silica)	Toluene	1.62 ± 0.064
$DiNH_2@SiO_2$ (III) (mesoporous silica)	Ethanol	1.3 ± 0.040

4.3.2 Aminopropyl-nanoscavengers ($NH_2@SiO_2$)

4.3.2.1 Morphology and particle size distribution of $NH_2@SiO_2$ (I)

The $NH_2@SiO_2$ (I) prepared by modifying preformed mesoporous silica with $NH_2Si(OEt)_3$ in toluene is the only batch studied by SEM and LSPSA as it was the most promising batch according to copper capacity measurement, as will be discussed in Section 4.3.2.5. Laser scattering particle size analysis of $NH_2@SiO_2$ (I) shows the size of the particles (main population) to be 581 nm (with 151 nm standard deviation) (Figure 4.7). This result did not match the size of the particles estimated from SEM images (Figure 4.8). The size of the particles, calculated by averaging measurements of fifty particles, was 248 ± 14 nm. The SEM results of the batch show that the morphology of the particles was spherical with sizes around 250 nm. These results confirmed that modification did not affect the size and the morphology of the modified particles.

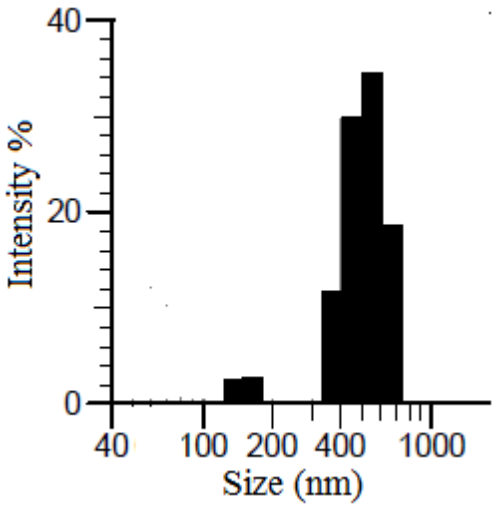

Figure 4.7 LSPSA of $NH_2@SiO_2$ (I) prepared in toluene

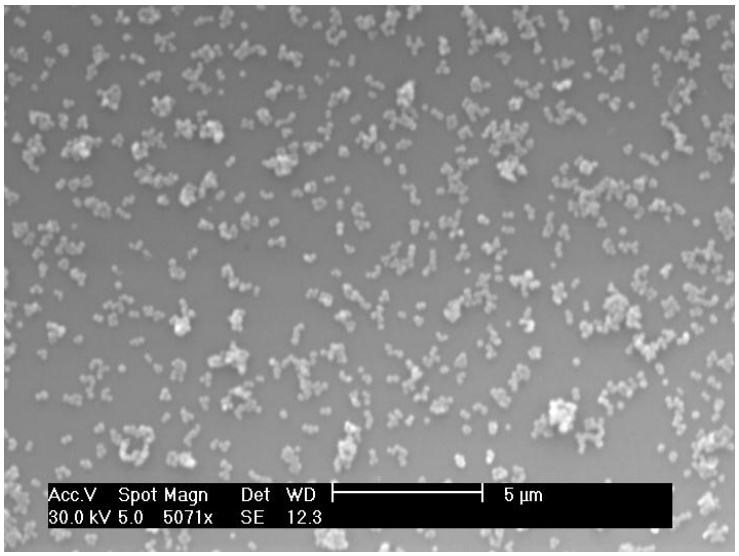

Figure 4.8 SEM image (5071X magnification) of $NH_2@SiO_2$ (I) prepared in toluene

4.3.2.2 Thermogravimetric study of $NH_2@SiO_2$

Modification of the silica surface was confirmed by thermogravimetric analysis. On the post grafting synthesis of $NH_2@SiO_2$ (I) in toluene there were in general three regions of weight loss on the TGA traces. The first change between 27 ºC and 126 ºC was a 4 % weight loss believed to be adsorbed water and residual solvent[14]. A 2.43 % weight loss between 126 to 342 ºC, and another 9 % weight loss between 342 and 773 ºC were due to oxidation of organic material[2] (Figure 4.9a). The thermogravimetric analysis of $NH_2@SiO_2$ (III) (prepared using the single pot method) revealed 18 % weight loss between 303 and 750 ºC (Figure 4.9b), as a result of the oxidation of organic materials. Some of this weight loss can also be attributed to oxidation of the template, as solvent extraction can not completely remove the template. TGA of $NH_2@SiO_2$ (IV) particles prepared from Stöber-type silica showed a 6 % weight loss between 126 and 773 ºC (Table 4.5). It is obvious that modification of pre-formed mesoporous silica with aminopropyl groups either in toluene or ethanol medium resulted in a higher loading of the aminopropyl moiety than modification of Stöber-type silica (Table 4.5). This is again due to the high surface area of mesoporous silica.

Table 4.5 Total weight loss of different $NH_2@SiO_2$ batches according to TGA

Batch	Solvent	Total weight loss (%) between 126 and 773 ºC
$NH_2@SiO_2$ (I) (mesoporous silica)	Toluene	11.43
$NH_2@SiO_2$ (II) (mesoporous silica)	Ethanol	10
$NH_2@SiO_2$ (III) (prepared during the formation of mesoporous silica)	Ethylene glycol	20
$NH_2@SiO_2$ (IV) (Stöber-type silica)	Toluene	6

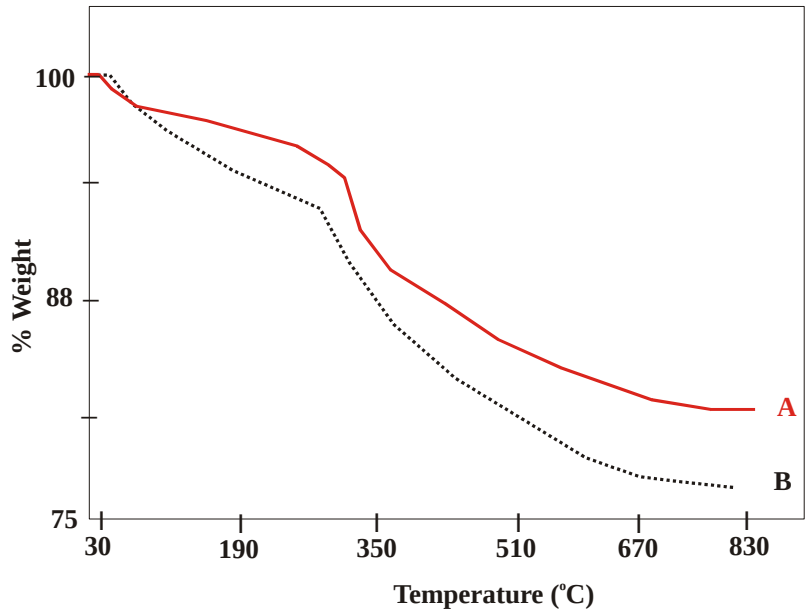

Figure 4.9 Thermogravimetric analysis of $NH_2@SiO_2$ particles prepared A) in toluene using mesoporous silica ($NH_2@SiO_2$ (I)) B) during the formation of mesoporous silica ($NH_2@SiO_2$ (III))

4.3.2.3 Infrared spectroscopy study of $NH_2@SiO_2$

In FT-IR spectroscopy the N-H stretching vibration at 3300 cm^{-1} is often too difficult to observe, especially when the silica particles are covered by a chemically bonded monolayer of aminopropyl moiety [11]. This band was not observed, even when the FT-IR spectroscopy was carried out for $NH_2Si(OEt)_3$ (Figure 4.10). The FT-IR spectroscopy (Figure 4.10) carried out of $NH_2@SiO_2$ (I) was prepared using post synthesis method in dried toluene, and revealed a weak band at 2940 cm^{-1} which might belong to a CH_2 asymmetric stretching mode, and a band at 1556 cm^{-1} which might come from deformation vibrations of N-H. On the other hand, two notable bands were detected at 2937 and 2873 cm^{-1} in the case of $NH_2@SiO_2$ prepared using the single pot approach. It can not be confirmed that these bands just refer to stretching vibrations of CH_2 groups on the $NH_2Si(OEt)_3$. As stated previously, the extraction of a template using a solvent cannot completely remove the entire template from the structure of $NH_2@SiO_2$. Therefore the bands may drive from alkyl groups of the remaining template in the $NH_2@SiO_2$ structure. In all IR spectra, a sharp and strong band was observed at 1066 cm^{-1}, which was attributed to the stretching mode of siloxane (Si-O-Si)[15] (Figure 4.10).

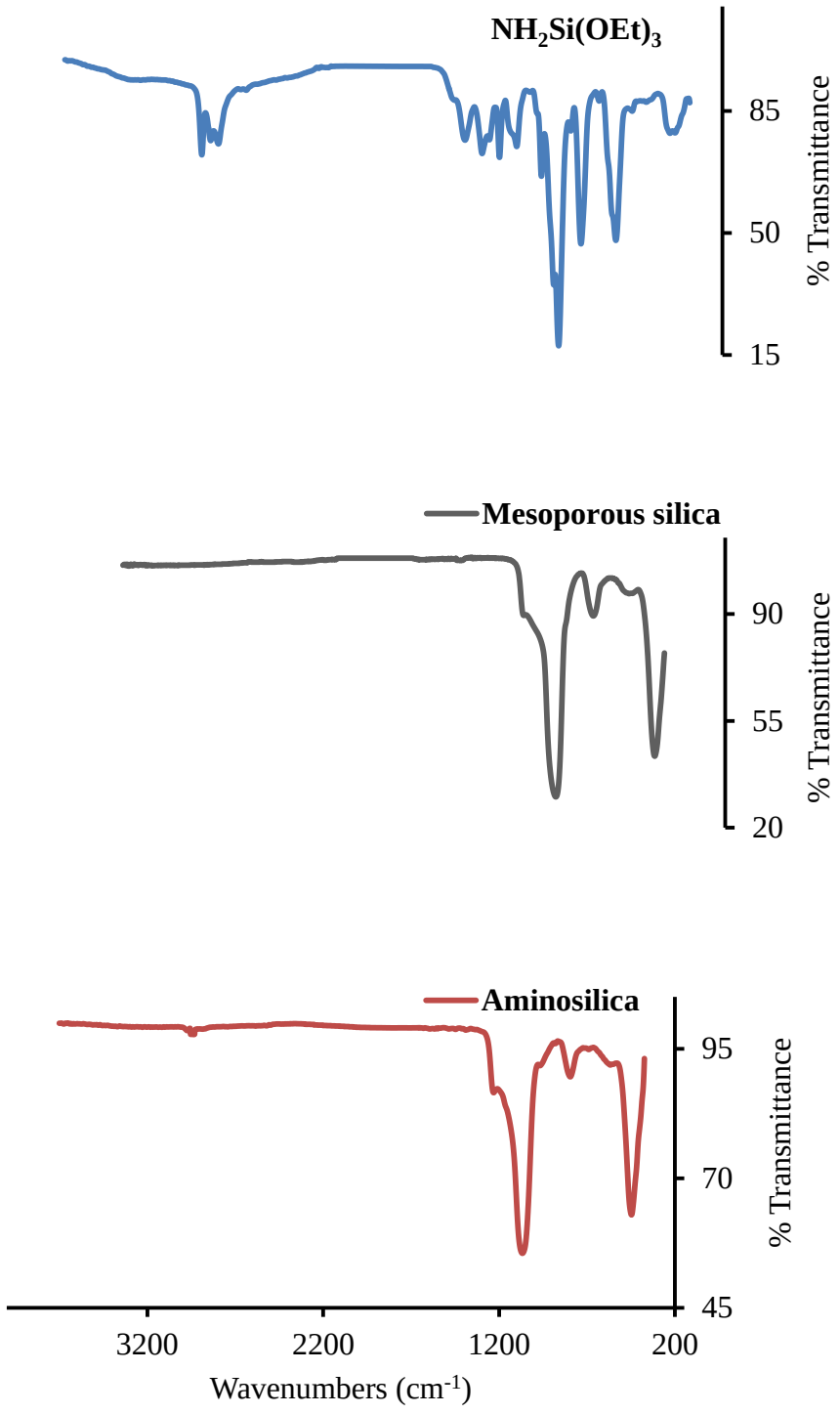

Figure 4.10 FT-IR spectroscopy of 3-aminopropyltriethoxysilane, mesoporous silica and aminosilica (NH_2@SiO_2 (I))

4.3.2.4 Colour test of $NH_2@SiO_2$

When white $NH_2@SiO_2$ particles were added to a copper (II) solution (1000 µg mL^{-1}), the colour of the recovered particles turned light blue. It was noted that the colour of the particles developed over time due to the attachment of more copper (II) ions. One hour was found to be more than enough to reach the clear light blue stage. Other researchers have also found that the colour of aminopropyl-silica particles turned pale blue after immobilization of Cu (II) on the surface of the particles[16].

4.3.2.5 Measurement of the copper capacity of $NH_2@SiO_2$ particles

To assess the functionalized amino groups on the silica surfaces, copper capacity measurements were carried out (Table 4.6). The preparation of amino-mesoporous silica in toluene gives the highest amine loading. The number of functionalized amine groups on the surface of mesoporous silica dropped when ethanol was used as a reaction solvent. Modification of mesoporous silica during the formation of the particles gives the lowest amine loading amongst the mesoporous silica modifications. Functionalization of the aminopropyl moiety on the surface of the Stöber-type silica gives a copper capacity 0.30 mmol g^{-1} which is three times the copper capacity obtained for the corresponding diamine. This could be as a result of steric hindrance caused by the diamine group.

Table 4.6 The copper capacity of different $NH_2@SiO_2$ batches

Batch	Solvent	Copper capacity ± SD, mmol g^{-1}, (n = 3)
$NH_2@SiO_2$ (I) (mesoporous silica)	Toluene	1.87 ± 0.07
$NH_2@SiO_2$ (II) (mesoporous silica)	Ethanol	1.23 ± 0.09
$NH_2@SiO_2$ (III) (prepared during particles formation mesoporous silica)	Ethylene glycol	1.0 ± 0.02
$NH_2@SiO_2$ (IV) (Stöber-type silica)	Toluene	0.3 ± 0.02

4.4 Conclusion

From the above study, it can be concluded that nano-sized silica particles can be modified with diamino or aminopropyl groups. Different types of solvents were used in attempts to increase the loading of amino groups on the surface of particles. The copper capacities of $DiNH_2@SiO_2$ batches prepared using ethanol and dried toluene as a solvent show no significant differences. The low surface area of the Stöber-type silica affects the immobilization of diamino group on the surface. The copper capacity of modified Stöber-type silica is around 17 times lower than that attained by modification of mesoporous silicas.

Both single pot synthesis and post grafting methods were applied to prepare $NH_2@SiO_2$ particles. According to the copper capacity results, the post synthesis method has a higher amine loading than single pot synthesis. There were many disadvantages arising from the single pot synthesis, such as long preparation time as well as difficulties with the removal of the template from the $NH_2@SiO_2$ structure by solvent extraction.

The morphology of $DiNH_2@SiO_2$ and $NH_2@SiO_2$ particles observed using scanning electron microscope was uniformly spherical. Moreover, the size of the particles confirmed by SEM was not affected by the modification. They were still around 250 nm.

4.5 References

(1) Yang, G.; Wu, J.; Xu, G.; Yang, L. *Colloids Surf. B-Biointerfac.* **2010**, *78*, 351-356.

(2) Shamim, T.; Gupta, M.; Paul, S. *J. Mol. Catal. A-Chem.* **2009**, *302*, 15-19.

(3) Fong, B.; Russo, P. S. *Langmuir* **1999**, *15*, 4421-4426.

(4) Soliman, E. M. *Anal. Lett.* **1997**, *30*, 1739-1751.

(5) Benhamou, A.; Baudu, M.; Derriche, Z.; Basly, J. P. *J. Hazard. Mater.* **2009**, *171*, 1001-1008.

(6) Oh, C.; Lee, J. H.; Lee, Y. G.; Lee, Y. H.; Kim, J. W.; Kang, H. H.; Oh, S. G. *Colloids Surf. B-Biointerfac.* **2006**, *53*, 225-232.

(7) Kemin, W.; Jiaofeng, P.; Xiaoxiao, H.; Weihong, T.; Huimin, L.; Xinli, X.; Yan, W. *Nanomed. Nanotechnol. Biol. Med.* **2006**, *2*, 113-120.

(8) Senda, Y.; Hidaka, T.; Matsumoto, J.; Shiragami, T.; Yasuda, M. *Bull. Chem. Soc. Jpn.* **2008**, *81*, 1518-1524.

(9) Kanan, S. A.; Tze, W. T. Y.; Tripp, C. P. *Langmuir* **2002**, *18*, 6623-6627.

(10) Blumel, J. *J. Am. Chem. Soc.* **1995**, *117*, 2112-2113.

(11) Pasternack, R. M.; Amy, S. R.; Chabal, Y. J. *Langmuir* **2008**, *24*, 12963-12971.

(12) Kallury, K. M. R.; Macdonald, P. M.; Thompson, M. *Langmuir* **1994**, *10*, 492-499.

(13) Piers, A.; Rochester, C. H. *J. Chem. Soc.-Faraday Trans.* **1995**, *91*, 359-365.

(14) Chen, H.; Zhou, S. X.; Gu, G. X.; Wu, L. M. *J. Disper. Sci. Technol.* **2004**, *25*, 837-848.

(15) Perez-Quintanilla, D.; Del Hierro, I.; Fajardo, M.; Sierra, I. *J. Mater. Chem.* **2006**, *16*, 1757-1764.

(16) Borgo, C. A.; Ferrari, R. T.; Colpini, L. M. S.; Costa, C. M. M.; Baesso, M. L.; Bento, A. C. *Anal. Chim. Acta* **1999**, *385*, 103-109.

Chapter 5
Dithiocarbamate-nanoscavengers ($NCS_2@SiO_2$) and their applications in the extraction of metal ions

5.1 Introduction

As has been discussed in Chapter 1, analytical instruments are frequently too insensitive to directly determine the low levels of concentration of trace metal ions in water. Trace metal measurements can also suffer from interferences from other materials in the sample. Under such circumstances preconcentration / extraction can be an essential step before measurement can take place. Examples of techniques that can be employed for this purpose are coprecipitation[1], chelating ion exchange[2], chelation-solvent extraction[3, 4], solvent evaporation[5] and solid phase extraction based on modified solid support (Section 1.3.2).

Dithiocarbamates bind to a large range of metal ions[6]. The versatility of the dithiocarbamate ligand is attributed to its small bite angle, leading to stabilization of a wide range of metal oxidation states[7-9]. The complexing capability of dithiocarbamate ligands comes from the donation of electrons on the sulfur atoms to the positive charge on the metal[10].

The surface of silica can be modified with dithiocarbamate moieties by converting a pre-formed amino-silica to its dithiocarbamate by reaction with carbon disulfide (CS_2). This can be performed under neutral pH conditions but adding base to the reaction medium is reported to improve the conversion of amine to dithiocarbamate[11]. In the 1970s, Leyden *et al.* prepared a series of dithiocarbamate-silicas by reacting pre-formed amino-silica with CS_2 in the presence of tetramethylammonium hydroxide and used these dithiocarbamate-silicas to preconcentrate metal ions[12-14]. Similar syntheses have employed sodium hydroxide[15-17]. Mahmoud *et al.* converted an amino-silica to its dithiocarbamate without adding base to the reaction medium[18, 19]. The main drawback of these two step syntheses is incomplete conversion of amine moieties into their

dithiocarbamates. This can be overcome by pre-forming the dithiocarbamated alkoxysilane and then reacting it with silica. Such a product has been used to extract Hg (II)[11].

Dithiocarbamates are frequently used for the extraction of metal ions as they establish stable complexes with many metal ions. Dithiocarbamate reagents possess some disadvantages in direct application to extract metal ions as the extraction requires use of some hazardous organic solvents. Immobilization of the dithiocarbamate moiety on solid support materials optimizes the ability of dithiocarbamates to preconcentrate metal ions.

In this chapter the two step syntheses of dithiocarbamate-nanoscavengers will be described. Mesoporous silicas were modified with mono and diamine groups (prepared as described in Chapter 4) and these materials were then reacted with carbon disulfide to produce mono- (Figure 5.1) and bis-dithiocarbamates (Figure 5.2). Following characterization, the dithiocarbamate-nanoscavengers were used to preconcentrate Cu^{2+}, Cd^{2+}, Ni^{2+}, Pb^{2+}, Co^{2+}, Cr^{3+}, Mn^{2+} and Zn^{2+} from water using a nanoscavenger dispersion extraction (NSDE) approach.

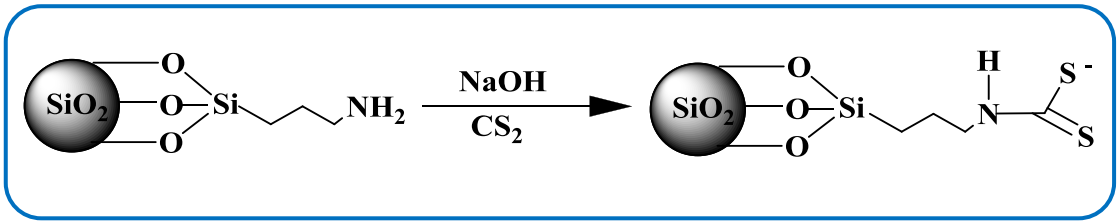

Figure 5.1 Synthesis of a monodithiocarbamate-nanoscavenger

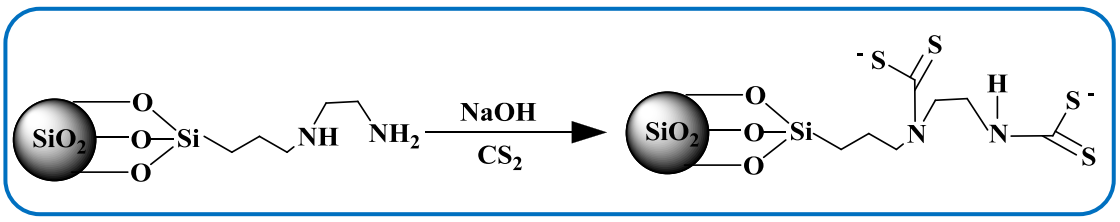

Figure 5.2 Synthesis of a bis-dithiocarbamate-nanoscavenger

5.2 Experiments

5.2.1 Materials

Carbon disulfide (99.9 %), hydrochloric acid (36 % (w/v), AR grade), tris(hydroxymethyl)aminomethane and sodium acetate were obtained from Aldrich (Poole, UK). 2-Propanol and sodium hydroxide was purchased from Fisher Scientific (Loughborough, UK). Chloroform (HPLC grade) was supplied by Rathburn (Walkerburn, UK). Nitric acid (AR grade), sodium diethyldithiocarbamate and tri-ammonium citrate were obtained from BDH limited (Poole, U.K).

A tris-buffer was prepared by dissolving of tris(hydroxymethyl)aminomethane (12.1 g) in deionised water (80 mL) in a beaker (200 mL). The solution was adjusted to the desired pH (7 or 9) using concentrated hydrochloric acid. Acetate buffer (1 M, pH = 4 or 5.7) was prepared by mixing acetic acid (211.75 mL, 1 M) and sodium acetate (38.25 mL, 1 M) together in a 500 mL beaker and the pH was adjusted to the desired pH by variation of the amount of acetic acid or sodium acetate.

Stock standard solutions (1000 µg mL^{-1}) of Cu^{2+}, Cd^{2+} , Ni^{2+}, Pb^{2+}, Co^{2+}, Cr^{3+}, Mn^{2+} and Zn^{2+} were individually prepared by dissolving (0.393, 0.274, 0.160, 0.496, 0.494, 0.770, 0.410 and 0.440 g) respectively of each metal salt ($CuSO_4.5H_2O$, $Cd(NO_3)_2.4H_2O$, $Ni(NO_3)_2.6H_2O$, $Pb(NO_3)_2$, $Co(NO_3)_2.6H_2O$, $Cr(NO_3)_3.9H_2O$, $MnSO_4.4H_2O$ and $ZnSO_4.7H_2O$) in 95 mL of deionised water and 5 mL of acetate buffer (pH = 5.7). The prepared standard solutions were stored in polyethylene containers (125 mL).

5.2.2 Analysis of metals

The metal ions (Cu^{2+}, Cd^{2+}, Ni^{2+}, Pb^{2+}, Co^{2+}, Cr^{3+}, Mn^{2+} and Zn^{2+}) were measured using a Perkin-Elmer 2380 atomic absorption spectrophotometer. The calibration was typically carried out in the range of 1 to 5 µg mL^{-1}. The employed measurement parameters are shown in Table 5.1.

Table 5.1 The FAAS parameters for metal ion analysis

Element	Slit width (nm)	Wavelength (nm)	Lamp current (mA)
Cu	0.7	325	4
Cd	0.7	228.8	3
Ni	0.7	232	5
Pb	2	217	5
Co	0.7	240.7	10
Cr	0.7	357.9	5
Mn	0.7	279.5	10
Zn	0.7	213.9	5

5.2.3 Characterization of the nanoscavengers

Preparation of the samples for the instruments was carried out according to the methods described in Section 3.1.2.

5.2.4 The synthesis of a monodithiocarbamate–nanoscavenger ($MNCS_2@SiO_2$)

Aminopropyl-nanoscavenger (2.4 g) (prepared as described in Section 4.2.4.1) and deionised water (80 mL) were transferred to a conical flask (250 mL) and sonicated for an hour. The mixture was stirred and NaOH (2 mL, 0.1 M), carbon disulfide (8 mL) and 2-propanol (8 mL) were added to the flask. The reactants were stirred for an hour at room temperature and then centrifuged for 5 minutes at 8400 *g*. The supernatant was removed and discarded. The pale yellow product was rinsed with 2-propanol 5 times and three additional times with methanol. The product was dried under continuous vacuum overnight and then stored in the dark under N_2 at 4 ºC.

5.2.5 Synthesis of a bis-dithiocarbamate-nanoscavenger ($BNCS_2@SiO_2$)

The experiment was carried out according to the method described in Section 5.2.4, except that the diamino-nanoscavenger (prepared as described in Section 4.2.3.2) was used instead of the aminopropyl-nanoscavenger.

5.2.6 Copper capacity measurement of the dithiocarbamate-nanoscavengers

This experiment was carried out according to the method described in Section 4.2.5.

5.2.7 Extraction of metals using the monodithiocarbamate–nanoscavenger

In this experiment, Cu^{2+}, Ni^{2+}, Pb^{2+}, Cd^{2+} Cr^{3+}, Mn^{2+}, Co^{2+} and Zn^{2+} (5 mL, 10 µg mL^{-1}) were spiked into a polyethylene bottle containing deionised water (1 L), tris-buffer (5 mL, pH =7, 1 M) and $MNCS_2@SiO_2$ (200 mg) (pre-sonicated in 5 ml of deionised water). The bottle was left for 2 hours and filtered using a 0.2 µm cellulose nitrate membrane filter. The filter was transferred to a polyethylene tube and a mixture of HCl and HNO_3 (5 mL, 1:1) was added to the tube and heated to 45 ºC for 2 hours using a water bath. The tube mixture was centrifuged and the acidic solution was transferred to a volumetric flask (10 mL). Deionised water (5 mL) was added to the tube, the contents shaken and centrifuged, then added to the volumetric flask. The volume was made up to the mark using deionised water. The concentration of each metal was measured by FAAS. This experiment was replicated three times.

5.2.8 The rate of metal uptake by the $MNCS_2@SiO_2$

This experiment was carried out according to the method described in Section 5.2.7, except that the equilibrium time allowed for the metals ions to react with the $MNCS_2@SiO_2$ was reduced from two hours to 15 minutes.

5.2.9 The affect of pH on metal extraction efficiencies using $MNCS_2@SiO_2$

A known weight of $MNCS_2@SiO_2$ (ca. 150 mg) was transferred to a glass vial (5 mL). Deionised water (5 mL) was added and the mixture was sonicated for 30 minutes. Deionised water (100 mL) was added to a low density polyethylene bottle (125 mL), with 1 mL of a mixture containing 20 µg mL^{-1} of each metal [Cu(II), Cd (II), Ni (II) and Pb (II)] (first group of metals) or (Co (II), Cr (III), Mn (II) and Zn (II)) [second group of metals]. The pH of each mixture was adjusted to pH = 4, using acetate buffer, or pH 7 or 9 using tris buffer. The $MNCS_2@SiO_2$ suspension was added to the bottle and the bottle was shaken gently and then left for an hour prior to filtration using a 0.2 µm cellulose nitrate membrane filter. The filter was carefully transferred to a sealed centrifuge tube (10 mL) and a mixture of HCl and HNO_3 (5 mL, 1:1) was added. The tube was left for 2 hours in a water bath at 45 ºC. The tube was centrifuged, the acidic solution was transferred to a volumetric flask (10 mL) and deionised water (5 mL) was added to the tube. It was shaken for 2 minutes and centrifuged, and the aqueous solution was added to the volumetric flask. The volume was accurately made up to the mark using deionised water and the concentrations of the metals were measured by FAAS.

5.2.10 Colorimetric determination of copper as a dithiocarbamate complex

Copper (II) was determined colorimetrically after solvent extraction of its diethyldithiocarbamate complex into chloroform (HPLC grade). Tap water (100 mL) was transferred into a separating funnel (250 mL) and the pH was adjusted to 7.0 using a triammonium citrate (10 % w/v) solution. Sodium diethyldithiocarbamate (2

mL, 1 mg mL^{-1}) was added to the funnel and the mixture was shaken for 5 minutes. Chloroform (2.5 mL) was added. The funnel was shaken vigorously for 5 minutes and the organic layer was collected into a volumetric flask (5 mL). The last step was repeated again. The organic layer was added to the volumetric flask and the volume was made up to the mark using chloroform. The absorbance was measured at 435 nm and the concentration was calculated according to a calibration curve derived from the extraction of standard copper solutions.

5.2.11 Calibration of the colorimetric approach

Standard solutions for colorimetric approach was prepared by spiking a known quantity of Cu (II) to deionised water (100 mL) and extracted and measured according to the method described in Section 5.2.10.

5.2.12 $MNCS_2@SiO_2$ extraction of Cu^{2+} from tap water

An aliquot (100 mL) of tap water was transferred to a low density polyethylene bottle (125 mL) and the pH was adjusted to 7.0 using triammonium citrate (10 mL, 10 % w/v) solution. $MNCS_2@SiO_2$ (100 mg) (pre-dispersed in 5 mL of deionised water) was added to the bottle mixture and mixed together. The solution was left for 2 hours prior to vacuum filtration through a 0.2 µm cellulose nitrate membrane filter. The filter was then transferred to a sealed centrifuge tube and a mixture of HCl and HNO_3 (2.5 mL, 1:1) was added. The tube was heated to 45 ºC for 2 hours using a water bath. The acidic solution was transferred to a volumetric flask (5 mL). Deionised water (2.5 mL) was added to the solid residue in the tube, shaken for 1 minute and centrifuged. The washings were added to the volumetric flask, and the volume was made up to the mark using deionised water. The concentration of copper in the solution was measured by FAAS.

5.3 Results and discussion

5.3.1 Morphology and particle size distribution

Scanning electron microscopy of dithiocarbamated nanoscavengers showed spherical particles (Figures 5.4a and 5.4b). The average size of the $MNCS_2@SiO_2$ particles was calculated from SEM image as 252 nm with 17 nm standard deviation. However, according to laser scattering particle size analysis (LSPSA) the mean diameter of the particles was 395 nm with 82 nm standard deviation (Figure 5.3).

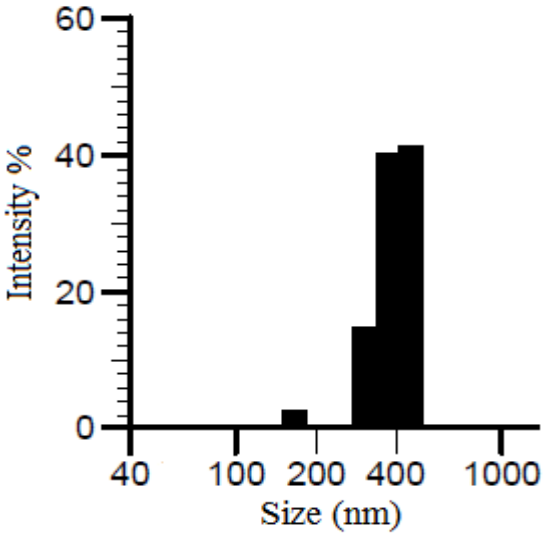

Figure 5.3 LSPSA of $MNCS_2@SiO_2$

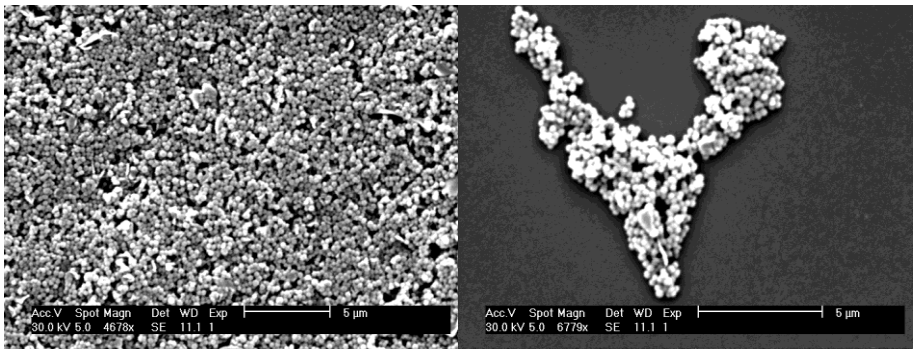

Figure 5.4 SEM images of a) $MNCS_2@SiO_2$ (4678X magnifications) and b) $BNCS_2@SiO_2$ (6779X magnifications)

The average size of $BNCS_2@SiO_2$ calculated from SEM images (Figure 5.4b) was 255 ± 20 nm and 446 ± 179 nm based on LSPSA measurement. The aggregation of the particles could be the main reason for obtaining higher average sizes in particles size measurements. The average sizes of nanoscavengers before and after introducing dithiocarbamate to the nanoscavengers according to the SEM measurements did not change (Table 5.2).

Table 5.2 The average particle sizes of some nanoscavengers

Type of nanoscavenger	SEM measurement (nm)	LSPSA measurement (nm)
$NH_2@SiO_2$ (I)	248 ± 14	581 ± 151
$MNCS_2@SiO_2$	252 ± 17	395 ± 82
$DiNH_2@SiO_2$ (II)	249 ± 24	551 ± 33
$BNCS_2@SiO_2$	255 ± 20	446 ± 179

5.3.2 Thermogravimetric analysis of dithiocarbamate-nanoscavengers

To confirm the dithiocarbamation of the silica, thermogravimetric analyses were carried out (Figure 5.5). With the $NH_2@SiO_2$ (I) (Table 5.3), 11 % weight loss occurred between 126 and 773 ºC (Figure 5.5a). In contrast, the TG trace of $MNCS_2@SiO_2$ showed around 15 % weight loss in the same area (Figure 5.5b). The 4 % increase in weight loss may be attributed to the dithiocarbamation. $BNCS_2@SiO_2$ showed ca. 23 % weight loss between 126 and 773 ºC, 5.3 % (Table 5.3) higher than $DiNH_2@SiO_2$ (II) (Figure 5.5c and d).

Table 5.3 Total weight loss of amino-nanoscavengers and dithiocarbamate-nanoscavengers

Batch	Total weight loss between 126 to 773 ºC (%)
$NH_2@SiO_2$ (I)	11
$MNCS_2@SiO_2$	15
$DiNH_2@SiO_2$ (II)	18.3
$BNCS_2@SiO_2$	23

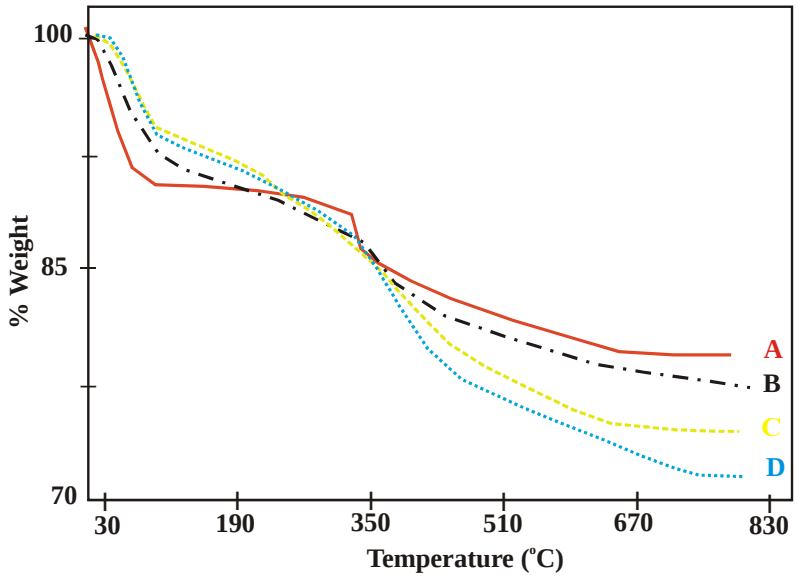

Figure 5.5 Thermogravimetric analysis of A) aminopropyl-nanoscavenger B) monodithiocarbamate-nanoscavenger C) diamino-nanoscavenger D) bis-dithiocarbamate-nanoscavenger

5.3.3 Infrared spectroscopy of dithiocarbamate-nanoscavengers

FT-IR of the dithiocarbamate-nanoscavengers showed CH_2 stretching bands of the hydrocarbon chain at 2975 and 2940 cm^{-1}. A broad and strong band for siloxane (Si-O-Si) appeared at 1060 cm^{-1} and a band due to Si–O bond stretching was observed at 951 cm^{-1}. The IR absorption of the dithiocarbamate moiety, usually exhibited at 1493.88, 1286.25, and 956.96 cm^{-1} (assigned to N-C=S)[20], did not appear in the dithiocarbamate-nanoscavengers spectrum. The absence of these bands may be attributed to signal overlap, in addition to the strong vibrational bands of the silica

framework[11]. Therefore the IR spectrum is not useful in confirming the linkage of the dithiocarbamate moiety to the silica.

5.3.4 Colour testing of dithiocarbamate-nanoscavengers

To further confirm the dithiocarbamation of the silica, a colour test was carried out. The dithiocarbamate-nanoscavenger particles were dispersed in copper (II) solution (1000 µg mL^{-1}, pH = 5.7). The colour of the particles immediately turned brown (Figure 5.6) inside the copper solution due to the dithiocarbamate-nanoscavengers complexing the copper. There was a noticeable change in the colour of the bis- and monodithiocarbamate-nanoscavengers when dispersed in the copper (II) solution. Whilst the amino-nanoscavengers when dispersed in the copper (II) solution were blue (as described in Section 4.3.2.4). The dithiocarbamate-nanoscavengers particles became brown. This is considered to be a reliable indicator of dithiocarbamate complexation.

Figure 5.6 The colour testing of a) $MNCS_2@SiO_2$ particles before dispersion in Cu (II) solution b) $MNCS_2@SiO_2$ particles after dispersion in Cu (II) solution

5.3.5 Measurement of the Cu capacities of dithiocarbamate-nanoscavengers

Copper capacity measurements were carried out to assess the dithiocarbamate moiety on the surface of the silicas. Dithiocarbamate-nanoscavenger capacities (Table 5.4) were similar to those of the amino-nanoscavengers but the copper capacities of the bis-dithiocarbamates were less than expected. This is believed to be due to difficulty of releasing copper from the bis-dithiocarbamate, due to chelation by two DTC ligands. It was noticed during the experiment that the colour of the silica after digestion was still light brown, implying that some copper remained on the silica. A stronger acid such as (aqua regia) should therefore be used in the digestion process to release all the copper (II) ions from the nanoscavengers. The copper capacities of dithiocarbamate-nanoscavengers prepared from mesoporous silica had a copper capacity seven times higher than that of materials prepared from a Stöber-type silica (Table 5.4). The high surface area of the mesoporous silica allows loading of more dithiocarbamate moiety on the surface of silica, therefore the copper capacity is substantial if compared to the dithiocarbamate-silica of the Stöber-type.

Table 5.4 The copper capacity of dithiocarbamate-nanoscavengers

Sample	Copper capacity ± SD mmol g^{-1} silica, (n = 3)	References
Monodithiocarbamate-nanoscavenger	1.13 ± 0.006	-
Bis-dithiocarbamate-nanoscavenger	0.93 ± 0.01	-
Dithiocarbamate-Stöber-type silica	0.2	21

5.3.6 The settling of dithiocarbamate-nanoscavengers from an aqueous suspension

The nanoscavenger dispersion extraction technique to extract metal ions from water is based on the dispersion of silica in water and then its recovery together with the

attached analytes. To avoid having to use agitation during the preconcentration process, the modified silica particles should remain suspended long enough to complete the extraction of the analytes. The stability of its suspension in water was reviewed by observing settlement of particles over time (Figure 5.7). The suspension was stable for more than 4 hours without noticeable settlement; enough to extract most target metal ions. Even if some of the dithiocarbamate-nanoscavenger particles settled, this would not prevent the attachment of metal ion to the nanoscavenger from continuing on the remaining suspended particles.

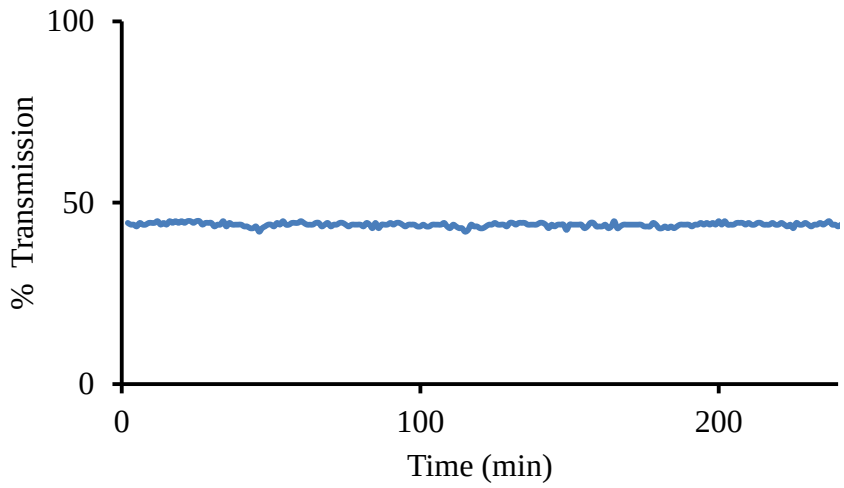

Figure 5.7 Settling of the dithiocarbamate-nanoscavenger from its suspension in water

5.3.7 Extraction of metals using $MNCS_2@SiO_2$

The ability of dithiocarbamate nanoscavenger to extract the metal ions can be predicted by considering the thermodynamic stabilities of the 1:1 metal-ligand complexes. Only the 1st formation constant for the metal-dithiocarbamate complex will be considered as it is expected that only one water molecule will be substituted with the ligand since the dithiocarbamate is not free in water but it is bonded to silica. Unfortunately the data of the 1st formation constant for metal-dithiocarbamate as far as I know is not available in the literatures to make comparison between the metal-dithiocarbamate complex in solution and the same metal-dithiocarbamate nanoscavenger.

The monodithiocarbamate-nanoscavenger was applied to the preconcentration of metal ions (Cu^{2+}, Cd^{2+}, Ni^{2+}, Pb^{2+}, Co^{2+}, Cr^{3+}, Mn^{2+} and Zn^{2+}) from synthetic water samples. These were prepared by spiking 50 µg of each metal ion into 1000 mL of deionised water. The recoveries obtained using the NSDE procedure are given in Table 5.5. All were almost 100 %, except for chromium (III) and manganese (II). The low recovery of chromium (III) (47 %) may be attributed to the slow replacement of surrounding water molecules by the dithiocarbamate-nanoscavenger. This is due to the Cr^{3+} has three electrons (d^3) which occupy t_2g orbital (low energy). Thus the ligand field stabilization energy (LFSE) of the ion in an octahedral ligand field would be high ($6/5\ \Delta o$) which makes complexes of Cr^{3+} kinetically inert[22, 23]. In addition the Cr is a hard metal thus its affinity to soft ligands will be low[24]. No recovery was detected for manganese (II). The poor recovery of Mn (II) may be attributed to the low affinity of dithiocarbamate-nanoscavenger to Mn (II), as it is a hard metal[25]. The dithiocarbamate-nanoscavenger had been able to preconcentrate most of the metal ions from 0.05 µg mL^{-1} to 5 µg mL^{-1} to obtain a 100 preconcentration factor. The preconcentration factor could potentially be enhanced by reducing the final volume of the extracted metal ion solution.

Table 5.5 The recovery of metals extracted from water using $MNCS_2@SiO_2$ (Initial sample contained 50 µg L^{-1} of each metal)

Metal	Preconcentration factor	% Average recovery ± SD, n = 3
Cu	100	102 ± 2
Cd	100	99 ± 0.6
Ni	100	105 ± 3
Pb	100	104 ± 4
Co	100	105 ± 1
Cr	100	47 ± 5
Mn	100	0 ± 0
Zn	100	101 ± 0.4

5.3.8 Rate of extraction of metal ions using $MNCS_2@SiO_2$

The equilibrium between the metal ions and the dithiocarbamate-nanoscavenger was reduced to 15 minutes, as employed by Howard and Khdary[21] in their solid phase dispersion extraction of Cu^{2+} using a bis-dithiocarbamate-silica. The recovery results were almost 100 % for Cu^{2+}, Cd^{2+}, Ni^{2+}, Pb^{2+}, Co^{2+} and Zn^{2+}. The rapid uptake of these ions by the dithiocarbamate-nanoscavenger can be attributed to the large available surface area of mesoporous silica, its high loading of dithiocarbamate and the high affinity of dithiocarbamate for most metal ions. No recovery was however observed for Mn^{2+} and Cr^{3+}. Manganese (II) is a hard metal so it is unlikely to be adsorbed by a soft ligand. In an aqueous solution, chromium (III) is hard to extract by ligand, due to its strong hydration by water molecules as Cr (III). This strong hydration around Cr (III) prohibits the access of chelating agents to the metal centre[26-28]. Displacement of coordinated water molecules by dithiocarbamate-nanoscavenger is therefore difficult. Increasing the equilibrium time can enhance the recovery of Cr (III). It was seen that the recovery of Cr (III) was 47 % when the equilibrium time was 2 hours.

5.3.9 The effect of pH on the preconcentration

Water sample pH was adjusted within the range 4 to 9. More extreme conditions were avoided as the dithiocarbamate decomposes under acidic conditions to sulfur compounds such as CS_2 and H_2S[29] and in strong base the silica particles dissolve. The affect of pH was studied at three pH levels (pH = 4, 7 and 9). The recoveries of Cu^{2+}, Cd^{2+}, Ni^{2+}, Pb^{2+} and Co^{2+} were almost 100 % from pH = 4 to pH = 9 (Table 5.6). Only 8 % of Cr (III) was recovered at pH = 4. This may be attributed to several reasons; first the kinetic inertness of Cr (III) hinders efficient complexation leading to poor recovery[30]. Therefore, many preconcentration methods for Cr (III) include conversion of Cr (III) to Cr (VI) step to enhance the recovery[31]. Secondly at low pH the affinity of ligand for Cr^{3+} was low due to competition with the H^+. Increasing the pH leads to deprotonation of the ligand and increases the affinity of the ligand for the metal ion[32]. Moreover, increasing the pH leads to the formation different Cr^{3+} species such as $CrOH^{2+}$, $Cr(OH)^+_2$ and $Cr(OH)_3$ which can be more easily extracted[31]. The

maximum recovery of Cr^{3+} was reached at the higher tested pH values. The recovery of Zn (II) dropped to 57 % at (pH = 4) due to increased competition between H^+ ions and Zn^{2+} at the low pH. The extraction of Mn (II) rose with increasing pH, perhaps due to precipitation at high pH values, of Mn (IV) oxide/hydroxide species resulting from its oxidation with subsequent adsorb on the surface of the nanoscavenger. These results coincided with those obtained by Sarmani *et al.*[25] in their study of the impact of pH on the retention of the Mn-diethyldithiocarbamate complex on a C_{18}-column. Their results showed that the Mn adsorption efficiency increased with increasing pH (7.5-8.5) of the sample solution[25]. It has also been found in another study that no Mn (II) was adsorbed on cross-linked chitosan at low pH (< 4)[33].

Table 5.6 Effect of pH on the extraction of metals using $MNCS_2@SiO_2$

		Average Recovery of Metal ± SD (n = 3)							
Buffer	pH	Cu	Cd	Ni	Pb	Co	Cr	Mn	Zn
Acetate-buffer	4	99±2	96±0.7	94±5	100±0	103±2	8±0	2±0	57±1
Tris-buffer	7	100±0	97±1	97±4	100±0	103±0	100±4	18±2.6	101±0.9
Tris-buffer	9	99±2	99±2	94±4	100±1	97±4	100±3	80±4	102±2

5.3.10 A comparison of Cu (II) determinations using $MNCS_2@SiO_2$ with a conventional colorimetric procedure

The NSDE preconcentration procedure was applied to extract copper (II) from samples of tap water collected from Southampton, United Kingdom. Fifteen tap water samples were collected from different sites across Southampton. $MNCS_2@SiO_2$ was used to extract copper (II) from the samples and after recovery of the copper it was determined by FAAS. The same samples were also analyzed using an established solvent extraction (SE) procedure based on the formation of a Cu (II) diethyldithiocarbamate complex and its extraction into chloroform. The Cu (II) was determined colorimetrically at 435 nm based on the extraction of standard solutions[34] (Section 5.2.11). The Cu concentrations obtained by the two approaches were plotted (Figure 5.8). The slope correlation calculated from the data was 1.0431 ± 0.010 at 95

% confidence level. In order to evaluate the variation in the approaches, the analysis of variance (ANOVA) method was applied. The statistical analysis of the obtained slope, at 95 % confidence level indicates that the slope is not statistically equal to 1. A 4 % difference between the two procedures, indicate to the concentration obtained using SE overall higher than the ones obtained using NSDE. This may be attributed to the preparation of standard solutions for the SE procedure which was carried out using the same procedure of preconcentration of Cu (II) from the sample. Thus the error which may come from losing some of Cu (II) during the sample preparation will be eliminated. However, the preconcentration of Cu (II) from samples using NSDE procedure was different from the preparation of standard solutions which was carried out by spiking the Cu (II) solution to the volumetric flask. Therefore there is a possibility of losing some of Cu (II) during the sample preparation using NSDE. Considering this experimental error, a good match of the Cu (II) concentration results in both methods emphasizes the accuracy of using a dithiocarbamate-nanoscavenger as a solid phase in NSDE to extract metals ions from water samples.

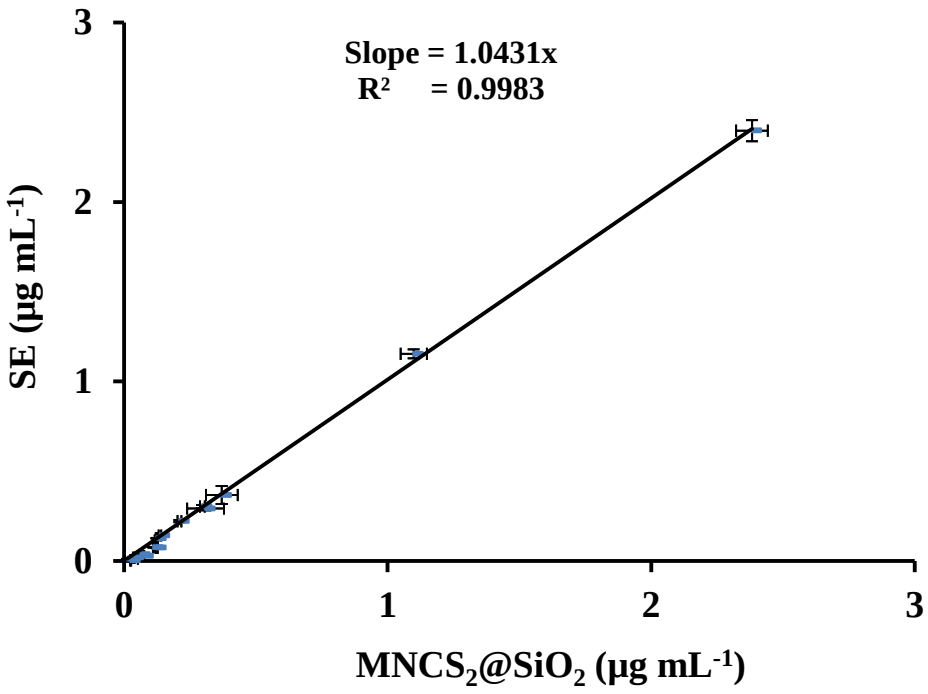

Figure 5.8 Correlation of Cu measurements obtained $MNCS_2@SiO_2$ nanoscavenger dispersion extraction and solvent extraction methods

5.4 Conclusion

The amino-nanoscavengers (Chapter 4) were reacted with carbon disulfide to produce dithiocarbamate-nanoscavengers to be used as solid phase nanoscavenger dispersion extractants to preconcentrate metal ions from an aqueous solution. The extraction of metal ions using the dithiocarbamate-nanoscavenger could be carried out without external (mechanical or manual) agitation.

SEM of dithiocarbamate-nanoscavengers indicated that the particle morphology and size did not change after grafting the dithiocarbamate moiety to the surface of the silica particles. Conversion of the amino-nanoscavengers to the corresponding dithiocarbamate was confirmed by thermogravimetric analysis, copper measurement and a colour test.

The $MNCS_2@SiO_2$ was used to preconcentrate eight metal ions (Cu^{2+}, Cd^{2+}, Ni^{2+}, Pb^{2+}, Co^{2+}, Cr^{3+}, Mn^{2+} and Zn^{2+}) from synthetic water samples. Essentially complete recovery was achieved for all metals except manganese (II) (0 % recovery) and chromium (III) (47 % recovery). The preconcentration factor was 100. Due to the strong affinity for dithiocarbamate to the metal ions, 15 minutes was found sufficient to extract most of the metal ions. The recoveries of most metals were not pH dependent and changing the pHs did not affect the recovery results. Only the recoveries of three metals (Cr^{3+}, Mn^{2+} and Zn^{2+}) were influenced by changing the pH of the sample. The extraction of these metals increased by changing the pH value to basic conditions.

In order to validate the dithiocarbamate-nanoscavenger for use as a new solid phase in the NSDE technique to preconcentrate metals ions from water, the same tap water samples were examined using NSDE and a conventional colorimetric procedure. The similarity in the concentrations obtained using both methods indicated that the dithiocarbamate-nanoscavengers represent a good new alternative the pre-concentration approach of metal ions from water samples.

5.5 References

(1) Buchanan, A. S.; Hannaker, P. *Anal. Chem.* **1984**, *56*, 1379-1382.

(2) Miyazaki, A.; Barnes, R. M. *Anal. Chem.* **1981**, *53*, 299-304.

(3) Rasmussen, L. *Anal. Chim. Acta* **1981**, *125*, 117-130.

(4) Sturgeon, R. E.; Berman, S. S.; Desaulniers, J. A. H.; Mykytiuk, A. P.; McLaren, J. W.; Russell, D. S. *Anal. Chem.* **1980**, *52*, 1585-1588.

(5) Thompson, M.; Ramsey, M. H.; Pahlavanpour, B. *Analyst* **1982**, *107*, 1330-1334.

(6) McClain, A.; Hsieh, Y. L. *J. Appl. Polym. Sci.* **2004**, *92*, 218-225.

(7) Mohammad, A.; Varshney, C.; Nami, S. A. A. *Spectroc. Acta Pt. A-Molec. Biomolec. Spectr.* **2009**, *73*, 20-24.

(8) Hogarth, G. *Transition Metal Dithiocarbamates: 1978-2003*; John Wiley & Sons Inc: New York, **2005**.

(9) Rafin, C.; Veignie, E.; Sancholle, M.; Postel, D.; Len, C.; Villa, P.; Ronco, G. *J. Agric. Food Chem.* **2000**, *48*, 5283-5287.

(10) Steggerda, J. J.; Cras, J. A.; Willemse, J. *Recl. Trav. Chim. Pays-Bas-J. Roy. Neth. Chem. Soc.* **1981**, *100*, 41-48.

(11) Goubert-Renaudin, S.; Gaslain, F.; Marichal, C.; Lebeau, B.; Schneider, R.; Walcarius, A. *New J. Chem.* **2009**, *33*, 528-537.

(12) Leyden, D. E.; Luttrell, G. H.; Nonidez, W. K.; Werho, D. B. *Anal. Chem.* **1976**, *48*, 67-70.

(13) Leyden, D. E.; Luttrell, G. H. *Anal. Chem.* **1975**, *47*, 1612-1617.

(14) Leyden, D. E.; Luttrell, G. H.; Sloan, A. E.; Deangelis, N. J. *Anal. Chim. Acta* **1976**, *84*, 97-108.

(15) Venkatesan, K. A.; Srinivasan, T. G.; Rao, P. R. V. *Colloid Surf. A-Physicochem. Eng. Asp.* **2001**, *180*, 277-284.

(16) Venkatesan, K. A.; Srinivasan, T. G.; Rao, P. R. V. *J. Radioanal. Nucl. Chem.* **2003**, *256*, 213-218.

(17) Venkatesan, K. A.; Srinivasan, T. G.; Rao, P. R. V. *Sep. Sci. Technol.* **2002**, *37*, 1417-1429.

(18) Mahmoud, M. E. *Anal. Chim. Acta* **1999**, *398*, 297-304.

(19) Mahmoud, M. E.; El-Essawi, M. M.; Fathallah, E. M. I. *J. Liq. Chromatogr. Relat. Technol.* **2004**, *27*, 1711-1727.

(20) Li, Y. J.; Xiang, B.; Ni, Y. M. *J. Appl. Polym. Sci.* **2004**, *92*, 3881-3885.

(21) Khdary, N. H. Ph.D. Thesis, Southampton University, Southampton, UK, **2006**.

(22) Jones, C. J. *d- and f-Block Chemistry.* , 1st ed.; Royal Society of Chemistry: Cambridge, **2001**.

(23) Cox, P. A. *Inorganic chemistry*, 2nd ed.; BIOS Scientific Publishers: London, **2004**.

(24) Pope, S. J. A.; Champness, N. R.; Reid, G. *J. Chem. Soc.-Dalton Trans.* **1997**, 1639-1644.

(25) Sarmani, S. B.; Abdullah, M. P.; Bobaker, A. M. *J. Radioanal. Nucl. Chem.* **2004**, *259*, 257-260.

(26) Tande, T.; Pettersen, J. E.; Torgrimsen, T. *Chromatographia* **1980**, *13*, 607-610.

(27) Subramanian, K. S. *Anal. Chem.* **1988**, *60*, 11-15.

(28) Wang, J. S.; Chiu, K. H. *Anal. Sci.* **2007**, *23*, 1337-1341.

(29) Kesari, R.; Gupta, V. K. *Talanta* **1998**, *45*, 1097-1102.

(30) Hsu, J. T.; Whang, C. W. *Chromatographia* **2010**, *71*, 957-961.

(31) Sperling, M.; Xu, S. K.; Welz, B. *Anal. Chem.* **1992**, *64*, 3101-3108.

(32) Koshcheeva, I. Y.; Khushvakhtova, S. D.; Levinskii, V. V.; Danilova, V. N.; Kholin, Y. V. *Geochem. Int.* **2007**, *45*, 178-184.

(33) Xue, A. F.; Qian, S. H.; He, G.; Han, X. F. *Analyst* **2001**, *126*, 239-241.

(34) Vogel, A. I. *Vogel's textbook of quantitative chemical analysis*; Longman Scientific & Technical: Harlow, **1989**.

Chapter 6

Hydroxyquinoline-nanoscavenger ($HQ@SiO_2$)

6.1 Introduction

8-Hydroxyquinoline (HQ) is one of the most commonly employed materials in analytical chemistry due to its selectivity for metallic ions in solution. Moreover it can react with several metal ions as bidentate ligand to form hydrophobic complexes. In general, it has the ability to form a stable chelating complex of 1:2 mole ratio with many divalent metal cations[1, 2]. However, Stary *et al.* [3] found that HQ can form two kinds of complexes with nickel ions at different levels of pH. The complexation with metal ions takes place by de-protonation of the HQ and the complex is therefore more effectively formed under basic conditions than under acidic ones[1].

The incorporation of HQ into a wide variety of solid supports was studied for potential extractors of metal ions from water prior their determination by FAAS[4, 5]. Such materials can preconcentrate metal ions from very dilute solution allowing the detection limit to be highly improved. HQ can be attached to methylated polystyrene[6] and polystyrene divinyl benzene gel[7, 8]. Cellulose and polyacrylonitrile[9] have also been modified with HQ to extract metal ions from water. Immobilization of HQ on the silica gel surface has been found to be a promising approach to the enrichment of transition metals from water. The immobilization of HQ onto silicone tubing was used as preconcentrator for Mn, Co, Ni, Cu, Cd, Pb and Zn from sea water prior to their determination by ICP-MS. The recovery results of the metals were highly dependent on pH. The recovery experiments performed at pH 5.3 produced poor recovery results with no recovery for Pb and Mn and less than 10 % recovery obtained for Ni and Cd. The best recovery results were obtained at pH 8.2 with recovery levels between 35 and 95 %[5]. Moreover, Malamas *et al.*[10] immobilized HQ on silica and used it for preconcentration of Cu, Co, Cd, Pb, Ni and Zn from a complex matrix at pH 6.5 with 25 minutes as a time sampling. A 500-fold preconcentration factor was obtained from 100 mL of solution. These techniques of preconcentration were based on packing the HQ immobilized silica into a column

into which the sample is injected. Column blocking, interferences, difficulties to preconcentrate large volumes of sample and no possibility of doing the preconcentration in the field are the major drawbacks of these techniques. A new technique therefore is required to simplify the preconcentration using HQ modified silica.

Many synthetic procedures to functionalize HQ onto the silica gels have been reported[11-15] but these procedures usually involve many steps. The simplest procedure has been reported by Goswami *et al.*[16]. The procedure involves two steps, first the reaction of silica gel with $NH_2Si(OEt)_3$ and second, the formation of a Schiff base by its reaction with 5-formyl-8-hydroxyquinoline (FHQ). This procedure was used to prepare HQ@SiO_2. For higher modification of HQ into the solid substrate, spherical mesoporous silica has been selected to be the solid support. The high surface area of mesoporous silica compared to other solid supports provides opportunities to modify more HQ into the surface. The nanoscavenger was applied to preconcentrate 8 metal ions from synthetic water samples using the NSDE approach.

This chapter describes the development of an HQ solid phase nanoscavenger that has been based on 250 nm spherical mesoporous silica particles. The mesoporous silica is first modified with an amino-silane and then coupled to HQ (Figure 6.1). The functionalized silica particles with HQ facilitate the extraction of a variety of different metal ions.

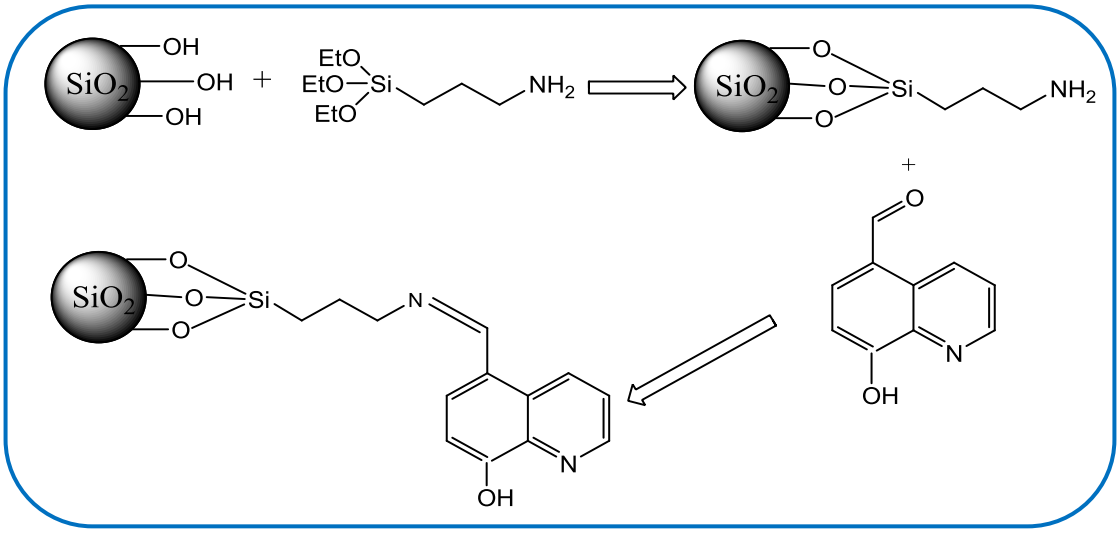

Figure 6.1 Schematic overview of 8-HQ-nanoscavenger synthesis

6.2 Preparation of $HQ@SiO_2$

6.2.1 Materials

Hydrochloric acid [37 % (w/v), AR grade] was obtained from Aldrich (Poole, U.K). HQ (99 %) was supplied by Alfa Aesar (Heysham, U.K) .Nitric acid (AR grade) was purchased from BDH limited (Poole, U.K). Anhydrous diethyl ether, toluene and ethanol were reagent grade. Water (>14 Mohm.cm) was purified by reverse osmosis followed by deionisation using an Elga Option 4 system. Cellulose nitrate membrane filters (Whatman 47 mm diameter, pore size 0.2 μm) were supplied by Fisher Scientific (Loughborough, U.K). All apparatus was soaked in nitric acid [5 % (v/v)] and rinsed with deionised water before use. Tris-buffer solution was prepared by dissolving 12.1 g of tris(hydroxymethyl)aminomethane in 1 L of water and adjusting the pH to 7.0 and 9.0 using concentrated hydrochloric acid. Stock standard solutions of each metal (containing 1000 μg mL^{-1} of metal ions) was prepared by dissolving a known amount of the metal salt in deionised water to give 100 mL of solution.

6.2.2 Analysis of metal ions

The measurements were carried out according to the method described in Section 5.2.2.

6.2.3 Characterization of $HQ@SiO_2$

Preparation of the samples for the instruments was carried out according to the methods described in Section 3.1.2.

6.2.4 Synthesis of 5-formyl-8-hydroxyquinoline

HQ was converted to its 4-formyl derivative using a variation of the method described by Goswami *et al.*[16]. To a two necked round-bottomed flask (250 mL) were transferred 8-hydroxyquinoline (10 g), ethanol (40 mL) and aqueous sodium hydroxide (25 mL) (20 g of NaOH dissolved in 25 ml of water). The mixture was

refluxed while chloroform (11 mL) was added dropwise over a period of an hour. After refluxing for 24 hours, the solvent was removed on a rotary evaporator. The resulting residue was dissolved in deionised water (250 mL) and the solution was made slightly acidic using diluted HCl (until the pH of the solution reached 5.5). The resulting brown coloured sticky solid was filtered off and left overnight in an oven at 40 ºC. The solid was mixed with anhydrous sodium sulfate until it became free flowing and extracted for 24 hours with anhydrous diethyl ether using a Soxhlet apparatus. The solvent was evaporated off, resulting in a yellow solid material.

6.2.5 Attachment of 5-formyl-8-hydroxyquinoline to the amino-nanoscavenger

FHQ (0.60 g) was transferred to a two necked round-bottomed flask (500 mL) fitted with a reflux condenser and anhydrous diethyl ether (200 mL) was added. The mixture was sonicated for 10 minutes and $NH_2@SiO_2$ (I) (Prepared as described in Section 4.2.4.1) (4.00 g) was added. The mixture was sonicated for an hour and stirred for 24 hours at room temperature. The mixture was left in the fume cupboard until all solvent evaporated. The excess of FHQ was removed by extracting the product for 24 hours in a Soxhlet apparatus with ethanol. The product was dried under continuous vacuum for 5 hours.

6.2.6 Measurement of the copper capacities of $HQ@SiO_2$

This experiment was carried out according to the method described in Section 4.2.5.

6.2.7 Extraction of metals using the $HQ@SiO_2$

This experiment was carried out according to the method described in Section 5.2.7.

6.2.8 Rate of metal uptake by the HQ@SiO_2

To two low density polyethylene bottles (1 L), containing deionised water (1 L) was added a HQ@SiO_2 suspension (250 mg of nanoscavenger dispersed in 5 ml of tris-buffer, pH = 7, 1 M) and the contents of each bottle were mixed. 1 mL of a solution containing 50 µg mL^{-1} of each of Cu (II), Ni (II), Pb (II) and Cd (II) [First group of metals] or, Co (II), Cr (III), Mn (II) and Zn (II) [Second group], were added to the bottle. The solutions were left for different equilibrium times (1 minute, 30 minutes, 1 hour, 3 hours, 6 hours, 15 hours and 24 hours) prior to vacuum filtration through a 0.2 µm cellulose nitrate membrane filter. The filter was then transferred to a polyethylene tube (10 mL) and a mixture of HCl and HNO_3 (1:1) (5 mL) was added to each tube. The tube was heated to 45 ºC for 2 hours using a water bath, then centrifuged for an hour and the acidic solution was transferred to a volumetric flask (10 mL). Deionised water (5 mL) was added to each tube, shaken for 2 minutes and centrifuged; the aqueous solution was added to the volumetric flask. The volume was made up to the mark using deionised water and the metal concentrations in the resulting solutions were measured by FAAS.

6.2.9 Effect of pH on metal extraction efficiencies

This experiment was carried out according to the method described in Section 5.2.9.

6.2.10 Colorimetric determination of copper as its dithiocarbamate complex

This experiment was carried out according to the method described in Section 5.2.10.

6.2.11 Calibration of the colorimetric approach

This experiment was carried out according to the method described in Section 5.2.11.

6.2.12 HQ@SiO_2 extraction of Cu^{2+} from tap water

This experiment was carried out according to the method described in Section 5.2.12 but replacing the nanoscavenger to be HQ@SiO_2.

6.3 Results and discussion

6.3.1 Synthesis of FHQ

FHQ was prepared by a variation of the method reported by Goswami *et al.*[16]. The reaction time was increased to 24 hours to increase the yield; the product was extracted with anhydrous diethyl ether in a Soxhlet apparatus achieving around 20 % yield. The ^{13}C NMR spectrum of the product showed a signal at 192 ppm for the carbon of the aldehyde group and in the ^{1}H NMR spectrum a singlet signal appears at δ 10.1 ppm for O=C-H . Moreover the FT-IR spectrum demonstrated C-H stretching bands from the aldehyde group at 2828 and 2755 cm^{-1} and a band at 1685 cm^{-1} from the carbonyl (CO) group. All of these results confirm the formation of 5-formyl-8-hydroxyquinoline.

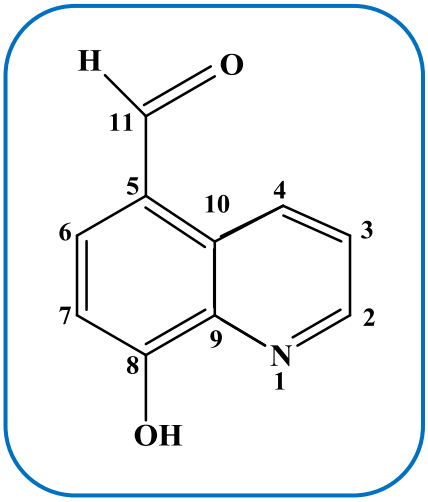

Figure 6.2 The structure of FHQ

Table 6.1 ^{13}C NMR spectrum result of FHQ

Carbon atom position	C_2	C_3	C_4	C_5	C_6	C_7	C_8	C_9	C_{10}	C_{11}
Signal (ppm)	147	124	140	121	134	110	148	137	128	192

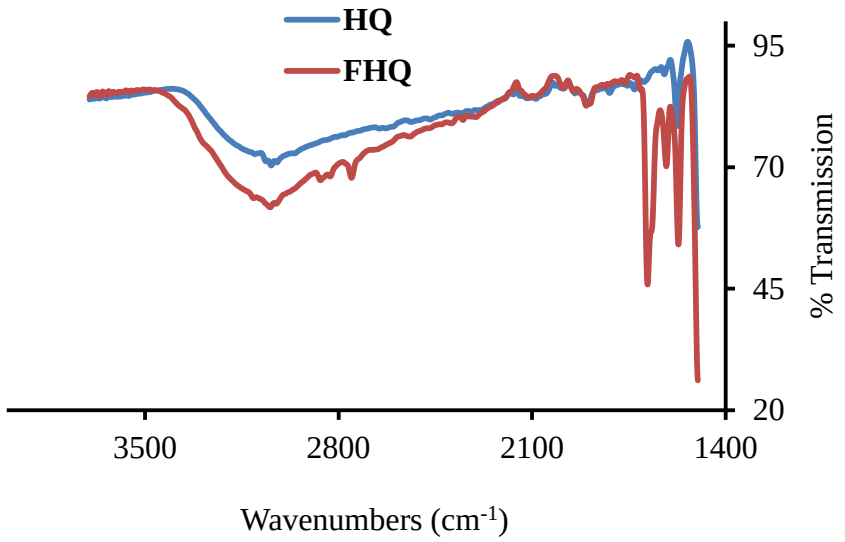

Figure 6.2 FT-IR spectrum of HQ and FHQ

6.3.2 Synthesis of the HQ@SiO_2

The final step in the preparation of HQ@SiO_2 was achieved by condensing NH_2@SiO_2 with FHQ in anhydrous diethyl ether to form a Schiff base. This caused the surface of the silica to turn brown which could be a good sign of successful loading of HQ onto the surface of the silica.

6.3.2.1 Morphology and particle size distribution

Scanning electron microscope showed spherical particles with a mean diameter around 249 ± 10 nm (Figure 6.3). Laser scattering particle size analysis indicated a monodispersed population of particles with a mean diameter of 236 ± 35 nm (Figure 6.4). There had been no significant change of particle morphology, population or the size compared to the original silica. These results showed that the particles remain

within the size range required for colloidal dispersion (250 nm) which allows them to be used for the extraction of metal ions from the water using the nanoscavenger dispersion extraction approach. Dispersed particles of this size, can stay suspended long enough for enrichment of the metal ions to occur. The copper capacity of the HQ@SiO$_2$ was 1.34 ± 0.1 mmol g^{-1}.

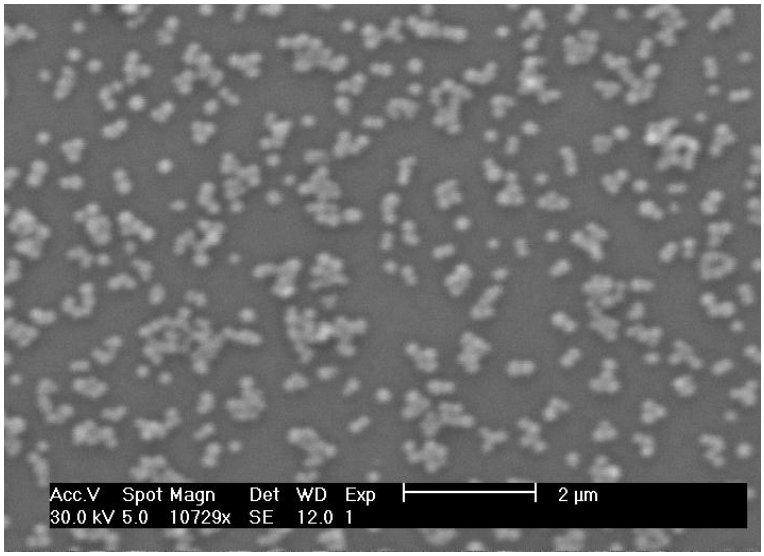

Figure 6.3 SEM image (10729 X) of HQ@SiO$_2$

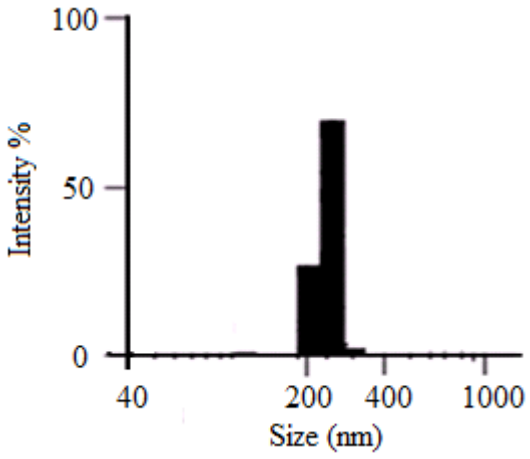

Figure 6.4 LSPSA of HQ@SiO$_2$

6.3.2.2 Thermogravimetric analysis of HQ@SiO$_2$

Thermogravimetric analysis was carried out in air over the temperature range from 25 to 800 ºC. The TGA suggested a significant loading of 8-quinolinol on the silica surface. Figure 6.5b showed a 7 % weight loss between 25 to 125 ºC that was attributed to the thermodesorption of physically adsorbed water and remaining solvent[17]. A 2.7 % weight loss in the 125 to 304 ºC region was attributed to thermal decomposition of 8-hydroxyquinoline on the surface of silica. Between 304 and 773 ºC oxidation of the remaining organic materials on the surface of silica particles resulted in a further 16 % weight loss. The HQ@SiO$_2$ lost 7 % more weight between 125 and 773 ºC than the NH$_2$@SiO$_2$ which is confirmed the attachment of FHQ to the silica surface (Figure 6.5a).

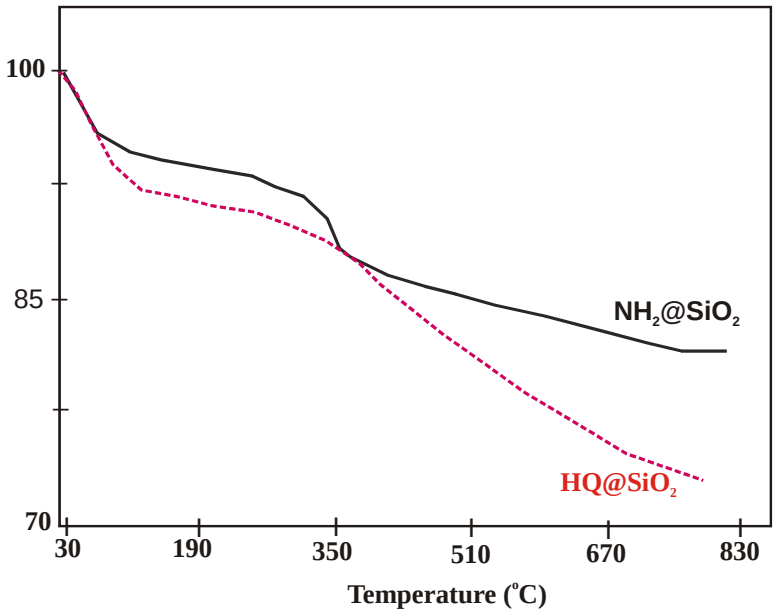

Figure 6.5 Thermogravimetric analysis of a) NH$_2$@SiO$_2$ b) HQ@SiO$_2$

6.3.2.3 Infrared spectroscopy of HQ@SiO$_2$

In order to confirm the linkage of 8-hydroxyquinoline to the silica surface infrared spectroscopy was carried out between 4000 and 200 cm^{-1}. The FT-IR spectrum (Figure 6.6) showed bands at 2978, 2935 and 2895 cm^{-1} due to C-H stretches. The band of CO which appears at 1685 cm^{-1} in the 5-F-8-HQ spectrum was found to be

absent from the HQ@SiO$_2$ spectrum. A stretching band appears at 1627 may be attributed to forming C=N[16]. The bands at 1595, 1548, 1505 and 1471 cm^{-1} may be assigned to ring vibrations. The broad and strong band which appears at 1060 cm^{-1} attributed to siloxane (–Si–O–Si–). Most of the structure of silica consists of Si-O-Si, causing its band to become strong, and weakening other functional groups.

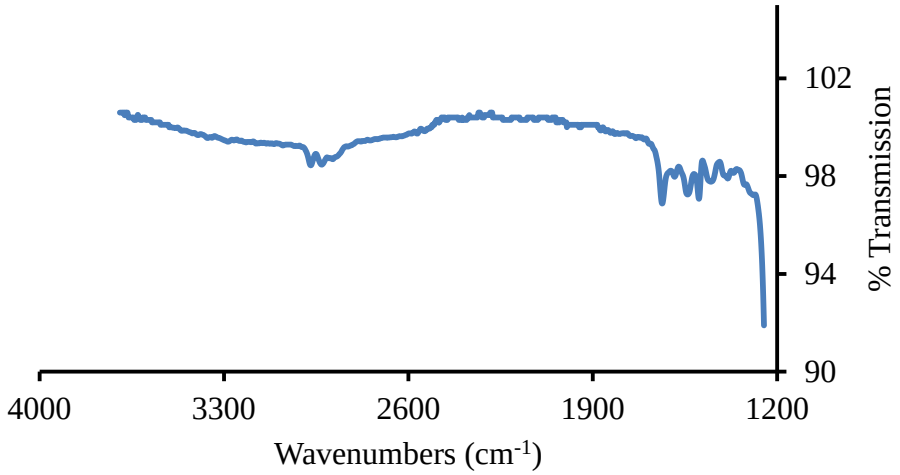

Figure 6.6 FT-IR spectroscopy of HQ@SiO$_2$

6.3.3 The settling of the HQ@SiO$_2$ particles from an aqueous suspension

Stability of the nanoscavenger particles in aqueous suspension is an essential factor of the nanoscavenger concept of NSDE as the particles must remain dispersed in the solution. This allows the particles to move naturally throughout the sample solution without external agitation. The stability of a HQ@SiO$_2$ suspension was therefore assessed by measuring the settling rate of the particles over an extended time period (Figure 6.7). Light transmission remained essentially constant for more than 7 hours, demonstrating extremely low sedimentation.

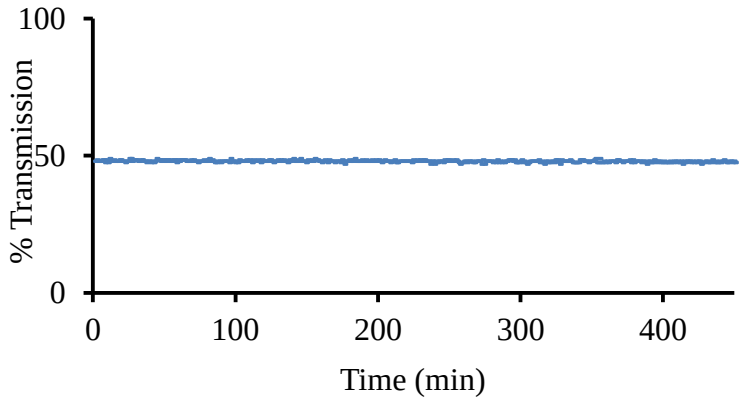

Figure 6.7 Settling of HQ@SiO$_2$ from its suspension in water

6.3.4 Extraction of metals ions from water using the HQ@SiO$_2$

As mentioned in Section 5.3.7 it is difficult to interpret thermodynamically the obtained results of metal chelation with hydroxyquinoline in the absence of the data of formation constant for metal-hydroxyquinoline complexes. The ability of HQ@SiO$_2$ to enrich metal ions from water was tested by spiking aliquots of metal ions into two of 1 L water samples. To a first 1 L water sample was added 50 µg of each of four metals (Cu^{2+}, Cd^{2+}, Ni^{2+} and Pb^{2+}). To a second 1 L water sample was added 50 µg of Co^{2+}, Cr^{3+}, Mn^{2+} and Zn^{2+}. The HQ@SiO$_2$ (200 mg) was dispersed in each water sample and the complexed metal was collected by filtration. The metal ions were released from the nanoscavenger by acidification and oxidation using a mixture of HCl and HNO_3 (1:1). The recovery results of eight metals were more than 92 % on all metals except Mn, which had a 45 % recovery (Table 6.2). The low affinity of Mn as a hard metal to HQ@SiO$_2$ may be the main reason for the low recovery. The recovery of Mn can be enhanced by increasing the pH of the water sample or by increasing the equilibration time as discussed later[18]. Soylak and Tuzen[19] reported that manganese can be efficiently extracted from water in the pH range 8-10. The preconcentration factor of 100-fold can be improved by decreasing the final volume of the extracted metals.

Table 6.2 The recovery of metals extracted from water using the HQ@SiO_2 (Initial sample contained 50 µg L^{-1} of each metal)

Metal	Preconcentration factor	% Average recovery ± SD, n = 3
Cu	100	98 ± 2
Cd	100	92 ± 2
Ni	100	109 ± 0
Pb	100	100 ± 0
Co	100	98 ± 2
Cr	100	104 ± 10
Mn	100	45 ± 8
Zn	100	92 ± 0

6.3.5 Rate of metal uptake from dilute solution by the HQ@SiO_2

The extraction of metals over time was studied to evaluate the optimized time for metal extraction using HQ@SiO_2. In general water with low pH (< 7) is acidic and H^+ can leach the metal ion from the container. Basic conditions cause the precipitation of many metal ions. Therefore a tris buffer was added to avoid any change of pH during sample preparation which could affect the recovery results. The pH of the water sample was adjusted to pH = 7. The recoveries of the first group of metal ions: Cu^{2+}, Cd^{2+}, Ni^{2+} and Pb^{2+} (Figure 6.8) and the second group of metal ions: Co^{2+}, Cr^{3+}, Mn^{2+} and Zn^{2+} (Figure 6.9) were drawn versus equilibration times. An equilibrium time of 1 minute was found to be sufficient to reach almost maximum uptake of Zn and for Pb and Mn to reach 70 % uptake. Only 51, 34, 50, 67 and 8 % of the maximum recovery was however achieved for Cu, Cd, Ni, Co and Cr respectively. The extraction of the metals increases with time, with lead reaching maximum uptake within 60 minutes and Cu and Ni reaching more than 90 % uptake in the same equilibration time. For most of the metals 3 hours was found to be sufficient to attain maximum uptake onto the nanoscavenger, the exception being Cd, which needed more than 6 hours. Overall, the results showed that once all the metal ions had reached their maximum extraction, increasing the time between the metal ions and the nanoscavenger has no significant effect on the extraction.

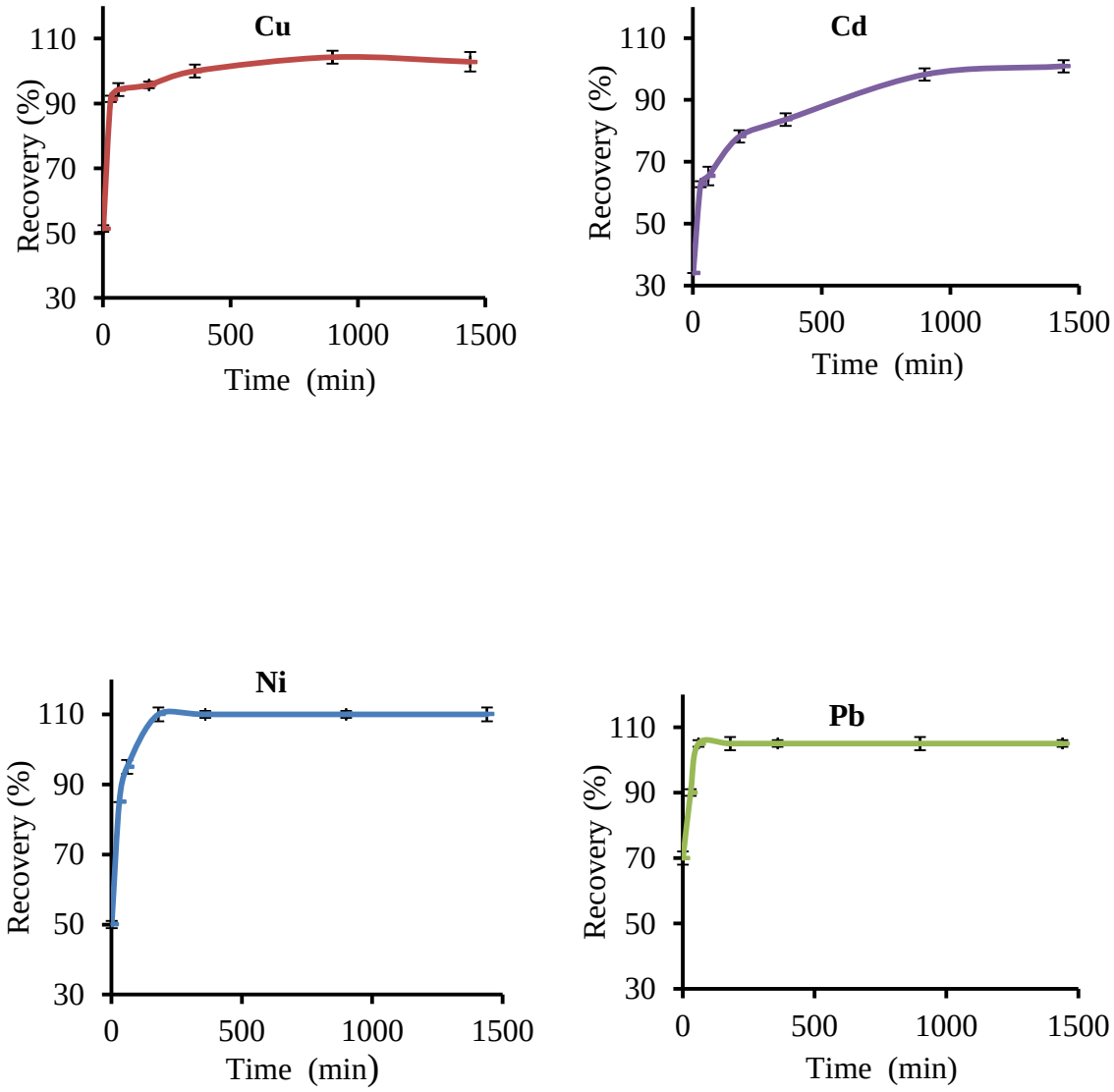

Figure 6.8 Effect of time on metal ion uptake by $HQ@SiO_2$ (First group)

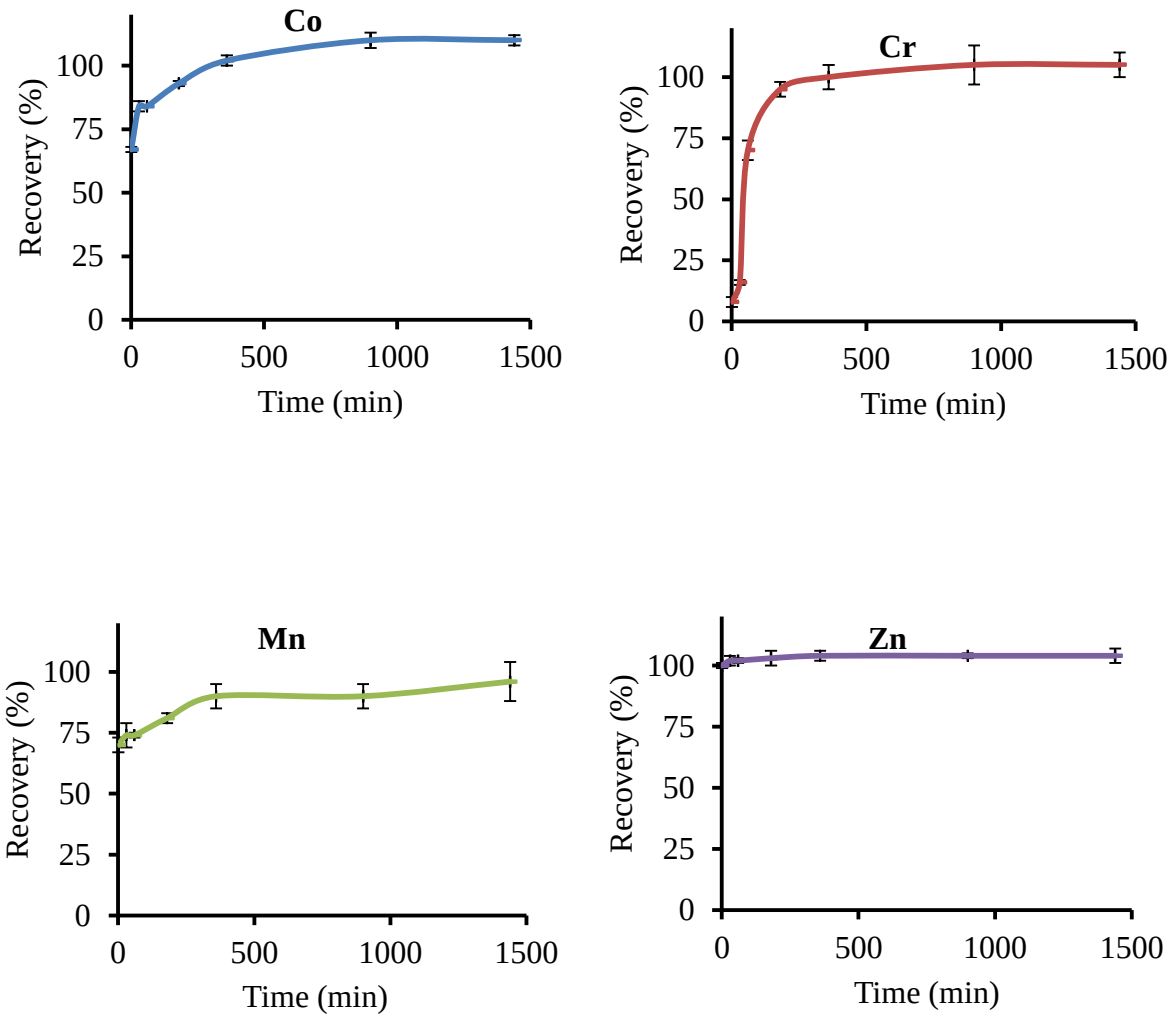

Figure 6.9 Effect of time on metal ion uptake by $HQ@SiO_2$ (Second group)

6.3.6 Effect of pH on the metal enrichment

The pH of the sample solution is an important factor in the extraction of metal ions from solution. Buffers were therefore added to the sample solution to maintain accurate pH values between 4 and 9. This pH range was chosen to avoid strong acid or base conditions because the chelating group on the surface of the nanoscavenger will be damaged by strong acid medium (pH < 4) and a pH > 9 is high enough to dissolve the silica. Acetate buffer was used to adjust the pH of the sample solution to 4 and tris buffer to adjust the sample solution to 7 and 9. Table 6.3 illustrates the

recovery of the metals from different pH media. It shows that some metals, such as Co, Zn and Ni, have not been influenced significantly by changing the pH value. However, Cd, Cr, Mn and Pb recoveries improved by increasing the pH. This was especially true for Cr, which had no recovery at all at pH = 4. The reason for the decrease in the extraction of some metals concurrent with a decrease in the pH value might be that the concentration of hydrogen-ion rises as the pH value lowers, which increases the tendency towards replacement of the metal from the chelate by hydrogen ions[20]. In general, binding of the metal ions to the complexing agent decreases with decreasing the pH value due to the increasing competition between the metal ions and H^+. For the Mn (II) it was reported in several articles[18, 21-23] that the optimized pH value to extract Mn was in the pH range 8-10 as discussed in Section 5.3.9. The extraction of the Cu ion reduces slightly as pH rises which may be attributed to loss of some copper as a result of precipitating copper with increasing the pH value.

Table 6.3 Effect of pH on the extraction of metals using HQ@SiO_2

		Average % Recovery of Metal ± SD (n = 3)							
Buffer	pH	Cu	Cd	Ni	Pb	Co	Cr	Mn	Zn
Acetate-buffer	4	99±2	83±1	97±6	39±9	105±9	0	8±3	93±2
Tris-buffer	7	92±4	97±2	97±6	100±0	100±0	95±2	80±0	98±0
Tris-buffer	9	92±0	98±2	103±6	100±0	100±0	93±2	102±3	98±2

6.3.7 A comparison of Cu (II) determinations using a HQ@SiO_2 with a conventional colorimetric procedure

The performance of a HQ@SiO_2 in the nanoscavenger dispersion extraction procedure was evaluated by comparing it against a widely adopted procedure based on solvent extraction of a copper complex. For this experiment water samples were

collected from a variety of domestic water sources across Southampton, UK. The first method was a colorimetric procedure involving solvent extraction of the Cu diethyldithiocarbamate complex into chloroform. The Cu was determined by measurement of the absorbance of the resulting chloroform extract at 435 nm. The concentration of Cu was calculated based on calibration with standard solutions. The second method employed the HQ@SiO_2 to extract the Cu ion from the water with subsequent measurement of the extracted Cu ion by FAAS. The concentration of Cu from the NSDE method was plotted against the concentration measured using the colorimetric method (Figure 6.10). The slope of the line was 1.0176 ± 0.0099 which is statically equal to 1 at the 95 % confidence level. The result proved that the Cu concentrations measured by both approaches was identical. The good agreement of the results obtained by the two methods suggests the HQ@SiO_2 approach to be a promising new method for the extraction of metals from water. The Cu concentrations on the tap water samples were found to range from 0.03 to 0.95 µg mL^{-1}.

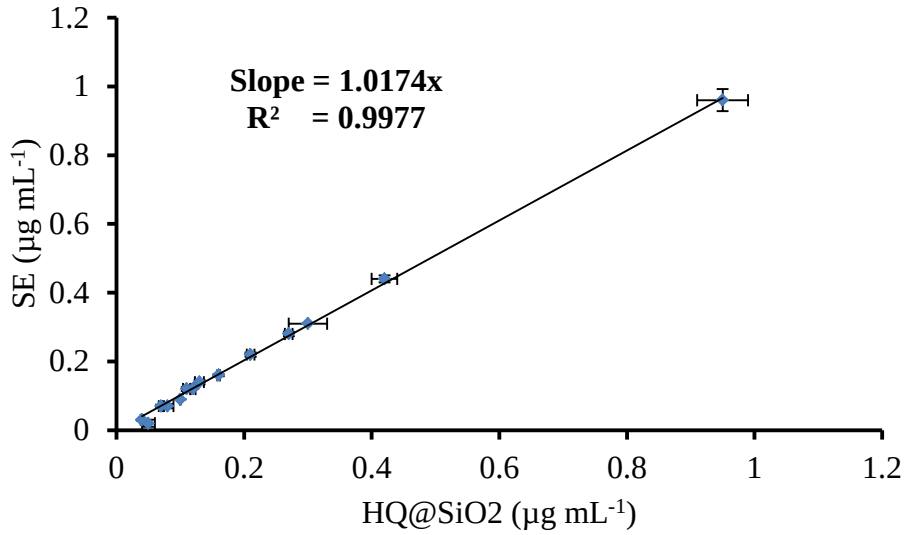

Figure 6.10 Correlation of Cu measurements obtained HQ@SiO_2 nanoscavenger dispersion extraction and solvent extraction methods

6.4 Conclusion

Mesoporous silica of (250 nm) was modified with $NH_2Si(OEt)_3$ (as described in Section 4.2.3.1) and then reacted with FHQ to chemically anchor HQ onto the particles through a Schiff base condensation reaction. The colour of the particles changed to be brown after loading HQ giving a good sign of successful modification. The thermogravimetric analysis, infrared spectroscopy and copper capacity measurement are all confirmed the immobilization of HQ on the silica particles.

Scanning electron microscope and laser scattering particle size analysis confirm the size of HQ@SiO_2 particles still in colloidal range of size (250 nm) regardless of two steps modifications. This lead to a good dispersion of the HQ@SiO_2 particles which remained suspended in water more than 7 hours without noticeable sedimentation. The good dispersion of the nanoscavenger in water leads to a high recovery results.

The HQ@SiO_2 was applied to enrich eight metal ions (Cu^{2+}, Cd^{2+}, Ni^{2+}, Pb^{2+}, Cr^{3+}, Co^{2+}, Mn^{2+} and Zn^{2+}). The recovery result of the metals was greater than 92 % with 100-fold preconcentration factor. When the HQ@SiO_2 was utilized to preconcentrate Cu^{2+} from tap water samples, the concentrations of Cu^{2+} that was found was similar of the concentrations found by results which were carried out using solvent extraction. These results attained from primary investigations of HQ@SiO_2 give a good indication of using HQ@SiO_2 as promising solid phase to preconcentrate metal ions from water samples using NSDE technique.

6.5 References

(1) Kim, Y. S.; Shin, J. H.; Choi, Y. S.; Lee, W.; Lee, Y. I. *Microchem. J.* **2001**, *68*, 99-107.

(2) Oprea, G.; Michnea, A.; Mihali, C. *Am. J. Appl. Sci.* **2007**, *4*, 592-596.

(3) Stary, J. *Curr. Cont./Phys. Chem. Earth Sci.* **1981**, 16-16.

(4) Nickson, R. A.; Hill, S. J.; Worsfold, P. J. *Anal. Proc.* **1995**, *32*, 387-395.

(5) Willie, S. N.; Tekgul, H.; Sturgeon, R. E. *Talanta* **1998**, *47*, 439-445.

(6) Willie, S. N.; Sturgeon, R. E.; Berman, S. S. *Anal. Chim. Acta* **1983**, *149*, 59-66.

(7) Jonas, P. M. M.; Eve, D. J.; Parrish, J. R. *Talanta* **1989**, *36*, 1021-1026.

(8) Askun, H.; Gulbakan, B.; Celikbicak, O.; Uzun, C.; Guven, G.; Salih, B. *J. Appl. Polym. Sci.* **2008**, *107*, 2714-2722.

(9) Wen, B.; Shan, X. Q.; Xu, S. G. *Analyst* **1999**, *124*, 621-626.

(10) Malamas, F.; Bengtsson, M.; Johansson, G. *Anal. Chim. Acta* **1984**, *160*, 1-10.

(11) Weetall, H. H. *Biochim. Et Biophys. Acta* **1970**, *212*, 1-7.

(12) Hill, J. M. *J. Chromatogr.* **1973**, *76*, 455-458.

(13) Sugawara, K. F.; Weetall, H. H.; Schucker, G. D. *Anal. Chem.* **1974**, *46*, 489-492.

(14) Fulcher, C.; Crowell, M. A.; Bayliss, R.; Holland, K. B.; Jezorek, J. R. *Anal. Chim. Acta* **1981**, *129*, 29-47.

(15) Marshall, M. A.; Mottola, H. A. *Anal. Chem.* **1983**, *55*, 2089-2093.

(16) Goswami, A.; Singh, A. K.; Venkataramani, B. *Talanta* **2003**, *60*, 1141-1154.

(17) Araujo, A. S.; Jaroniec, M. *Thermochim. Acta* **2000**, *363*, 175-180.

(18) Sarmani, S. B.; Abdullah, M. P.; Bobaker, A. M. *J. Radioanal. Nucl. Chem.* **2004**, *259*, 257-260.

(19) Soylak, M.; Tuzen, M. *J. Hazard. Mater.* **2006**, *138*, 195-200.

(20) Martell, A. E.; Calvin, M. *Chemistry of the metal chelate compounds*, 2nd ed.; Prentice-Hall: New York, **1953**.

(21) Lemos, V. A.; David, G. T. *Microchem. J.* **2010**, *94*, 42-47.

(22) Citak, D.; Tuzen, M.; Soylak, M. *J. Hazard. Mater.* **2010**, *173*, 773-777.

(23) Kenduzler, E.; Turker, A. R.; Yalcinkaya, O. *Talanta* **2006**, *69*, 835-840.

Chapter 7

Mercaptobenzamide-nanoscavenger ($SH@SiO_2$)

7.1 Introduction

The surface of silica gel can be easily modified by thiol moieties to produce thiol-silica to extract metal ions from water. Sahin *et al.*[1] modified silica gel with 3-mercaptopropyltrimethoxysilane and used it for selective separation and preconcentration of selenite (Se^{4+}) from aqueous solutions containing Se^{4+} and selenate (Se^{6+}). Furthermore, they applied mercapto-silica for trace metal preconcentration[2], namely Cu^{2+}, Cd^{2+}, Pb^{2+} and Zn^{2+} and extracted As (III)[3] and Sb (III) from highly saline aqueous solutions. This type of sorbent has only one ligand centre (-SH) which means no chelation between metal and ligand will take place. This will increase the chance to leach the metal ions during sample preparation.

Rudner *et al.*[4] synthesized a new adsorbent material mercaptobenzamide-silica gel possessing multiligand centres by reacting aminopropyl-silica gel with methyl thiosalicylate. The product was packed into a column located in the loop of an injection valve. The sample was introduced and eluted, the final extracted sample being introduced to the instrument on line. The main disadvantages of this procedure are complexity, especially as the column needs at least 3 months before it can be reused and it is time consuming to prepare the column. It is flushed with 2 M nitric acid after each operation. Moreover, the ability of mercaptobenzamide-silica gel sorbent to extract Cd from water was investigated by Pavon and his workers[5]. They found that the recovery results were pH dependent and the optimized pH to extract Cd was at pH 8. A new simple approach (nanoscavenger dispersion extraction), using mercaptobenzamide-nanoscavenger ($SH@SiO_2$) is established in this chapter to preconcentrate elements from aqueous samples.

The synthesis of mercaptobenzamide-nanoscavenger was accomplished in two steps. Firstly, mesoporous silica (prepared as described in Section 3.3.1.4) was modified with a 3-aminopropyltriethoxysilane in dried toluene (as described in Section

4.2.4.1). The aminopropyl-nanoscavenger was then reacted with methyl thiosalicylate by displacement of methoxy groups to produce mercaptobenzamide-nanoscavenger[6] (Figure 7.1).

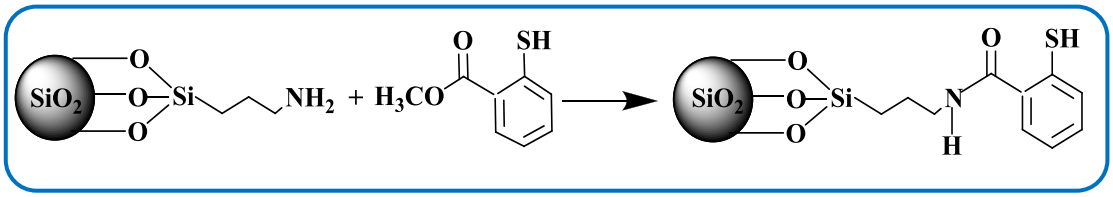

Figure 7.1 Synthesis of SH@SiO_2

The mercaptobenzamide-nanoscavenger has a unique characteristic if compared to the other nanoscavengers in that it contains three atoms (sulfur, oxygen and nitrogen) as donor sites. These ligands atoms are located to form two different chelating angles (bite angles). The presence of a number of chelating centres may increase the complexing capacity of SH@SiO_2 nanoscavenger for one or more metal ions with superb selectivity. In addition, the chelate complex enhances the stability of metal ions on the nanoscavenger and may prevent leaching of metal ions during the sample preparation.

The prepared SH@SiO_2 was characterised using variety of techniques such as SEM, LSPSA, TGA and FT-IR. The capability of mercaptobenzamide-nanoscavenger as an extracting agent for trace metal ions was investigated by applying SH@SiO_2 to preconcentrate eight metal ions from water samples prior to their determination by FAAS.

7.2 Preparation of SH@SiO_2

7.2.1 Materials

Methyl thiosalicylate (methyl 2-mercaptobenzoate) (97 %), hydrochloric acid [36 % (w/v), AR grade], tris(hydroxymethyl)aminomethane and sodium acetate were purchased from Aldrich (Poole, UK). Chloroform (HPLC grade) was supplied by

Rathburn (Walkerburn, UK). Nitric acid (AR grade), sodium diethyldithiocarbamate and triammonium citrate were obtained from BDH limited (Poole, U.K).

Tris(hydroxymethyl)aminomethane and acetate buffer were prepared as described in Section 5.2.1. Stock standard solutions (1000 µg mL^{-1}) of Cu^{2+}, Cd^{2+}, Ni^{2+}, Pb^{2+}, Co^{2+}, Cr^{3+}, Mn^{2+} and Zn^{2+} were individually prepared according to the method described in Section 5.2.1.

7.2.2 Analysis of metal ions

The measurements were carried out according to the method described in Section 5.2.2.

7.2.3 Characterization of mercaptobenzamide-nanoscavenger

Preparation of the samples for the instruments was carried out according to the methods described in Section 3.1.2.

7.2.4 Synthesis of $SH@SiO_2$

Aminopropyl-nanoscavenger (prepared as described in Section 4.2.4.1) (4 g) and ethanol (200 mL) were transferred to a two neck round-bottomed flask (500 mL). The mixture was sonicated for an hour and heated to 90 ºC. Ethanol (30 mL) and methylthiosalicylate (5 mL) were transferred to a dropping funnel, mixed together and added slowly to the reaction flask. The reaction was left to proceed at 90 ºC for 24 hours. The suspended solid was isolated by centrifugation, rinsed five times with ethanol and dried under continuous vacuum.

7.2.5 Measurement of the copper capacity of $SH@SiO_2$

The experiment was carried out according to the method described in Section 4.2.5.

7.2.6 Extraction of metals using $SH@SiO_2$

This experiment was carried out according to the method described in Section 5.2.7.

7.2.7 Rate of metal uptake by $SH@SiO_2$

This experiment was carried out according to the method described in Section 6.2.8.

7.2.8 Effect of pH on metal extraction efficiencies using $SH@SiO_2$

This experiment was carried out according to the method described in Section 5.2.9.

7.2.9 Colorimetric determination of copper as a dithiocarbamate complex

This experiment was carried out according to the method described in Section 5.2.10.

7.2.10 Calibration of the colorimetric approach

This experiment was carried out according to the method described in Section 5.2.11.

7.2.11 $SH@SiO_2$ extraction of Cu^{2+} from tap water

This experiment was carried out according to the method described in Section 5.2.12 but replacing the nanoscavenger with $SH@SiO_2$.

7.3 Results and discussion

7.3.1 Morphology and particle size distribution

The size and morphology of the particles are very important, as they affect the stability of the particles when suspended in water. Thus laser scattering particle size analysis and scanning electron microscopy were carried out to ensure that the size of

the particles was as close as possible to the targeted size (250 nm) with spherical morphology. The LSPSA showed the size to be 400 nm (47 nm standard deviation) (Figure 7.2). SEM showed that the particles were spherical and their averaged size was 240 ± 20 nm (Figure 7.3). Aggregation of some particles during measurement could be the main reason for unexpected results in LSPSA measurement. The SEM result confirmed that the morphology and the size of particles had not been influenced by the two step modification. The averaged size of SH@SiO_2 particles was still close to the colloidal range with spherical morphology.

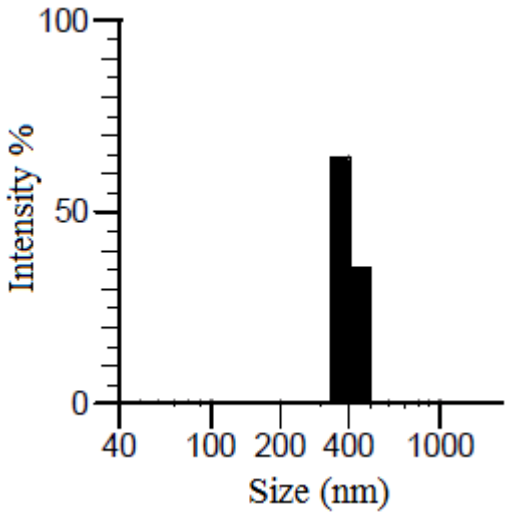

Figure 7.2 LSPSA of SH@SiO_2

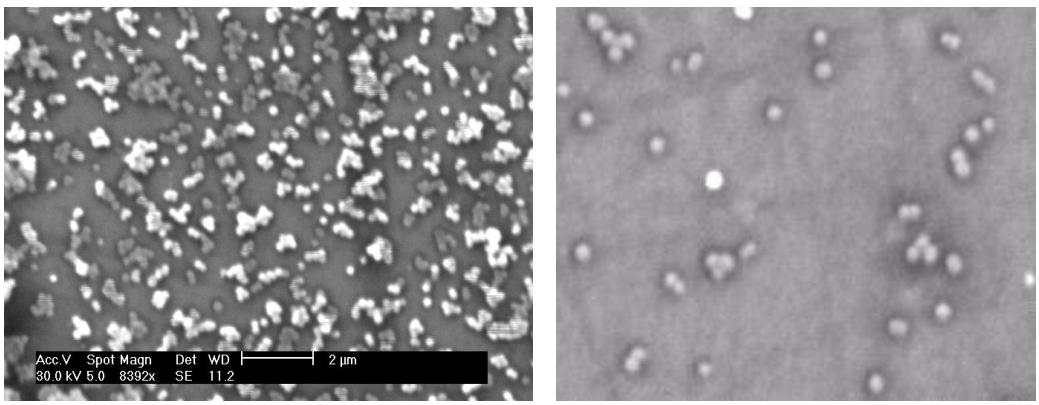

Figure 7.3 SEM images (8392X) of SH@SiO_2

7.3.2 Thermogravimetric analysis of $SH@SiO_2$

In order to confirm the anchoring of the thiol moiety to the surface of the silica particles, thermogravimetric analysis was applied. The TGA was carried out for the $NH_2@SiO_2$ and the $SH@SiO_2$ nanoscavengers (Figure 7.4). The TGA traces of $NH_2@SiO_2$ showed a 3 % weight loss between 124 and 340 ºC, followed by a 7 % weight loss between 340 and 773 ºC. In contrast, in the TGA trace of $SH@SiO_2$ most of the physically adsorbed water and remaining solvent were lost between 27 and 124 ºC. Around 4 % of weight loss between 124 and 344 ºC corresponded to the complete removal of water and remaining solvent from the structure of $SH@SiO_2$ and the start of combustion of organic materials. The last area of weight loss (14 %) occurred between 344 and 773 ºC, and was attributed to complete oxidation of organic materials from the silica surface. The increased weight loss (8 %) in the $SH@SiO_2$ trace gave a good sign of successful linkage of the thiosalicylate group to the silica surface. Rudner *et al.*[4] found a large mass loss (11%) between 300 and 650 ºC in the TGA of thiosalicylate-silica gel, corresponding to a loss in the thiosalicylate group. It is obvious that mesoporous silica loads more of the thiosalicylate groups compared to silica gel, because of the large surface area of the mesoporous silica.

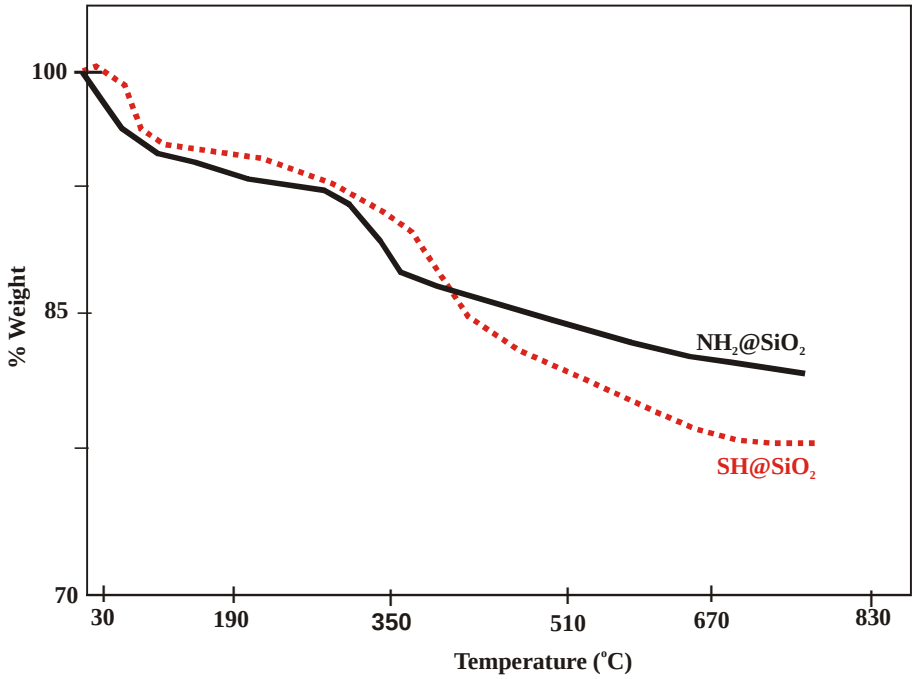

Figure 7.4 Thermogravimetric analysis of a) $NH_2@SiO_2$ b) $SH@SiO_2$

7.3.3 Infrared spectroscopy of $SH@SiO_2$

For additional confirmation of the anchoring of the thiosalicylate moiety to the surface of silica particles, FT-IR spectroscopy of $SH@SiO_2$ was carried out. Figure 7.5 shows the FT-IR spectra of $SH@SiO_2$. The large mass of silica compared to the small mass of the organic groups on the surface of the silica made it difficult to distinguish these groups. Most of the bands belonging to the groups on the surface of silica were weak and difficult to assign. The FT-IR of the $SH@SiO_2$ spectrum shows bands at 2933 and 2879 cm^{-1} that may correspond to a stretching vibration of the alkyl groups. A band at 2644 cm^{-1} can be attributed to an S-H stretching vibration[3]. In addition, bands at 1595, 1569, 1551, 1446 cm^{-1} may be attributed to C-$C_{aromatic}$ ring vibrations.

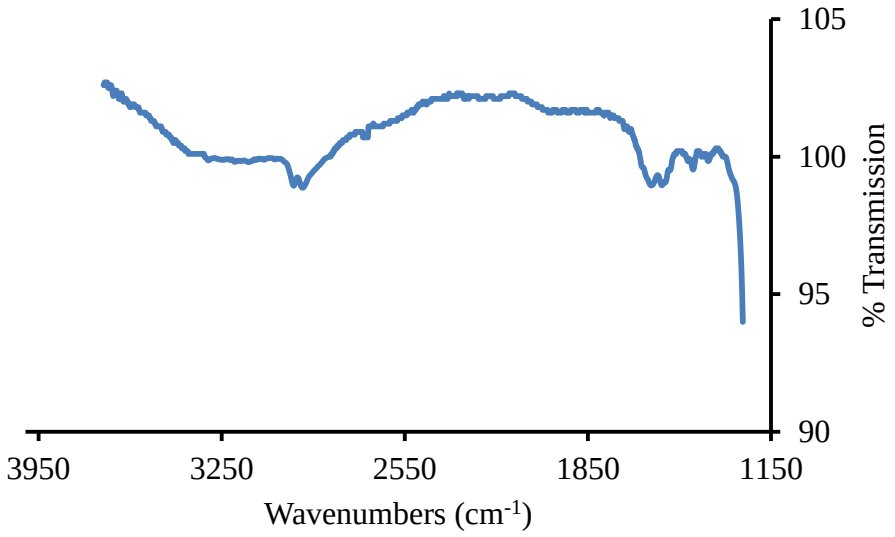

Figure 7.5 FT-IR spectroscopy of $SH@SiO_2$

7.3.4 Colour test and copper capacity measurement of $SH@SiO_2$

A colour test may reveal signs of loading of a thiosalicylate moiety on the surface of silica. Figure 7.6a illustrates the image of $SH@SiO_2$ particles prior to dispersal in a Cu (II) solution, in light yellow. The colour of the particles then turned to light blue (Figure 7.6b) after dispersal in 1000 µg mL^{-1} of Cu (II) solution. The change in colour is attributed to the attachment of divalent copper to the bidentate ligand or to the residual unreacted amine groups. Further confirmation of immobilization of thiosalicylate on the silica surface is the copper capacity result, which showed around 1.8 ± 0.06 mmol g^{-1} of copper per silica.

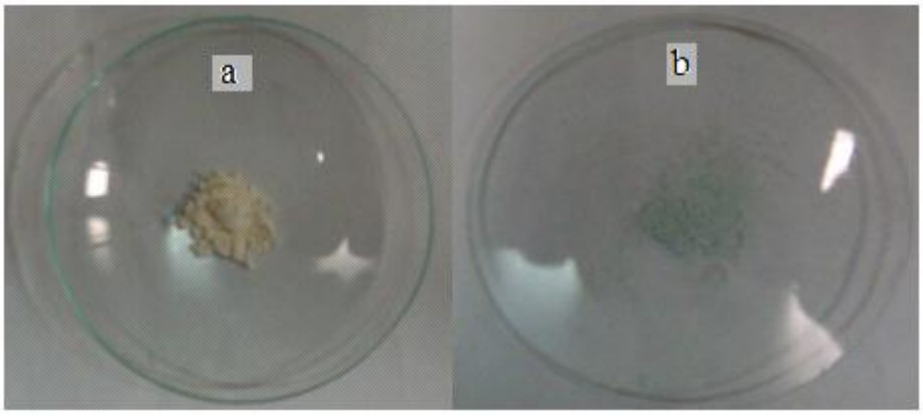

Figure 7.6 Colour tests of $SH@SiO_2$ particles a) prior to extraction of Cu^{2+} b) after extraction of Cu^{2+}

7.3.5 The settling of SH@SiO$_2$ particle from an aqueous suspension

The SH@SiO$_2$ nanoscavenger particles were synthesized for use in the NSDE technique to preconcentrate metal ions from water. This technique is simply based on dispersing the nanoscavenger particles into the water sample; the particles move naturally through the sample, thus no external agitation is required. Therefore the stability of the particles in an aqueous solution should be examined. The SH@SiO$_2$ particles were dispersed into deionised water and the settlement of the particles was observed over time using UV/Vis spectroscopy apparatus. Figure 7.7 shows that the particles remained suspended in the deionised water for more than 6 hours and no obvious settlement of the particles was noticed. This period of time will be more than enough to extract most of the metal ions from the aqueous solution. Even if some of the nanoscavenger particles precipitate, it will not prevent the attachment of metal ions to the nanoscavenger particles[7].

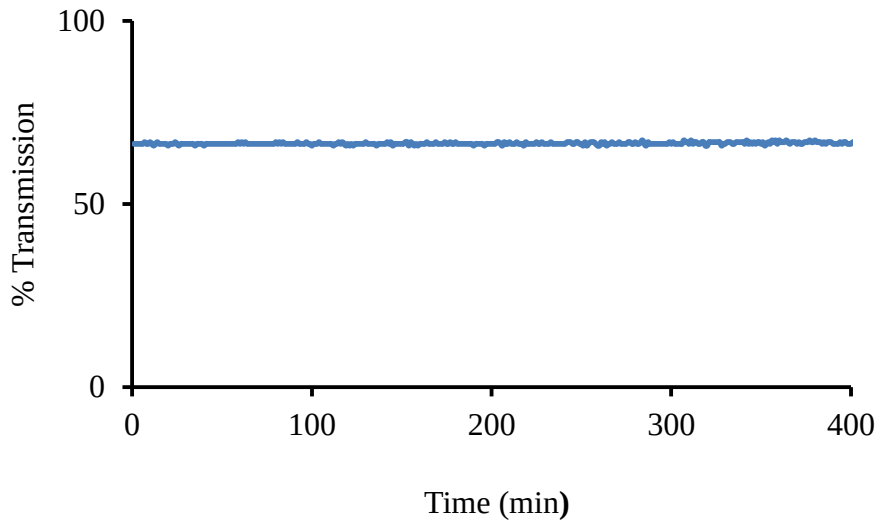

Figure 7.7 Settling of the SH@SiO$_2$ nanoscavenger from its suspension in water

7.3.6 Extraction of metal ions using SH@SiO$_2$

The formation constants for metal ion and oxygen and sulphur-donor ligands data are not available in the literature to predict thermodynamically the ability of

mercaptobenzamide-nanoscavenger to make strong chelating complex with metal ions. The SH@SiO_2 nanoscavenger was applied to preconcentrate and extract 8 metal ions from a synthetic water sample. The deionised water samples were spiked by 50 µg of each Cu^{2+}, Cd^{2+}, Ni^{2+}, Pb^{2+}, Co^{2+}, Cr^{3+}, Mn^{2+} and Zn^{2+}. The SH@SiO_2 nanoscavenger particles (200 mg) were suspended in the water samples and the particles with attached metals were recovered by filtration. The metals were released from ligands by acid (HCl: HNO_3, 1:1), as water cannot release the metals. This is probably due to the strong stability of the complex formed by metal ions and the ligand used. The precision of the method expressed as standard deviation for three replicates. The recovery results illustrated in Table 7.1, fall into three groups. The first group consisted of Cu^{2+}, Cd^{2+}, Pb^{2+} and Zn^{2+}, with recovery results of 99, 94, 90 and 90 %, respectively. The second group showed 30, 42 and 48 % recovery results for Ni^{2+}, Co^{2+} and Cr^{3+}, respectively. The third group recorded the lowest recovery results for Mn^{2+}, which suggests that the affinity of SH@SiO_2-nanoscavenger to this metal is very low. The metal ions do not exist in water as free ions, but are surrounded by water molecules, which are considered as a weak ligand. Attachment of the ligand to the SH@SiO_2 nanoscavenger required replacement of some water molecules around the metal ions by the ligands on the surface of the nanoscavenger. The mercaptobenzamide moiety has three donor atoms, O, N and S, which act as a bidentate ligand forming chelates with metal ions. The stability between the metal ions and the ligand depends on how easy the metals (Lewis acid) accept the electron pair donation from the ligands (Lewis base). The result showed that copper had the highest recovery results due to its highly complex stability constant with most of the ligands[8]. In the same manner, high recovery results for Cd^{2+}, Pb^{2+} and Zn^{2+} may be attributed to a good complexing constant between the metal and the ligand. The reason behind the low recoveries of Ni^{2+} and Co^{2+} is unclear, especially these metals exhibited high recovery with dithiocarbamate-nanoscavenger and hydroxyquinoline-nanoscavenger. In the case of Cr^{3+}, the recovery results were 48 %, which can be improved by increasing the equilibration time between the metal and the ligand, as will be discussed later. As discussed in Section 5.3.7 the Cr^{3+} (d^3) is kinetically inert towards ligand substitution[9]. Two hours is not enough to accomplish 100 % recovery. Manganese recorded no recovery at all, and this may be attributed to the fact that Mn is most likely to bind to a hard ligand according to hard soft acid base theory.

Table 7.1 The recovery of metals extracted from water using SH@SiO_2 (Initial sample contained 50 µg L^{-1} of each metal)

Metal	Preconcentration factor	% Average recovery ± SD, n = 3
Cu	100	99 ± 0.76
Cd	100	94 ± 1.15
Ni	100	30 ± 0
Pb	100	90 ± 1.36
Co	100	42 ± 1.6
Cr	100	48 ± 2
Mn	100	0 ± 0
Zn	100	90 ± 0.1

7.3.7 The effect of time on the extraction of metal ions using SH@SiO_2

The effect of time on the extraction of metal ions from water was studied by measuring the recovery results of metals over different periods. The recovery results for the metal ions were plotted against time. The error bars on the figure were calculated based on the standard deviation for three replicates to express the precision of the method. The time had no effect on the recovery results for Cu^{2+}, Cd^{2+}, Pb^{2+} (Figure 7.8) and Zn^{2+} (Figure 7.9), as they reached maximum recovery within one minute and no further change was observed afterwards. In addition, increasing the time did not improve the recovery results for manganese, and it was confirmed that manganese can not be extracted by SH@SiO_2 at this pH. On the other hand, increasing the equilibration time had a slight effect on the extraction of Ni^{2+} (Figure 7.8) and Co^{2+} (Figure 7.9). It was noted that the recovery of Ni^{2+} increased by 15 % when the time was extended to 30 minutes. The recovery remained constant in the equilibrium times from 30 minutes to 6 hours before the recovery dropped to 40 % after 15 hours. This means, there was leaching of Ni^{2+} from ligand due to substitution of Ni^{2+} by some cations. The recovery of Co^{2+} was increased from 40 % to 48 % when the equilibrium time increased to 1 hour, after which there was no significant change in the recovery with increasing the time. Meanwhile, the highest effect of time on the extraction of metals was in the recovery of Cr^{3+}. The recovery results of Cr^{3+} (Figure 7.9) had been just 7 % at 1 minute equilibrium, but it

increased gradually with increasing the equilibration time to reach maximum within 24 hours. The gradual increase in the recovery of Cr^{3+} over time may because the attachment of the Cr^{3+} to the SH@SiO_2 nanoscavenger is kinetically slow.

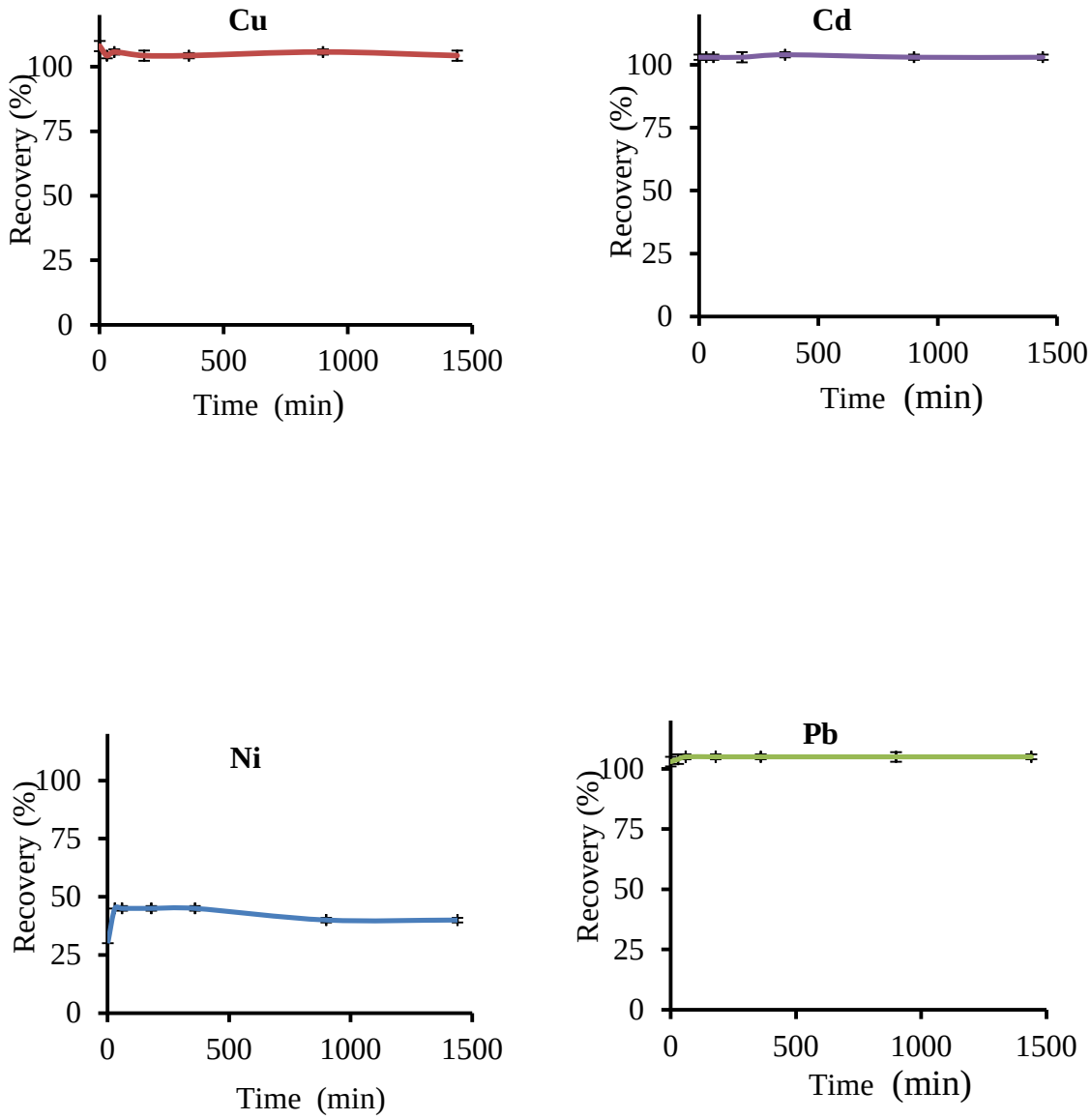

Figure 7.8 Effect of time on metal ion uptake by SH@SiO_2 (first group)

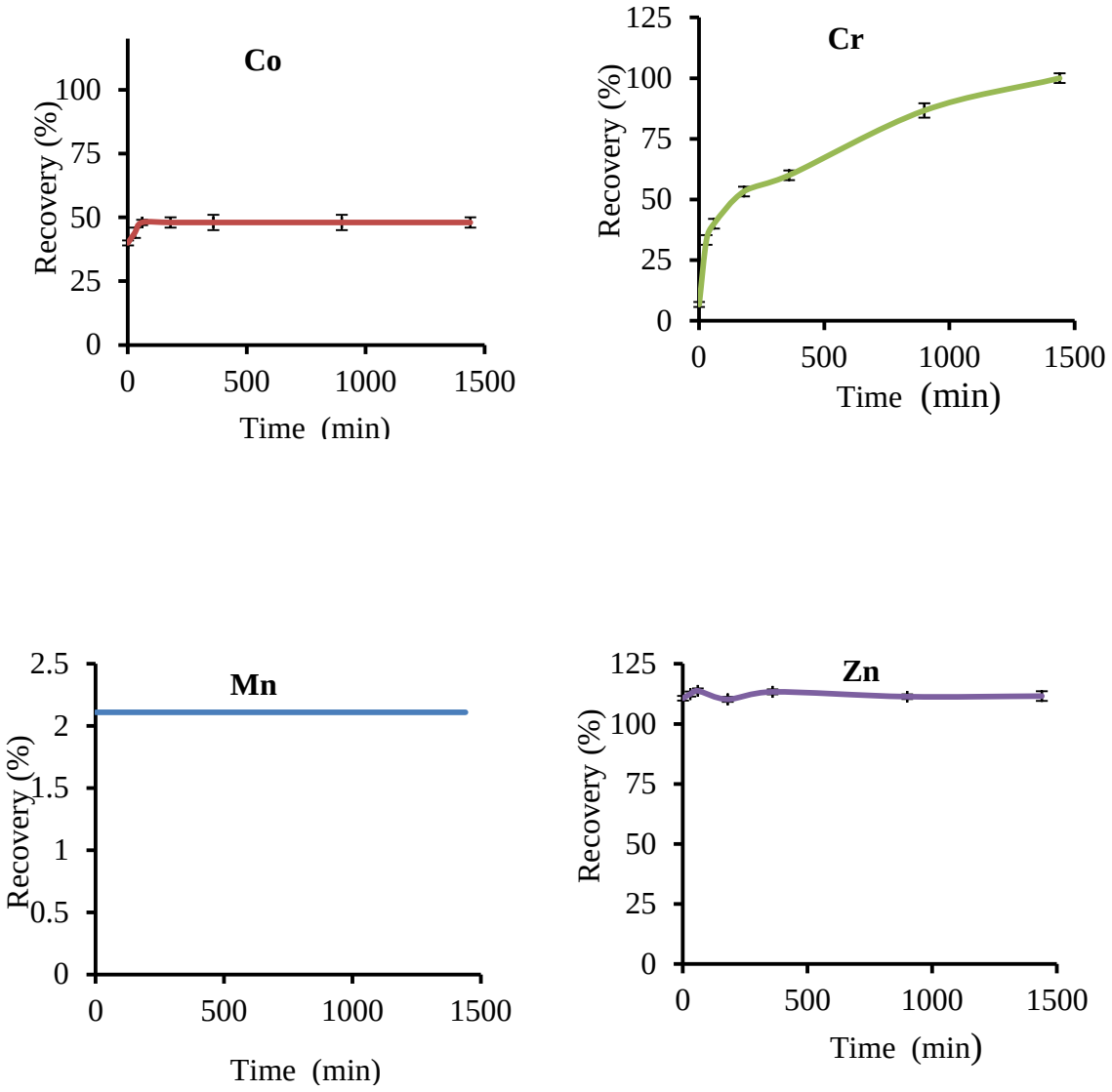

Figure 7.9 Effect of time on metal ion uptake by $SH@SiO_2$ (second group)

7.3.8 The effect of pH on the preconcentration of metals using SH@SiO_2

Table 7.2 summarizes the recovery results attained at different pH values. As illustrated in the table, at pH = 4 only 83, 55, 50, 30 and 22 % recovery results were obtained for Co^{2+}, Cu^{2+}, Pb^{2+}, Ni^{2+} and Cr^{3+} respectively, while the SH@SiO_2 nanoscavenger did not show any tendency to extract Cd^{2+}, Mn^{2+} and Zn^{2+} at this pH. The low recovery of some of the metals at this pH (acidic conditions) may be attributed to the protonation of the donor atoms in the ligand, which blocks the binding of the ligand to the metal ions, leading ultimately to loss of the chelate.

Increasing the pH value affected all metal recovery results, as shown in the recovery results of the metals at pH 7. The copper and cobalt reached their maximum at this pH, and the recovery results for cadmium, lead, chromium and zinc were more than 90 %. The recovery results for nickel and manganese were 55 and 15% respectively. It has been reported in literatures[10-13] that the optimized pH to preconcentrate Mn^{2+} from water at pH > 7. The improvements in the recovery results of the metals may be due to a decrease in the degree of protonation of the donor atom, which leads to good binding between metal ions and ligand atoms.

At pH = 9 most of the metal ions reached their maximum recoveries. The most noticeable effect of the pH on the recovery results was observed on the extraction of nickel and manganese, which recorded 91 and 77 % respectively. The increasing recovery results for the two metals could be due to precipitation of the metals at this high pH value[10]. In addition, the effect of deprotonation of the ligand leads to more successful binding between ligand atoms and metal ions.

Table 7.2 Effect of pH on the extraction of metals by SH@SiO_2

		Average Recovery of Metal ± SD (n = 3)							
Buffer	pH	Cu	Cd	Ni	Pb	Co	Cr	Mn	Zn
Acetate-buffer	4	55±2.3	0±0	30±5	50±0	83±0	22±2.9	0±0	0±0
Tris-buffer	7	100±0	96±2.5	55±0	93±0	100±1	98±2	15±0	92±0.66
Tris-buffer	9	100±1.73	99±1.9	91±0	100±0.2	100±0	102±2.9	77±2.8	102±3

7.3.9 A comparison of Cu (II) determinations using SH@SiO_2 with a conventional colorimetric procedure

The accuracy of SH@SiO_2 nanoscavenger as a solid phase extractor of metal ions in the analytical field was evaluated. The concentration of extracted Cu^{2+} from tap water using a NSDE technique with a SH@SiO_2 nanoscavenger was applied as solid phase and compared to the one attained using a conventional extraction technique (colorimetric). The colorimetric procedure involved solvent extraction of the Cu^{2+} diethyldithiocarbamate complex into chloroform. The Cu^{2+} was determined colorimetrically at 435 nm. The concentration of Cu^{2+} was calculated using calibration with standard solutions. Fifteen tap water samples were collected from different places across Southampton, UK. The concentrations of Cu^{2+} ions in tap water samples was obtained using NSDE and plotted against the one attained by the colorimetric method, as shown in Figure 7.10.

The slope of the line was 1.0292 ± 0.015 which is statically equal to 1 at the 95 % confidence level. This indicates that the concentration of Cu^{2+} obtained using the colorimetric method was overall similar to the one obtained using NSDE. The good agreement of the results attained from the two analytical approaches of extraction, suggests the accuracy of the SH@SiO_2 nanoscavenger method as a promising new approach to extract of metal ions from water samples. Furthermore, the Cu^{2+}

concentrations in the tap water samples were found to range from 0.087 to 0.84 µg mL^{-1}.

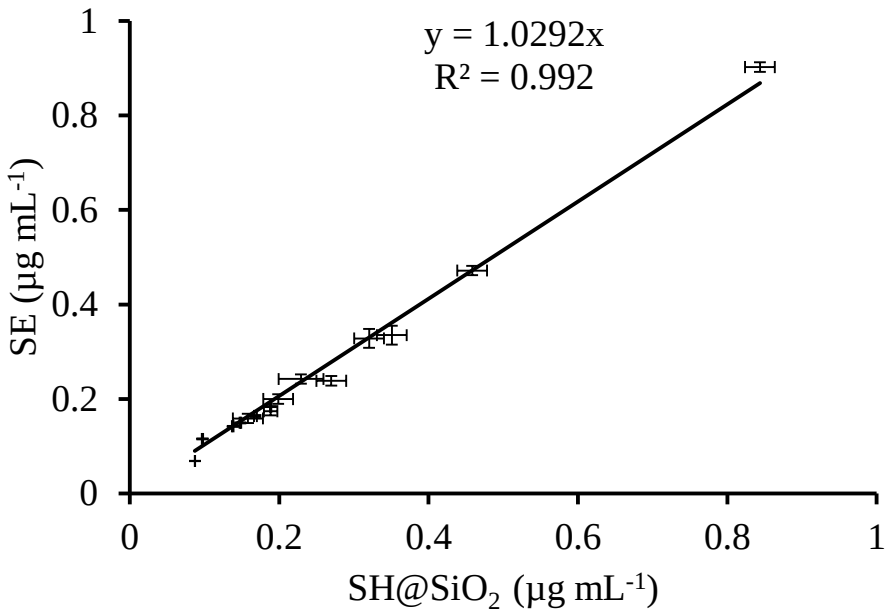

Figure 7.10 Correlation of extracted Cu measurements obtained using SH@SiO_2 nanoscavenger dispersion extraction and solvent extraction methods

7.4 Conclusion

Mesoporous silica particles have been successfully modified with aminopropyl following anchoring by thiosalicylate moiety to the surface of silica particles. The SEM results confirmed that the morphology of the particles was spherical and the size of the particles was unchanged from the original size of the mesoporous silica, despite the two modifications that had taken place.

The SH@SiO_2 nanoscavenger was applied to extract/preconcentrate eight metal ions from synthetic samples at pH = 7. This pH has been selected to be close to the pH of natural water. It has a good ability to extract Cu^{2+}, Cd^{2+}, Pb^{2+} and Zn^{2+} with recovery results more than 90%. Therefore SH@SiO_2 nanoscavenger can be used selectively to extract these metal ions from aqueous solution in presence of Mn^{2+}, Ni^{2+}, Co^{2+} and Cr^{3+}. The recovery results could be enhanced by increasing the equilibration time between the metal ions and the ligands or by raising the pH.

The ability of the SH@SiO_2 nanoscavenger as a solid phase extractor of metal ions was assessed by comparing the concentration of Cu^{2+} in tap water samples to the ones attained using the well-known colorimetric approach. The obtained result confirmed the similarity of the results attained using the two methods certify the possibility of using the SH@SiO_2 nanoscavenger as a tool to extract metal ions from water.

The results obtained from primary investigation of the nanoscavenger indicate that the SH@SiO_2 nanoscavenger offers a simple and cost effective approach to the preconcentration of metal ions from water.

7.5 References

(1) Sahin, F.; Volkan, M.; Howard, A. G.; Ataman, O. Y. *Talanta* **2003**, *60*, 1003-1009.

(2) Volkan, M.; Ataman, O. Y.; Howard, A. G. *Analyst* **1987**, *112*, 1409-1412.

(3) Howard, A. G.; Volkan, M.; Ataman, O. Y. *Analyst* **1987**, *112*, 159-162.

(4) Rudner, P. C.; Pavon, J. M. C.; Rojas, F. S.; de Torres, A. G. *J. Anal. At. Spectrom.* **1998**, *13*, 1167-1171.

(5) Zougagh, M.; De Torres, A. G.; Pavon, J. M. C. *Talanta* **2002**, *56*, 753-761.

(6) Grivas, J. C.; Navada, K. C. *J. Org. Chem.* **1971**, *36*, 1520-1522.

(7) Howard, A. G.; Khdary, N. H. *Analyst* **2005**, *130*, 1432-1438.

(8) Agrawal, Y. K.; Tandon, S. G. *J. Inorg. Nucl. Chem.* **1974**, *36*, 869-873.

(9) Cox, P. A. *Inorganic chemistry*, 2nd ed.; BIOS Scientific Publishers: London, **2004**.

(10) Sarmani, S. B.; Abdullah, M. P.; Bobaker, A. M. *J. Radioanal. Nucl. Chem.* **2004**, *259*, 257-260.

(11) Kenduzler, E.; Turker, A. R.; Yalcinkaya, O. *Talanta* **2006**, *69*, 835-840.

(12) Lemos, V. A.; David, G. T. *Microchem. J.* **2010**, *94*, 42-47.

(13) Citak, D.; Tuzen, M.; Soylak, M. *J. Hazard. Mater.* **2010**, *173*, 773-777.

Chapter 8
Dual functionality nanoscavenger ($HOC_{18}@SiO_2$)

8.1 Introduction

C_{18}-silica phases are the most used sorbents in SPE, being used for the extraction and preconcentration of many organic materials. With the increasing demand to separate similar materials, the development of approaches to synthesize solid phase sorbent has been necessary. Materials can be made in which the silica surface is modified by more than one functional group. Silva *et al.*[1], for example, prepared a stationary phase with both the polar thiocarbamate group and a non-polar C_{18} group which could be used in reversed phase HPLC. When compared with other C_{18} reversed phase materials, the results were better for basic solutes and not significantly different for non-polar solutes using the C_{18}-thiocarbamate stationary phase. A new mixed-functionality silica material has also been synthesized by linking of glycidoxypropyl and phenyl groups to the surface of silica. The oxirane ring was hydrolyzed to the diol group by refluxing the prepared materials in perchloric acid solution (pH 3.0). The resulting material, when packed in a column, could be used for the analysis of hydrophobic and hydrophilic drugs in serum[2].

The most common ways to functionalize the surface of silica are to react a chlorosilane or an alkoxysilane with silanol groups on the surface of the silica. A catalyst, or at least a trace of water, is essential for the hydrolysis of the groups (chloro or alkoxy) to silanol. The most widely reported mechanism for the linkage of groups to the surface of silica reaction is that the chlorosilane is first hydrolyzed by water, eliminating HCl. This is followed by condensation of the resulting hydroxyl group to the silica surface to form a strong Si-O-Si surface bond and eliminate H_2O (Figure 8.1). Further condensations can occur between the free hydroxyl groups of the silane and the hydroxyl groups on the silica surface or with nearby silane molecules forming a cross-linked layer of polymer. The main advantage of this bond (Si-O-Si) is stability, making the modified silica phase suitable for extracting organic

materials. The occurrence of the first step, the hydrolysis of the chlorosilane to a silanol by the surface water, is amply supported by the literature[3-8].

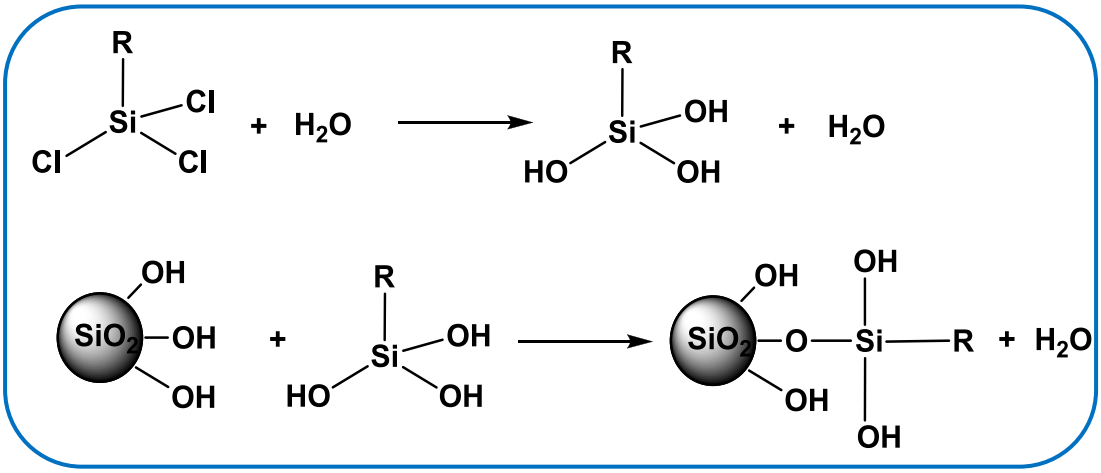

Figure 8.1 Schematic reaction between silica particles and $C_{18}SiCl_3$, where R = $C_{18}H_{37}$

This chapter describes the synthesis of dual functionality nanoscavengers to preconcentrate organic materials from aqueous samples. The nanoscavenger is functionalized with octadecyl and diol groups and will be referred to as HOC_{18}-nanoscavenger. The octadecyl moiety is present for the preconcentration of organic materials from water and the diol groups are essential to allow the particles to disperse in water (i.e. to make them wettable). Four approaches have been evaluated for the preparation of material having a reasonable quantity of C_{18} yet sufficient diol groups to allow it to disperse easily in water.

The preparation of HOC_{18}-nanoscavenger1 was carried out by modifying mesoporous silica with $C_{18}SiCl_3$ prior to removal of the template. The later removal of the template left pores containing hydroxyl groups. HOC_{18}-nanoscavenger2 and HOC_{18}-nanoscavenger3 were prepared in two individual steps. In the first step, $C_{18}Si(OMe)_3$ or $C_{18}SiCl_3$ and 3-glycidoxypropyltrimethoxysilane ($GSi(OMe)_3$) were added together to pre-formed mesoporous silica. The second step was to open the epoxy ring by treating the nanoscavenger with an acid solution. The HOC_{18}-nanoscavenger4 was prepared in three individual steps. In the first step, mesoporous silica particles were modified with $GSi(OMe)_3$. The product of the first step was then

reacted with $C_{18}SiCl_3$. The final step was to open the epoxy ring and produce diol groups in an attempt to increase the wettability of the particles (Figure 8.2). It is essential that the opening of the epoxy ring is the last step to prevent reaction of $GSi(OMe)_3$ or $C_{18}SiCl_3$ with the diol groups.

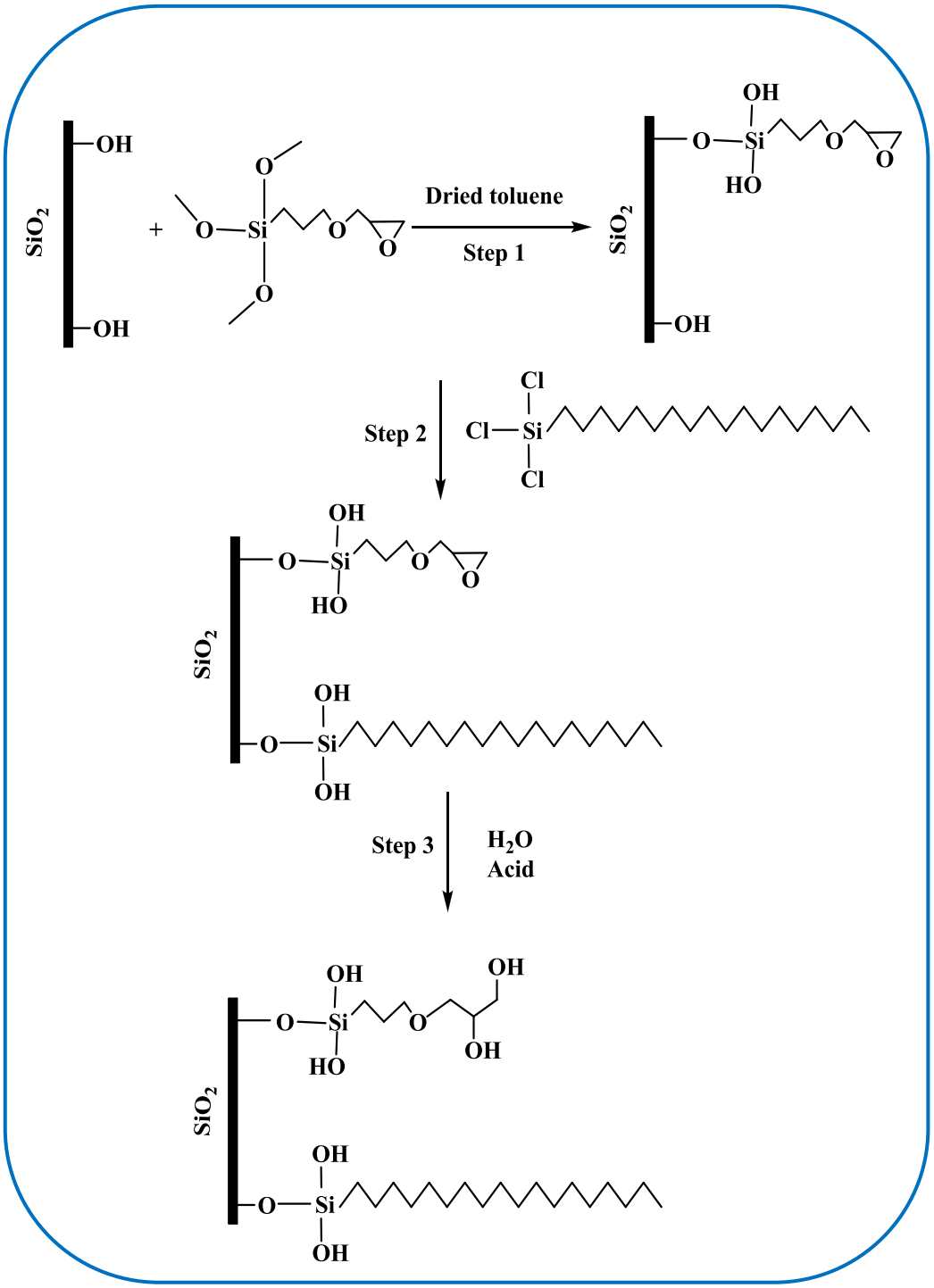

Figure 8.2 The preparation of a HOC_{18}-nanoscavenger (assuming the modifier attaches to the surface from one point)

To validate the HOC_{18}-nanoscavengers as a suitable analytical tool for the extraction of organic materials, they were applied in a nanoscavenger dispersion extraction (NSDE) of some estrogenic compounds, polynuclear aromatic hydrocarbons (PAHs) and tributyltin (TBT).

8.2 Experiments

8.2.1 Materials

Octadecyltrichlorosilane (90 %), octadecyltrimethoxysilane (94 %), 3-glycidoxy-propyltrimethoxysilane (98 %), tributyltin chloride (96 %), 17α-ethynylestradiol (98 %), estriol (98 %) and estrone (99 %) were obtained from Aldrich (Poole, UK). Acetonitrile, methanol and n-hexane were HPLC grade and supplied by Fisher Scientific (Loughborough, UK). Toluene (laboratory grade) and sodium hydroxide were purchased from Fisher Scientific (Loughborough, UK). Octadecane (99 %), 1-octadecanol, hexadecanol (99 %) and phosphorus pentoxide (99.99 %) were purchased from Aldrich. A standard solution containing 13 PAH compounds (EPA polynuclear aromatic hydrocarbons Mix B-Supelco) was obtained from Aldrich. The mixture contains 500 µg mL^{-1} of each compound.
All glassware was washed with detergent and water, rinsed with acetone and then deionised water prior to use.

8.2.2 Characterization of HOC_{18}-nanoscavengers

Preparation of the samples for the instruments was carried out according to the methods described in Section 3.1.2.

8.2.3 Synthesis of HOC_{18}-nanoscavengers

Four different methods were used to prepare HOC_{18}-nanoscavengers.

8.2.3.1 Modification of mesoporous silica (with template) with $C_{18}SiCl_3$ (HOC_{18}-nanoscavenger1)

To a two necked round-bottomed flask (100 mL) fitted with a condenser, was transferred 1 g of mesoporous silica (prepared as described in Section 3.3.1.4 except that the template was not removed) and dried toluene (40 mL). The mixture was sonicated for an hour under N_2. The mixture was then heated at 100 ºC under N_2 and stirred for 15 minutes. $C_{18}SiCl_3$ (1 mL) was dissolved in dried toluene (10 mL) and added slowly through a dropping funnel. The reaction was left to proceed at 100 ºC under stirring and N_2 for 12 hours. The suspension was then centrifuged and rinsed five times with dried toluene and two more times with ethanol. The white product was dried under continuous vacuum. Removal of the surfactant was carried out for 24 hours in Soxhlet apparatus using ethanol/hydrochloric acid solution.

8.2.3.2 Synthesis of HOC_{18}-nanoscavenger2

Synthesis of this nanoscavenger was carried out in two steps:

8.2.3.2a Modification of the silica surface with $C_{18}Si(OMe)_3$ and $GSi(OMe)_3$ to synthesize HOC_{18}-nanoscavenger2

Mesoporous silica (1 g) (prepared as described in Section 3.3.1.4) was dispersed in dried toluene (80 mL) in a two necked round-bottomed flask (250 mL) fitted with a condenser. The mixture was stirred using a magnetic stirrer and left until the temperature was stable at 80 ºC. Dipropylamine (1 mL) and $C_{18}Si(OMe)_3$ (0.5 mL) were added to the reaction mixture. Five minutes later, $GSi(OMe)_3$ (0.5 mL) was added to the reaction mixture. The reaction was left to proceed at 80 ºC for 7 hours under N_2. The product was isolated by centrifugation, rinsed with dried toluene five times and dried under continuous vacuum.

8.2.3.2b Opening the epoxy ring

Deionised water (100 mL) was transferred to a round-bottomed flask (250 mL), and the pH was adjusted to 3, using HCl. C_{18}-mesoporous silica (1 g) (prepared as

described in Section *8.2.3.2a*) was added and the mixture was sonicated for 15 minutes. The reaction mixture was refluxed at 100 ºC overnight. The white precipitate was isolated, rinsed with deionised water five times and dried in an oven at 60 ºC.

8.2.3.3 Modification of the surface of silica with $C_{18}SiCl_3$ and $GSi(OMe)_3$ to prepare HOC_{18}-nanoscavenger3

This experiment was carried out according to the method described in Section *8.2.3.2a*, with the following changes: no base was used in this reaction; $C_{18}SiCl_3$ and $GSi(OMe)_3$ were mixed together in dried toluene (20 mL) and added through a dropping funnel. Opening the epoxy ring was carried out according to the method described in Section *8.2.3.2b*.

8.2.3.4 Synthesis of HOC_{18}-nanoscavenger4

In this approach the HOC_{18}-nanoscavenger4 was prepared in three individual steps:

8.2.3.4a Synthesis of glycidoxypropyl-mesoporous silica

Mesoporous silica (2 g) (prepared as described in Section 3.3.1.4 and then dried at 120 ºC overnight) and dried toluene (150 mL) were transferred to a two necked round-bottomed flask (250 mL) fitted with a condenser. The mixture was sonicated for 15 minutes and heated at 95 ºC for an hour under N_2. $GSi(OMe)_3$ (1 mL dissolved in 10 mL of dried toluene) was then added slowly through a dropping funnel. The reaction was left to proceed at 90 ºC for 7 hours. The white solid was isolated by centrifugation, rinsed with dried toluene five times and then dried under continuous vacuum for 5 hours.

8.2.3.4b Synthesis of C_{18}-mesoporous silica using $C_{18}SiCl_3$

Glycidoxypropyl-mesoporous silica (2 g) (prepared as described in Section *8.2.3.4a*) and dried toluene (150 mL) were transferred to a two necked round-bottomed flask (250 mL). The mixture was sonicated for 15 minutes and $C_{18}SiCl_3$ (1 mL dissolved

in 10 mL of dried toluene) was slowly added dropwise using a dropping funnel. The reaction mixture was stirred at 90 ºC under N_2 for 7 hours. The precipitate was filtered and rinsed with dried toluene five times and twice with ethanol, and dried under continuous vacuum for 6 hours.

8.2.3.4c Opening the epoxy ring

This experiment was carried out according to the methods described in Section *8.2.3.2b*.

8.2.4 Measurement of octadecyl groups on the surface of silica

The quantity of octadecyl groups which chemically bonded to the surface of silica were evaluated using Genieser method[9]. This method is based on release of octadecane and octadecanol from the surface of silica by alkali fusion and subsequently analyzed by GC. The sum of both of the products gives the amount of octadecyl loaded on the surface.

8.2.4.1 Preparation of standard solutions of octadecane, octadecanol and hexadecanol

Stock solutions were prepared by dissolving 100 mg quantities of octadecane, octadecanol and hexadecanol individually in 100 mL of hexane. Appropriate dilutions were carried out to obtain mixtures containing octadecane, octadecanol and hexadecanol (40, 40 and 20 µg mL^{-1}), (20, 20 and 20 µg mL^{-1}) and (10, 10 and 20 µg mL^{-1}) respectively.

8.2.4.2 Digestion of HOC_{18}-nanoscavengers

HOC_{18}-nanoscavenger (10 mg) was transferred into a small test tube, KOH (100 mg) was added and the tube was left in a desiccator (containing P_2O_5) overnight. Triethylene glycol dimethyl ether (200 µL) was added to the tube, which was heated in a sand bath at 216 ºC for 2 hours. After one minute of cooling, deionised water

(250 µL) was added, followed by 1-hexadecanol (100 µL, 1 mg mL^{-1}), as an internal standard, and hydrochloric acid (140 µL, 37 % w/v). The tube was shaken for 3 minutes, and then n-hexane (2 mL) was added. The tube was shaken for 3 minutes and then centrifuged. The organic supernatant was transferred to a volumetric flask (5 mL) and the volume was made up to the mark using n-hexane. 1 µL was injected into the GC (Perkin-Elmer 8700). Table 8.1 gives the chromatographic conditions that were used.

Table 8.1 The chromatographic conditions of the GC

Parameters	Setting		
Oven temperature (ºC)	60	200	250
Iso time (minute)	3	0	5
Ramp rate (ºC /minute)	25	5	0
Injector temperature	250 ºC		
Detector temperature	300 ºC		
Type of injection	Splitless		
Carrier gas	Nitrogen		
flow rate	1 mL / min		
Column	Phase: (5 % phenyl)- 95 % methylpolysiloxane, Alltech Econo-cap SE-54, 30 m x 0.25 mm x 0.25 µm, (Part No. 19647)		
Detector	FID		

8.2.5 Preconcentration of estrogenic compounds

8.2.5.1 Preparation of standard solutions of estrogenic compounds

Stock solutions were prepared by dissolving 20 mg of each compound (estriol, estrone, β-estradiol and 17α-ethynylestradiol) individually in 10 mL of methanol (HPLC grade). 1 mL of each solution was transferred to a small sample vial and kept in the fridge. Appropriate dilutions were carried out to obtain mixtures containing the

four compounds, estriol, estrone, β-estradiol and 17α-ethynylestradiol (5, 2, 1 and 0.5 µg mL^{-1} each). The dilutions were carried out using water: acetonitrile (55:45 %).

Analysis of the samples of the estrogenic compounds was carried by HPLC under the following conditions:
Column: Symmetry ® C_{18} 5 µm (3.9 x 150 mm)
Mobile phase: water: acetonitrile (65: 35 %).
Flow rate: 1 mL min^{-1} .
Detector: UV at 220 nm.
Injection: 20 µL.
Sample: in water : acetonitrile (55 : 45 %).

8.2.5.2 Recovery of estrogenic compounds

A standard solution (0.5 mL) containing 20 µg mL^{-1} of each of the four estrogenic compounds (estriol, estrone, β-estradiol and 17α-ethynylestradiol) was added to a volumetric flask containing deionised water (500 mL). HOC_{18}-nanoscavenger (150 mg) (pre-dispersed in 5 mL of deionised water) was added to the volumetric flask. The volumetric flask was left for an hour and then the suspended particles were collected by filtration using a 0.22 µm polyvinylidene fluoride (PVDF) polymer membrane filter. The membrane filter was transferred to a test tube, 1 mL of acetonitrile (HPLC grade) was added and the tube was sonicated and then shaken for 10 minutes. The extract was then centrifuged and the supernatant was transferred to a volumetric flask (5 mL). Addition of acetonitrile to the test tube was repeated once more. The volume of the volumetric flask was made up to the mark using deionised water and the solutions were analyzed by HPLC.

8.2.6 Extraction of PAHs

8.2.6.1 Preparation of standard solution of PAHs

0, 2, 4, 6 and 10 µL of PAHs as supplied (500 µg mL^{-1}) were transferred to volumetric flasks (1 mL) to prepare 0, 1, 2, 3 and 5 µg mL^{-1} of PAHs standard

solution. The volumes of the volumetric flasks were made up to the mark using dichloromethane (HPLC grade).

8.2.6.2 Uptake of PAHs using HOC_{18}-nanoscavenger4

HOC_{18}-nanoscavenger4 (300 mg) was transferred to a glass vial (5 mL) and deionised water (5 mL) was then added. The mixture was sonicated for an hour and transferred to a volumetric flask (500 mL), almost filled with deionised water. A 30 µL aliquot of the 500 µg mL^{-1} PAHs standard was added to the volumetric flask and left for 2 hours. The suspension was filtered using a 0.22 µm PVDF polymer membrane filter. The filter was transferred to a glass vial (20 mL). Dichloromethane (5 mL) was added to the vial followed by 1 g of anhydrous sodium sulfate (Na_2SO_4) (dried in an oven at 400 ºC overnight) to dry the extract. The vial was left for 30 minutes and the dichloromethane extract was separated from the solid and transferred to a volumetric flask (10 mL). The previous step was repeated using dichloromethane (5 mL) and the volume of the volumetric flask was made up to the mark using dichloromethane. The concentrations of the compounds were determined using GC, based on the standard solution.

8.2.7 Extraction of TBT using HOC_{18}-nanoscavenger4

This work was carried out in collaboration with Awad Alrashdy (Member of Alan Howard's research group)

8.2.7.1 Preconcentration of tributyltin chloride (TBTCl)

HOC_{18}-nanoscavenger4 (200 mg) was transferred to a glass vial containing deionised water (10 mL) and the mixture was sonicated for an hour. The suspension was transferred to a volumetric flask (1000 mL) almost filled with deionised water. 5 µL of 0.5 µg (Sn) mL^{-1} as TBT (2.5 ng of TBTCl by mass) was added to the flask using a Hamilton microlitre syringe. The flask was left for 4 hours. The suspended particles were then recovered by filtration using a 0.22 µm PVDF polymer membrane filter.

The filter was transferred to a glass vial (20 mL) and dried overnight in desiccator, using an activated silica gel desiccant.

8.2.7.2 Derivatization

The dried filter paper was cut into small pieces inside a PTFE caped glass vial. Hexane (1 mL) was added to the glass vial and mixed well with the filter paper pieces. Hexylmagnesium bromide Grignard reagent (1 mL, 2 M in ether) was then added and the reaction was left to proceed at ca. 20 ºC for 2 hours. Aqueous hydrochloric acid (2 mL, 5 % v/v) was added to quench the excess Grignard reagent.

8.2.7.3 Isolation

After the reaction had finished, the aqueous layer was discarded and the hexane layer was dried using activated anhydrous Na_2SO_4.

8.2.7.4 Measurement

The dried hexane layer was transferred to a volumetric flask (1 mL) and the volume of the flask was made up to the mark using hexane. The extracted solution (5 µL) was injected into a gas chromatograph which was fitted with a capillary column, coupled with a pulsed flame photometric detector (GC-PFPD).

8.3 Results and discussion

8.3.1 Morphology and particle size analysis

The HOC_{18}-nanoscavenger1 (prepared from silica with template present), and HOC_{18}-nanoscavenger3 (modification mesoporous of silica with $C_{18}SiCl_3$ and $GSi(OMe)_3$) were found to float when dispersed in water. These two nanoscavengers lacked the main purpose of this kind of nanoscavenger, which is to obtain wettable particles. No morphology and particle size distribution studies were therefore carried out on these two materials.

LSPSA of HOC_{18}-nanoscavenger2 showed the average particles size to be 274 nm (Table 8.2), with a high standard deviation which could be due to aggregation of the particles (Figure 8.3).

Table 8.2 LSPSA and SEM of mesoporous silica, HOC_{18}-nanoscavenger2 and HOC_{18}-nanoscavenger4

Material	LSPSA Average size ± SD (nm)	SEM Average size ± SD, (nm)
Mesoporous silica	299 ± 52	250 ± 35
HOC_{18}-nanoscavenger2	274 ± 150	225 ± 30
HOC_{18}-nanoscavenger4	230 ± 23 nm	251 ± 18

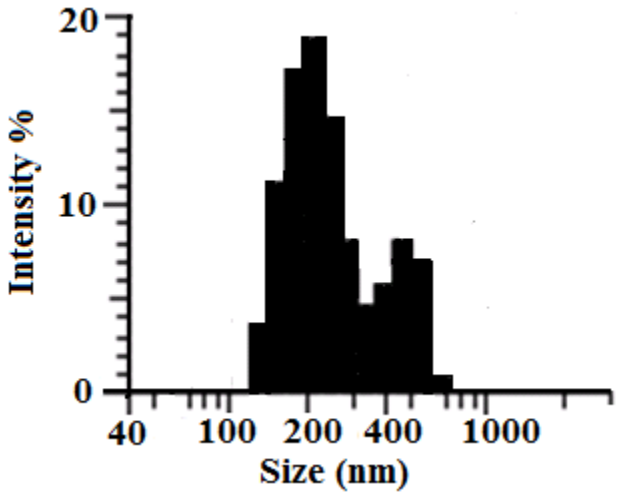

Figure 8.3 LSPSA of HOC_{18}-nanoscavenger2 (Prepared by modification of mesoporous silica with C_{18}TMOS and $GSi(OMe)_3$)

The SEM image of HOC_{18}-nanoscavenger2 showed the particles to be spherical (Figure 8.4) and the average size from SEM images was 225 ± 30 nm (Table 8.2).

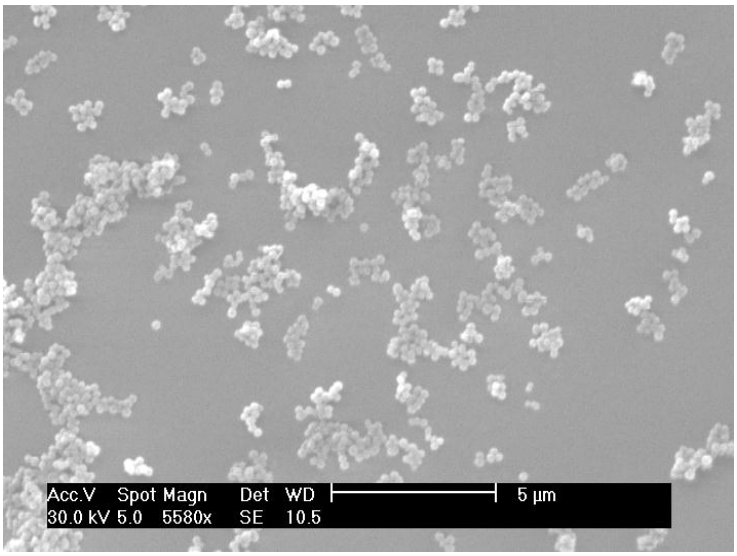

Figure 8.4 SEM image (5580X) of HOC_{18}-nanoscavenger2 (prepared by modification of mesoporous silica with $C_{18}SiCl_3$ and $GSi(OMe)_3$)

The LSPSA result for HOC_{18}-nanoscavenger4 (Figure 8.5) shows the average particle size to be 230 ± 23 nm. The good dispersion of the nanoscavenger helps to attain an accurate result from the LSPSA. Figure 8.6 shows the morphology of the particles to be spherical. When the morphology and the average size of the particles of HOC_{18}-nanoscavenger4 were compared with the starting materials (preformed mesoporous silica prepared as described in Section 3.3.1.4) (Table 8.2), they were found to be similar, despite the two modifications of the silica. Overall, the HOC_{18}-nanoscavenger4 gave the best particle morphology and average particle size out of the four HOC_{18}-nanoscavengers.

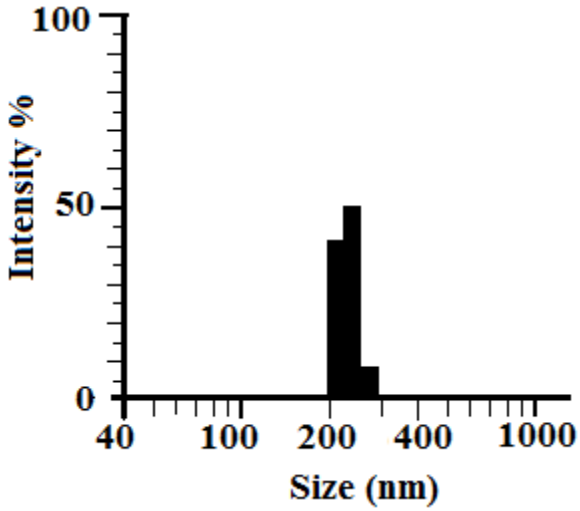

Figure 8.5 The LSPSA of HOC_{18}-nanoscavenger4, prepared by modification of mesoporous silica with $C_{18}SiCl_3$ and $GSi(OMe)_3$ in a three-step synthesis

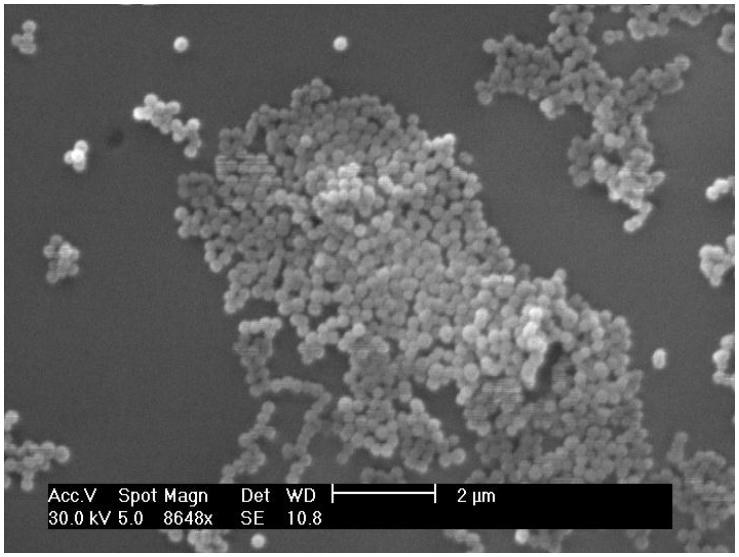

Figure 8.6 SEM image (8648X) of HOC_{18}-nanoscavenger4, prepared by modification of mesoporous silica with $C_{18}SiCl_3$ and $GSi(OMe)_3$ in a three-step synthesis

8.3.2 Infrared spectroscopy

The loading of the C_{18} moiety on the surface of silica was studied using FT-IR. Figure 8.7 shows the FT-IR spectrum of HOC_{18}-nanoscavenger1. The three bands at

2989, 2930, 2855 cm^{-1} could be attributed to asymmetric stretching vibration of CH_2 and CH_3. However, it can not be certain whether or not the bands just came from the CH_2 and CH_3 of the C_{18} moiety on the silica surface or from both the alkyl groups of the C_{18} moiety and the template. It is clear from the floating of the HOC_{18}-nanoscavenger1 after dispersal in water that the surface of the particles is hydrophobic. It might be that the surface of the silica is covered by a multilayer of octadecyl moiety, and that hinders the complete extraction of the template by the solvent.

The FT-IR spectrum of HOC_{18}-nanoscavenger2 (Figure 8.7) showed weak bands at 2958, 2930 and 2866 cm^{-1}, attributable to the asymmetric stretching vibration of CH_2 and CH_3. The existence of CH_2 and CH_3 can confirm successful modification but can not confirm whether the loading took place of both of the groups (octadecyl and glycidoxypropyl) or for just one of them on the surface of the silica.

The FT-IR spectrum of HOC_{18}-nanoscavenger3 showed two strong bands at 2922 and 2849 cm^{-1}, attributable to the alkyl groups (Figure 8.7). The bands can most likely be attributed to the dominance of the C_{18} moiety on the surface of the silica, as the particles were floated on water.

The HOC_{18}-nanoscavenger4 was prepared in three individual steps. In the first step, the surface of the preformed silica was modified with glycidoxypropyl moiety. The FT-IR of glycidoxypropyl-silica showed three weak bands at 2951, 2932 and 2857 cm^{-1}, attributable to the asymmetric stretching vibration of CH_2, which could be a sign of the successful loading of the glycidoxypropyl group on the silica surface. After reaction between glycidoxypropyl-silica and $C_{18}SiCl_3$, the bands attributed to the stretching of CH_2 or CH_3 appear clearly on the spectrum, due to loading of the C_{18} groups on the silica surface (Figure 8.7).

All FT-IR spectra for the four HOC_{18}-nanoscavengers showed a strong sharp band at around 1070 cm^{-1} corresponding to the backbone Si-O-Si bond siloxane group. Free silanol of groups appears at 950 cm^{-1} of unmodified mesoporous silica. After reaction this band either reduces in intensity or disappears completely from the spectrum , due to reaction with the modifier[10]. The symmetric and asymmetric

stretching vibration of epoxy groups, which normally appears at 1250 and 904 cm^{-1}, did not appear in any nanoscavenger spectrum, due to the position of this group near the strong Si-O-Si band. The hydroxyl groups (bands at around 3500 cm^{-1}) generated from the hydrolysis of epoxy to diol groups are hard to distinguish from the hydroxyl groups from water adsorbed on the silica surface.

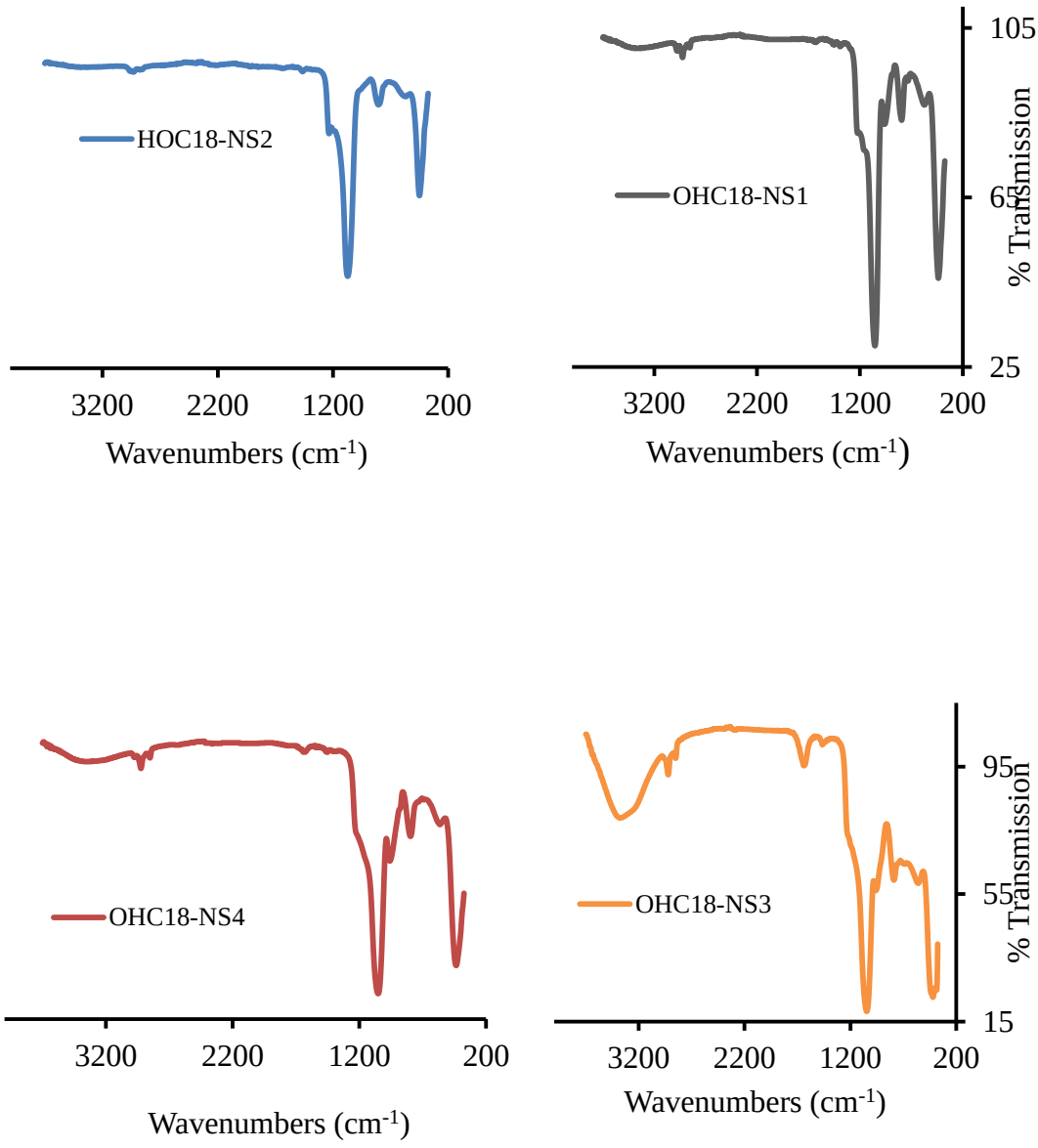

Figure 8.7 FT-IR spectra of HOC_{18}-nanoscavenger1, HOC_{18}-nanoscavenger2, HOC_{18}-nanoscavenger3 and HOC_{18}-nanoscavenger4

8.3.3 Thermogravimetric analysis (TGA)

Thermogravimetric analysis was carried out on the HOC_{18}-nanoscavengers between room temperature and 800 ºC in air. The TGA traces of HOC_{18}-nanoscavenger1 prior to extraction of the template (Figure 8.8) showed three main weight loss steps. The first weight loss was between 37 and 164 ºC and is attributed to loss of residual solvent and adsorbed water. The second step, a sharp weight loss between 164 and 350 ºC, results from oxidation of the octadecyl moiety and the template. The last step, between 350 and 773 ºC, with only 1 % of weight loss attributed to lose of the remaining of organic materials. The TGA traces for C_{18}-nanoscavenger1 (Figure 8.8), shows between 200 and 773 ºC a weight loss of 36 % prior to the extraction reduced to 18 % after extraction, due to the removal of the template (Table 8.3).

Combustion of HOC_{18}-nanoscavenger2 (Figure 8.8) shows four weight loss steps. The first is associated with combustion of residual solvent and adsorbed water. The second and third weight loss steps were between 226 and 650 ºC, and are attributed to the oxidation of the organic materials. The removal of organic materials from the silica started with sharp decomposition in the octadecyl group and glycidoxypropyl on the surface of the silica, in the region of weight loss between 226 and 430 ºC. The remaining of the organic material was gradually burnt off between 430 and 650 ºC. There was no significant weight loss after 650 ºC.

The TGA curve obtained for HOC_{18}-nanoscavenger3 (Figure 8.8) shows 27 % of the weight loss occurring between 180 and 484 ºC, which indicates a high loading of organic groups on the silica surface. The high organic content in the HOC_{18}-nanoscavenger3 could be attributed to cross linking among the octadecyl-trichlorosilane itself or to glycidoxypropylsilane causing multilayer coating of the organic groups[11, 12].

The TGA trace of glycidoxypropyl-silica (Figure 8.9) shows a 8.5 % weight loss in the region of temperature between 200 and 773 ºC. However, after inserting an octadecyl moiety in glycidoxypropyl-silica, the weight loss in the same area was 18.5

% (Figure 8.9). The 10 % increase in the weight loss is attributed to the pyrolysis of the octadecyl group (Table 8.3).

All TGA traces for the HOC_{18}-nanoscavengers showed a dramatic weight loss in the temperature region from ~ 200 to 400 ºC, which is assigned to the degradation of the surface grafted organic materials. The remained organic material was burnt off between 400 and 600 ºC. The highest weight loss was recorded for C_{18}-nanoscavenger3 (Table 8.3), which indicates a multilayer of C_{18} moiety.

Table 8.3 The weight loss of HOC_{18}-nanoscavengers

Materials	Weight loss (%) between 200-773 ºC
HOC_{18}-nanoscavenger1 before extraction	36
HOC_{18}-nanoscavenger1 after the extraction	18
HOC_{18}-nanoscavenger2	19
HOC_{18}-nanoscavenger3	28
Glycidoxypropyl-silica	8.5
HOC_{18}-nanoscavenger4	18.5

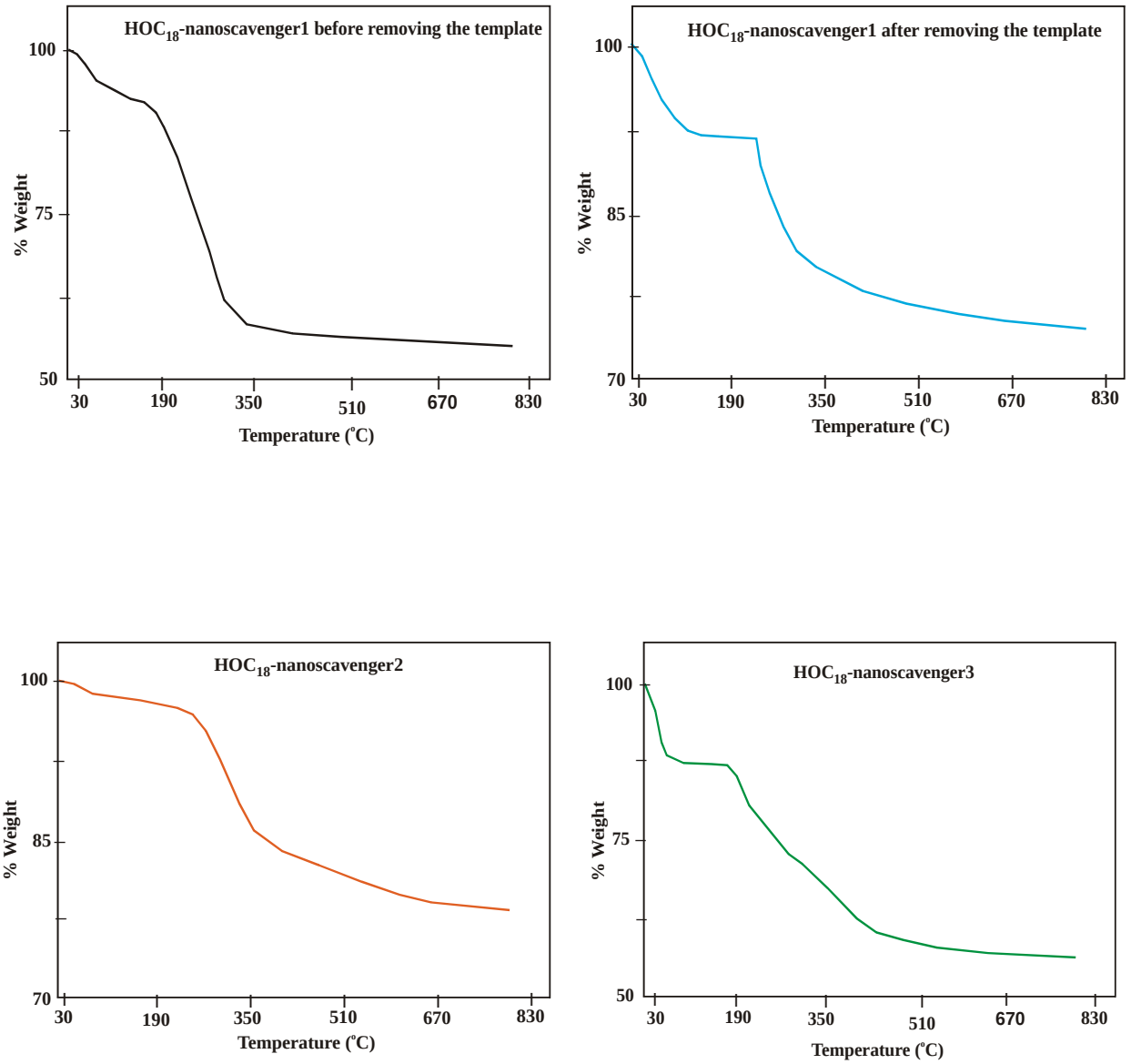

Figure 8.8 TGA traces of HOC_{18}-nanoscavenger1 before and after removing the template, HOC_{18}-nanoscavenger2 and HOC_{18}-nanoscavenger3

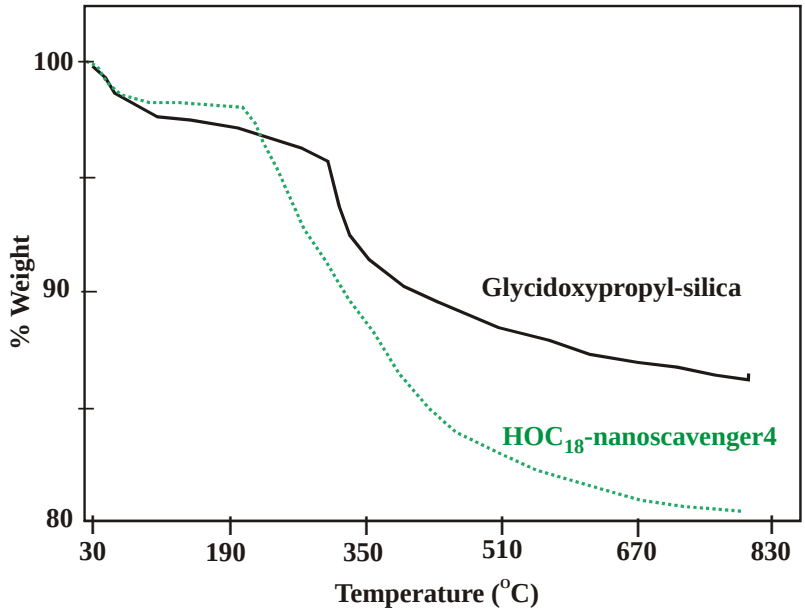

Figure 8.9 TGA traces of glycidoxypropyl-silica and HOC_{18}-nanoscavenger4

8.3.4 The settling of HOC_{18}-nanoscavenger from aqueous suspension

The stability of the sol resulting from the dispersion of particles in water was assessed by measuring light transmission over time. The stability of the nanoscavenger particle suspension in water is essential, to the nanoscavenger approach and rapid sedimentation or floating has to be avoided. HOC_{18}-nanoscavenger4 was chosen for study as HOC_{18}-nanoscavenger1 and HOC_{18}-naoscavenger3 were highly hydrophobic, so floated when dispersed in water. Transmission changed little over time (Figure 8.10) and good stability of the particle suspension in water was achieved over 8 hours. The existence of surface diol groups helped them to achieve wettability and easily disperse in water.

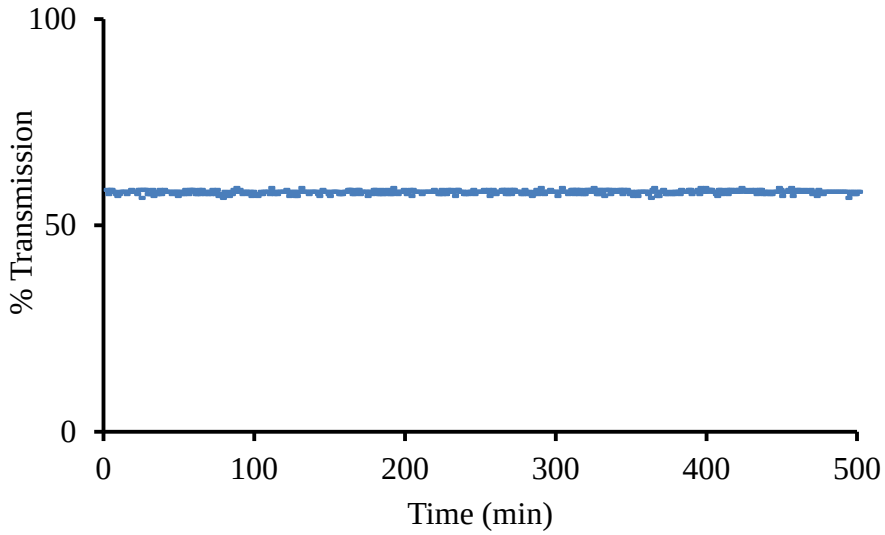

Figure 8.10 Settling of HOC_{18}-nanoscavenger4 from its suspension in water

8.3.5 Measurement of octadecyl groups on the silica

The octadecyl contents on the silicas were assessed using the Genieser method[9], which is based on cleaving the stable Si-C bond using a base[13]. Analysis of released octadecane and 1-octadecanol (Table 8.4) showed that HOC_{18}-nanoscavenger3 contained more octadecyl groups than the other HOC_{18}-nanoscavengers. This could be attributed to a multilayer of octadecyl groups on the silica surface as a result of cross-linking of $C_{18}SiCl_3$. The introduced octadecyl groups increased gradually with the increase in the relative amount of $C_{18}SiCl_3$ or $C_{18}Si(OMe)_3$ used in the reaction. Most of the cleavage products were n-octadecane and a small amount of 1-octadecanol. 1-Octadecanol was detectable in analysis only in C_{18}-nanoscavenger2. The ratio of n-octadecane to 1-octadecanol is reported to be affected considerably by changing the reaction temperature or the concentration of the suspending ether[9].

Table 8.4 Octadecane and 1-octadecanol released from the HOC_{18}-nanoscavengers

Materials	Octadecane (mmol g^{-1})	Octadecanol (mmol g^{-1})
HOC_{18}-nanoscavenger2	0.5 ± 0.2	0.025
HOC_{18}-nanoscavenger3	1.5 ± 0.1	-
HOC_{18}-nanoscavenger4	0.80 ± 0.15	-

8.3.6 Preconcentration of estrogenic compounds using HOC_{18}-nanoscavengers

The HOC_{18}-nanoscavengers were used in NSDE to preconcentrate four estrogenic compounds (estriol, β-estradiol, 17α-ethynylestradiol and estrone) from aqueous solutions (10 µg of each compound was spiked into 500 mL of deionised water). Table 8.5 shows the recovery of the compounds using different HOC_{18}-nanoscavengers. HOC_{18}-nanoscavenger2 extracted only 8-29 % of the estrogenic compounds. This low recovery may be attributed to the low octadecyl content of the silica. The recovery results improved with HOC_{18}-nanoscavenger3, but the recovery was still less than 50 %, in spite of HOC_{18}-nanoscavenger3 having the highest loading of octadecyl amongst all the HOC_{18}-nanoscavengers. The poor wettability of HOC_{18}-nanoscavenger3 caused the particles to float away from the target, probably the main reason for the low recovery of the compounds using HOC_{18}-nanoscavenger3. The highest recovery results were achieved with HOC_{18}-nanoscavenger4. The recovery results for estriol, β-estradiol, 17α-ethynylestradiol and estrone were 35, 88, 91 and 96 %, respectively. It was noted that the recovery of the compounds increased with the increased retention time of the compounds in HPLC chromatograms as a result of improving the affinity of the compounds toward the hydrophobic groups. The recovery of estriol was the lowest of the four, as a result of its low affinity to the C_{18} group as noted in the HPLC chromatogram (Figure 8.11) the retention time (2.23 minutes) was very low.

Table 8.5 Recovery of estrogenic compounds extracted from water using HOC_{18}-nanoscavengers (Initial sample contained 20 µg L^{-1} of each compound)

Compound	Preconcentration factor	Recovery of HOC_{18}-nanoscavenger2 (%) ± SD	Recovery of HOC_{18}-nanoscavenger3 (%) ± SD	Recovery of HOC_{18}-nanoscavenger4 (%) ± SD
Estriol	100	8 ± 1	12 ± 0	35 ± 1
β-estradiol	100	24 ± 2	42 ± 2	88 ± 3
17α-ethynyle-stradiol	100	22 ± 4	45 ± 1	91 ± 5
Estrone	100	29 ± 1	38 ± 3	96 ± 1

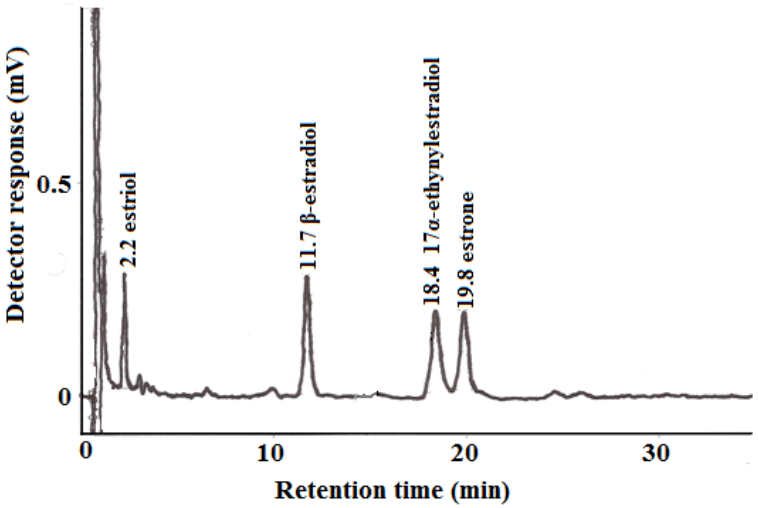

Figure 8.11 HPLC chromatogram of estrogenic compounds (2 µg mL^{-1})

8.3.7 Extraction of PAHs from water using HOC_{18}-nanoscavenger4

The ability of HOC_{18}-nanoscavenger4 to preconcentrate organic compounds was assessed by applying this approach to extract 13 compounds of PAHs from water prior to analysis by gas chromatography. HOC_{18}-nanoscavenger4 was applied in nanoscavenger dispersion extraction. The recovery of the PAHs compounds ranged from 35 % to over 100 %, as shown in Table 8.6. Most of the compounds exhibited a strong affinity for HOC_{18}-nanoscavenger4. The extraction of the organic compounds from water is based on the hydrophobic interaction between the octadecyl group on the solid phase and the target analytes. The first four compounds (Table 8.6) showed low recoveries. This may attributed to their low water solubility, making them not available for the suspended nanoscavenger particles to extract. The chromatogram of the PAH compounds under study is presented in Figure 8.12.

Table 8.6 The recovery of PAHs compounds extracted from water using the HOC_{18}-nanoscavenger4 (Initial sample contained 30 µg L^{-1} of each compound)

Number	Compound	% Recovery ± SD (n =4)
1	Acenaphthylene	48 ± 1
2	Fluorene	35 ± 1
3	Phenanthrene	67 ± 2
4	Anthracene	59 ± 2
5	Pyrene	95 ± 4
6	Benzo(a)anthracene	95 ± 1
7	Chrysene	101 ± 5
8	Benzo(b)fluoranthene	106 ± 8
9	Benzo(k)fluoranthene	109 ± 6
10	Benzo(a)pyrene	100 ± 2
11	Indeno(1,2,3-cd)pyrene	108 ± 9
12	Dibenzo(a,h)anthracene	105 ± 8
13	Benzo(ghi)perylene	105 ± 6

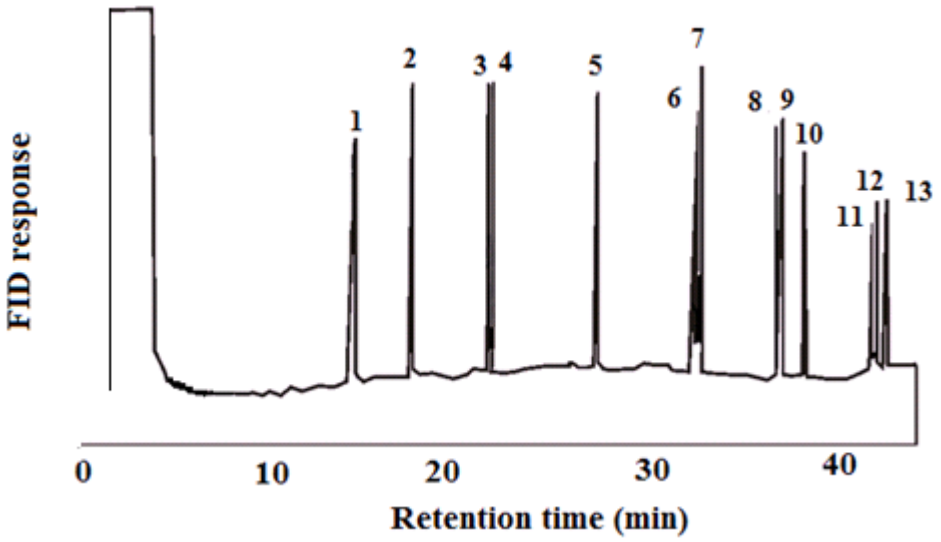

Figure 8.12 Chromatogram of 13 PAH compounds (2.5 µg mL^{-1})

8.3.8 Extraction of TBT from water using HOC_{18}-nanoscavenger4

In order to further investigate the utility of HOC_{18}-nanoscavenger4 for preconcentration of organic materials. It was applied to extract TBT from water using the NSDE approach. The analysis was carried out in four steps. The first step involved preconcentration of tributyltin chloride (TBTCl) using HOC_{18}-nanoscavenger4. The concentration of TBT was calculated according to the concentration of tin, and will be written in the form ng (Sn) / L as TBT. The initial concentration of TBT in the water was 2.5 ng (Sn) / L as TBT. In the second step, the TBTCl was hexylated using a Grignard reagent solution (Figure 8.13).

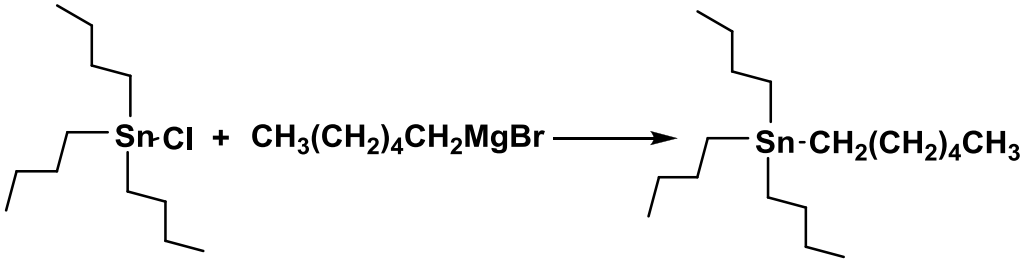

Figure 8.13 The hexylation of tributyltin chloride using a Grignard reagent solution

The substituted alkyl group in the Grignard reagent was selectively chosen as a hexyl group for all the TBT as hexyl alkyltin is sufficiently stable[14, 15]. Thus the hexyl tributyltin is not volatile at room temperature and it is extremely volatile at high temperatures. The rate of hexylation of the TBTCl when loaded on the HOC_{18}-nanoscavenger4 was highly dependent on time and shaking which eventually affect the recovery results. The recovery was found to be 87.5 % when the sample was vigorously shaken for 30 minutes, increasing to 97 % when the shaking time was increased to 120 minutes. The reasons for the improvement in the recovery with increased reaction time are: some TBTCl may be localized with the pores of the nanoscavenger and some of the nanoscavenger particles are held inside the pores of the filter paper. Therefore the Grignard reagent needs time to penetrate pores to reach the TBTCl. In addition, some of the Grignard was quenched by water before reaching the TBTCl. Increasing the reaction time is therefore essential to obtain good recovery of TBT. The next step was to add hydrochloric acid to quench the excess of

derivatization reagent remaining in the organic layer. In the third step the organic layer containing tributylhexyltin was isolated from the aqueous layer and dried using Na_2SiO_4. In the last step, the dried TBT was collected in 1 mL volumetric flask and determined by gas chromatography. A pulsed flame photometric detector was used to detect the tin in the sample. The concentration of TBT was calculated based on the standard solutions.

8.3.8.1 Rate of TBTCl uptake by HOC_{18}-nanoscavenger4

The time required to reach maximum extraction of TBTCl was investigated. TBTCl was extracted using HOC_{18}-nanoscavenger4 over a range of equilibrium times (30 to 240 minutes). Recovery increased with increasing equilibrium time (Figure 8.14) from 73 % in 30 minutes to approximately 90 % after four hours.

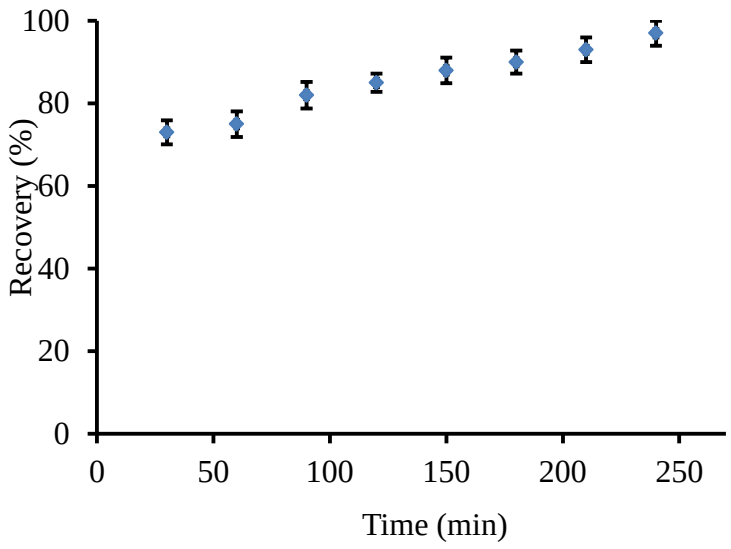

Figure 8.14 Effect of time on TBTCl uptake by HOC_{18}-nanoscavenger4 (Initial sample contained 2.5 ng (Sn) L^{-1} as TBT)

8.3.8.2 Extraction efficiency

The extraction efficiency of the nanoscavenger dispersion extraction approach to preconcentrate tributyltin using HOC_{18}-nanoscavenger4 as a solid phase was assessed. Nine synthetic water samples (1 L) containing 2.5 ng (Sn) L^{-1} as (TBTCl) were extracted using HOC_{18}-nanoscavenger4 and hexylated as described in Section 8.2.7. The extracted TBT was collected in 1 mL of hexane. In the mean time, 5 µL of 0.5 µg (Sn) mL^{-1} as (TBTCl) was spiked into 1 mL of hexane and hexylated. The experiment was replicated nine times. The extracted TBT was collected in 1 mL of hexane. The TBT obtained from extracted and spiked samples was measured using GC and every sample was measured nine times. All the measurements of extracted and spiked TBT were carried out under the same conditions. The recovery of TBT was calculated. This approach offers a number of advantages:

a) Any loss of the TBT during the hexylation step would be similar in extracted and spiked TBT, as the TBT in both procedures reacts with the Grignard reagent.
b) The effect of the Grignard reagent on the hexylation of TBT will be analogous for extracted and spiked TBT.
c) The difference in concentrations between extracted and spiked TBT, which can occur during the drying process, will be negligible, as they will both go through the drying process.

The recovery results ranged from 90 to 100 %, with a mean of 95 ± 3.7 (Table 8.7). The chromatogram for extracted TBT using C_{18}-nanoscavenger4 is illustrated in Figure 8.15.

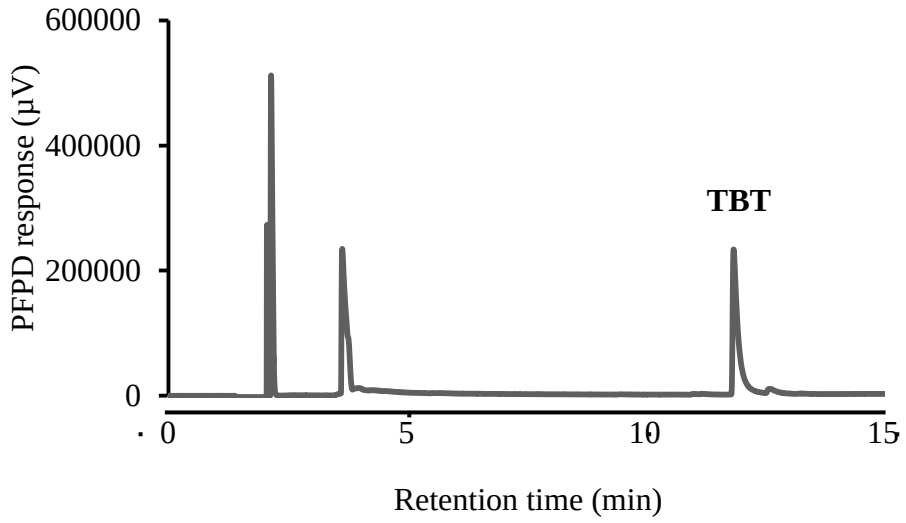

Figure 8.15 Typical chromatogram obtained from extracted TBT (2.5 ng mL^{-1}) using HOC_{18}-nanoscavenger4

Table 8.7 The recoveries of tributyltin using HOC_{18}-nanoscavenger4 (Initial sample contained 2.5 ng (Sn) L^{-1} as TBT)

Spiked water sample	Average recovery results (%) ± RSD, n = 9 (each experiment)
1	98 ± 3.3
2	93 ± 2.9
3	95 ± 3.7
4	97 ± 4
5	100 ± 3.1
6	90 ± 2.9
7	93 ± 3
8	92 ± 4.3
9	95 ± 0.8

The recovery results show that HOC_{18}-nanoscavenger4 dispersion extraction is a promising approach to the preconcentration of TBT from aqueous samples.

8.4 Conclusion

Four different approaches were carried out in attempt to prepare a nanoscavenger containing dual functionality groups. The octadecyl group functionalized the surface of a nanoscavenger to uptake the organic materials from water. It is essential to increase the wettability of the hydrophobic particles by incorporation of diol groups on the surface of the nanoscavenger; otherwise the nanoscavenger will float on the water. Among the four HOC_{18}-nanoscavegers, HOC_{18}-nanoscavenger4, prepared in a three-step reaction, was found to be the most promising for purposes of this study. In the preparation of HOC_{18}-nanoscavenger4, the glycidoxypropyl group was firstly introduced to the surface of the silica in limited quantities to avoid of glycidoxypropyl groups impeding the loading of octadecyl groups onto the interior surfaces during silanization.

The morphology of HOC_{18}-nanoscavengers was found to be spherical using SEM, and the average size of particles was 230-274 nm based on the type of HOC_{18}-nanoscavenger. This means no affect of modifications in the morphologies and the sizes of the particles. The quantities of loaded octadecyl groups on the silica surface were found to be based on the method of preparation. The octadecyl groups were determined by the Genieser method[9] to be 0.5–1.5 mmol g^{-1} as octadecane.

All four HOC_{18}-nanoscavengers were employed to preconcentrate some estrogenic compounds, and only HOC_{18}-nanoscavenger4 was used to preconcentrate PAHs and TBT. The recovery of hydrophobic compounds by HOC_{18}-nanoscavenger increases with increasing affinity of the hydrophobic on the nanoscavenger to the target compound. The recovery results of estriol, β-estradiol, 17α-ethynylestradiol and estrone were 8-35, 24-88, 22-91, 29-96 %, respectively based on the HOC_{18}-nanoscavengers type. High recoveries of some of PAH compounds was achieved using C_{18}-nanoscavenger4 with 50-fold preconcentration factor.

A 95 ± 3.7 % of TBT was recovered using C_{18}-nanoscavenger4 at a preconcentration factor of up to 1000-fold. The good recovery results for organic compounds indicated that using HOC_{18}-nanoscavenger as a solid phase in nanoscavenger dispersion

extraction is a novel and promising approach to extract organic materials from water, with less solvent, more economical and less time preconcentration features. In addition, this new approach is capable of being used with large water samples.

8.5 References

(1) Silva, R. B.; Silva, C. R.; Airoldi, C.; Collins, C. H.; Jardim, I. *Microchem. J.* **2006**, *82*, 150-158.

(2) Haginaka, J.; Wakai, J. *Chromatographia* **1990**, *29*, 223-227.

(3) Tripp, C. P.; Hair, M. L. *J. Phys. Chem.* **1993**, *97*, 5693-5698.

(4) Tripp, C. P.; Hair, M. L. *Langmuir* **1992**, *8*, 1120-1126.

(5) Tripp, C. P.; Hair, M. L. *Langmuir* **1992**, *8*, 1961-1967.

(6) Angst, D. L.; Simmons, G. W. *Langmuir* **1991**, *7*, 2236-2242.

(7) Silberzan, P.; Leger, L.; Ausserre, D.; Benattar, J. J. *Langmuir* **1991**, *7*, 1647-1651.

(8) Khdary, N. H. Ph.D. Thesis, Southampton University, Southampton, UK, **2006**.

(9) Genieser, H. G.; Gabel, D.; Jastorff, B. *J. Chromatogr.* **1982**, *244*, 368-372.

(10) Sales, J. A. A.; Airoldi, C. *J. Non-Cryst. Solids* **2003**, *330*, 142-149.

(11) McElwee, J.; Helmy, R.; Fadeev, A. Y. *J. Colloid Interface Sci.* **2005**, *285*, 551-556.

(12) Brambilla, R.; Dos Santos, J. H. Z.; Miranda, M. S. L.; Frost, R. L. *Thermochim. Acta* **2008**, *469*, 91-97.

(13) Kohjiya, S.; Ikeda, Y. *J. Sol-Gel Sci. Technol.* **2003**, *26*, 495-498.

(14) Leroy, M. J. F.; Quevauviller, P.; Donard, O. F. X.; Astruc, M. *Pure Appl. Chem.* **1998**, *70*, 2051-2064.

(15) Ebdon, L.; Hill, S. J.; Rivas, C. *Trac-Trends Anal. Chem.* **1998**, *17*, 277-288.

Chapter 9 Conclusions and Future work

9.1 Conclusions

9.1.1 Aims of the study

The main aim of the study was to develop novel nanoscavengers and to use them to preconcentrate analytes from water using nanoscavenger dispersion extraction (NSDE) techniques. The initial steps were focussed on the synthesis of 250 nm sized spherical silica particles with high surface area. Once this had been achieved, the silicas were modified with different functional groups for use as extracting agents. The ability of modified silicas to preconcentrate analytes from water was then assessed by applying the materials for the extraction of metal ions and organic compounds from water samples.

9.1.2 Synthesis of the nanoscavenger

9.1.2.1 Choosing the solid phase support

Spherical silica particles were selected to be the solid phase support for the preparation of the nanoscavengers. Silica was chosen for the following reasons: the materials to make it are commercially available and inexpensive; it is thermally stable; it does not swell in organic solvents; and it is easy to dispose of safely. In addition, the surface of silica is covered by silanol groups which are highly active and readily functionalized by chemically straightforward silylation reaction[1].

9.1.2.2 Size and uniformity of the nanoscavenger

The size of the nanoscavenger particles was selectively chosen to be around ca. 250 nm. The size of the particles is neither too large to cause rapid sedimentation, nor too small to make the recovery of the particles difficult and expensive. Smaller particle sizes (less than 100 nm) need powerful centrifuges to recover the particles which

take a long time to achieve. In addition there is the possibility of losing small particles during filtration or centrifugation. In contrast, large particle sizes (more than 500 nm) require mechanical suspension to avoid rapid sedimentation prior to extraction of the analytes.

The uniformity of the particle size (250 nm) makes the filtration and centrifugation process straightforward. By choosing the appropriate pore-size filter paper, no particles go through the pores and less loss of analytes is ensured. Moreover, variety in particle size can cause loss of those sample particles which have not been settled by centrifugation.

Particles with optimized homogenous size (around 250 nm) are therefore offering advantages of good equilibrium times between the nanoscavenger and the analyte leading to high recoveries.

9.1.2.3 Production of 250 nm silica with a high surface area

Two types of silica were used in an attempt to achieve of 250 nm spherical particles with a high surface area: Stöber-type silica and mesoporous silica. Firstly Stöber-type silica was synthesized by mixing TEOS with methanol. Ammonium hydroxide was then added to the mixture and the reaction was carried at room temperature. Silica particles with ca. 250 nm diameters, and having a surface area around ca. 20 $m^2\ g^{-1}$, were obtained. This surface area was considered to be too small and three approaches were therefore explored in attempts to increase it. Firstly, BTEE was added to TEOS to break up the structure of the silica particles with a C-C bridge. However, the adsorption isotherm measurements showed that this was not successful as there was no increase in surface area. Similarly, the addition of sodium fluoride during the formation of the particles did not achieve the desired result. The next approach was to use sucrose as a template. Whilst this increased the surface area, it only did so only to 110 $m^2\ g^{-1}$, and it caused an increase in the particle size to 412 ± 24 nm. None of these results were considered to be sufficiently effective.

Mesoporous silicas were selected as they are known to have a high surface area (around 1000 $m^2\ g^{-1}$)[2]. In order to achieve the desired particle size, four approaches

were evaluated. In these methods, several factors were manipulated: changing the type and amount of solvent, the silica precursor and the type of template (see Table 3.6 in Section 3.3.2.2). However, three of these resulted in the particle size being too large and/or some particles being irregular spheres, amorphous or aggregated, causing difficulty for their dispersion in water. The fourth method, using TMOS as a silica precursor and C_{12}TMABr as a template in ethylene glycol solvent, resulted in a surface area of around 1325 m^2 g^{-1} and uniform spherical particles of ca. 250 nm (Figure 9.1). The use of ethylene glycol increased the viscosity of the reaction solution when compared to methanol or ethanol; as a consequence, the number of primary particles increased and the particle size decreased[3].

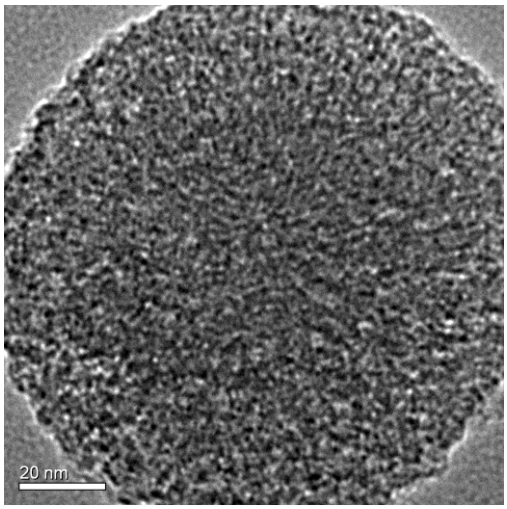

Figure 9.1 TEM image of mesoporous silica prepared using TMOS and C_{12}TMABr

9.1.3 Choosing the functional groups for extraction

Chelating groups were attached to the mesoporous silica surface to bind with a wide range of metal ions. Three different groups were evaluated: dithiocarbamate, hydroxyquinoline and mercaptobenzamide. For the extraction of organic materials, a dual functionality (diol and C_{18}) functionalized silica was developed. Diol was necessary to make the surface wettable because C_{18} alone would hinder the dispersion of the particles in water due to the poor wettability of a completely C_{18}-functionalized silica surface.

For metal extractions the silicas were initially modified with the aminoalkoxysilanes (Z-6094 and $NH_2Si(OEt)_3$) to immobilize diamine and monoamine groups respectively. The quantitative loading of these groups on the surface of the silicas were assessed by copper capacity measurements. Higher copper capacities were obtained when mesoporous silica was used due to large surface areas of the mesoporous silicas compared to the Stöber-type silicas. The amino-nanoscavengers were not used directly to extract the metal ions from water but rather as starting materials for the preparation of a range of new chelating nanoscavengers.

The dithiocarbamate-nanoscavengers, hydroxyquinoline-nanoscavenger and mercaptobenzamide-nanoscavenger were prepared by reacting amino-nanoscavengers with CS_2, FHQ and methyl 2-mercaptobenzoate reagents, respectively, in an appropriate solvent. The successful modifications of the silica surfaces with these groups were proven by FT-IR, TGA, copper capacity and colour tests.

For the extraction of organic materials, modification of the silica surface with octadecylsilane gave highly hydrophobic silica particles which hardly dispersed in water. A novel method was therefore developed based on functionalizing the silica surface with two different groups. The dual-functionality nanoscavenger was prepared by modifying mesoporous silica with $GSi(OMe)_3$ and C_{18} groups were then incorporated. Opening the epoxy groups to generate diol resulted in an improvement of the dispersion of HOC_{18}-nanoscavengers in water samples and the recovery of organic materials.

9.1.4 Nanoscavengers applications

The nanoscavengers were applied to preconcentrate a group of metal ions and organic materials, using the nanoscavenger dispersion extraction technique. Eight metal ions, Cu^{2+}, Cd^{2+}, Ni^{2+}, Pb^{2+}, Co^{2+}, Cr^{3+}, $Mn^{2+}$and Zn^{2+}, were preconcentrated using the dithiocarbamate-nanoscavenger, the hydroxyquinoline-nanoscavenger and the mercaptobenzamide-nanoscavenger. The recoveries of most of the metals extracted using the nanoscavengers were almost 100 %. A fast equilibration time (15

minutes) and maximum metal recovery was found when the dithiocarbamate-nanoscavenger was used to preconcentrate the metals. However, around 2 hours equilibration time was needed to reach maximum recovery with the mercaptobenzamide-nanoscavenger and the hydroxyquinoline-nanoscavenger. The nanoscavenger dispersion extraction technique was compared with a complexation solvent extraction technique to extract Cu^{2+} from tap waters collected from Southampton. The results showed no obvious differences between the two approaches.

The HOC_{18}-nanoscavengers were applied to preconcentrate three groups of organic materials: estrogenic compounds, PAHs and TBT from water. The recoveries of estrogenic compounds from water were 35 % of estriol, 88 % of β-estradiol, 91 % of 17α-ethynylestradiol and 96 % of estrone. These results parallel the analyte polarities demonstrating poor distribution coefficient for the more polar analytes. The recovery results were found to be improved by increasing the dispersion of the HOC_{18}-nanoscavengers in the water samples. HOC_{18}-nanoscavenger4 with improved dispersion was therefore selected to extract 13 PAH compounds and TBT from water. Most of the PAHs exhibited high affinities for the HOC_{18}-nanoscavenger4, resulting in good recovery results of these compounds. The extraction of TBT from spiked water samples using HOC_{18}-nanoscavenger4 resulted in high recovery results (95 %). These good recoveries of TBT encouraged the application of the HOC_{18}-nanoscavenger4 to the preconcentration of TBT from real water samples. This is still under investigation by Awad Alrashdy (Alan Howard research group member).

9.1.5 The advantages of nanoscavengers dispersion extraction over other solid phase extraction techniques

The nanoscavenger dispersion extraction technique offers a number of advantages compared to alternatives such as solvent extraction and disk or cartridge solid phase extraction. Firstly, the nanoscavenger can be mixed with a large volume sample with no further shaking being required and the particles can then be easily recovered by filtration. Thus for large investigations, much less work is needed and many samples can be processed in parallel.

It is possible to selectively extract target analytes by functionalizing the silica surface with specifically selected groups such as a chelating agents, ion exchange groups[4], cyclodextrins or octadecane, having a high affinity toward the target analytes whether they be organic or inorganic materials. On the other hand, extraction using disk or cartridge for example, may require pre-treatment of them by immobilization extraction agent before the extraction process take place.

After initial mixing, NSDE requires no further mechanical agitation, as the particles remain naturally suspended and move naturally due to Brownian motion and sedimentation. This facilitates their use in the field. When appropriate only small quantities of solid need to be transported, as opposed to litres of liquid sample. Furthermore, performing this process in the field limits contamination, oxidation and loss which might otherwise occur during transportation and pre-analysis storage.

The long term dispersion of particles in water (more than 5 hours for most of the nanoscavengers) and well controlled particle size offer an additional advantage during filtration in that the controlled settling of the particles into the pores of the filter membrane leads to a reduced tendency for filter blockage and rapid filtration. On the other hand, in the extraction of the analytes using disk or cartridge systems, the flow rate through the sorbent must be slow enough to ensure that the analytes are retained on the sorbent. The rapid filtration that disks may offer can cause incomplete retention of the analytes, especially with large volume samples due to poor analytes capacity leading to lower recovery[5-7].

In addition this technique is environmentally friendly as the use of organic solvents is avoided in the extraction of metal ions and only small quantities (1-5 mL) of organic solvents are required to preconcentrate organic materials. These quantities are considered minute compared to the large volume of organic solvent used with solvent extraction and solid phase extraction-cartridges. Moreover, only a small quantity of complexing agent is functionalized on the silica surface, which is less than that used in solvent extraction. At the end of a preconcentration process using nanoscavenger dispersion extraction only a small quantity of nanoscavenger (50-200 mg) needs to be disposed of safely. In contrast, in the solvent extraction technique a

large quantity of solvent has to be safely discarded, and in the solid phase extraction cartridge technique, the disposal of two materials is necessary: the cartridge and the sorbent.

9.2 Future work

In this project the synthesis, modification and applications of nanoscavengers have been highlighted. This primary investigation of the preparation and applications of the nanoscavengers needs to be further developed to expand the range of nanoscavenger procedures and to confirm their applicability in many fields such as water purification and medical applications. Further studies and applications of nanoscavengers which may be carried out in the future are highlighted below.

9.2.1 Effect of calcination on mesoporous silica structure

The template can be removed from mesoporous silica structure either *via* solvent extraction or calcination[8, 9] at high temperature; the latter being the most common method due to its simplicity. Calcinations can however decrease the pore size and surface area, as well as collapsing the mesoporous channels[10, 11] and dehydroxylation the surface silanol groups. All of these affect the modification of mesoporous silica. Thus the impact of high temperatures on the surface silanol concentration and pore size should be investigated in further work. In addition, the effect of treating mesoporous silica with acid to rehydroxylate the surface and improve the modification of mesoporous silica surface could be investigated.

9.2.2 Further studies of existing nanoscavengers

A number of further studies of nanoscavengers are possible, such as the effect of interference of some metal ions on their extraction ability; the optimal acid concentration required releasing the metals from nanoscavengers; and the possibility of the reuse of nanoscavengers and the cycling number at which the nanoscavenger can still be used with high recovery. In addition to identify the method detection limit and improve it.

9.2.3 Preparation of new nanoscavengers

In this study, nanoscavengers have been successfully prepared by modifying mesoporous silica with extracting agents such as dithiocarbamates and hydroxyquinoline. When applied to extract metal ions from water, good recovery results were obtained. It is obvious that extraction of metal ions from water using solid phase relies on the affinity of the metal to the extracting group. A wide range of chelating groups can be used to enhance the selectivity of the nanoscavenger. As such example 5-amino-1,3,4-thiadiazole-2-thiol[12] which has multi extraction positions can functionalize the surface of mesoporous silica for preparation of a new nanoscavenger therefore may be investigated in future.

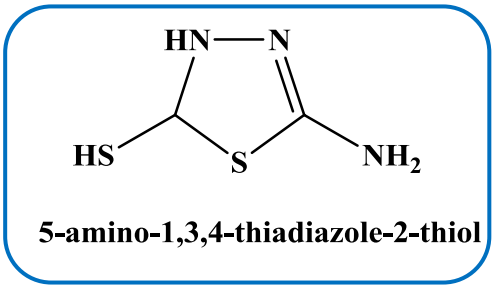

5-amino-1,3,4-thiadiazole-2-thiol

9.2.4 Further applications of nanoscavengers in the analytical fields

Nanoscavengers have been used to extract and concentrate metal ions by chelation and organic materials by exploitation of hydrophobic interactions between the analyte and the nanoscavengers. The nanoscavenger can immobilize unstable elements that might otherwise be lost during transport and storage. Moreover the extracted sample is very small and significantly easier to transport than the liquid sample. These three aspects are particularly advantageous in locations where analytical instruments are unavailable.

Arsenic is a suitable element to illustrate the potential application of nanoscavengers in difficult circumstances. Arsenic is a toxic metalloid which has contaminated natural waters all over the world. In developing countries, such as Bangladesh, there

are few high quality analytical facilities, and this means that hundreds of samples of water have to be transported to wherever suitable instruments are available to measure the arsenic. This process is unsatisfactory as the analyte can be lost during transportation and unconcentrated samples are excessively large and difficult to transport. To provide a better means of sampling under such conditions, a mercapto-nanoscavenger could be prepared by reacting mesoporous silica with 3-mercaptopropyltrimethoxysilane. A similar large particle silica gel has been applied to the batch and column preconcentration of arsenite from water samples that also contain arsenate, monomethylarsonate and dimethylarsinate[13]. Arsenite is the most toxic form of arsenic. A nanoscavenger dispersion extraction technique, based on mercapto-nanoscavenger, could therefore be developed for the selective recovery of arsenite from water in presence of arsenate.

The amine-nanoscavenger that has been prepared in this work can also be used to incorporate other functional agents onto the silica. It has been reported, for example, that aminopropyl silica can be reacted to give an aminothioamidoanthraquinone silica for the preconcentration of metal ions such as Ni (II) and Cd (II) from water. This has been used in a column technique[14] but such a modification of mesoporous silica could be investigated as the basis of a new NSDE technique for the collection of metals from water. Aminopropyl-mesoporous silica can also be potentially reacted with salicylaldehyde to give a nanoscavenger material for the preconcentration of U(VI) from water[15].

Preconcentration of phenolic compounds from water by solvent evaporation or by extraction are very difficult because they are volatile. The solid phase extraction using 8-decanoloxy-7-(3,5-dinitrobenzoyloxy)propoxypropylsilylated silica gel has however been shown to be more efficient[16]. A new nanoscavenger for phenols extraction could therefore be developed by the reaction of glycidoxypropyl-mesoporous silica with 3,5-dinitrobenzoic acid and the product could be employed to preconcentrate phenols from water.

The affinity of a wide range of organic materials for hydrophobic ‘reverse phase’ material has been widely exploited in both HPLC and in conventional solid phase extraction systems. HOC_{18}-nanoscavengers have already been prepared in this

project and following further characterization these could be evaluated for the preconcentration of phenylurea pesticides such as tebuthiuron, diuron and propanil from an aqueous solution[17, 18]. The C_{18}-silicas are also potentially useful for the extraction/preconcentration of metal chelate complexes.

9.2.5 Nanoscavengers for direct aspiration into ICP-MS

Preconcentration of metal ions from water using solid phase extraction requires the sorbent to be recovered with attached metals by filtration or centrifugation. The metal ions can then be released from the sorbent by using acid. The last step can be avoided by using nanoscavengers. With the recovered nanoscavenger with attached metal dispersed in water and the sol can be directly aspirated into an ICP-MS. The high temperature of the plasma is capable of releasing the metal ions from the complexing agent on the nanoscavenger surface[19, 20].

9.2.6 Extraction of TBT and determination as total tin

The HOC_{18}-nanoscavenger has successfully extracted TBT from water. With the concentration of TBT being determined by GC coupled with a pulsed flame photometric detector (PFPD).This detector is uncommon, and sample preparation is lengthy as the TBT has to be derivatized. A simpler technique could be developed to extract and determine TBT based on HOC_{18}-nanoscavenger dispersion extraction and following redispersion in 5 ml of water, direct aspiration into an ICP-MS. Assuming the selective extraction of alkyltins from the water, with the nanoscavenger rejecting the inorganic species, total tin measurement would be a good estimate of organotin species.

9.2.7 Magnetic nanoscavengers

Magnetic nanoscavengers can be prepared by modifying mesoporous magnetic nanoparticles ($MSiO_2@Fe_3O_4$) with suitable extractant function groups. There are two steps in the preparation of $MSiO_2@Fe_3O_4$. First, a magnetic material such as Fe_3O_4 is encapsulated within a silica shell *via* a Stöber-type method. The surface area

of the obtained material is normally low, but an improvement can be achieved in a second step, which is re-encapsulating the prepared magnetic silica using TEOS templated by $C_{16}TMABr$[21]. A high surface area will be generated after removing the template from the particle structure. The main advantage of magnetic nanoscavenger particles is that the particles can be easily recovered from water by applying a magnet, removing the need for filtration or centrifugation.

9.4 References

(1) Peng, Y.; Li, Z. M.; Zeng, Y. B.; Xie, X. A.; Wang, H. D.; Li, L.; Liu, X. M. *Microchim. Acta* **2010**, *170*, 17-26.

(2) Liu, C. Y.; Wang, S. Y.; Rong, Z. H.; Wang, X. Q.; Cu, G. N.; Sun, W. J. *J. Non-Cryst. Solids* **2010**, *356*, 1246-1251.

(3) Yamada, Y.; Yano, K. *Micropor. Mesopor. Mater.* **2006**, *93*, 190-198.

(4) Nesterenko, P. N.; Shaw, M. J.; Hill, S. J.; Jones, P. *Microchem J.* **1999**, *62*, 58-69.

(5) Bjorklund, L. B.; Morrison, G. M. *Anal. Chim. Acta* **1997**, *343*, 259-266.

(6) Moghimi, A.; Poursharifi, M. J. *Asian J. Chem.* **2009**, *21*, 2541-2548.

(7) Khdary, N. H. Ph.D. Thesis, Southampton University, Southampton, UK, **2006**.

(8) Schuth, F. *Ber. Bunsen-Ges. Phys. Chem. Chem. Phys.* **1995**, *99*, 1306-1315.

(9) Dattelbaum, A. M.; Amweg, M. L.; Ruiz, J. D.; Ecke, L. E.; Shreve, A. P.; Parikh, A. N. *Mechanism of surfactant removal from ordered nanocomposite silica thin films by deep-UV light exposure*; Materials Research Society: Warrendale, **2004**.

(10) Hozumi, A.; Yokogawa, Y.; Kameyama, T.; Hiraku, K.; Sugimura, H.; Takai, O.; Okido, M. *Adv. Mater.* **2000**, *12*, 985-987.

(11) Kundu, D.; Zhou, H. S.; Honma, I. *J. Mater. Sci. Lett.* **1998**, *17*, 2089-2092.

(12) Tzvetkova, P.; Vassileva, P.; Nickolov, R. *J. Porous Mater.* **2010**, *17*, 459-463.

(13) Howard, A. G.; Volkan, M.; Ataman, O. Y. *Analyst* **1987**, *112*, 159-162.

(14) Ngeontae, W.; Aeungmaitrepirom, W.; Tuntulani, T. *Talanta* **2007**, *71*, 1075-1082.

(15) Jamali, M. R.; Assadi, Y.; Shemirani, F.; Hosseini, M. R. M.; Kozani, R. R.; Masteri-Farahani, M.; Salavati-Niasari, M. *Analytica Chimica Acta* **2006**, *579*, 68-73.

(16) Biernat, J. F.; Makuch, B. *Pol. J. Environ. Stud.* **2000**, *9*, 71-75.

(17) Spliid, N. H.; Koppen, B. *J. Chromatogr. A* **1996**, *736*, 105-114.

(18) Sagratini, G.; Manes, J.; Giardina, D.; Damiani, P.; Pico, Y. *J. Chromatogr. A* **2007**, *1147*, 135-143.

(19) Hill, S. J.; Dawson, J. B.; Price, W. J.; Shuttler, I. L.; Tyson, J. F. *J. Anal. At. Spectrom.* **1996**, *11*, R281-R325.

(20) Hill, S. J.; Dawson, J. B.; Price, W. J.; Riby, P.; Shuttler, I. L.; Tyson, J. F. *J. Anal. At. Spectrom.* **1994**, *9*, R213-R247.

(21) Chen, D. Y.; Jiang, M. J.; Li, N. J.; Gu, H. W.; Xu, Q. F.; Ge, J. F.; Xia, X. W.; Lu, J. M. *J. Mater. Chem.* **2010**, *20*, 6422-6429.